THÈSE

présentée à

L'UNIVERSITÉ DES SCIENCES ET TECHNIQUES DE LILLE

pour obtenir le grade de

DOCTEUR ES SCIENCES PHYSIQUES

par

Didier TANRÉ

INTERACTION RAYONNEMENT-AEROSOLS APPLICATIONS A LA TELEDETECTION ET AU CALCUL DU BILAN RADIATIF

Soutenue le 19 mars 1982 devant la Commission d'Examen :

Membres du Jury :	M.	SOULAGE	Président
	M.	BOLLE	Rapporteurs
	M.	HERMAN	
	M.	KAUFMAN	
	Mme	LENOBLE	Examinateurs
	M.	DESCHAMPS	
	M.	RASOOL	
	M.	REVAH	

U.E.R. DE PHYSIQUE FONDAMENTALE

Ce travail a été effectué au Laboratoire d'Optique Atmosphérique de l'Université des Sciences et Techniques de Lille, dirigé par Madame Lenoble, Professeur. Je suis particulièrement heureux de pouvoir lui exprimer ici ma profonde reconnaissance pour m'avoir accueilli dans son laboratoire et pour avoir participé à ce travail.

Cette étude a été dirigée par Monsieur Herman, Professeur, ses conseils, sa coopération en ont permis l'aboutissement. Il est certain que, sans lui, ce travail ne serait pas ce qu'il est aujourd'hui. Je voudrais de même exprimer ma gratitude envers Monsieur Deschamps, chargé de Recherche au C.N.R.S., qui a joué à diverses reprises un rôle essentiel dans le développement de ces travaux. Les articles inclus dans cette thèse suffisent à témoigner de leur étroite collaboration.

Monsieur Bolle, Professeur à l'Université d'Innsbruck et Monsieur Kaufman du Goddard Space Flight Center de la N.A.S.A. ont bien voulu juger mon travail et apporter leur critique, je les en remercie très vivement.

Monsieur Rasool, responsable des projets scientifiques à la N.A.S.A., Monsieur Revah, Directeur adjoint du Centre de Recherches en Physique de l'Environnement Terrestre et Planétaire et Monsieur Soulage, Professeur à l'Université de Clermont-Ferrand, m'ont fait l'honneur de participer à mon jury, je tiens à leur témoigner mes sincères remerciements.

Le Centre National d'Etudes Spatiales (C.N.E.S.) a non seulement financé la majeure partie de nos travaux mais m'a apporté personnellement son soutien financier ; qu'il soit ici remercié. Avec une attention plus particulière, je remercie Monsieur De Leffe de la Division Observation de la Terre du C.N.E.S. de Toulouse pour les échanges fructueux que nous avons eus avec lui et qui sont à l'origine d'une partie de ce travail.

Mes remerciements vont également à l'ensemble des membres du laboratoire et plus particulièrement à l'équipe informatique, Mademoiselle Deroo et Monsieur Gonzales, au secrétariat, Mesdames Devaux et Théroux et à Monsieur Panhaleux qui par sa disponibilité des derniers instants a permis la réalisation de cet ouvrage.

Je tiens aussi à remercier l'ensemble du personnel technique de l'U.E.R., et surtout Messieurs Carey, Fauquembergue et Vilain de l'atelier de reproduction ainsi que Monsieur Raffaud qui a reproduit une partie des dessins.

Lire ce travail dans son intégralité a du parfois s'avèrer pénible pour Martine qui s'est chargée de la frappe du manuscrit. Cette dernière page doit lui procurer un soulagement bien compréhensible. C'est donc par elle que je tiens à conclure ces remerciements.

à Frédérique

SOMMAIRE

-=-=-=-=-=-=-=-

Interaction Rayonnement_Aérosols Applications à la Télédétection et au Calcul du Bilan Radiatif

INTRODUCTION

Les processus qui régissent le transfert radiatif en atmosphère claire sont de deux types, les processus d'absorption gazeuse, (principalement H_2O, O_3, NO_2, CO_2 et O_2) et les processus de diffusion (molécules et aérosols). Si l'absorption et la diffusion par les molécules sont bien paramétrisées par contre le rôle des aérosols est encore assez mal cerné. Leurs sources étant très diverses (érosion, pollution atmosphérique, éruption volcanique...), il est clair que aussi bien l'abondance de ces particules que les paramètres définissant leur influence sur le rayonnement ne sont pas simplement modélisables, les mesures satellitaires vont donc être délicates à interpréter si on ne s'affranchit pas de cette perturbation sur le rayonnement.

Les propriétés des aérosols étant très variables, notre démarche a été d'effectuer des simulations numériques du transfert radiatif sur un échantillonage d'aérosols représentatifs, afin de dégager par quels principaux paramètres ils influencent l'allure du champ de rayonnement. Ces simulations ont été faites sur des modèles d'atmosphère tenant compte des conditions réalistes de mesure (inhomogénéités verticales pour l'atmosphère, inhomogénéités horizontales pour le sol) et les calculs ont été conduits aussi exactement que possible (en particulier, avec prise en compte de la polarisation), mais ils s'avèrent lourds et couteux. Nous avons donc été amenés à développer une formulation analytique simple du signal satellitaire, les comparaisons effectuées avec les calculs exacts montrent que sa précision est tout à fait satisfaisante. L'établissement de ce formalisme fait l'objet de la partie I (chapitre I).

L'exploitation de ces calculs montre l'importance de trois paramètres, l'épaisseur optique en aérosols leur facteur d'anisotropie (caractéristique de leur diagramme de diffusion) et leur albédo. La formulation que nous avons dégégée nous a permis d'estimer facilement le signal satellitaire ce qui s'avère indispensable si l'on veut optimiser les performances des capteurs des expériences spatiales. Ces résultats ont été appliqués en particulier aux bilans de flux prévisionnels des expériences S.P.O.T. 1 (Satellite Probatoire d'Observation de la Terre) du C.N.E.S. (Centre National d'Etudes Spatiales) et O.C.M. (Ocean Color Monitoring) de l'E.S.A. (Agence Spatiale Européenne).

De façon générale, on peut schématiquement distinguer deux types d'applications, la télédétection de la couleur de l'océan (O.C.M.) et la télédétection des ressources terrestres (S.P.O.T.) où le but est d'éliminer l'influence de l'atmosphère sur les mesures de réflectances de sol.

Dans le cas de l'océan, les réflectances marines sont faibles devant la composante atmosphérique qui correspond au rayonnement diffusé dans l'atmosphère. Cette composante purement atmosphérique représente le signal parasite qu'il faut éliminer. Cela fait l'objet du Chapitre II, Partie I.

En ressources terrestres, où les réflectances de sol sont élevées, l'effet perturbateur principal va plutôt provenir de l'environnement. En effet, le capteur va recevoir non seulement un signal provenant de la cible mais aussi un signal provenant de son environnement, correspondant aux photons réfléchis par les surfaces voisines et qui sont diffusés ensuite par l'atmosphère dans la direction du capteur. On a également un effet du deuxième ordre par rapport aux effets d'environnement qui provient des écarts à la loi de lambert de la plupart des réflectances de surface. Ceci sera étudié dans le chapitre III, partie I.

La correction de ces différentes perturbations nécessite en tout premier lieu de connaitre l'épaisseur optique des aérosols. On aborde là l'aspect télédétection des aérosols. On peut envisager l'utilisation simultanée des calculs théoriques et de mesures expérimentales afin de développer des algorithmes d'inversion permettant de remonter aux propriétés optiques des aérosols, mais le problème reste très complexe. La modélisation nous a permis d'envisager de remonter à l'épaisseur optique en aérosols uniquement à partir des mesures satellitaires. Cette méthode est basée sur l'analyse fine des histogrammes des réflectances d'une scène donnée. Une première étude sur les données LANDSAT nous a montré la faisabilité de la méthode (chapitre III, partie I).

Le deuxième volet de ce travail a été consacré à l'aspect énergétique de l'interaction rayonnement aérosols pour aborder l'étude de leur impact climatique. En perturbant le rayonnement, les aérosols modifient l'albedo de la planète pour la partie visible du spectre et modifient les processus d'émission et d'absorption pour la partie infrarouge. Pour intégrer ces effets radiatifs dans des modèles climatiques évolutifs déjà existants, la prise en compte doit se faire d'une manière simple et précise afin de ne pas alourdir les temps de calcul déjà prohibitifs des modèles de circulation générale. La modélisation vue en partie I, directement adaptée aux calcul du bilan radiatif dans le visible a été généralisée aux longueurs d'onde infrarouges. Nous nous sommes d'abord intéressés aux aérosols stratosphériques, ce qui simplifie le problème et constitue une première approche du problème. Les aérosols stratosphériques forment une couche de faible épaisseur optique et relativement stable située au dessus de la couche diffusante formée par les molécules d'air, les aérosols troposphériques et les nuages. Par ailleurs, le rôle radiatif est à priori simple puisque nous n'avons pas dans ce cas de phénomènes de couplage ou de "feedback" avec les nuages comme ce peut être le cas avec les aérosols troposphériques.

L'expression analytique simple obtenue, permet de tester l'influence des divers paramètres (albedo du système troposphére-sol, absorption, facteur d'anisotrope et épaisseur optique des aérosols) sur le bilan climatique de la planète. Cette étude fait l'objet de la partie II.

PARTIE I

TELEDETECTION

INTRODUCTION

En atmosphère claire (sans nuages), les mesures de réflectance des surfaces terrestres, faites au moyen de la mesure du rayonnement solaire réfléchi vers l'espace, sont perturbées par deux processus, un processus d'absorption par certains gaz atmosphériques (O_3, H_2O et CO_2 principalement) et un processus de diffusion par les aérosols et par les molécules. Généralement, les bandes spectrales d'observation sont choisies dans des fenêtres atmosphériques transparentes, et l'absorption par les gaz peut être négligée ; le seul terme perturbateur reste la diffusion atmosphérique (molécule et aérosols).

Nous nous proposons, dans cette partie, de modéliser le signal satellitaire en fonction des paramètres optiques caractérisant l'atmosphère et la surface respectivement. Nous envisagerons alors deux cas pratiques d'application de cette modélisation : la mesure de la couleur de l'océan, entre 0,4 et 0,7 µm, (domaine spectral intéressant pour la chlorophylle) où les signaux cherchés sont faibles par rapport au signal atmosphérique lui même qui sera à retrancher de la mesure, l'observation de paysages terrestres, entre 0,7 et 1 µm, (domaine spectral intéressant pour la végétation) où la principale perturbation provient du mélange des signatures de cibles voisines.

La correction de ces effets demande de connaitre en particulier l'épaisseur optique des aérosols. On propose une méthode pour atteindre ce paramètre essentiel à partir d'un satellite ; une étude de faisabilité en a été faite dans le cas du satellite LANDSAT.

Enfin, on suppose généralement les réflectances du type lambertien ; on examinera les problèmes que soulèvent les écarts, par rapport à cette simple loi, des réflectances réelles des cibles.

I - MODÉLISATION DU SIGNAL (ANNEXE 1)

Examinons de manière qualitative comment se pose le problème.

Le rayonnement solaire qui arrive au voisinage de la terre servant de source primaire, nous cherchons quelle fraction de ce rayonnement percevra un satellite qui vise la terre. La cible désignera la portion de la surface terrestre interceptée par le champ de l'appareil.

Imaginons d'abord qu'on enlève l'atmosphère. Tout le rayonnement solaire éclairera la surface. Elle n'en absorbera en général qu'une partie, le reste étant renvoyé vers l'espace. Les seuls photons que l'on captera ici seront ceux que la cible, et elle seule, renvoie précisément dans la direction du satellite, et ils seront intégralement captés. Ce signal, directement relié aux propriétés de la cible, est le signal utile ; on l'observerait directement, dans ce cas idéal.

Interposons l'atmosphère, et dénombrons les photons qui parviennent encore jusqu'au détecteur, en suivant comme précédemment de simples trajets directs du soleil à la cible puis de la cible au satellite. Typiquement, par rapport au cas idéal, on n'en comptera plus qu'environ 70 pour cent à 850 nm, et 40 pour cent à 450 nm. Ces seuls

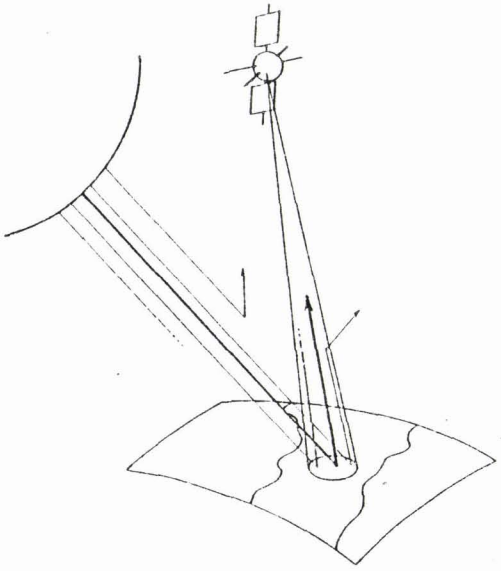

photons directement transmis feront donc paraître la cible nettement plus absorbante qu'elle ne l'est, et un premier point sera d'évaluer avec précision cet effet de transmission directe de l'atmosphère.

Les photons qui manquent dans ce premier bilan ont disparu à partir de deux mécanismes : l'absorption et la diffusion.

Quelques uns d'entr'eux ont été absorbés par les aérosols ou certaines molécules gazeuses (O_2, H_2O..). Ils contribuent à échauffer l'atmosphère qui réémet cette énergie, mais à des longueurs d'onde beaucoup plus grandes dans l'infra-rouge. Pour notre bilan ces photons correspondent à une perte nette, mais très faible. En effet, l'absorption des aérosols est faible dans le visible, et on évitera en général l'absorption gazeuse en faisant les observations en dehors des bandes d'absorption moléculaire les plus intenses. Ces pertes par absorption seront à évaluer ici en tant que termes correctifs.

La presque totalité des photons non transmis seront ici diffusés. Dans ce second mécanisme, l'interaction du photon avec un aérosol ou une molécule est élastique ; il est aussitôt réémis, sans changement de longueur d'onde, mais dans une direction différente de sa direction d'incidence. Après une ou plusieurs diffusions, ces photons finiront par atteindre la surface ou par ressortir vers l'espace. Ils réapparaîtront donc dans nos bilans, mais sous la forme maintenant de faisceaux diffus, plus complexes que les faisceaux directs précédents.

Considérons pour commencer les photons ainsi extraits du faisceau solaire incident, avant qu'ils n'atteignent la surface, et qui sont finalement rétrodiffusés vers l'espace.

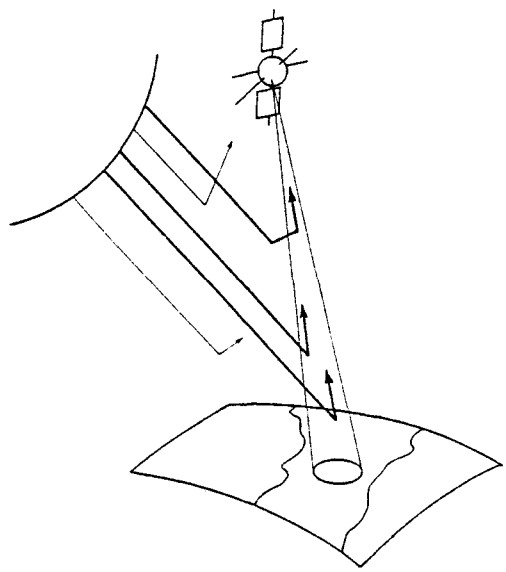

Le détecteur en captera une partie : ceux qui subissent leur dernière diffusion dans le champ de l'appareil avec une direction finale convenable. Ce nouveau signal est purement parasite. Entièrement créé dans l'atmosphère, il ne transporte aucune information sur la surface. Il superposera simplement au signal utile venant de la cible un fond continu qu'on devra déterminer.

Le reste des photons extraits du faisceau solaire finiront par traverser l'atmosphère à quelques pertes près par absorption. Ceux-là contribuent à illuminer la surface, sous la forme d'un faisceau diffus, et compensent partiellement l'atténuation du faisceau solaire direct. Ils formeront donc en général une composante utile. On leur réservera quand même une formulation particulière, pour le cas où l'on voudrait analyser comment la réponse d'une surface peut varier suivant le type d'illumination qu'elle reçoit.

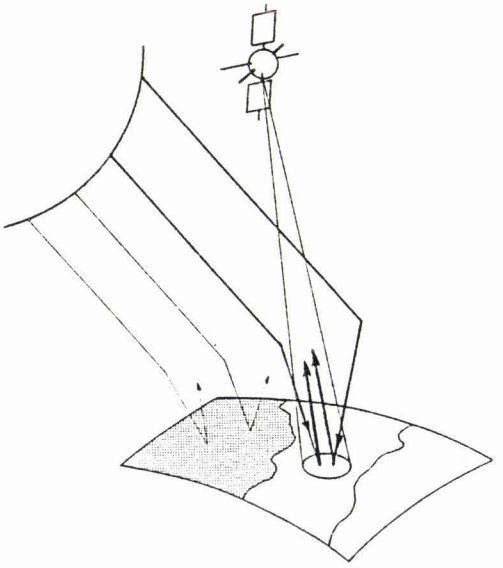

On fera la même analyse pour les photons qui se trouvent maintenant diffusés sur leurs trajets retour, depuis la surface vers l'espace, lorsqu'on interpose l'atmosphère.

Considérons encore pour commencer ceux qui finissent par ressortir vers l'espace, par transmission diffuse à travers l'atmosphère. Comme précédemment, une partie d'entr'eux sera captée par le détecteur, à partir d'une dernière diffusion dans le champ de visée. Cette troisième composante du signal doit être analysée soigneusement. Si les propriétés de la surface sont assez uniformes, dans le voisinage de la cible, ce sera une composante utile dont on devra conserver l'information. Mais si la scène observée est inhomogène, cette composante

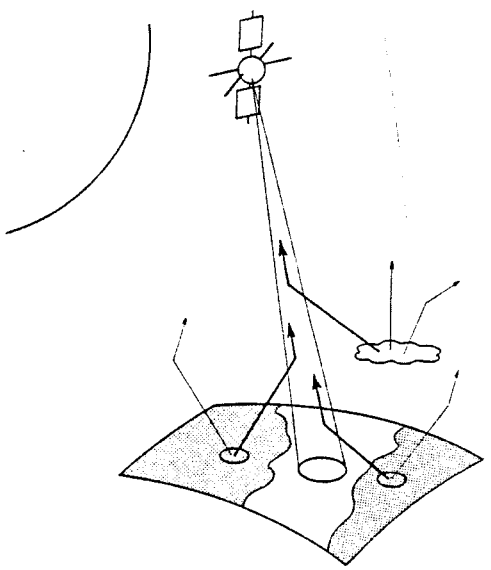

induira au contraire des effets parasites d'environnement très génants.

Enfin les photons qui reviennent vers la surface, rétrodiffusés par l'atmosphère, vont donner une troisième composante à son illumination totale. On voit ici s'amorcer le phénomène classique du "trapping", avec l'emprisonnement du photon qui interagit successivement

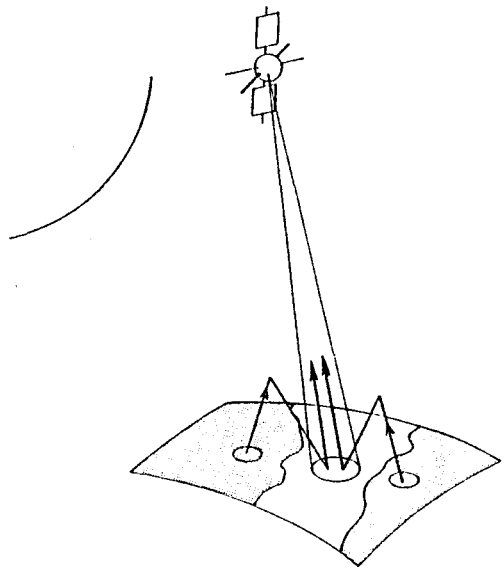

avec la surface et l'atmosphère. Dans le cas présent ce phénomène s'atténue très vite, et cette série d'interactions converge rapidement.

Passons de cette analyse qualitative à une formulation analytique du signal, dans le cas simple d'un réflecteur lambertien. On généralisera ensuite cette formulation au cas d'un sol non homogène ou présentant une réflectance de caractère directionnel.

I-1 - FORMULATION ANALYTIQUE DANS LE CAS D'UN REFLECTEUR LAMBERTIEN HOMOGENE

On suppose la réflectance de tout le site uniforme et lambertienne, de valeur ρ. Chaque point du sol reçoit un éclairement qui est l'addition des processus suivants :

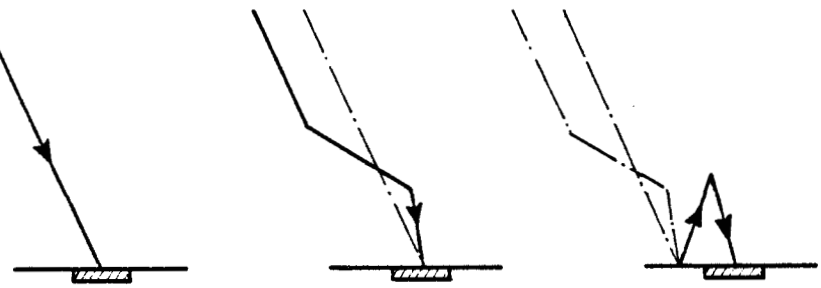

(a) (b) (c)

a) Un éclairement direct, qui correspond à l'éclairement solaire en haut de l'atmosphère, $\mu_s E_s$, atténué en $e^{-\tau/\mu_s}$ lors de sa traversée de l'atmosphère ; soit

$$\mu_s E_s e^{-\tau/\mu_s} \qquad \text{(I-1)}$$

où τ est l'épaisseur optique de l'atmosphère et θ_s = Arcos μ_s l'angle solaire zénithal.

b) Un éclairement diffus intrinsèque à l'atmosphère (c'est à dire pour $\rho = 0$), qui correspond aux photons arrivant au sol uniquement après diffusion par l'atmosphère ; soit l'éclairement solaire en haut de l'atmosphère, $\mu_s E_s$, pondéré par un facteur de transmission diffus, $t_d(\theta_s)$:

$$\mu_s E_s t_d(\theta_s) \qquad \text{(I-2)}$$

La somme des facteurs de transmission direct, $e^{-\tau/\mu_s}$, et diffus, $t_d(\theta_s)$, définit un facteur de transmission total (direct + diffus) qu'on notera $T(\theta_s)$:

$$T(\theta_s) = e^{-\tau/\mu_s} + t_d(\theta_s) \qquad \text{(I-3)}$$

c) Enfin un éclairement diffus traduisant l'influence de la réflexion du sol, et qui correspond aux réflexions puis diffusions successives des photons par le sol et l'atmosphère, soit :

$$\mu_s E_s T(\theta_s) \{\rho s + \rho^2 s^2 + \ldots\} \qquad \text{(I-4)}$$

où s, facteur de réflexion atmosphérique pour une source isotrope, est l'albedo sphérique de l'atmosphère.

L'éclairement au niveau du sol, $E(\theta_s)$, somme des 3 composantes précédentes, s'écrit donc

$$E(\theta_s) = \mu_s E_s T(\theta_s) \ (1 + \rho s + \rho^2 s^2 + \ldots)$$
$$E(\theta_s) = \mu_s E_s \frac{T(\theta_s)}{1-\rho s} \qquad \text{(I-5)}$$

La réflectance étant lambertienne, la luminance réfléchie par le sol (en bas de l'atmosphère) sera isotrope et uniforme, et donnée par :

$$L^{\uparrow}_{sol} = \frac{\rho}{\pi} E(\theta_s) = \frac{\rho}{\pi} \mu_s E_s \frac{T(\theta_s)}{1-\rho s} \qquad \text{(I-6)}$$

La luminance en haut de l'atmosphère $L^*(\theta_s, \theta_v, \phi_v)$ (où ϕ_v est la différence d'azimuth entre les directions d'incidence et d'observation) est par ailleurs la somme de 3 contributions :

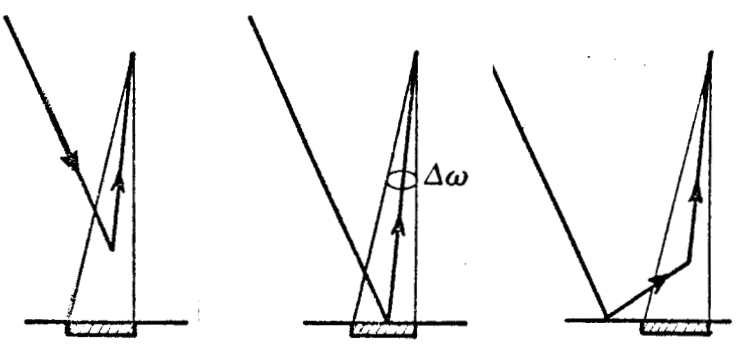

a) la luminance intrinsèque à l'atmosphère (i.e. $L^* = L_a$ pour $\rho = 0$) :

$$L_a = \frac{\mu_s E_s}{\pi} \rho_a \qquad \text{(I-7)}$$

b) Le signal réfléchi provenant de l'élément dS visé dans la direction d'observation, $L^{\uparrow}_{sol}$, affecté du facteur de transmission directe : $e^{-\tau/\mu_v}$

$$\mu_s E_s \frac{T(\theta_s)}{1-\rho s} \frac{\rho}{\pi} e^{-\tau/\mu_v} \qquad \text{(I-8)}$$

où $\theta_v = \text{Arcos } \mu_v$ est l'angle de visée.

c) Et le signal réfléchi provenant, par diffusions dans l'atmosphère, de l'environnement de l'élément dS, et affecté du facteur de transmission diffuse $t'_d(\theta_v)$:

$$\mu_s E_s \frac{T(\theta_s)}{1 - \rho s} \frac{\rho}{\pi} t'_d(\theta_v) \qquad \text{(I-9)}$$

Au total :

$$L^*(\theta_s, \theta_v, \phi_v) = \frac{\mu_s E_s}{\pi} \{\rho_a(\theta_s, \theta_v, \phi_v) + \rho \frac{T(\theta_s)}{1-\rho s} (e^{-\tau/\mu_v} + t'_d(\theta_v))\} \qquad \text{(I-10)}$$

Si on exprime les différentes grandeurs en réflectance équivalente définie par

$$\rho^* = \frac{\pi L^*}{\mu_s E_s} \quad , \qquad \text{(I-11)}$$

l'expression de la réflectance apparente d'un site homogène et lambertien sera finalement donnée par,

$$\rho^*(\theta_s, \theta_v, \phi_v) = \rho_a(\theta_s, \theta_v, \phi_v) + \rho \frac{T(\theta_s)\ T'(\theta_v)}{1 - \rho s} \quad . \qquad \text{(I-12)}$$

où

$$T'(\theta_v) = e^{-\tau/\mu_v} + t'_d(\theta_v) \qquad \text{(I-13)}$$

Il suffit donc pour décrire les effets de diffusion atmosphérique, de connaitre les 4 fonctions suivantes :

- $\rho_a(\theta_s, \theta_v, \phi_v)$, qui représente la réflectance atmosphérique intrinsèque (i.e. la réflectance de l'atmosphère pour un sol non réfléchissant) et dépend fortement des conditions géométriques d'éclairement et d'observation.

- $T(\theta_s)$, facteur de transmission total de l'atmosphère diffusante (rapport de l'éclairement (direct + diffus) au sol à l'éclairement incident en haut de l'atmosphère), qui ne dépend que de l'angle zénithal θ_s.

- $T'(\theta_v)$, facteur de transmission total correspondant à des photons injectés au niveau du sol et transmis en haut de l'atmosphère (nous montrerons que les fonctions T et T' physiquement différentes sont en fait identiques).

- et s, albédo sphérique de l'atmosphère, indépendant des conditions géométriques d'éclairement et d'observation.

I-2 - FONCTIONS ATMOSPHERIQUES

Nous avons illustré les fonctions atmosphériques précédentes pour différentes conditions de mesures

(R) correspond à des conditions de mesure idéales en télédétection, atmosphère moléculaire pure.

(23) correspond à des conditions moyennes d'observation, diffusion moléculaire et une concentration en aérosols correspondant à une visibilité au sol de 23 km.

(5) correspond à des conditions limites d'observation pour l'utilisation de la télédétection,diffusion moléculaire et visibilité de 5 km.

Réflectance atmosphérique intrinsèque

Eclairons d'abord l'atmosphère par le faisceau solaire, sous l'incidence μ_s, et calculons le transfert du rayonnement, en supposant la réflectance du sol nulle. Soient, dans ces conditions,

$L_a(\theta_s, \theta_v, \phi_v)$ la luminance diffuse qui ressort vers l'espace, et $L_a^{\downarrow}(\theta', \phi')$ la luminance diffuse qui parvient au niveau du sol.

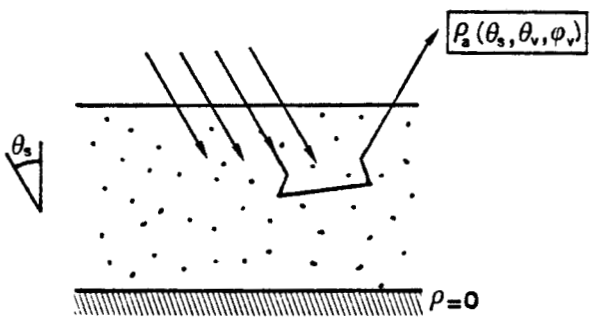

La réflectance intrinsèque de l'atmosphère, $\rho_a(\theta_s, \theta_v, \phi_v)$, définie précédemment (eq I-7) est donnée par

$$\rho_a(\theta_s, \theta_v, \phi_v) = \frac{\pi L_a}{\mu_s E_s} \qquad \text{(I-14)}$$

Les figures I-1 et I-2 montrent cette réflectance atmosphérique propre en fonction de θ_v pour λ = 450 et 850 nm. On est amené à faire les constatations suivantes,

. L'analyse de la réflectance atmosphérique ρ_a en fonction de l'angle d'observation θ_v (ce qui correspond au signal mesuré par un radiomètre à balayage placé sur un satellite) montre que ρ_a varie peu pour des conditions moyennes de visées ($\theta_v < 45°$) et un soleil proche du zénith ($\theta_s = 15°$). Ceci n'est conservé, lors d'incidences solaire plus rasantes ($\theta_s = 60°$), que dans le plan ($\phi_v = 90°, 270°$) ; le signal mesuré présente au contraire un fort degré d'anisotropie dans le plan ($\phi_v = 0$; 180°), plus particulièrement dû à la diffusion par les aérosols.

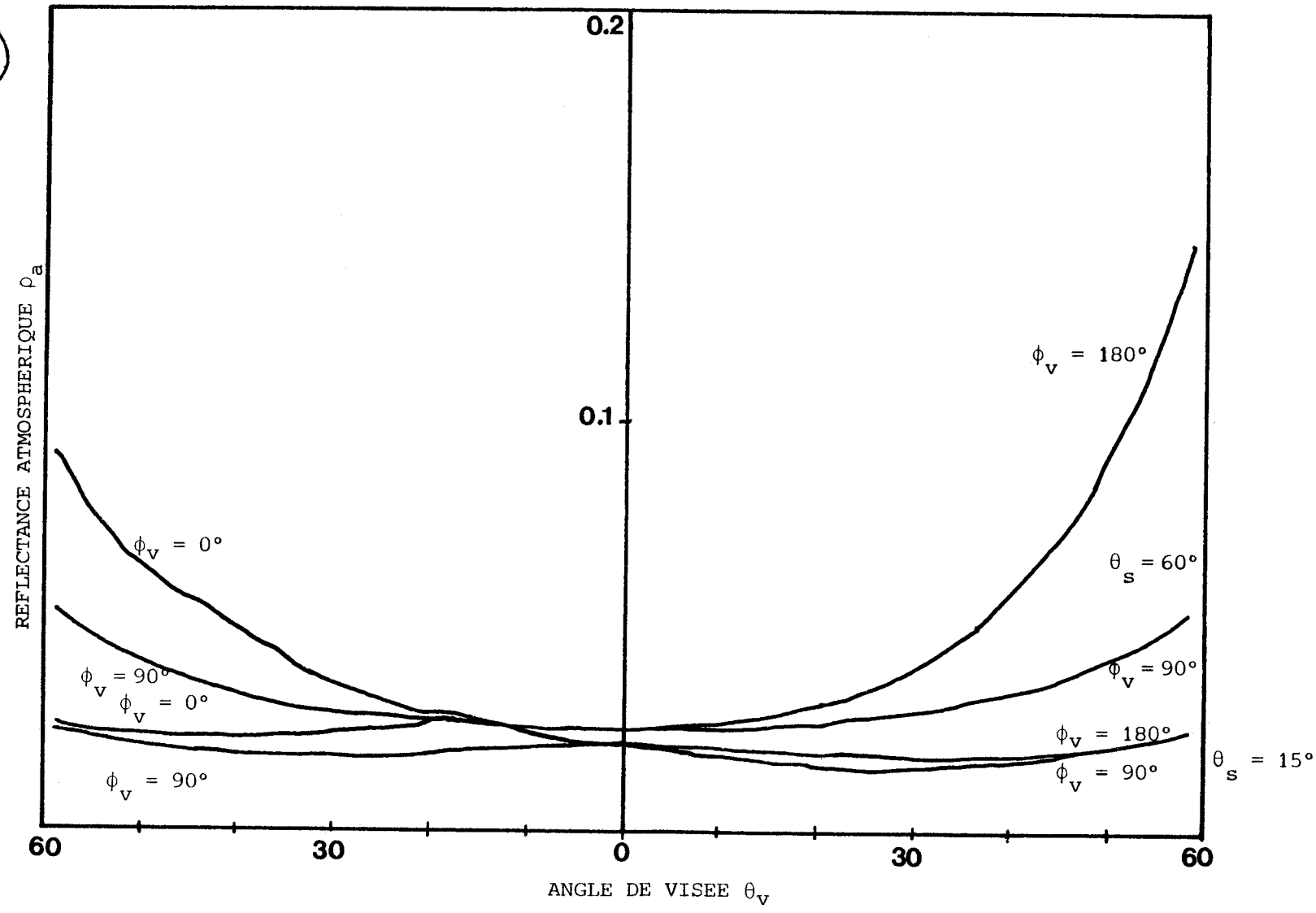

FIGURE I-1 : Variabilité de la réflectance atmosphérique ρ_a, en fonction de la géométrie d'observation. Observations à 850 nm, dans des conditions de visibilité moyennes : (V-23). Simulations d'un balyage dans le plan d'incidence du soleil (ϕ = 0° et 180°), et d'un balayage dans le plan perpendiculaire au plan d'incidence (ϕ_v = 90°), en considérant deux hauteurs différentes du soleil (θ_s = 15° et 60°) dans chacun des cas.

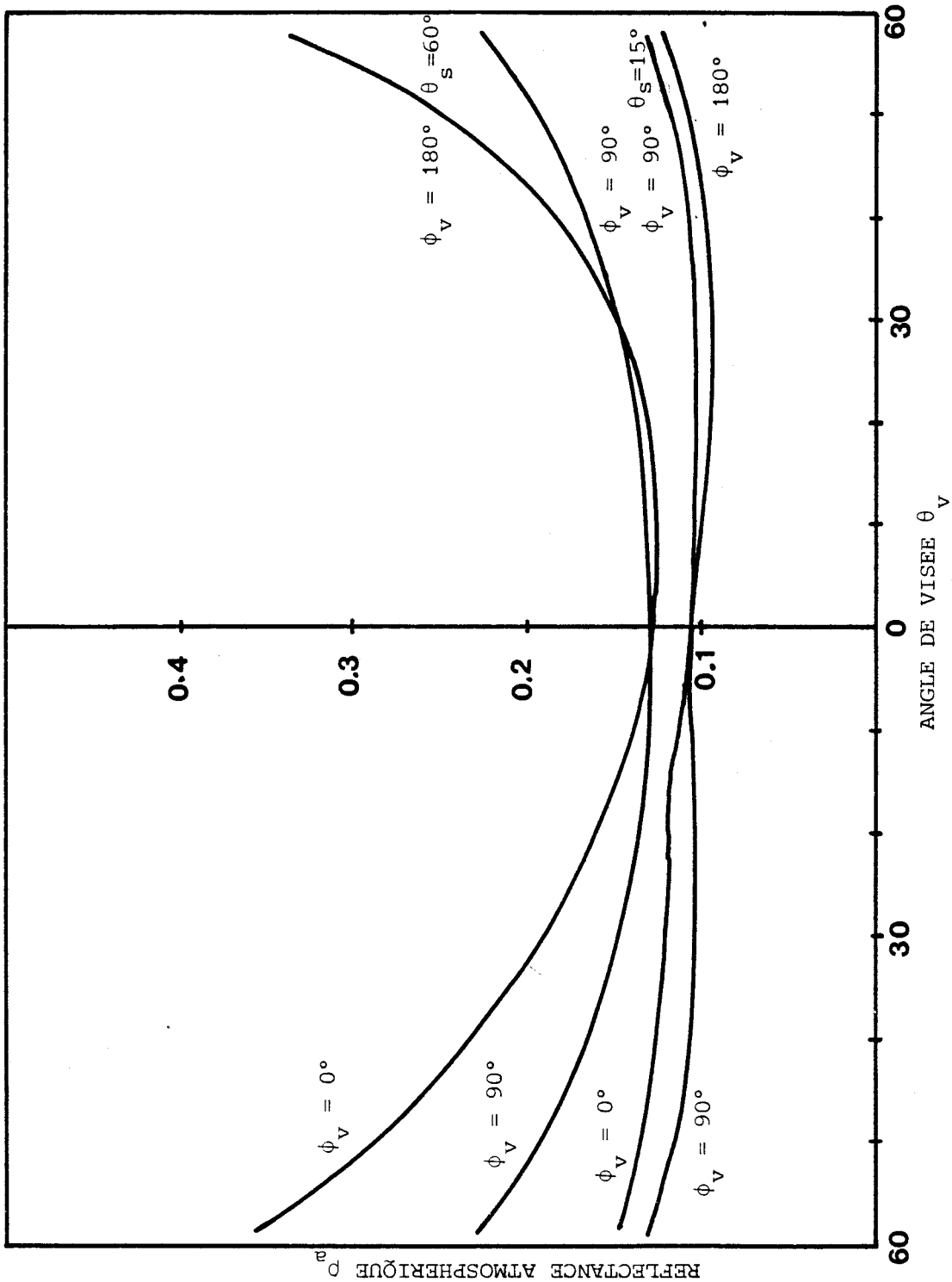

FIGURE I-2 : Même légende que Figure I-1, mais pour des observations à 450 nm.

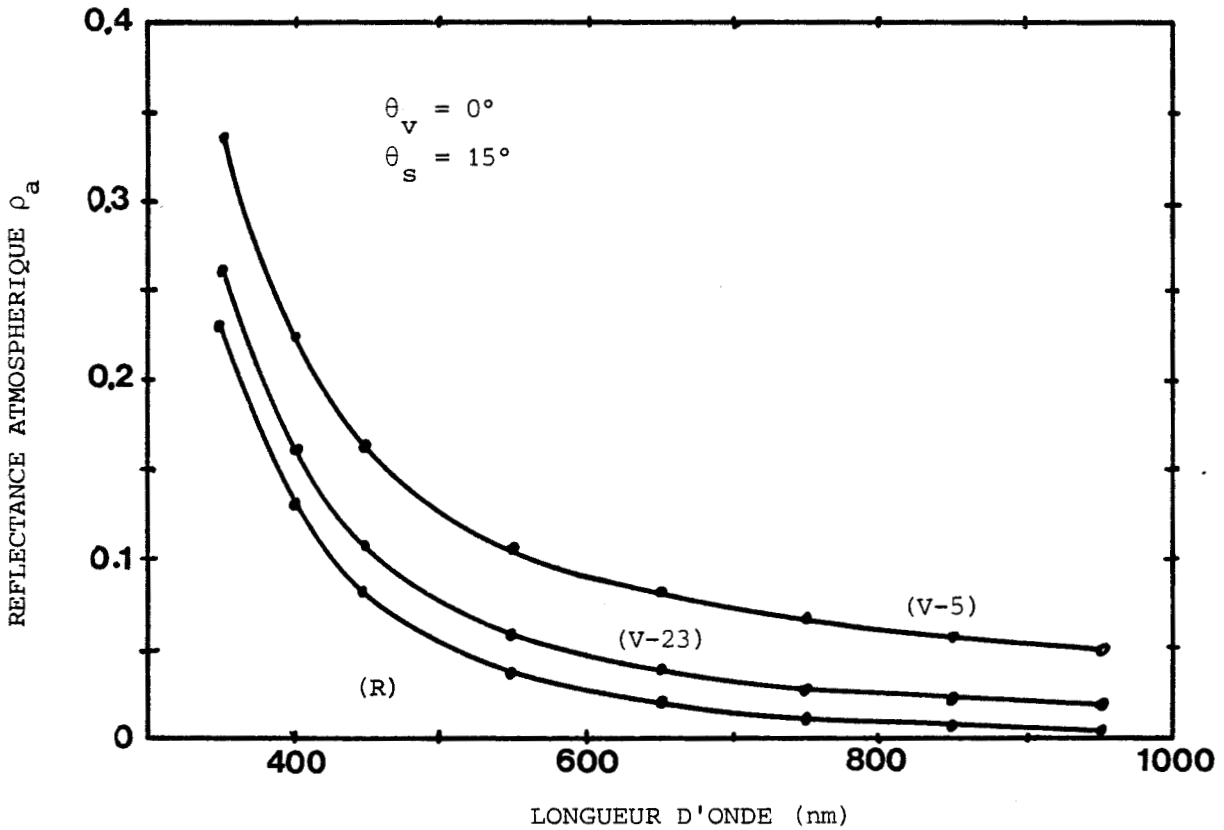

FIGURE I-3 : Réflectance atmosphérique ρ_a en fonction de la longueur d'onde, cas d'une incidence solaire faible θ_s = 15° et d'une observation verticale θ_v = 0°

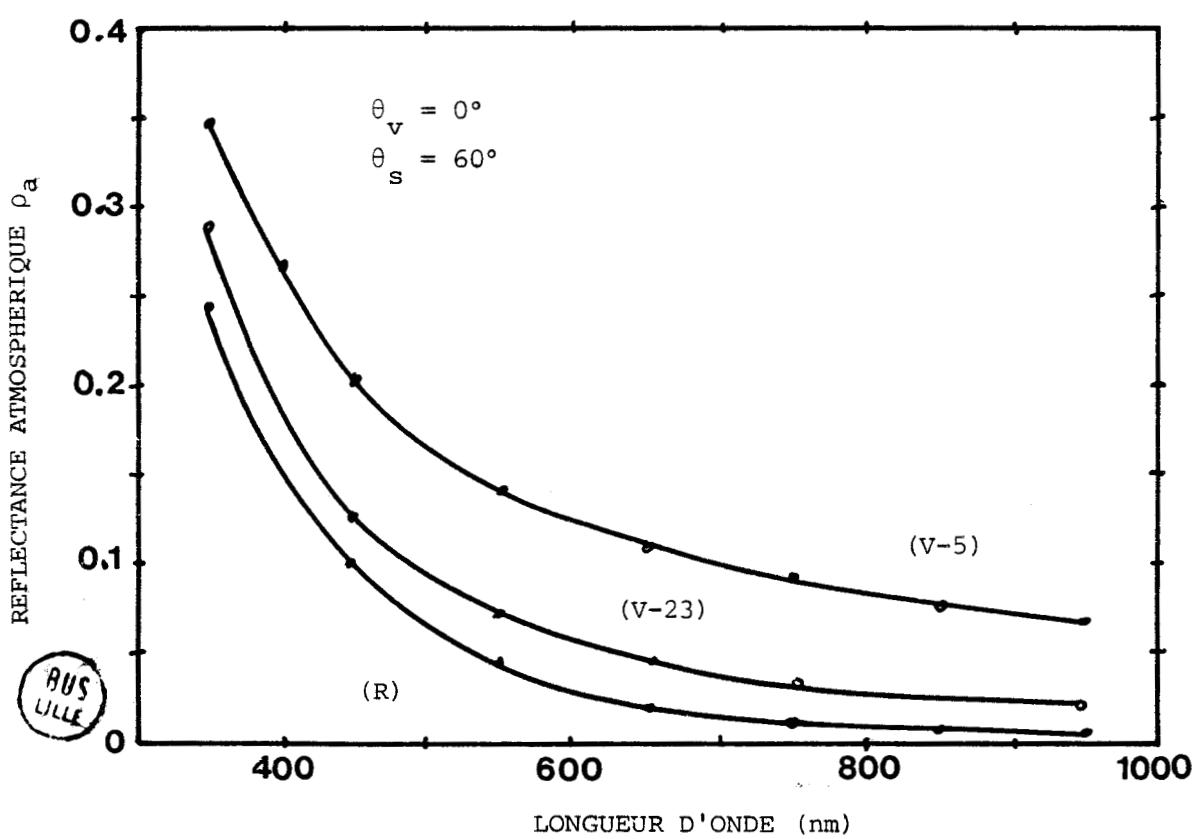

FIGURE I-4 : Même légende que figure I-3 mais pour θ_s = 60°

En télédétection, on utilise souvent des données multispectrales. Les figures I-3 et I-4 nous donnent la dépendance en longueur d'onde de la réflectance pour une observation verticale et deux directions d'incidence. On constate la grande dépendance spectrale du ρ_a, la diffusion moléculaire variant en λ^{-4} et celle des aérosols, typiquement, en λ^{-1}. Pour un modèle moyen d'atmosphère ρ_a passe de 15 % à 400 m à 5 % dans le rouge.

. A λ = 850 nm, la diffusion moléculaire est faible et la réflectance atmosphérique provient essentiellement de la diffusion par les aérosols. A λ = 450 nm, les propositions sont inversées et on se trouve en présence d'une forte composante de diffusion moléculaire.

Fonctions de transmission

L'éclairement total du sol se décompose

- en un éclairement par le faisceau solaire direct transmis :

$$E_{sol}^{direct} = \mu_s E_s e^{-\tau/\mu_s} \qquad \text{(I-15)}$$

- et en un éclairement par le rayonnement atmosphérique diffus $L_a^{\downarrow}(\theta', \phi')$:

$$E_{sol}^{diffus} = \int_0^{2\pi} \int_0^{\pi/2} L_a^{\downarrow}(\theta', \phi') \cos\theta' \, d\omega'. \qquad \text{(I-16)}$$

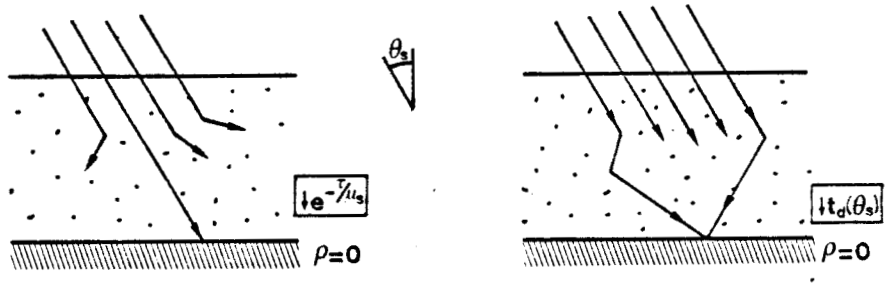

On a le facteur de transmission directe de l'atmosphère (abstraction faite de l'absorption gazeuse).

$$e^{-\tau/\mu_s} = \frac{E_{sol}^{direct}}{\mu_s E_s} \quad ; \qquad \text{(I-17)}$$

et on a défini (eq I-2) le facteur de transmission diffuse de l'atmosphère, $t_d(\theta_s)$, par

$$t_d(\theta_s) = \frac{E_{sol}^{diffus}}{\mu_s E_s} \quad . \tag{I-18}$$

Eclairons maintenant l'atmosphère par le sol, en y supposant une source diffuse, étendue à toute sa surface, et de luminance isotrope égale à $1/\pi$; soit un éclairement incident unité. Supposons toujours le sol noir, et calculons le transfert du rayonnement.

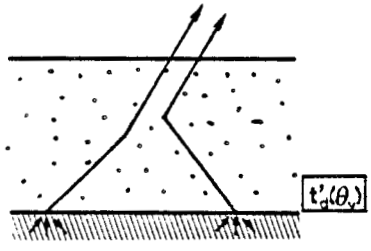

On observera maintenant depuis l'espace, en plus de la luminance directement transmise, $e^{-\tau/\mu_v}/\pi$, une luminance diffuse, correspondant à des photons initialement injectés en dehors du point de la surface que l'on vise, et qu'on notera

$$t'_d(\theta_v) \tag{I-19}$$

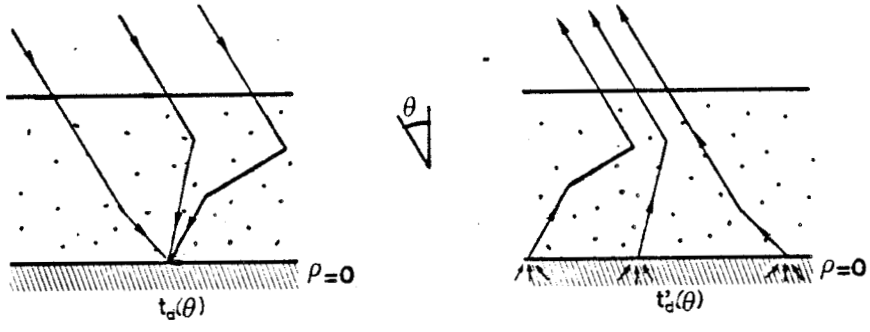

On peut montrer que les fonctions $t_d(\theta)$ et $t'_d(\theta)$ sont en fait iden-

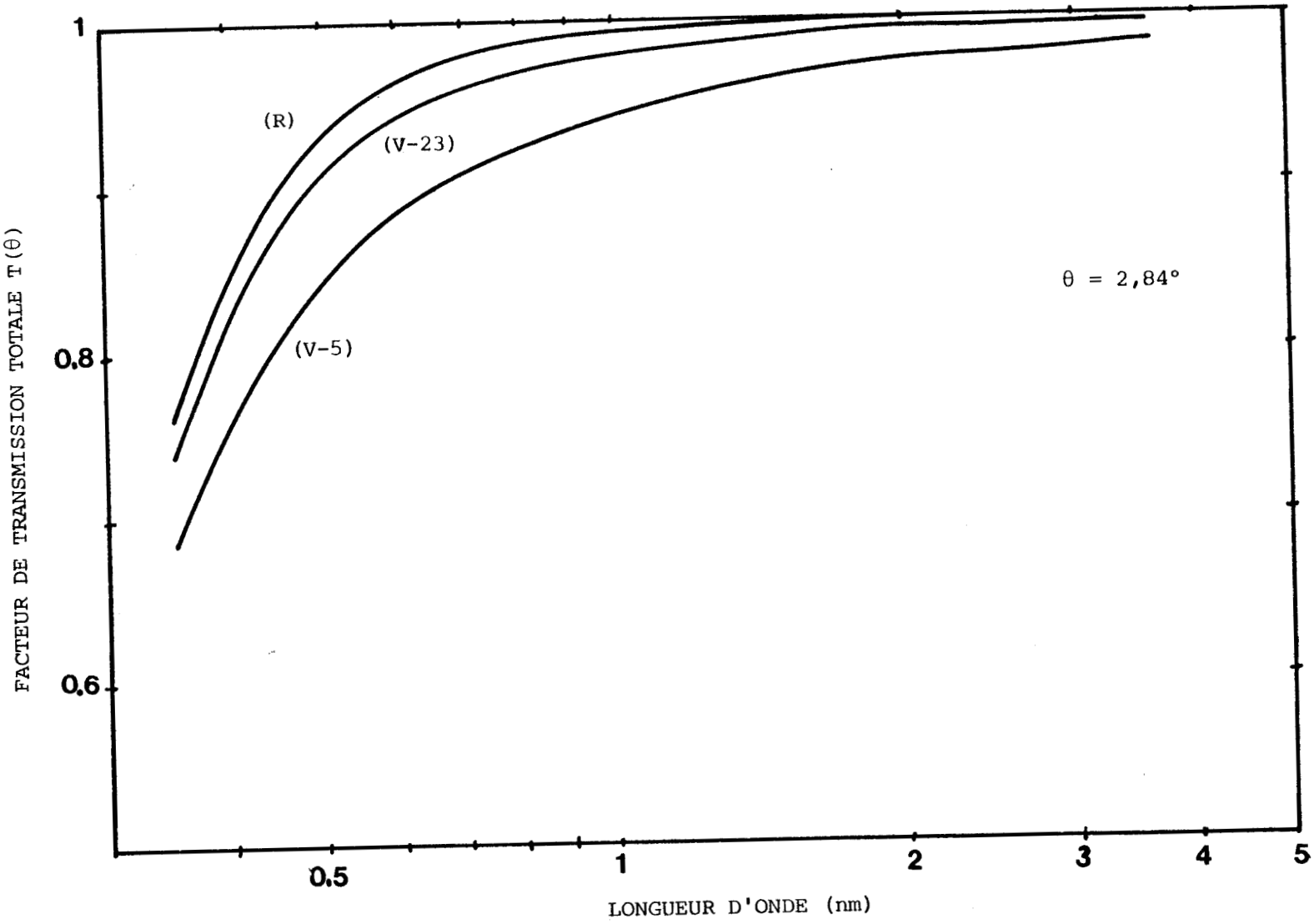

FIGURE I-5 : *Facteur de transmission totale, T(θ), pour une direction voisine de la verticale (θ= 2,84°), en fonction de la longueur d'onde d'observation et de la quantité totale d'aérosols (modèle (R), (V-23) et (V-5)).*

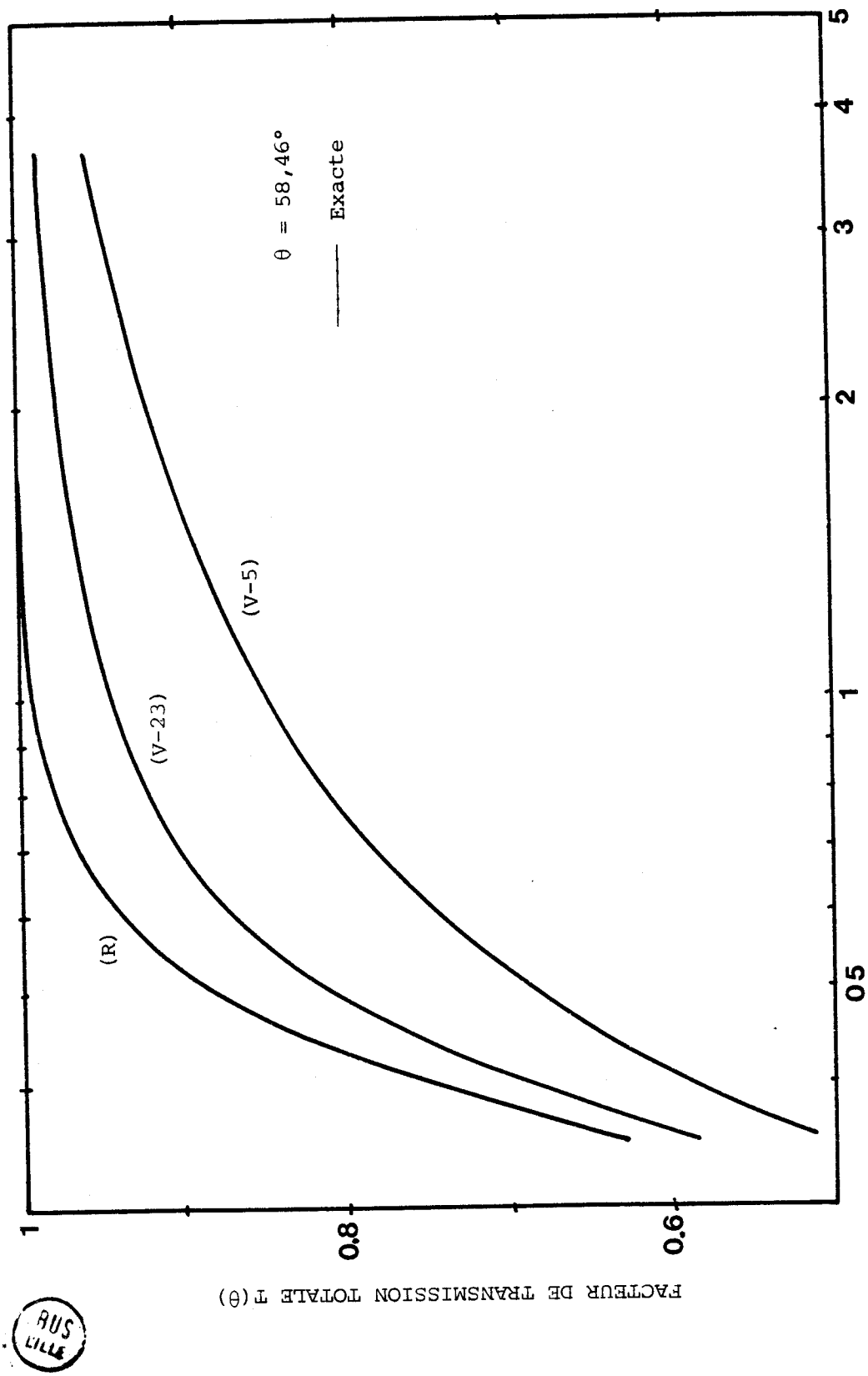

FIGURE I-6 : Même légende que Figure I-5, mais pour θ = 58,46°

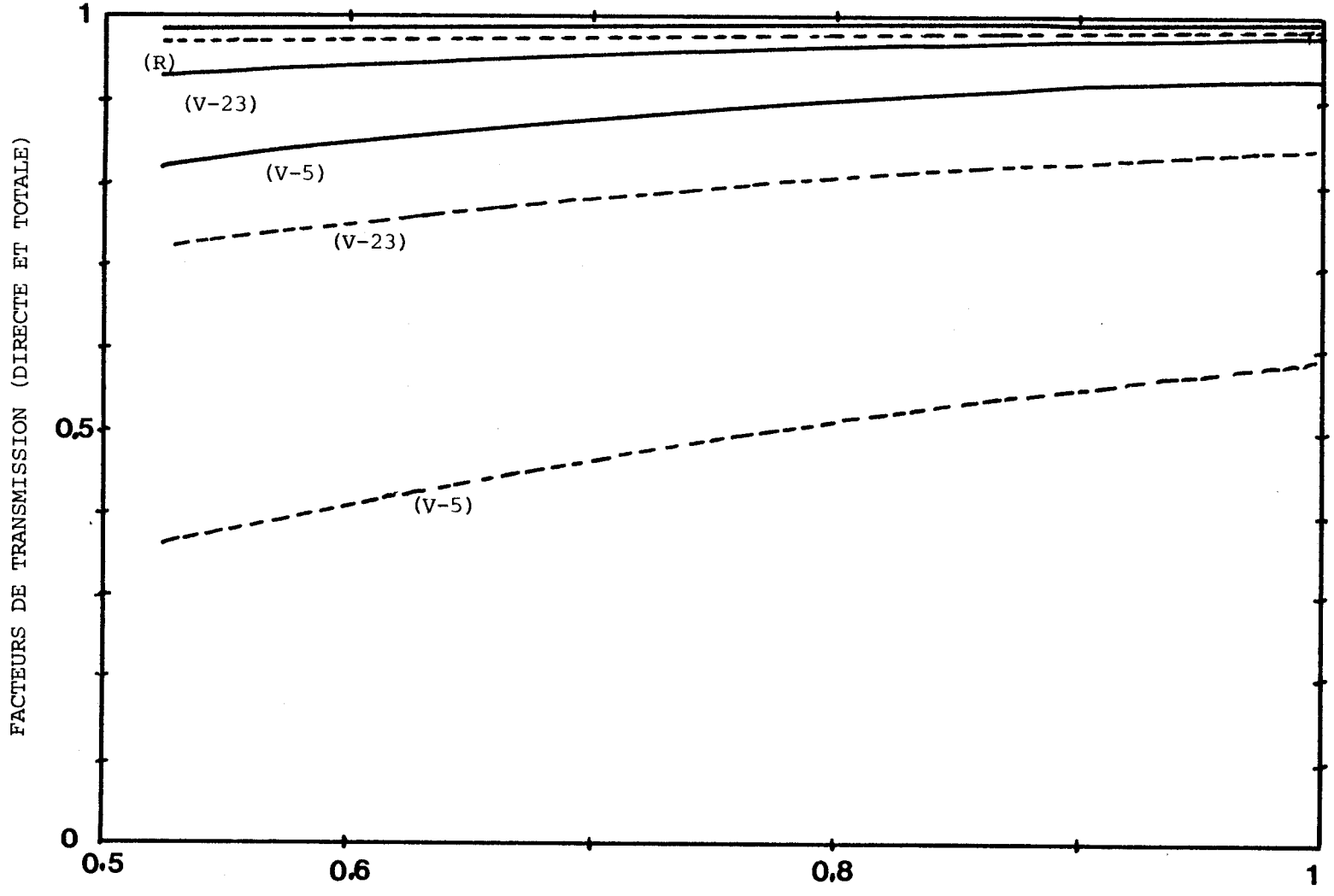

Figure I-7 : Importance de l'éclairement diffus de la cible par rapport à son seul éclairement direct, ou, importance de la contribution de l'environnement par rapport à la seule contribution directe de la cible :

En traits pleins : facteur de transmission totale, $T(\theta)$
En pointillés : facteur de transmission directe, $exp(-\tau/\mu)$
Résultats, en fonction de $\cos\theta$, pour les 3 modèles d'atmosphère.
λ = 850 nm.

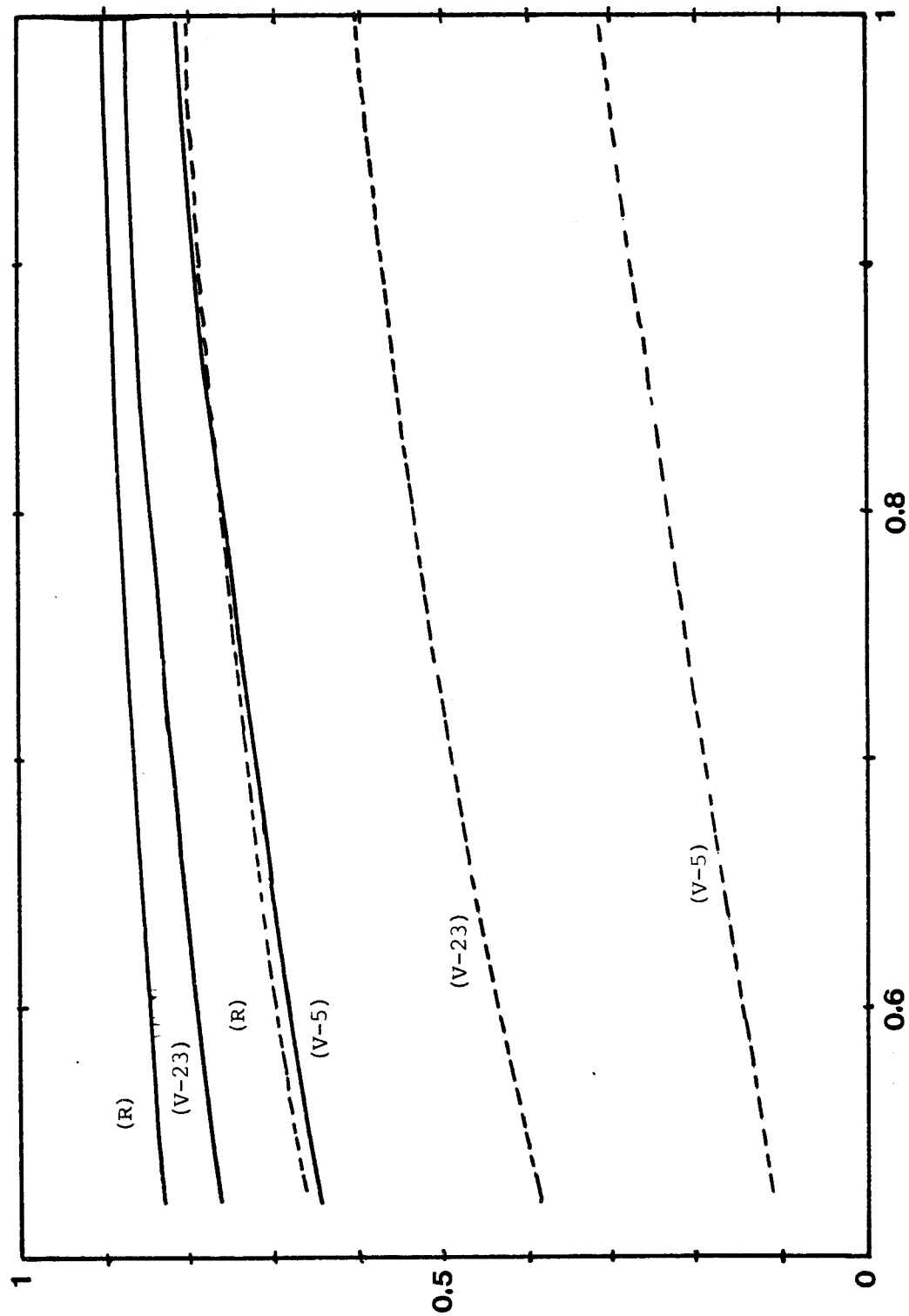

FIGURE I-8 : Même légence que Figure I-7, mais pour une longueur d'onde λ = 450 nm.

tiques (l'origine physique étant que ces fonctions correspondant à des photons qui dévrivent des trajectoires identiques, au sens de propagation près) de sorte qu'on n'utilisera par la suite qu'une seule fonction de transmission diffuse de l'atmosphère, $t_d(\theta)$; mais dont la signification sera différente suivant la variable considérée :

$t_d(\theta_s)$ sera le facteur de transmission diffus au niveau du sol (noir), pour un éclairement unité du sommet de l'atmosphère, par un faisceau directionnel dans la direction θ_s ;

$t_d(\theta_v)$ sera le facteur de transmission diffus en haut de l'atmosphère, pour un éclairement diffus étendu à la surface.

Les figures I-5 et I-6 illustrent la dépendance en longueur d'onde de la fonction de transmission totale $T(\theta)$ (Eq. I-15) pour deux directions θ = 2,84° et 58,46. On peut observer la prépondérance de la diffusion moléculaire aux longueurs d'onde les plus courtes.

Quant aux variations de $T(\theta)$ (Eq. I-13) en fonction de l'angle, les figures I-7 et I-8 (respectivement à λ = 850 et 450 nm) nous montrent que si on se limite à des directions d'observation ou d'incidence inférieures à 60°, la dépendance angulaire est faible. Nous avons reporté aussi les contributions respectives du facteur de transmission directe par rapport au facteur de transmission totale.

albedo sphérique

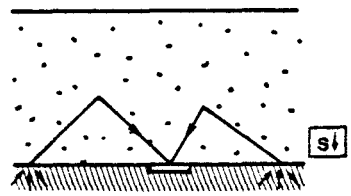

Enfin, l'éclairement de la surface correspondant à la luminance $\ell^{\downarrow}(\theta', \phi')$ que rétrodiffuse l'atmosphère vers le sol, s'identifie à l'albédo sphérique de l'atmosphère, s :

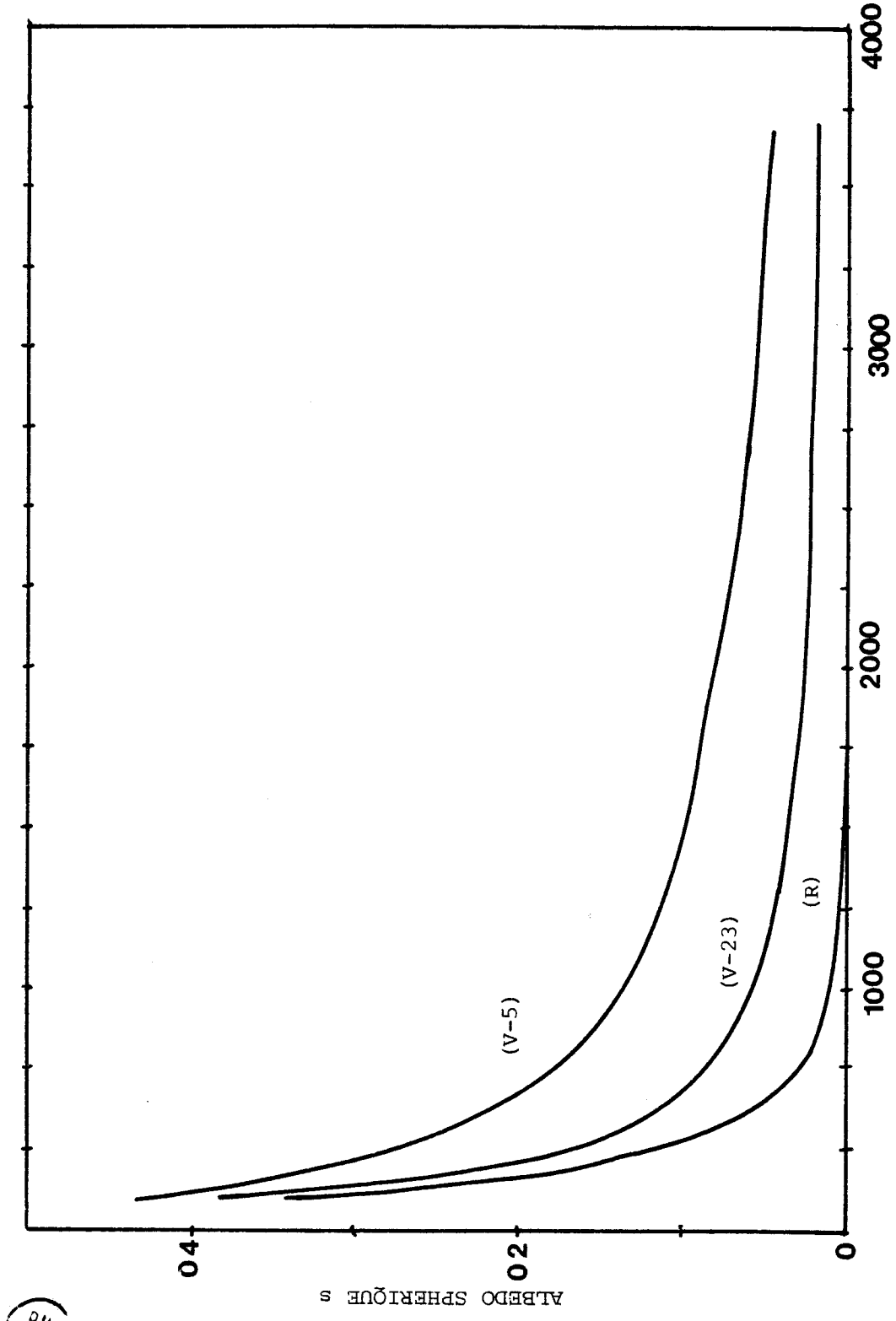

FIGURE I-9 : Albédo sphérique de l'atmosphère, s, en fonction de la longueur d'onde et de la quantité totale d'aérosols (modèles (R), (V-23) et (V-5)).

$$s = \int_0^{2\pi} \int_0^{\pi/2} \ell\psi(\theta', \phi') \cos\theta' \, d\omega'. \qquad \text{(I-20)}$$

La figure I-9 illustre sa dépendance en longueur d'onde, on remarquera que, même dans le bleu, pour une atmosphère moyenne et une réflectance de sol de l'ordre de 50 %, la contribution des interactions multiples ne représente que 10 à 15 % du signal ; de sorte que ces termes (en $1/(1-\rho s)$) seront le plus souvent négligés.

I-3 - CAS D'UN SOL NON HOMOGENE ET NON LAMBERTIEN

Généralisons maintenant la modélisation précédente au cas d'un sol non homogène et non lambertien. Ce travail est détaillé dans la publication n° 1 (TANRE et al, 1979) et nous nous contenterons d'en rappeler ici les principaux résultats.

Supposons d'abord notre cible, infiniment petite et de réflectance lambertienne ρ, placée dans un environnement uniforme et également lambertien, mais de réflectance ρ_e différente de ρ. Le signal atmosphérique s'écrit sous la forme :

$$\rho^*(\theta_s,\theta_v,\theta_v) = \rho_a(\theta_s, \theta_v, \phi_v) + \rho \frac{T(\theta_s)\, e^{-\tau/\mu_v}}{1 - \rho_e s} + \rho_e \frac{T(\theta_s)\, t_d(\theta_v)}{1 - \rho_e s} \qquad \text{(I-21)}$$

Si la réflectance de l'environnement n'est pas uniforme, la modélisation (I-21) restera formellement exacte, à condition d'y définir convenablement ρ_e. Il est clair qu'on devra, pour cela, définir le poids relatif dans le signal d'un point donné du voisinage, en fonction de sa distance à la cible.

Supposons connue la réflectance du sol, $\rho(r, \psi)$, en tout point M' de coordonnées polaires (r, ψ) autour du point visé M, pris comme origine. On définit la fonction de diffusion atmosphérique, $F(r)$ (on se restreindra par simplicité à une observation au nadir), telle que

$$\rho_e = \frac{1}{2\pi} \int_0^{2\pi} \int_0^{\infty} \rho(r, \psi) \frac{dF(r)}{dr} \, dr \, d\psi \quad . \qquad \text{(I-22)}$$

F(r) sera appelée la fonction d'environnement. Sa signification physique est la suivante : F(r) représente la probabilité pour qu'un photon, envoyé depuis l'espace vers le point M puis diffusé par l'atmosphère, atteigne la surface à l'intérieur d'un cercle de rayon r autour de M. Réciproquement, une fraction F(r) du rayonnement provenant de l'environnement de la cible correspond à des photons initialement rediffusés par la surface intérieure à un cercle de rayon r centré sur M. F(r) est une fonction croissante de r, avec $F(0) = 0$ et $F(\infty) = 1$ par normalisation.

Cette fonction F(r) dépend des propriétés optiques de l'atmosphère, fonction de phase et épaisseur optique, ainsi que de la répartition verticale des aérosols. Ces aspects seront étudiés plus loin mais en première approche (fig. I-10), on aura une portée typique de l'ordre de 1 km.

Supposons maintenant que l'on veuille mesurer les effets bidirectionnels que peut présenter la cible, et considérons un site sensiblement uniforme, de réflectance non lambertienne $\rho(\theta_s, \theta_v, \phi_v)$.

La seule composante du signal qui conserve à priori toute l'information cherchée sera le terme directement transmis en

$$e^{-\tau/\mu_s}\ \rho(\theta_s, \theta_v, \phi_v)\ e^{-\tau/\mu_v} \quad . \tag{I-23}$$

En première approximation, on affectera une même valeur moyenne, $\bar{\rho}$, proche de l'albédo du sol, à la réponse du sol sous l'éclairement solaire diffus $t_d(\theta_s)$ et à sa transmission diffuse $t_d(\theta_v)$ à travers l'atmosphère. En séparant dans (I-12) le seul terme utile (I-23), la réflectance apparente s'écrira alors

$$\rho^*(\theta_s, \theta_v, \phi_v) = \rho_a(\theta_s, \theta_v, \phi_v) + (\rho - \bar{\rho})e^{-\tau/\mu_s}\ e^{-\tau/\mu_v} + \bar{\rho}\ \frac{T(\theta_s)\ T(\theta_v)}{1 - \rho s} \tag{I-24}$$

Cette modélisation peut donner l'ordre de grandeur des contrastes directionnels espérés, et de leur sensibilité aux paramètres atmosphériques. Elle conduit toutefois à des estimations un peu pessimistes de ces contrastes, la forte diffusion des aérosols dans la direction avant

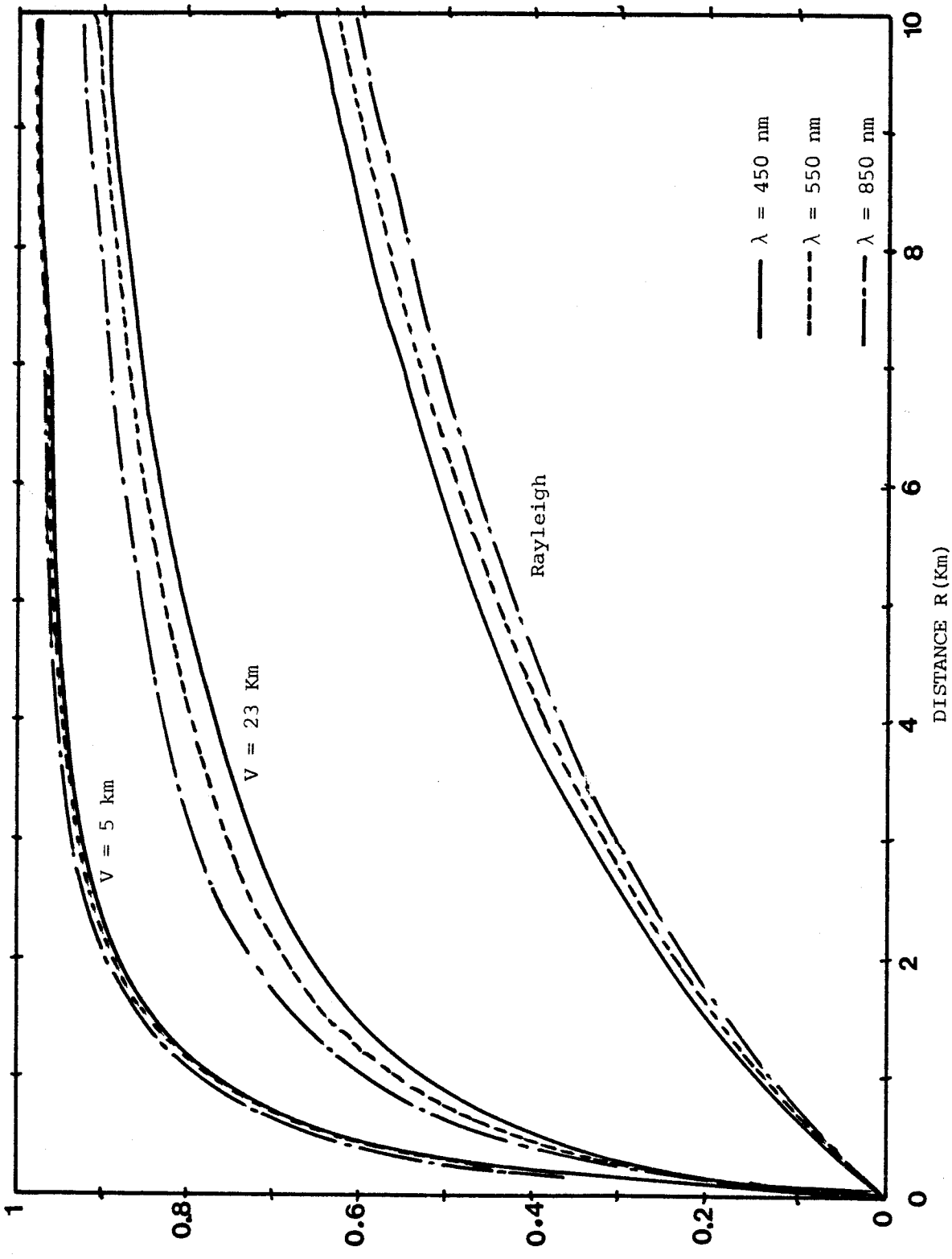

FIGURE I-10 : Contribution de l'environnement

conservant dans $t_d(\theta_s)$ et $t_d(\theta_v)$ une directionnalité sensible.

En négligeant le terme de série géométrique, la réflectance apparente dans le cas général d'un sol non homogène et non lambertien s'écrit donc

$$\rho^*(\theta_s, \theta_v, \phi_v) = \rho_a(\theta_s, \theta_v, \phi_v) + \rho(\theta_s, \theta_v, \phi_v)\ e^{-\tau/\mu_s}\ e^{-\tau/\mu_v}$$
$$+ \bar{\rho}(\theta_s, \theta_v, \phi_v)\ t_d(\theta_s)\ e^{-\tau/\mu_v} \qquad \text{(I-25)}$$
$$+ \rho_e(\theta_s, \theta_v, \phi_v)\quad T(\theta_s)\ t_d(\theta_v)$$

Cette modélisation n'est plus rigoureuse hors du cas d'un sol homogène et lambertien, puisque le couplage résiduel sol atmosphère fait que les deux réflectances moyennes $\bar{\rho}$ et ρ_e dépendent en fait légérement du type d'atmosphère. Nous reviendrons plus en détail sur ces problèmes de réflectances moyennes, mais la formulation (I-25) représente une excellente approximation du signal.

Nous avons vu (Annexe 1) les ordres de grandeur des différentes composantes de cette formulation, nous l'appliquerons dans la suite à deux cas différents,

(i) en observations marines, où mis à part des mesures effectuées près des côtes ou dans le voisinage de nuages, on pourra considérer que les sites sont homogènes sur des distances de l'ordre de la portée de F(r) et que les réflectances sont lambertiennes. On pourra écrire alors

$$\rho^*(\theta_s, \theta_v, \phi_v) = \rho_a(\theta_s, \theta_v, \phi_v) + \rho_w \frac{T(\theta_s)\ T(\theta_v)}{1 - \rho_w s} \qquad \text{(I-26)}$$

où ρ_w est de l'ordre du pourcent, le problème revient donc à estimer la réflectance atmosphérique ρ_a qui est d'un ordre de grandeur supérieure au signal utile ρ_w.

(ii) en observations terrestres, où la prise en compte de l'environnement s'avère indispensable. A un ordre de grandeur plus petit, le caractère directionnel de la réflectance des sites pourra également représenter une source d'erreur. Dans ce cas,

$$\rho^*(\theta_s, \theta_v, \phi_v) = \rho_a(\theta_s, \theta_v, \phi_v) + \rho \frac{T(\theta_s)\ e^{-\tau/\mu_v}}{1 - \rho_e s} + \rho_e \frac{T(\theta_s)\ t_d(\theta_v)}{1 - \rho_e s} \qquad \text{(I-27)}$$

Les réflectances des sols ρ, en infra-rouge proche par exemple, étant élevées, le morcellement fréquent, la principale source d'erreur proviendra de la contamination du voisinage de réflectance ρ_e.

ANNEXE 1

Reprinted from APPLIED OPTICS, Vol. 18, page 3587, November 1, 1979

Atmospheric modeling for space measurements of ground reflectances, including bidirectional properties

D. Tanre, M. Herman, P. Y. Deschamps, and A. de Leffe

A fairly accurate analytical expression of the measured reflectance is established for the general case of a non-Lambertian and nonuniform ground by separating the atmospheric and surface effects. The signal is nearly linear in the function of intrinsic atmospheric reflectance, the actual target reflectance, and two average ground reflectances, angular and spatial, to be defined. Contrast reduction by the atmosphere, defined in the cases of Lambertian and directional ground reflectances, has been evaluated using this formulation.

I. Introduction

The three main mechanisms by which terrestrial atmosphere perturbs the measurements of ground reflectances from space are (1) aerosol and molecular backscatterings change the measured target reflectances, (2) for nonuniform sites the measurement is altered by the contribution of the target background, and (3) the bidirectional properties of the target reflectance are partially smoothed over by the atmospheric scattering processes.

The study of these different atmospheric effects has been considerably developed. Atmospheric models assuming the ground to be uniform and Lambertian have been studied extensively.[1–5] These computations give the intrinsic atmospheric radiation for quite varied conditions and also permit the evaluation of contrast degradation for sites of large dimensions or for small targets in a uniform background.[1,2,7] Several attempts have been made to account for the diffuse radiation field corresponding to a nonuniform ground albedo with the aid of the adding procedure, the Fourier transformation method, or the invariant imbedding technique.[6,7] Finally, the influence of the bidirectional character of the reflectance has also been studied.[8,9]

These studies improve our knowledge of various atmospheric and surface effects, but their influences are most frequently considered separately. These effects generally occur simultaneously, and it is of interest to specify their relative importance in the function of experimental conditions (sun elevation, aerosol content, wavelength, type of target reflectance) and to evaluate measurement sensitivity to the variations of these conditions within the framework of multitemporal, multiangular, or multispectral observations. Consider a mean atmosphere above a ground for which the reflectance $\rho_\lambda(M,\mathbf{S}_0,\mathbf{S})$ depends upon the point M and upon the incidence and observation directions $\mathbf{S}_0$ and $\mathbf{S}$. The apparent reflectance $\rho_\lambda^*(M,\mathbf{S}_0,\mathbf{S})$ of M, observed from a satellite in direction $\mathbf{S}$ when the sun is in direction $\mathbf{S}_0$, will depend not only upon the actual target reflectance $\rho_\lambda(M,\mathbf{S}_0,\mathbf{S})$ and the atmospheric reflectance $\rho_{a\lambda}(\mathbf{S}_0,\mathbf{S})$ but also upon spatial and angular mean reflectances to be defined (see, e.g., Refs. 10 and 11). An exact numerical simulation of the actual problem is obviously out of the question, but the study of a simple case of a uniform and Lambertian ground proves sufficient to give fairly precise answers to the following questions:

Which are the mean reflectances to be defined and how are they related to experimental conditions?

To what extent is the measurement a linear function of these mean reflectances?

What are the relative contributions of these quantities to the apparent reflectance $\rho^*(M,\mathbf{S},\mathbf{S}_0)$; and how do these contributions vary in function of observation conditions.

A. de Leffe is with Centre National d'Etudes Spatiales, Division Observation de la terre, 31055 Toulouse, France; the other authors are with Universite des Sciences et Techniques de Lille, Laboratoire d'Optique Atmospherique, 59650 Villeneuve d'Ascq, France.

Received 1 March 1979.
0003-6935/79/213587-08$00.50/0.

II. Signal Analysis in the Case of a Homogeneous Lambertian Surface

Let it be given that the ground is of uniform Lambertian reflectance. The atmosphere and particularly the atmospheric aerosol concentration are assumed to be horizontally uniform. This study deals with monochromatic quantities, but subscript λ will be omitted to simplify notation. Last, rather than being expressed as radiance I, the various quantities will be expressed exclusively in terms of equivalent reflectance defined as

$$\rho^* = \frac{\pi I}{\mu_0 f}, \tag{1}$$

where f is the solar flux at the top of the atmosphere, and $\Theta_0 = \arccos\mu_0$ is the zenithal solar angle.

It is practical to express the signal received by the satellite in the function of successive orders of radiation interactions in the coupled ground–atmosphere system.[10,11] If ρ is the ground reflectance, the apparent reflectance is written

$$\begin{aligned}\rho^*(M,S_0,S) = {} & \rho_a(\mu_0,\mu,\phi) + \exp(-\tau/\mu_0)\rho\exp(-\tau/\mu) \\ & + E(\mu_0)\rho\exp(-\tau/\mu) \\ & + [\exp(-\tau/\mu_0) + E(\mu_0)]\rho E'(\mu) \\ & + \left\{\sum_{n=1}^{\infty}[\exp(-\tau/\mu_0) + E(\mu_0)](\rho r)^n\right\} \\ & \times \rho[\exp(-\tau/\mu) + E'(\mu)],\end{aligned} \tag{2}$$

where
- τ is the optical thickness of the atmosphere,
- $\Theta = \arccos\mu$ is the zenithal viewing angle,
- ϕ is the azimuthal angle,
- $\rho_a(\mu_0,\mu,\phi)$ is the intrinsic atmospheric contribution in terms of reflectance [Fig. 1(a)],
- $\rho\exp(-\tau/\mu_0)\times\exp(-\tau/\mu)$ is the term that contains the information resulting from direct solar radiation reflected by the target [Fig. 1(b)],
- $\rho E(\mu_0)\times\exp(-\tau/\mu)$ is the contribution resulting from diffuse downward solar radiation attaining the ground at point M [Fig. 1(c)], and
- $\rho[\exp(-\tau/\mu_0) + E(\mu_0)]E'(\mu)$ represents the first-order contribution of the target background [Fig. 1(d)].

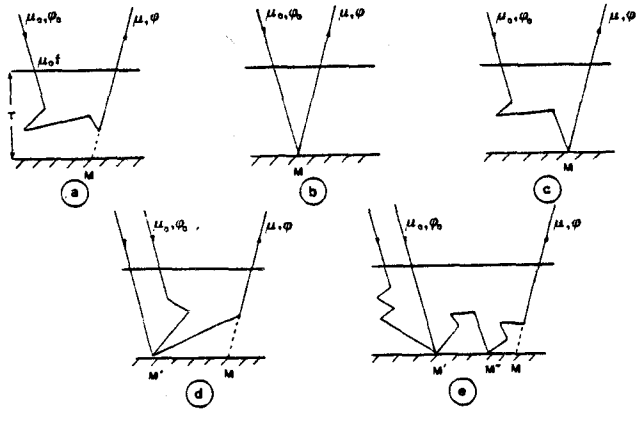

Fig. 1. Successive orders of radiation interactions in the ground–atmosphere system.

The geometrical series in Eq. (2) corresponds to higher orders of interaction with the ground, the term $[\exp(-\tau/\mu_0) + E(\mu_0)](\rho r)^n$ corresponds to radiation having interacted n times with the ground [Fig. 1(e)]. Equation (2) is also written as

$$\begin{aligned}\rho^*(M,S_0,S) = {} & \rho_a(\mu_0,\mu,\phi) + \frac{\rho}{1-\rho r}[\exp(-\tau/\mu_0) \\ & + E(\mu_0)][\exp(-\tau/\mu) + E'(\mu)].\end{aligned} \tag{3}$$

For a homogeneous atmosphere, functions $E(\mu_0)$ and $E'(\mu)$ are identical in accordance with the reciprocity principle

$$E(\mu) = E'(\mu). \tag{4}$$

Due to the presence of aerosols, the real atmosphere is inhomogeneous, but Eq. (4) is numerically well verified and will be accepted for the remainder of this paper. Equation (3) is written as

$$\begin{aligned}\rho^*(M,S_0,S) = {} & \rho_a(\mu_0,\mu,\phi) + \frac{\rho}{1-\rho r}[\exp(-\tau/\mu_0) \\ & + E(\mu_0)][\exp(-\tau/\mu) + E(\mu)].\end{aligned} \tag{5}$$

In accordance with the above definitions, the normalized quantities $E(\mu_0)$ and r are given by

$$E(\mu_0) = \frac{1}{\mu_0 f}\int_0^{2\pi}\int_0^{-1} I_d^-(\tau,\mu_0,\mu,\phi)\mu d\mu d\phi, \tag{6}$$

where $I_d^-(\tau,\mu_0,\mu,\phi)$ is the downward diffuse radiance at the bottom of the atmosphere for $\rho = 0$, and

$$r = \frac{1}{\pi}\int_0^{2\pi}\int_0^{-1} I^-(\tau,\mu)\mu d\mu d\phi, \tag{7}$$

where $I^-(\tau,\mu)$ is the downward radiance at the ground level for the case of an incident upward isotropic radiation at the bottom of the atmosphere [$I^+(\tau,\mu) = 1$].

III. Signal Analysis in the Case of a Non-Homogeneous Non-Lambertian Ground Surface

Let it now be assumed that the ground reflectance depends upon the target M and the observation and incidence directions and thus is written $\rho(M,\mu_0,\mu,\phi)$. In this case, Eq. (2) is no longer exact but remains interesting. Each of the terms (1) implicitly defines the different spatial and angular averages that must be made for $\rho(M,\mu_0,\mu,\phi)$, (2) gives the weight of these averages in the total signal, and (3) allows one to estimate the linearity of the measured signal. Equation (2) is now written as

$$\rho^*(M,\mu_0,\mu,\phi) = \rho_a(\mu_0,\mu,\phi) + \rho(M,\mu_0,\mu,\phi)\exp(-\tau/\mu_0)\exp(-\tau/\mu) + \bar{\rho}(M,\mu_0,\mu,\phi)\exp(-\tau/\mu)E(\mu_0) + \langle\rho(M,\mu_0,\mu,\phi)\rangle[E(\mu_0) + \exp(-\tau/\mu_0)]E(\mu) + \langle\rho(M,\mu_0,\mu,\phi)\rangle r\left[\frac{\bar{\rho}(M,\mu_0,\mu,\phi)\exp(-\tau/\mu) + \langle\rho(M,\mu_0,\mu,\phi)\rangle E(\mu)}{1 - \langle\rho(M,\mu_0,\mu,\phi)\rangle r}\right][E(\mu_0) + \exp(-\tau/\mu_0)]. \quad (8)$$

The first three terms of this development are precisely defined:

$\rho_a(\mu_0,\mu,\phi)$ is still the intrinsic atmospheric reflectance ($\rho = 0$).

$\rho(M,\mu_0,\mu,\phi)\exp(-\tau/\mu_0)\exp(-\tau/\mu)$ gives direct information about the target.

$\bar{\rho}(M,\mu_0,\mu,\phi)E(\mu_0)\exp(-\tau/\mu)$ rigorously allows us to define an average angular reflectance of the target M as

$$\bar{\rho}(M,\mu_0,\mu,\phi) = \frac{1}{\mu_0 E(\mu_0)}\int_0^{2\pi}\int_0^{-1}\rho(M,\mu',\mu,\phi'-\phi)\,I_d^{\downarrow}(\tau,\mu_0,\mu',\phi')\mu' d\mu' d\phi'. \quad (9)$$

$\langle\rho(M,\mu_0,\mu,\phi)\rangle\,E(\mu)[\exp(-\tau/\mu_0) + E(\mu_0)]$ defines the average reflectance of the environment $\langle\rho(M,\mu_0,\mu,\phi)\rangle$ in the same way, but this definition is not so easily formulated. If $t(\mu,x,y)$ is the contribution to $E(\mu)$ per unit area of ground at a point M' with horizontal coordinates $(x,y,)$, a reasonable definition of $\langle\rho\rangle$ seems to be

$$\langle\rho(M,\mu_0,\mu,\phi)\rangle = \frac{1}{E(\mu)}\int_{-\infty}^{+\infty}\int_{-\infty}^{+\infty}\bar{\rho}(M')t(\mu,x,y)dxdy, \quad (10)$$

where $\bar{\rho}(M')$ is the average angular reflectance of M', which could be specified only by the analysis of $t(\mu,x,y)$. Such an accurate definition of $\bar{\rho}(M')$ is superfluous for what follows, and it is sufficient to state that $\bar{\rho}(M')$ could be given as either $\bar{\rho}(M',\mu_0,\mu,\phi)$ or $\rho(M',\mu_0,\mu,\phi)$.

The use of the preceding averages [$\bar{\rho}(M,\mu_0,\mu,\phi)$ and $\langle\rho(M,\mu_0,\mu,\phi)\rangle$] in the last term of Eq. (8) is approximate but acceptable. Since the corresponding term is quite small, this approximation proves sufficient. Equation (8) may also be more simply written with a good degree of approximation assuming $(\rho - \bar{\rho})\,\langle\rho\rangle\,r \simeq 0$:

$$\rho^* \simeq \rho_a + \frac{1}{1 - \langle\rho\rangle r}(A\rho + B\bar{\rho} + C\,\langle\rho\rangle), \quad (11)$$

with $A = \exp(-\tau/\mu)\exp(-\tau/\mu_0)$,

$B = \exp(-\tau/\mu)E(\mu_0)$,

$C = E(\mu)\,[\exp(-\tau/\mu_0) + E(\mu_0)]$, and

where A, B, and C allow us to obtain the relative contributions of the defined reflectances ρ, $\bar{\rho}$, and $\langle\rho\rangle$.

In Eq. (8), the signal is developed in such a way as to separate atmospheric properties from ground properties. This task is not exactly accomplished because $\bar{\rho}(M,\mu_0,\mu,\phi)$ and $\langle\rho(M,\mu_0,\mu,\phi)\rangle$ are still dependent upon atmospheric properties by way of Eqs. (9) and (10). But the study of the development coefficients of Eq. (8) will give some information about the relative weights of the various atmospheric effects. It will be seen in Sec. V that the remaining influence of the atmospheric properties upon $\bar{\rho}$ and $\langle\rho\rangle$ is much smaller than upon their respective weights.

IV. Atmospheric Functions

In order to define the dependence of atmospheric functions $\rho_a(\mu_0,\mu,\phi)$, $E(\mu)$, and r, it is necessary to calculate intrinsic atmospheric radiances for different experimental conditions and different atmospheric models. The considered atmospheric models consist of a Rayleigh atmosphere to which is added a variable aerosol concentration. Optical thickness and phase function for Rayleigh scattering have been adopted from the estimations of Hoyt.[12] The aerosol scattering properties correspond to the aerosol model used by McClatchey *et al.*[13] The particle scattering cross section and the phase function were computed from the size distribution using Mie theory. For this, the refractive index of the particles was assumed to be real (that is, no absorption) and equal to 1.50. Table I gives the corresponding optical thicknesses for visibilities of 5 km, 10 km, 23 km, and 30 km. The vertical profiles of aerosol concentration are the ones given by McClatchey *et al.* for visibilities of 5 km and 23 km. In fact the aerosol vertical profile only slightly affects the radiation field, and the main parameter remains the optical thickness. The radiances were computed by the successive orders of scattering method.[14] The computations were made for four wavelengths (λ = 450 nm, 550 nm, 650 nm, and 850 nm) and four zenithal solar angles (θ_0 = 15°, 41.4°, 60°, and 75.5°). By using these computations, $E(\mu_0)$ and r can be obtained directly from Eqs. (6) and (7).

Table I. Optical Thicknesses for Four Wavelengths and Four Visibilities

Wavelength (nm)	Visibility (km)			
	5	10	23	30
450	0.9306	0.6719	0.2801	0.1771
550	0.7801	0.5570	0.2348	0.1468
650	0.6681	0.4756	0.2011	0.1254
850	0.5151	0.3680	0.1550	0.0970

Table II. Function r for Four Wavelengths and for Three Atmosphere Models

Wavelength (nm)	Molecular atmosphere	Turbid atmosphere (V = 23 km)	Turbid atmosphere (V = 5 km)
450	0.1605	0.2128	0.3080
550	0.0807	0.1403	0.2432
650	0.0438	0.1038	0.2056
850	0.0157	0.0698	0.1606

Table III. Function $E(\mu)$ for Several Zenithal Angles ($\mu = \cos\Theta$)

Solar zenith angle Θ (deg)	Wavelength (nm)	Molecular atmosphere	Turbid atmosphere (V = 23 km)	Turbid atmosphere (V = 5 km)
15	450	0.0992	0.2647	0.4822
	550	0.0466	0.2076	0.4414
	650	0.0243	0.1715	0.4004
	850	0.0083	0.1284	0.3339
41.4	450	0.1235	0.3065	0.5107
	550	0.0592	0.2452	0.4805
	650	0.0310	0.2044	0.4438
	850	0.0107	0.1547	0.3793
60	450	0.1723	0.3707	0.5206
	550	0.0860	0.3085	0.5162
	650	0.0458	0.2622	0.4941
	850	0.0160	0.2025	0.4425
75.5	450	0.2793	0.4457	0.4616
	550	0.1564	0.4103	0.4966
	650	0.0872	0.3677	0.5071
	850	0.0315	0.3000	0.4995

Table IV. Atmospheric Contribution $\rho_a(\mu,\Phi,\mu_0,\Phi_0)$ for Vertical Observation (μ = 1)

λ_{nm}	$\Theta°$	Atmosphere models: Rayleigh	V = 23 km	V = 5 km
450	15	0.0838	0.1050	0.1603
550	15	0.0367	0.0567	0.1071
650	15	0.0184	0.0366	0.0815
850	15	0.0061	0.0208	0.0559
450	60	0.0988	0.1281	0.2027
550	60	0.0448	0.0708	0.1420
650	60	0.0228	0.0454	0.1096
850	60	0.0077	0.0250	0.0747

The values obtained for r and $E(\mu)$ are recorded, respectively, in Tables II and III. The following formulas, based on the Eddington method, have been proven to give a good approximation of r and $E(\mu)$ and can be extended to other aerosol models:

$$r \simeq (0.92\tau_r + \alpha\tau_p)\exp[-(\tau_r + \tau_p)], \quad (12a)$$

$$E(\mu) \simeq \exp(-\tau/\mu)\{\exp[(0.52\tau_r + \beta\tau_p)/\mu] - 1\}, \quad (12b)$$

with $\alpha = 1 - \langle\cos\Theta\rangle$ and $\beta = \frac{1}{2}(1 + \langle\cos\Theta\rangle)$, where $\langle\cos\Theta\rangle$ is the anisotropy factor of the aerosol scattering phase function. This factor remains quite constant (about $\frac{2}{3}$) for most of the aerosol models,[14] and variations of r and $E(\mu)$ as a function of wavelength are mainly due to variations of τ_p.

Table IV gives some values of $\rho_a(\mu_0,\mu,\varphi)$. ρ_a increases with decreasing wavelengths and visibilities, and values higher than 0.1 may be found at shorter wavelengths. A parameterization of ρ_a is not convenient because of the variable angular effects. Also, the intrinsic contribution ρ_a only modifies the absolute level of the measured reflectances and does not change the relative contributions of the other terms.

Figure 2 represents the relative contributions A, B, and C of reflectances ρ, $\bar{\rho}$, and $\langle\rho\rangle$ vs the zenithal solar angle Θ_0 when viewing at the nadir for three wavelengths (450 nm, 550 nm, and 850 nm) and three optical thicknesses corresponding to visibilities of 10 km, 23 km, and 30 km. The results are interpolated from Table III. It is clear that, except for exceptional visibilities and near IR wavelengths, the contributions of the three terms are of the same order.

In a first approximation, the results in Fig. 2 are representative of the atmospheric effects due to a given optical thickness τ_p and are independent of the particle model used for the computations. Apart from knowing $\rho_a(\mu_0,\mu,\phi)$, the atmospheric parameter to be determined in order to define Eq. (11) is thus the aerosol optical thickness τ_p at the wavelengths used.

V. Average Reflectances

The sensitivity of averages $\bar{\rho}$ and $\langle\rho\rangle$ to the atmospheric properties is more difficult to evaluate, since it depends upon the exact nature of the target or site involved.

The bidirectional effect was studied with the aid of the experimental results of Kriebel[15] corresponding to the reflectance of the savannah at λ = 520 nm. By introducing these experimental values of $\rho(\mu_0,\mu,\phi)$ and the radiances $I_d(\tau,\mu_0,\mu,\phi)$ obtained in the theoretical computations into Eq. (9), $\bar{\rho}$ was computed for different solar incidence angles, for different viewing angles, and for three atmospheric models: Rayleigh, V = 23 km, and V = 5 km at λ = 450 nm and 850 nm. The values thus obtained for $\bar{\rho}$ are found in Figs. 3(a) and 3(b) as a function of the actual values of reflectance ρ.

It is clear that the variations of $\bar{\rho}$ between visibilities of 5 km and 23 km are rather small and that the knowledge of coefficient B [Eq. (11)] is sufficient for definition of the contribution of the bidirectional effects. However, the strongly directional atmospheric radiation corresponding to aerosol scattering reduces the degradation of the signal obtained for the pure molecular scattering.

From Fig. 3 it may be seen that $\bar{\rho}$ preserves partly the bidirectional effect of ρ and could be approximately written as

$$\bar{\rho} = \bar{\rho}_0 + a\rho, \quad (13)$$

with a = 0.1 for the Rayleigh scattering and a between 0.3 and 0.5 for V = 5 km and V = 23 km; a would generally depend upon the degrees of anisotropy of both the atmospheric scattering and the ground reflectance; a would tend to 0 for an isotropic scattering or a specular reflection; and a would be close to 1 for a strong forwardscattering and a near Lambertian reflectance.

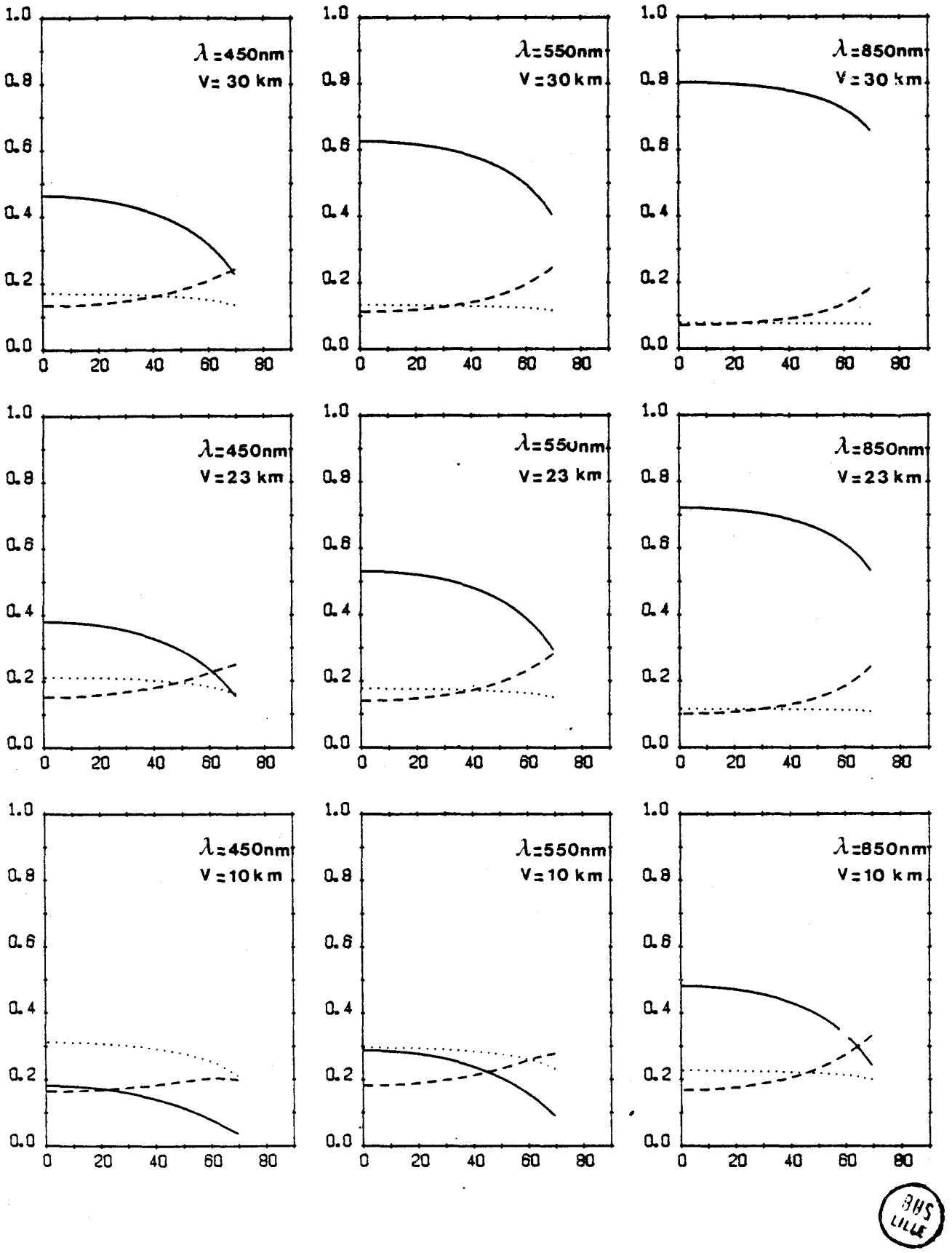

Fig. 2. Relative contributions A, B, and C of reflectances ρ, $\bar{\rho}$, and $\langle\rho\rangle$ vs the zenithal solar angle, for a vertical observation (A is represented by a solid line, B is represented by a dashed line, and C is represented by a dotted line).

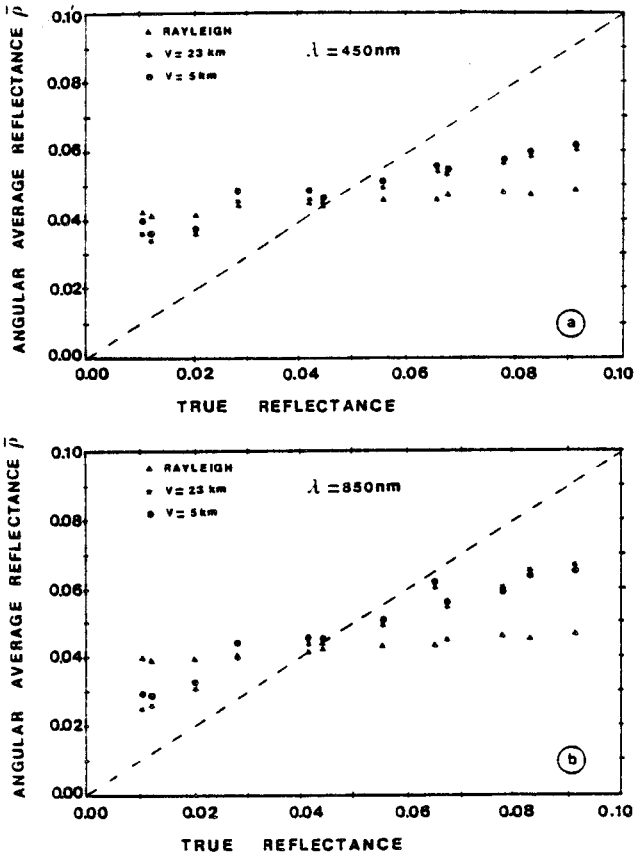

Fig. 3. Angular average reflectance $\bar{\rho}$ for the incident diffuse radiation vs true reflectance for three atmosphere models at $\lambda = 450$ nm [Fig. 4(a)] and 850 nm [Fig. 4(b)]. Each point corresponds to different geometric conditions (solar incidence and observation angle).

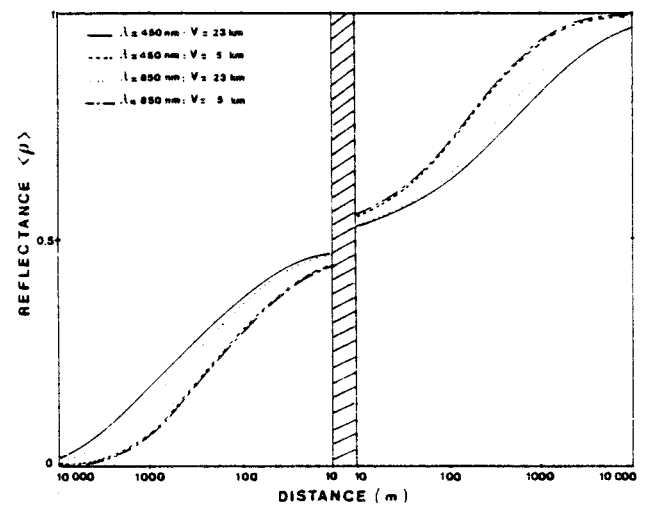

Fig. 4. Average reflectance of environment vs the distance between the target M and the separation of the two half planes ($\rho_0 = 0$ and $\rho_1 = 1$) for two of McClatchey's models ($V = 23$ km and $V = 5$ km) at $\lambda = 450$ nm and $\lambda = 850$ nm.

Spatial average reflectance $\langle\rho\rangle$ was evaluated by considering the case of a ground composed of two infinite half planes with uniform Lambertian reflectances ρ_1 and ρ_2. The computation of $\langle\rho\rangle$ was made by using the approximation of primary scattering for the evaluation of $t(\mu,x,y)$ in Eq. (10). Figure 4 gives the values of $\langle\rho\rangle$ thus obtained for the three above defined atmosphere models and at wavelengths 450 nm and 850 nm. The residual interaction cannot be entirely neglected, particularly in the critical zone of 500 m, but, if one notes that the weighting of $\langle\rho\rangle$ is from 40% to 20% between visibilities of 5 km and 23 km, the linearity of Eq. (11) remains quite accurate in the first approximation.

VI. Application: Definition of Spatial or Directional Contrast

In what follows, we attempt to generalize the notion of contrast reduction in the case of bidirectional reflectance properties. Contrast reduction is defined as the variation of the available signal after atmospheric degradation, as compared with the original signal. If ρ_1 and ρ_2 are the exact reflectances in two different measurement conditions, and ρ_1^* and ρ_2^* are the measured apparent reflectances [Eq. (1)], the contrast reduction R is expressed as

$$R = \frac{\rho_1^* - \rho_2^*}{\rho_1 - \rho_2}, \tag{14}$$

which allows expression of the information loss when viewing through the atmosphere. Spatial contrast is obtained by giving reflectance values ρ_1 and ρ_2 for two neighboring targets for which the atmosphere can be considered identical. This notion will be extended to include the case of a target having bidirectional reflection properties. In this case, ρ_1 and ρ_2 correspond to different incidence or viewing angles for the same target. For the sake of practicability, it will be considered that the bidirectional measurements are made under fixed illumination conditions with an observation angle $\pm\Theta$ in the incidence plane.

The effects due to the term ρ_a [Eq. (2)] will be neglected, which is rigorously exact for the spatial contrast; in the case of bidirectional measurements, however, ρ_a is dependent upon geometrical conditions and perturbs the measurement, but this effect will not be evaluated here. The effects due to the multiple interactions between the ground and the atmosphere will also be neglected. In order to evaluate contrast reduction, we consider the following cases:

(1) Spatial contrast between Lambertian sites of large dimensions ($\langle\rho\rangle = \bar{\rho} = \rho$). From Eqs. (11) and (14) we obtained

$$R = A + B + C,$$

$$R = [\exp(-\tau/\mu_0) + E(\mu_0)][\exp(-\tau/\mu) + E(\mu)]. \tag{15}$$

This case typically corresponds to the remote sensing

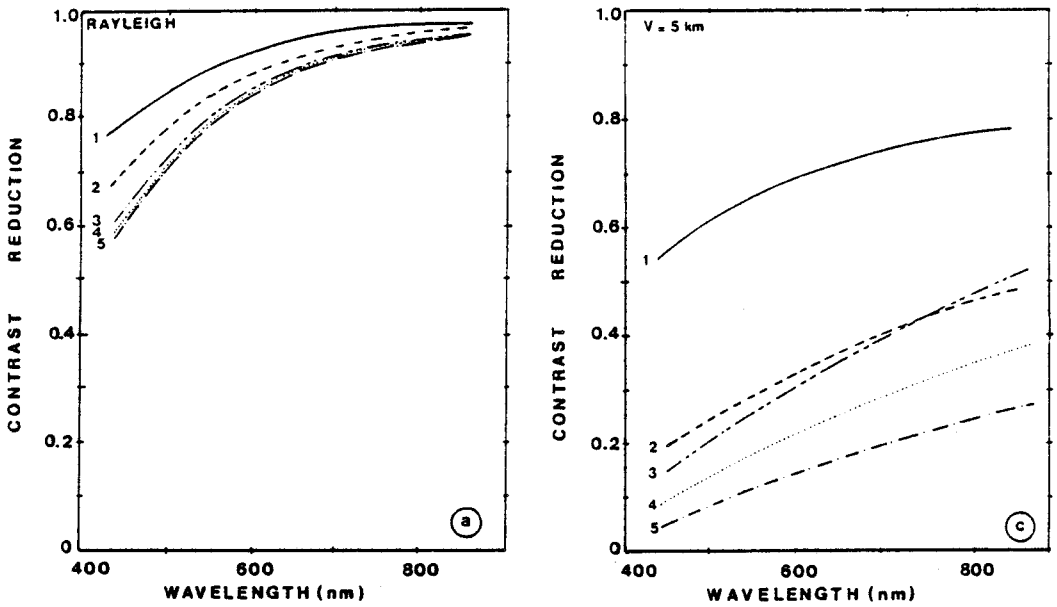

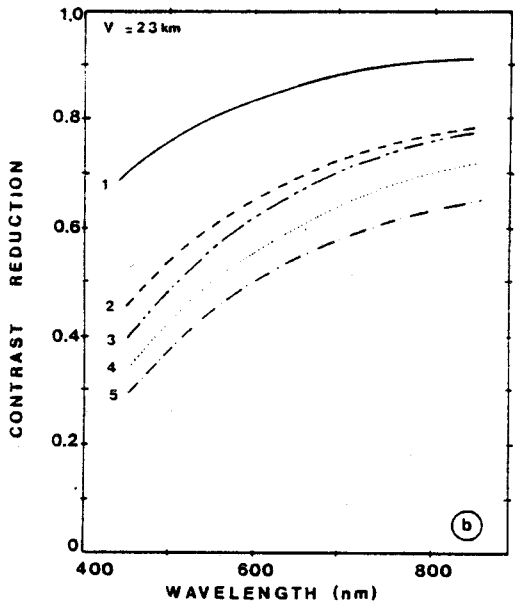

Fig. 5. Contrast reduction vs wavelength for three atmosphere models: (1) large Lambertian targets; (2) small Lambertian targets; (3) and (4) are the same as (1) and (2) but for the directional reflectance of the savannah, and (5) specular reflectance.

of the ocean and other large uniform areas such as a desert or forest. The results in Fig. 4 show that the uniform area must have a minimum dimension of several kilometers.

(2) Spatial contrast between Lambertian targets of small dimensions ($\bar{\rho} = \rho$; $\langle \rho \rangle$ = constant):

$$\left.\begin{aligned} R &= A + B, \\ R &= [\exp(-\tau/\mu_0) + E(\mu_0)] \exp(-\tau/\mu). \end{aligned}\right\} \quad (16)$$

This case corresponds to the definition of the contrast reduction in remote sensing commonly found when the broken ground is of small dimensions (on the order of 100 m, see Fig. 4).

(3) Directional contrast for sites of large dimensions. It is obvious that only the direct flux of the solar radiation is useful in the measurement of the bidirectional reflectance properties. However, it is seen in Figs. 3(a) and 3(b) that a small fraction a of the diffuse flux preserves the directional properties of the target. If the site is homogeneous over large dimensions, these properties are also partly preserved for the contribution of directions other than the direction of observation. Thus

$$R = [\exp(-\tau/\mu_0) + aE(\mu_0)][\exp(-\tau/\mu) + aE(\mu)]. \quad (17)$$

The following values of a were adopted from the results of the example dealing with the savannah [Figs. 3(a) and 3(b)]:

a = 0.1 for the Rayleigh scattering,

a varying linearly from 0.3 to 0.5 between 450 nm and 850 nm for an atmosphere containing aerosols.

(4) Directional contrast for targets of small dimensions. The background contributes in a constant (or random) way to the directional effect, thus

$$R = [\exp(-\tau/\mu_0) + aE(\mu_0)] \exp(-\tau/\mu_0). \quad (18)$$

(5) The extreme case of a perfectly specular reflection can also be considered as the limit of contrast degradation

$$R = \exp(-\tau/\mu_0) \exp(-\tau/\mu). \quad (19)$$

The contrast reductions corresponding to the different cases above are plotted as a function of wavelength (450–850 nm) in Figs. 5(a)–5(c). The geometrical conditions are incidence at 41.4° and observation at +30° in the plane of incidence. The results correspond to three atmosphere models: Rayleigh atmosphere, which represents an ideal case and the best

possible atmospheric conditions; visibility of 23 km, which represents good standard conditions in remote sensing; visibility of 5 km, generally considered to be the lowest limit in remote sensing problems.

The contrast between Lambertian sites of large dimensions (case 1) is always relatively good ($R > 0.5$), even for 5-km visibility. In all other cases, contrasts deteriorate much more rapidly for 23-km or 5-km visibility. The contrasts become inferior to 0.5 for $\lambda = 500$ nm in the case of 23-km visibility and for $\lambda = 850$ nm in the case of 5-km visibility.

It is particularly interesting to note that the loss of contrast in directional effects (cases 3 and 4) is about the same as the loss of spatial contrast in the case of neighboring sites of small dimensions (case 2). This should allow the feasibility of bidirectional reflectance measurements to be evaluated by a study of the spatial contrast between sites of small dimensions as obtained in present remote sensing measurements. Measurement of the bidirectional properties of the target thus seems possible if given that the measurement is limited to good atmospheric conditions and to the upper limit of the visible spectrum. It must nonetheless be remembered that we have not taken into account the variations of ρ_a as a function of the geometrical conditions. In a rough analysis, the ρ_a variations expressed as reflectance are on the order of 0.05. This limits measurements to well-defined bidirectional reflectances, which in practical terms means the study of vegetation in the near IR region.

VII. Conclusion

A fairly accurate analytical expression of the measured reflectance was established for the general case of a non-Lambertian and nonuniform ground. The signal is quite linear as a function of the intrinsic atmospheric reflectance, the actual target reflectance, and two average reflectances, angular and spatial. These two average reflectances remain slightly dependent upon atmospheric properties. For atmospheric corrections, it appears that, except for the intrinsic atmospheric reflectance, the only unknown necessary for the definition of the relative weights of these different terms is the total optical thickness.

Other problems have not been studied here. The relationship between the average angular reflectance and the true reflectance should be generalized to include other types of directional reflectances, and the sensitivity of the average spatial reflectance to the aerosol distribution, for example, should be studied.

The formulation of the signal as described can be quite practical. In particular, it allows a fast and simple evaluation of the different notions of contrast and, more generally, should be useful in the optimization of the correction algorithms for a given type of measurement.

The authors thank J. Lenoble for her keen interest and useful advice and F. Martin for his aid in the translation of this paper. This work has been supported by the Centre National d'Etudes Spatiales under contract CNES/77/0737.

References

1. S. Q. Duntley, J. I. Gordon, J. H. Taylor, C. T. White, A. R. Boileau, J. E. Tyler, R. W. Austin, and J. L. Harris, Appl. Opt. **3**, 549 (1964).
2. R. S. Fraser, J. Opt. Soc. Am. **54**, 289 (1964).
3. B. M. Herman, S. R. Browing, and R. J. Curran, J. Atmos. Sci. **28**, 419 (1971).
4. S. Ueno and S. Mukaï, in *Proceedings of the IFAC Symposium on Environmental Systems Planning, Design, and Control*, H. Akashi, Ed. (Pergamon, Oxford, 1977), pp. 423–428.
5. H. R. Gordon, Appl. Opt. **17**, 1631 (1978).
6. A. P. Odell and J. A. Weinman, J. Geophys. Res. **80**, 5035 (1975).
7. Y. Kawata, Y. Haba, T. Kusaka, Y. Terashita, and S. Ueno, in *Proceedings of the Twelfth International Symposium on Remote Sensing of Environment*, Ann Arbor (1978), pp. 1241–1257.
8. P. Koepke, and K. T. Kriebel, Appl. Opt. **17**, 260 (1978).
9. K. L. Coulson, E. L. Gray, and G. M. Bouricius, "A Study of the Reflection and Polarization Characteristics of Selected Natural and Artificial Surfaces," Technical Information Series, Report R65SD4, Space Sciences Laboratory, General Electric Co. (1965).
10. K. L. Coulson and H. Jacobowitz, "Proposed Calibration Target for the Visible Channel of a Satellite Radiometer," NOAA Technical Report NESS 62 (1972).
11. S. Ueno, Y. Haba, Y. Kawata, T. Kusaka, and Y. Terashita, in *Remote Sensing of the Atmosphere: Inversion Methods and Application*, A. L. Fymat and V. E. Zuev, Eds. (Elsevier, New York, 1979).
12. D. V. Hoyt, J. Appl. Meteorol. **16**, 432 (1977).
13. R. A. McClatchey, R. W. Fenn, J. E. A. Selby, F. E. Voltz, and J. S. Garing, "Optical Properties of the Atmosphere," AFCRL 71-0279, Environmental Research Paper 354 (1971).
14. D. Tanré, "Etude de l'influence des Aérosols sur le Rayonnement Terrestre Retrodiffusé," Thèse de 3e Cycle, Université de Lille (1977).
15. K. T. Kriebel, Appl. Opt. **17**, 253 (1978).

II - APPLICATION COULEUR DE L'OCÉAN (ANNEXES 2 ET 3)

Pour des observations océanographiques, dans le but de remonter à la concentration en pigments chlorophylliens il convient de distinguer, dans la réflectance de la cible, la contribution de l'eau de mer proprement dite de celle de l'interface eau-mer (phénomène du "glitter").

Le glitter ne dépend que de l'état de surface de la mer, principalement conditionné par la vitesse du vent. Un exemple d'indicatrice dans le plan d'incidence du soleil est donné. L'effet directionnel est évidemment très prononcé, la réflectance restant maximum au voisinage de la direction de réflexion spéculaire ($\phi = 0$, $\theta = \theta_s$).

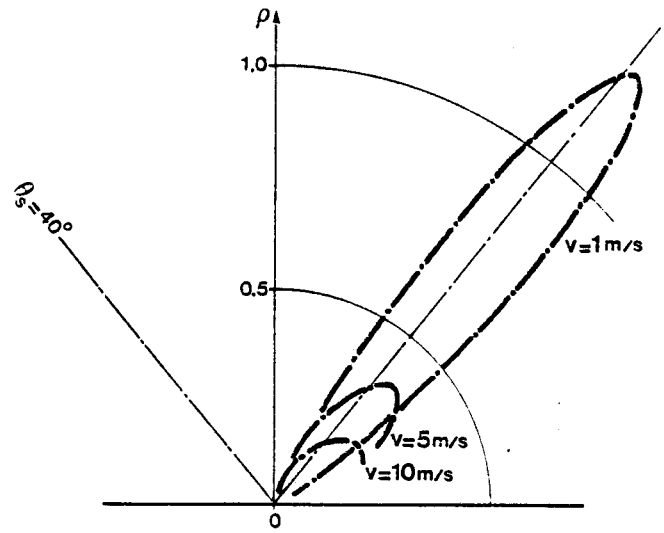

Indicatrices de réflectance du glitter, dans le plan d'incidence du soleil pour différentes valeurs de la vitesse du vent, v. Les réflectances sont calculées à partir d'une modélisation de l'état de surface de la mer. Résultats pour un angle d'incidence $\theta_s = 40°$.

Ce phénomène de réflexion pure est défini, en amplitude, par l'indice de réfraction de l'eau et varie peu avec la longueur d'onde. Ceci permettra d'ailleurs de l'éliminer assez bien, en tant que phénomène parasite, en opérant sur les différences des réflectances observées à plusieurs longueurs d'onde.

La réflectance bidirectionnelle associée à la rétrodiffusion de l'eau de mer est beaucoup plus isotrope. Un exemple d'indicatrice est

présenté dans le cas d'un soleil au zénith ; on voit que, pour cette contribution, l'assimilation à une simple réflectance de Lambert constitue une bonne approximation.

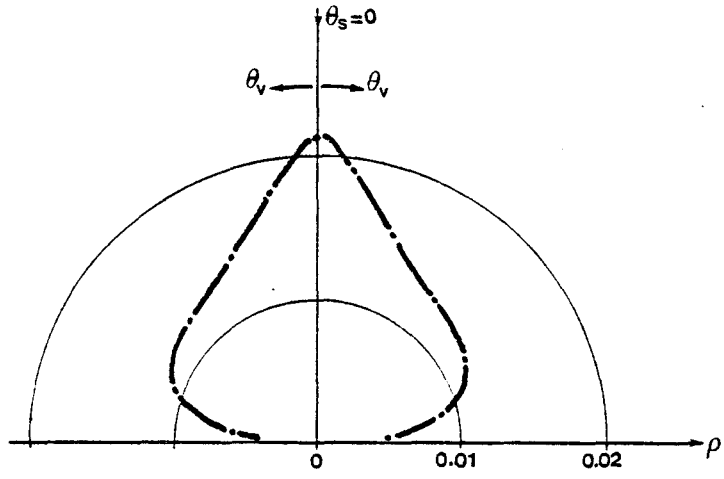

Indicatrice de réflectance associée à la rétrodiffusion de l'eau de mer. Cas d'un soleil au zénith. Les résultats sont calculés à partir d'un modèle de la diffusion de l'eau de mer.

La réflectance correspondante est pratiquement nulle dans l'infrarouge (au delà de 850 nm), les phénomènes de diffusion étant alors inhibés par la très forte absorption propre de l'eau. Vers les courtes longueurs d'onde, surtout pour les eaux très pures, la réflectance croît un peu, avec l'efficacité croissante de la diffusion moléculaire de l'eau. Pour des eaux plus troubles, la diffusion des différentes suspensions marines peut devenir déjà sensible à partir de 700 nm. Mais, de façon générale, les réflectances qu'on aura à mesurer ne dépasseront pas ici quelques pour cent et sont à comparer aux valeurs de la réflectance atmosphérique propre qui pour une atmosphère moyenne passe de 15 % à 400 m à 5 % à 700 nm.

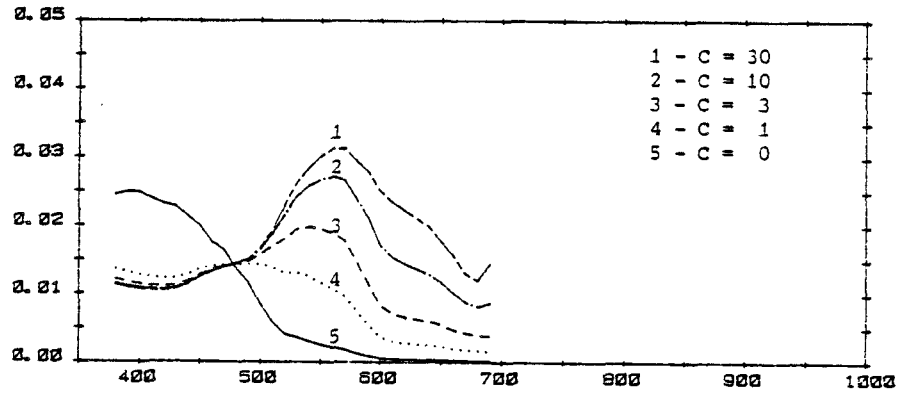

Dépendance spectrale de l'albédo de l'eau de mer. Spectres calculés pour une turbidité moyenne et différentes concentrations, C, de la chlorophylle (C en mg/m^3).

Dans le cas d'observations marines, l'approximation d'une réflectance lambertienne est donc justifiée et le terme perturbateur essentiel est la réflectance atmosphérique qui est d'ordre de grandeur supérieur au signal utile entre λ = 400 nm et λ = 550 nm où l'on veut obtenir ρ_w. Or, suivant la concentration et le type d'aérosols, les variations de ρ_a sont elles mêmes de l'ordre de quelques pourcents. Une solution consiste à mesurer ρ_a à partir de l'espace à des longueurs d'onde pour lesquelles la réflectance de l'eau peut être supposée nulle et à extrapoler ces mesures, pour en déduire ρ_a aux longueurs d'onde utiles.

Deux précautions sont à prendre, éviter les conditions géométriques proches des conditions de réflexion spéculaire et travailler sur des surfaces suffisamment étendues (1 km) pour ne pas être géné par l'environnement.

Des premiers résultats obtenus de cette façon avec le CZCS (Coastal Zone Color Scanner) semblent indiquer que la concentration en pigments peut être ainsi estimée avec une précision d'un facteur 2, des mesures in situ donnent un facteur 0.5.

Ces résultats encourageants montrent la faisabilité de l'expérience et l'on peut espèrer améliorer la précision (i) en développant des algorithmes de correction plus poussés et (ii) en définissant des mesures annexes sur les propriétés optiques de l'atmosphère.

Ces études ont fait l'objet de deux publications (annexe 2 et 3) dont nous allons rappeler ici les principaux résultats.

Nous ferons avant tout les hypothèses suivantes,

- l'absorption par les gaz (principalement O_3) sera paramétrisée comme un facteur de transmission multiplicatif du signal, et découplée des processus de diffusion ;

- l'absorption par les aérosols sera négligée ;

- la luminance rétrodiffusée par l'eau de mer sera supposée isotrope ;

- nous supposerons que nous nous trouvons en dehors de la tache du glitter.

Ces hypothèses simplificatives n'enlèvent rien à la validité des résultats obtenus, le système atmosphère-océan restant décrit presque exactement.

Ces conditions étant réalisées, la réflectance apparente mesurée par le satellite ρ^* s'écrit sous la forme (Eq I-12)

$$\rho^*(\theta_s, \theta_v, \phi) = \rho_a(\theta_s, \theta_v, \phi) + \rho_w \frac{T(\mu_v)\ T(\mu_s)}{1 - \rho\ s} \qquad \text{(II-1)}$$

En océanographie, les réflectances ρ_w sont faibles, comme l'albédo sphérique s atteint au maximum 30 % dans le bleu pour de faibles visibilités, il parait réaliste de négliger les intéractions multiples atmosphère océan et d'écrire ρ^* sous la forme,

$$\rho^*(\theta_s, \theta_v, \phi) = \rho_a(\theta_s, \theta_v, \phi) + \rho_w\ T(\mu_s)\ T(\mu_v) \qquad \text{(II-2)}$$

Cette mise en équation (II-2) permet une première estimation des perturbations dues à l'atmosphère, elles sont de deux sortes :

(i) une augmentation du niveau des réflectances par la réflectance atmosphérique ρ_a due à la rétrodiffusion des molécules et des aérosols ;

(ii) une diminution de la contribution de la réflectance de l'océan due aux fonction de transmission sur les trajets soleil-océan, océan-satellite.

Il est intéressant de distinguer dans la réflectance atmosphérique le rôle des molécules, composante stable et modélisable et le rôle des aérosols, composante variable, et donc de linéariser le signal atmosphérique sous la forme,

$$\rho_a(\theta_s, \theta_v, \phi) = A\ \rho_R^a(\theta_s, \theta_v, \phi) + B\ \rho_p^a(\theta_s, \theta_v, \phi) \qquad \text{(II-3)}$$

où $\rho_R^a(\theta_s, \theta_v, \phi)$ est la réflectance moléculaire,

et $\rho_p^a(\theta_s, \theta_v, \phi)$ est la réflectance due aux aérosols,

l'essentiel du problème des mesures de couleur de l'océan comme on l'a vu étant de déduire la réflectance atmosphérique ρ_a à $\lambda \simeq 400$ nm à partir de ρ_a mesurée à $\lambda > 700$ nm.

La formulation (II-3) nous permet de dégager deux sources d'erreur,

(iii) l'estimation de la réflectance aérosols ρ_p^a dans l'extrapolation en longueur d'onde

(iv) l'estimation des coefficients A et B.

Dans un premier papier (annexe 2), nous avons supposé que A = B = 1 et que l'estimation de la réflectance ρ_p^a se faisait à l'aide d'une seule longueur d'onde (λ = 670 nm), la dépendance spectrale de ρ_p^a étant faite à partir d'une étude statistique. Pour le calcul des fonctions de transmission $T(\mu_s)$ et $T(\mu_v)$ (dont l'évaluation est moins cruciale que celle de la réflectance atmosphérique ρ_a), le Rayleigh était parfaitement pris en compte, mais la contribution des aérosols l'était à partir d'un modèle moyen des particules.

Toutes ces hypothèses étaient faites dans le but d'appliquer l'algorithme aux premiers résultats de l'expérience C.Z.C.S., où le nombre de canaux utiles était restreint (440, 520, 550 et 670 nm). La correction atmosphérique, nécessairement simplifiée, ainsi obtenue, nous donnait des résultats limités en précision, l'estimation de la concentration en pigments chlorophylliens s'effectuant à un facteur 1,5 à 3 près (en supposant connue la relation entre la concentration et la réflectance dans le bleu et le vert). Rappelons que des mesures in-situ semblent indiquer une précision d'un facteur 0.5 sur cette concentration.

Les expériences spatiales futures devraient comporter un plus grand nombre de canaux, en particulier des canaux additionnels dans le proche infrarouge afin de mieux évaluer les effets d'atmosphère. Parallèlement les algorithmes de correction doivent être développés et améliorés de façon à tenir compte des processus actuellement négligés. Ce travail a fait l'objet d'une publication (annexe 3) dans laquelle nous reprenons les points suivants.

(i) processus d'interaction entre les diffusions atmosphériques par les molécules et les aérosols ;

(ii) utilisation de mesures à deux longueurs d'onde dans le proche infra-rouge ;

(iii) évaluation des termes de transmission.

On montre dans ce travail, que l'équation II-3 dans laquelle on pose A = B = 1 constitue une bonne approximation tant que les diffusions multiples restent dans des limites raisonnables par rapport à la diffusion primaire, c'est à dire pour de faibles épaisseurs optiques en aérosols τ_p. En dépit de ce résultat, il est intéressant de posséder une formulation de $\rho_a(\theta_s, \theta, \phi)$ qui reste valable aux incidences rasantes, aux concentrations en aérosols élevées et aux courtes longueurs d'onde. On a donc cherché à modéliser le terme de couplage Rayleigh-Aérosols, ce qui donne une expression de la réflectance atmosphérique plus complexe mais plus précise.

Pour atteindre la réflectance atmosphérique ρ_p^a dans le bleu, nous utilisons deux mesures dans le proche infra-rouge, domaine de longueur d'onde où la réflectance de la mer peut être considérée comme nulle. Nous soustrayons à ces mesures la composante Rayleigh (les interactions molécules et aérosols étant négligeables dans ces canaux) et on extrapole la réflectance ρ_p^a des aérosols dans le bleu à partir de ces mesures corrigées.

A partir d'un certain nombre de modèles d'aérosols, nous avons pu estimer la précision de cette extrapolation ; il apparait que l'ordre de grandeur de l'erreur introduite ($\Delta\rho$) est de quelques milliémes quelle que soit la visibilité ($\frac{\Delta\rho}{\rho} \simeq 5$ %).

En plus de la réflectance atmosphérique ρ_a, on doit encore estimer les fonctions de transmission $T(\theta_s)$ $T(\theta_v)$ pour lesquelles nous avons à notre disposition une expression analytique approchée,

$$T(\mu) = \exp(-(\tau_R + b_p\tau_p)/\mu) \qquad \text{(II-4)}$$

avec $b_p = \frac{1}{2}(1 - \langle\cos\theta\rangle_p)$.

Le paramètre que nous devons atteindre est donc le produit $b_p\tau_p$.

De même, les albédos plan $A_p(\mu_s)$ et sphérique S_p des aérosols peuvent s'écrire avec une bonne précision sous la forme

$$A_p(\mu_s) = 1 - \exp(-\frac{b_p\tau_p}{\mu_s}) \qquad \text{(II-5)}$$

$$S_p = 2\, b_p\tau_p \exp(-2b_p\tau_p) \qquad \text{(II-6)}$$

où l'on retrouve le même paramètre $b_p\tau_p$ à déterminer.

Pour déterminer ce paramètre, nous avons étudié sa corrélation avec la réflectance ρ_p^a, seule grandeur connue, obtenue à partir de la mesure de ρ^a dans le rouge après soustraction de la composante moléculaire. La corrélation est telle que l'estimation du coefficient $b_p\tau_p$ semble possible à 20 % près à partir de la connaissance de ρ_p^a à 650 ou 850 nm.

Si on reprend la formulation du signal marin ρ_w, l'erreur introduit sur les fonctions de transmission $T(\mu_s)$ et $T(\mu)$ par l'incertitude sur le paramètre $b_p\tau_p$, n'entraine pas d'erreurs importantes sur la réflectance vraie ρ_w.

Quant à la modélisation du couplage, l'incertitude sur les albédos plan et sphérique des aérosols ne dégrade pas notre formalisme qui reste plus performant que la simple addition des réflectances ρ_R^a et ρ_p^a et restitue bien la plupart des écarts systématiques observés au soleil couchant et aux faibles visibilités.

L'erreur résiduelle de l'algorithme est due principalement à l'extrapolation en longueur d'onde de la réflectance propre des aérosols. Si on veut augmenter la précision, des informations supplémentaires sur les aérosols deviennent nécessaires.

Pour plus de détails, on se reportera aux annexes 2 et 3 où tout ce qui précéde est largement développé.

ANNEXE 2

AN ALGORITHM FOR REMOTE SENSING OF WATER COLOR FROM SPACE

M. VIOLLIER, D. TANRÉ, P. Y. DESCHAMPS
Laboratoire d'optique atmosphérique (ERA 466) Université des sciences et techniques de Lille, U.E.R. de Physique Fondamentale 59655 Villeneuve d'Ascq CEDEX - (France)

(Received 12 October, 1979)

Abstract. The ocean color algorithm proposed in this paper takes into account the effects of Rayleigh and aerosol scattering. The inherent reflectance and the diffuse transmittance of the Rayleigh atmosphere are expressed as functions of optical thickness and satellite measurement geometry with the aid of simple and accurate formulas. In the case of a turbid atmosphere, from which the aerosol optical thickness is unknown, the aerosol contribution is estimated with the aid of a measurement in a channel where the ocean is a blackbody (in the red or near infrared). If the relationship between the ocean color and the chlorophyll-like pigment concentration is assumed to be known at sea level, it is shown that the chlorophyll-like pigment concentration at an open ocean site can be determined from space to within a factor of 1.5 to 3 (uncertainty equal to 0.2 to 0.5 log interval), depending on the atmospheric turbidity.

1. Introduction

Several airborne experiments have already shown the feasibility of ocean color measurements in the determination of the relative chlorophyll richness of water masses (Clarke *et al.*, 1970; Arvesen *et al.*, 1973; Miller *et al.*, 1977; Wilson *et al.*, 1978; Viollier *et al.*, 1978a). Most of the experiments were carried out at low altitude in order to minimize the masking effects of the atmosphere in the spectral range for which the ocean has a useful spectral signature (0.4 to 0.7 μm).

The realization of these ocean color measurements from space, notably by the CZCS experiment (Coastal Zone Color Scanner, Hovis, 1978) poses the problem of eliminating atmospheric influences in a more crucial and complex way. Examples of the magnitude of this effect are given by the theoretical computations of Kattawar and Humphreys (1976), and by the experimental results of Hovis *et al.* (1973). The main difficulty in the correction of atmospheric effects is due to the presence of aerosol, for which optical characteristics are variable in both time and space. Curran (1972) has evaluated the accuracy required of aerosol optical thickness measurements for chlorophyll content determinations. Gordon (1978) has proposed the correction of the aerosol influence by measurements at 0.7 μm or longer, where the ocean becomes a blackbody. This method assumes (1) the independence of scattering effects due to molecules and aerosols, (2) the linear dependence of the aerosol effect upon optical thickness. These hypotheses are verified in the present article by means of accurate computations of diverse terms of atmospheric perturbation, and simple formulas have been found to facilitate quick and accurate correction. The developed atmospheric correction algorithm is finally applied to the measurement of chlorophyll-like pigment concentration in accordance with the method already proposed

Boundary-Layer Meteorology **18** (1980) 247–267. 0006–8314/80/0183–0247$03.15.

by Viollier *et al.* (1978a), and the accuracy with which chlorophyll-like pigment concentration can be determined from satellites is estimated.

2. Model

The radiative transfer in the ocean-atmosphere system is modelled in the following way. The radiance $I_\lambda((\theta, \phi), (\theta_0, \phi_0))$ measured from space, at wavelength λ, is systematically expressed as a reflectance

$$R_\lambda((\theta, \phi), (\theta_0, \phi_0)) = \frac{\pi I_\lambda((\theta, \phi), (\theta_0, \phi_0))}{E_{0\lambda} \cos \theta_0} \tag{1}$$

where $E_{0\lambda}$ is the solar spectral irradiance at the top of the atmosphere, and (θ, ϕ) and (θ_0, ϕ_0) represent the observation and incidence directions. Notation will be simplified by deleting subscript λ from optical terms. The several contributions of the measured reflectance can be split up in the following way:

$$R = R_a + R_0 + R_{a0} + R_{0a} + R' \tag{2}$$

where, in accordance with Figure 1, each term represents a possible radiation pathway:

- R_a: radiation scattered uniquely by the atmosphere (without an ocean reflection component).
- R_0: direct radiation reflected by the ocean (without atmospheric scattering).
- R_{a0}: diffuse sky radiation reflected towards the satellite.
- R_{0a}: direct radiation reflected and then scattered towards the satellite.
- R': reflected radiation which has been reflected and/or scattered more than twice.

The last term, R', is negligible when the target surface reflectance is a few percent, which is generally the case in measurement of ocean color. Terms R_0, R_{a0} and R_{0a} are all proportional to the ground reflectance ρ for an uniform Lambertian ground reflectance, and it is then possible to write

$$R = R_a + \rho T \tag{3}$$

and in this way to define the diffuse transmittance T.

Ocean reflectance

The ocean reflectance ρ_0 can be considered to be the addition of a perfectly diffuse reflectance ρ resulting from backscattering from the water mass and a surface specular reflectance ρ' which obeys Fresnel's laws

$$\rho_0((\theta, \phi), (\theta', \phi')) = \rho + \rho'(\theta)\delta(\theta - \theta')\delta(\phi - \phi') \tag{4}$$

where δ is the Dirac function. This model is valid only for a perfectly calm water surface. When the water surface is rough, the radiation reflected from the surface is no longer sent uniquely in the direction of the specular reflection, but rather is distributed around this direction (see Annex II). Part of this reflected radiation then

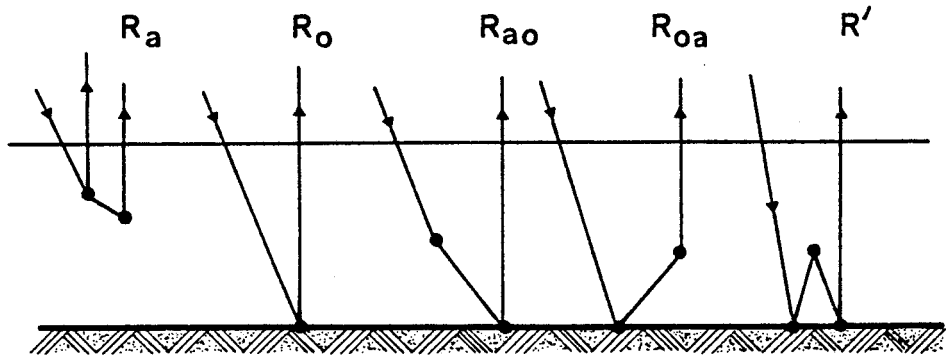

Fig. 1. The different pathways followed by radiation which upwells towards the satellite.

is directly measured by the satellite, and this constitutes the 'glitter' phenomenon. In this study we will suppose that the glitter can be ignored, which assumes the target surface to be perfectly smooth. Furthermore, as most of the surface reflected radiation will thus be sent in the direction of the specular reflection, it will be possible to get good approximate values for R_{a0}, R_{0a}, and R' by using expression (4).

Atmospheric absorption and scattering

In the range used for the measure of ocean color, 0.4 to 0.7 μm, the only notably absorbing atmospheric gas is ozone. The absorption due to ozone can be localized in the atmosphere above the scattering layers and its influence can be calculated separately (see Annex I).

In what follows, Rayleigh scattering due to molecules and Mie scattering due to aerosols have been taken into account. Two cases have been studied. The first case was that of a purely Rayleigh atmosphere, and simple and precise formulas for the evaluation of perturbation due to this kind of atmosphere have been developed; in the second case, aerosols (standard aerosol model, from McClatchey 1971) were added to the Rayleigh atmosphere and an attempt was made to demonstrate the linear relationship between optical thickness and the supplementary perturbation introduced by the aerosols.

Computations were made at wavelengths of 450, 550 and 650 nm, which cover the useful interval in the measure of ocean color (the CZCS channels are at 443, 520, 550, 670 and 750 nm). In what follows it is to be borne in mind that the spectral reflectance signature of the ocean has an amplitude of a few 10^{-2} and that an accuracy on the order of 10^{-3} is necessary for the determination of this signature.

3. Pure Rayleigh Atmosphere

The resolution of radiative transfer in a Rayleigh atmosphere poses no particular problem. Certain of these results can be found in the form of tables (Sekera and Kahle, 1966). Nevertheless, neither exact computer calculation nor the reading of a

table is entirely satisfactory for the pixel-by-pixel correction of the satellite image. What is really needed is the simplest possible formula giving reflectance with an accuracy of 10^{-3}.

With this in mind, we have compared the results of exact computations for a plane-parallel atmosphere which were obtained by the successive orders of scattering method (taking polarization into acount), with results obtained with the aid of approximate formulas. This comparison is made for terms R_a^M and T^M of Equation 3 (the superscript M indicating that they refer to a Rayleigh atmosphere).

Atmospheric reflectance R_a^M

This term corresponds to the apparent reflectance which is measured for a perfectly black surface ($\rho = 0$).

Table I gives the results of exact computations for optical thickness corresponding to 450, 550 and 650 nm, incidence angles θ_0 being of 15° and 60°, and observation angle θ being of 0° and 30° in a plane perpendicular to the plane of incidence ($\phi - \phi_0 = 90°$). These conditions correspond approximately to the geometrical configuration extremes that are possible in the observation of ocean color from space. The results are given for the exact computation, with and without polarization: as has already been pointed out (Plass *et al.*, 1976), it is necessary to account for polarization introduced by Rayleigh scattering in order to obtain the necessary accuracy.

For small optical thickness, multiple scattering becomes negligible and the calculation of single scattering gives a value $R_a^{M(1)}$ close to the exact value R_a^M with

$$R_a^{M(1)} = \frac{p(\chi)}{4(\mu + \mu_0)}\left[1 - \exp -\tau^M\left(\frac{1}{\mu} + \frac{1}{\mu_0}\right)\right] \tag{5}$$

where $\chi = \pi - \arccos(\cos\theta\cos\theta_0 + \sin\theta\sin\theta_0\cos(\phi - \phi_0))$ is the scattering angle, $\mu_0 = \cos\theta_0$, $\mu = \cos\theta$, or, since τ is small,

$$R_a^{M(1)} = \frac{p(\chi)}{4\mu\mu_0}\tau^M \tag{6}$$

with

$$p(\chi) = \tfrac{3}{4}(1 + \cos^2\chi) \tag{7}$$

for Rayleigh scattering.

The latter approximation was used to obtain the values recorded in Table I (column 3). It is interesting to note that the approximate expression (Equation 6) for single scattering gives much better results than does the exact expression (Equation 5). By using the approximate expression (Equation 6), residual errors of a few 0.001 occur, which can be very simply tabulated with an accuracy of 0.001 since the majority of the geometry-associated variations were taken into account in the term $p(\chi)/\mu\mu_0$. Other equations can be found which more exactly account for multiple scattering, but the accuracy obtained is hardly better than the accuracy obtained by

TABLE I

Comparisons between alternative computations of atmospheric reflectances due to Rayleigh scattering (R_a^M) both without and with specular reflectance from the sea surface, without and with polarization, and comparison between exact and approximate computations: 1 – exact without polarization; 2 – exact with polarization; 3 – approximated by Equation 6; 4 – exact with polarization; and 5 – approximated by Equation 9

		λ	Without specular reflection			With specular reflection	
		(nm)	1	2	3	4	5
$\theta = 0$	$\theta_0 = 15$	450	0.0791	0.0838	0.0809	0.0884	0.0842
		550	0.0355	0.0367	0.0356	0.0391	0.0370
		650	0.0181	0.0184	0.0180	0.0193	0.0187
	$\theta_0 = 60$	450	0.1009	0.0988	0.1011	0.1096	0.1091
		550	0.0453	0.0448	0.0444	0.0506	0.0479
		650	0.0229	0.0228	0.0225	0.0257	0.0243
$\theta = 30$	$\theta_0 = 15$	450	0.0816	0.0846	0.0822	0.0903	0.0855
		550	0.0364	0.0373	0.0361	0.0397	0.0375
		650	0.0185	0.0187	0.0183	0.0199	0.0190
	$\theta_0 = 60$	450	0.1119	0.1098	0.1109	0.1209	0.1197
		550	0.0501	0.0496	0.0487	0.0555	0.0526
		650	0.0253	0.0252	0.0247	0.0279	0.0267

equation 6 in the previously defined observation range. Equation 6 is simple, and seems to give the best results.

Specular reflection

The ocean reflection model was described in Section 2. The greater part of the radiation is reflected in the direction of specular reflection. Part of this radiation interacts with the atmosphere by scattering and makes a significant contribution to measured radiation.

This contribution can be approximated with sufficient accuracy by the following formula:

$$R_{\text{spec}} = (\rho'(\theta) + \rho'(\theta_0)) \frac{p(\chi')}{4\mu\,\mu_0} \tau^M \tag{8}$$

(with $p(\chi') = p(\chi)$ for $\chi' = \pi - \chi$) which accounts for radiation reflected after scattering and radiation scattered after reflection, with reflection coefficients $\rho'(\theta)$ and $\rho'(\theta_0)$. For nearly vertical sightings, $\rho'(\theta)$ is equal to 0.02, and the term R_{spec} is then of the order of 0.004 at 450 nm.

This term can easily be incorporated into R_a (in place of Equation 6) which becomes

$$R_a^{M(1)} = (1 + \rho'(\theta) + \rho'(\theta_0)) \frac{p(\chi)}{4\mu\,\mu_0} \tau^M . \tag{9}$$

With Table I (columns 4 and 5), it is possible to test the validity of this expression as compared with the exact computation. Differences of a few 0.001 exist, which can easily be tabulated as a function of the geometry of the problem.

DIFFUSE TRANSMITTANCE T^M

For a uniform Lambertian ground reflectance, the Rayleigh diffuse transmittance is defined by Equations 2 and 3:

$$\rho T^M = R_0^M + R_{a0}^M + R_{0a}^M \tag{10}$$

and the analytical expressions for the terms R_0^M, R_{a0}^M, R_{0a}^M are

$$R_0^M = \rho e^{-\tau^M/\mu_0} e^{-\tau^M/\mu} \tag{11}$$

$$R_{a0}^M = \rho E_a^M e^{-\tau^M/\mu} \tag{12}$$

$$R_{0a}^M = \rho(E_a^M + E_S^M) t^M(\mu) \tag{13}$$

where $t^M(\mu)$ is the appropriate transmittance and E_S^M and E_a^M are respectively the direct and diffuse components of the downwelling normalized irradiance. In accordance with the above conventions, each term is normalized to the incident irradiance outside of the atmosphere, $\mu_0 E_0$, divided by π; E_S^M and E_a^M are thus dimensionless transmission terms

$$E_S^M = e^{-\tau^M/\mu_0} \tag{14}$$

$$E_a^M = \tfrac{1}{2}(1 - e^{-\tau^M/\mu_0}). \tag{15}$$

Equation 15 is exact for only the single scattering approximation, but this approximation still gives good results when τ^M is not too large. The expression of the transmittance $t^M(\mu)$ is found to be identical to the expression of E_a^M:

$$t^M(\mu) = \tfrac{1}{2}(1 - e^{-\tau^M/\mu}). \tag{16}$$

Combining equations 11 to 16 yields

$$R_0^M + R_{a0}^M + R_{0a}^M = (\rho/4)(1 + e^{-\tau/\mu})(1 + e^{-\tau/\mu_0}) \tag{17}$$

which provides an expression for diffuse transmittance as previously defined by Equation 10

$$T^M(\mu, \mu_0) = \tfrac{1}{4}(1 + e^{-\tau^M/\mu})(1 + e^{-\tau^M/\mu_0}). \tag{18}$$

This formula is used further in the text (Table VI, column 3) and gives excellent accuracy in the retrieval of ground reflectances from synthetic data of R.

This model assumes the ground reflectance ρ to be uniform over horizontal distances of at least several kilometers. Ocean reflectance obviously is not completely uniform since fronts, eddies and various patches are present. Ocean reflectance variations are nevertheless small enough for the above model to remain valid as a first approximation. This is not the case for areas very close to the coast

where the change in reflectances between water and land is so large as to invalidate the model. Specific atmospheric corrections which acccount for this particular non-uniform case have not yet been developed.

If this limitation is accepted, formulas 9 and 18 are useful in the elimination of the influence of Rayleigh scattering.

4. Turbid Atmosphere

Aerosol scattering causes an additional perturbation of reflectance R_a and diffuse transmittance T. In marine or continental zones, the nature of aerosols can be extremely varied: water droplets, industrial or volcanic dust, etc. To study all possible cases present in nature would be impossible. An attempt thus will be made to demonstrate the general laws of radiative transfer in a turbid atmosphere with the aid of a standard aerosol model.

Aerosol model

Computations for an atmosphere containing aerosols were made using the standard model of McClatchey *et al.* (1971). For this model, particle characteristics are independent of altitude. The particles are assumed to be spherical, non-absorbing, of optical index $m = 1.50$, of the following size distribution:

$$n(r) = 0 \quad \text{if} \quad r < 0.02\ \mu\text{m}$$

$$n(r) = 10^{-4}C \quad \text{if} \quad 0.02 < r < 0.1\ \mu\text{m}$$

$$n(r) = Cr^{-4} \quad \text{if} \quad 0.1 < r < 10\ \mu\text{m}$$

$$n(r) = 0 \quad \text{if} \quad r > 10\ \mu\text{m}$$

$$C = 8.83\ 10^{-5}\ \mu\text{m}^{-4}.$$

The value of the phase function deduced from this model are presented in Table II.

McClatchey *et al.* (1971) selected two atmospheric aerosol distributions, one representative of a clear sky and one of a hazy sky. The two models correspond to horizontal visibilities of respectively 23 and 5 km. The optical thicknesses of the aerosols in these two models are presented in Table III.

Linearity of R_a^A as compared with τ^A

Tanré and Herman (1978) have demonstrated that for nearly vertical sightings ($\theta < 15°$) and aerosol optical thicknesses smaller than 0.5, the reflectance for a turbid atmosphere can be written as

$$R_a = R_a^M + R_a^A \tag{19}$$

where R_a^A is the reflectance due to a hypothetical atmosphere containing only aerosols; the term including the Rayleigh-aerosol interaction was found to be less than 3%.

TABLE II

Phase function of the aerosol model of McClatchey *et al.* (1971). The ratio between $p^A(\chi)$ at 450 and 650 nm (last column) emphasizes the dependence of $p^A(\chi)$ upon wavelength, particularly in backward directions. The angles chosen, χ, are those used in the approximate computations presented in this paper

Phase angle χ	Phase function $p^A(\chi)$ 450 nm	550 nm	650 nm	Ratio $p^A_{450}(\chi)/p^A_{650}(\chi)$
15°	8.54	8.39	8.31	1.03
41°	1.93	1.93	1.92	1.00
60°	0.80	0.81	0.82	0.97
120°	0.141	0.152	0.160	0.87
139°	0.153	0.166	0.175	0.88
165°	0.328	0.337	0.345	0.95

Unlike the Rayleigh reflectance, it would be superfluous to look for approximations of R_a^A as a function of aerosol optical thickness and phase function. That would not resolve the problem because the aerosol optical parameters are exceedingly variable in time and space. An attempt should instead be made to correlate the atmospheric correction directly with a satellite measurement. Gordon (1978) suggests a linear dependence of R_a on τ^A. Thus if one knows the spectral dependence of τ^A, the value of $R^A_{a\lambda}$ at a given wavelength can be deduced from R measured at a different wavelength, i.e., in the red where the radiance backscattered by the ocean becomes nil.

This is illustrated in Table IV which presents the results of exact computations of R_a^A for a vertical sighting ($\theta = 0$), and for three solar angles ($\theta_0 = 15°$, 41.41° and 60°), as well as by Table V, which presents the differences between the exact and approximate computations of R_a^A at 450 nm. The computations were made for the two cases, clear and hazy. The approximate determination of R_a^A at 450 nm (R^A_{a450}) is deduced from the exact value of R^A_{a650} by use of the linear relationship between R_a^A and τ^A.

Two equations were tried, first

$$R^A_{a450} = \varepsilon R^A_{a650} \tag{20}$$

TABLE III

Rayleigh optical thickness from Hoyt (1977), and aerosol optical thickness for the clear and hazy models from McClatchey *et al.* (1971)

λ (nm)	450	550	650
τ^M	0.2157	0.0948	0.0481
τ^A Clear	0.2801	0.2348	0.2011
τ^A Hazy	0.9305	0.7801	0.6681

TABLE IV

Turbid atmosphere: exact computations of the aerosol reflectance R_a^A. The zenith solar angles θ_0 are 15, 41.4 and 60°. The sighting is vertical ($\theta = 0$). R_a^A includes the Rayleigh-aerosol interaction

Clear Atmosphere			
λ (nm)	$\theta_0 = 15°$	$\theta_0 = 41.41°$	$\theta_0 = 60°$
450	0.0212	0.0200	0.0293
550	0.0200	0.0176	0.0260
650	0.0182	0.0154	0.0226
Hazy Atmosphere			
450	0.0765	0.0802	0.1039
550	0.0704	0.0713	0.0972
650	0.0631	0.0623	0.0868

where ε is the optical thickness ratio

$$\varepsilon = \tau^A(450)/\tau^A(650); \tag{21}$$

and second

$$R^A_{a450} = \varepsilon' R^A_{a650} \tag{22}$$

where $\varepsilon' = 0.9\varepsilon$.

In this case the factor 0.9 takes into account the average ratio of the phase function at 450 and 650 nm at the angles of backscattered radiation (see column 5 of Table II). In Table V it is seen that the use of coefficient $\varepsilon' = 0.9\varepsilon$ instead of ε notably reduces the differences, and this is of particular interest in the 'hazy' model. For the 'clear'

TABLE V

Disparity (in absolute value) between the exact value of R_a^A at 450 nm and the value as approximated by

$R^A_{a450} = \varepsilon R^A_{a650}$ where $\varepsilon = \frac{\tau^A_{450}}{\tau^A_{650}}$ column (1)

$R^A_{a450} = \varepsilon' R^A_{a650}$ where $\varepsilon' = 0.9\varepsilon$ column (2)

	θ_0	(1)	(2)
Clear	15°	+0.0041	+0.0015
	41.4°	+0.0014	−0.0007
	60°	+0.0022	−0.0011
Hazy	15°	+0.0114	+0.0023
	41.4°	+0.0066	−0.0024
	60°	+0.0170	+0.0046

model, the differences between exact and approximate computations of R_a^A are about 10^{-3}, which is equal to the magnitude of the desired accuracy.

The interaction between the specular reflection and the scattering can be incorporated into the expression of R_a^A in the same way as in the study of Rayleigh scattering (Equation 8). R_a^A is roughly given by the single scattering approximation

$$R_a^A = \{p^A(\chi) + (\rho'(\theta) + \rho'(\theta_0))p^A(\chi')\} \frac{\tau^A}{4\mu\,\mu_0} \tag{23}$$

where χ' and $\chi = \pi - \chi'$ respectively designate the forward and backward scattering directions. Given this equation, it is logical to consider that the previously demonstrated results remain valid, indicating that R_a^A is a linear function of τ^A. The algorithm based on Equation 20 thus remains applicable if the influence of the specular reflection upon the scattered radiation is taken into account.

Diffuse transmittance T

The diffuse transmittance expression (Equation 18) established for Rayleigh scattering is no longer valid in the case of aerosols. Unlike Rayleigh scattering, aerosol scattering is very dissymmetric. Typically 70% of the radiation is scattered forwards in an angle of $\pm 10°$ and can be considered directly transmitted. For an atmosphere containing only aerosols, one can write the approximation

$$R^A = R_a^A + \rho \exp -b\tau^A \left(\frac{1}{\mu_0} + \frac{1}{\mu}\right) \tag{24}$$

where b is a coefficient representing the part of the radiation scattered backward by the aerosols. With the McClatchey aerosol model, the best results were obtained by assuming b to be equal to 0.13.

If we consider the aerosol-Rayleigh mixture, the diffuse transmittance Equation 18 combined with equations 11 to 16 and 24 becomes:

$$T = \tfrac{1}{4}(1 + \exp -\tau^M/\mu_0)(1 + \exp -\tau^M/\mu) - \left[1 - \exp -b\tau^A\left(\frac{1}{\mu} + \frac{1}{\mu_0}\right)\right] \exp -\tau^M\left(\frac{1}{\mu} + \frac{1}{\mu_0}\right). \tag{25}$$

This expression has been used for the retrieval of ground reflectances ρ from synthetic data of R. Results of such computations are presented in Table VI for two cases of atmospheric turbidity. The retrieval of ρ is obtained by using Equation 3 in which R_a is assumed to be known. It can be seen that the errors in ρ are less than 0.002 when ρ is smaller than 0.05, which is the case in ocean sightings. The influence of aerosols upon the diffuse atmospheric transmittance thus can easily be calculated with the aid of Equation 25.

TABLE VI

Comparison of initial (ρ) and retrieval (ρ_r) values of the ocean reflectance supposing that R_a is known and using the expression of the diffuse transmittance (Equation 25). R is the reflectance at the top of the atmosphere. The computations were made for the case in which reflectance ρ is lambertian. The sighting is vertical ($\theta = 0$)

		Rayleigh		Clear		Hazy	
	ρ	R	ρ_r	R	ρ_r	R	ρ_r
$\theta_0 = 15°$	0	0.0838	—	0.1050	—	0.1603	—
	0.05	0.1247	0.0503	0.1437	0.0507	0.1936	0.0514
	0.10	0.1662	0.1014	0.1833	0.1026	0.2279	0.1043
$\theta_0 = 41.41°$	0	0.0860	—	0.1060	—	0.1662	—
	0.05	0.1257	0.0502	0.1430	0.0502	0.1969	0.0500
	0.10	0.1661	0.1014	0.1808	0.1015	0.2286	0.1017
$\theta_0 = 60°$	0	0.0988	—	0.1281	—	0.2027	—
	0.05	0.1362	0.0502	0.1615	0.0487	0.2289	0.0478
	0.10	0.1742	0.1012	0.1957	0.0986	0.2559	0.0971

5. Correction Algorithm

By examining the results of the preceding computations, the following method can be proposed for the elimination of atmospheric influences.

Measured radiances are expressed as reflectance $R(\theta, \phi; \theta_0\phi_0)$ with the aid of Equation 1, and then corrected for ozone absorption effects by a multiplicative factor which is a function of geometry (θ, θ_0) and of the average seasonal ozone quantity (see Annex I).

In what follows, subscript 1 will designate the wavelength for which the ocean is considered a black body, and 2 will designate the wavelength at which the correction is effected. Ocean reflectance ρ_2 can be retrieved from the reflectances R_2 and R_1 measured at the top of the atmosphere by the equation

$$\rho_2 = \{(R_2 - R_{a2}^M) - \varepsilon(R_1 - R_{a1}^M)\}T_2^{-1}. \tag{26}$$

In this equation Rayleigh reflectances R_{a1}^M and R_{a2}^M can be calculated with accuracy (see Equation 9) because they depend only upon optical thickness values τ_λ^M which are constant in time, and upon geometric variables (θ_0, ϕ_0) and (θ, ϕ).

Diffuse transmission T_2 can also be calculated with accuracy (Equation 25); uncertainty relative to the term $b\tau^A$ is of little consequence in the evaluation of T_2, which depends mainly upon Rayleigh scattering. The only unknown in Expression 26 is the coefficient $\varepsilon = \tau_2^A/\tau_1^A$. When lacking contemporary experimental determination of ε, one can use an average derived from a statistical study of on site measurements (see Annex III). The accuracy of the algorithm is limited essentially by the probable differences between the real and estimated values of ε.

The coefficient ε can vary a great deal. It generally is accepted that $\tau^A(\lambda)$ can be approximated by a power law

$$\varepsilon = \frac{\tau_2^A}{\tau_1^A} = \left(\frac{\lambda_2}{\lambda_1}\right)^{-\alpha}. \tag{27}$$

The parameter α depends mainly upon the aerosol size distribution and theoretically can vary between -0.2 and 2 (see, for example, Box and Lo, 1976). This leads to variations of ε between 0.9 and 3 for the spectral range considered here. Actual measurements show this variation to be less extensive, especially for ocean sites (see Annex III). With the aid of Equation 27, it is easy to establish that the uncertainty $\Delta\rho_2$ in ρ_2 can be expressed as a function of the uncertainty $\Delta\alpha$ in α by

$$\Delta\rho_2 = \frac{1}{T_2}\frac{\lambda_1}{\lambda_2} R_{a1}^A \alpha \Delta\alpha . \tag{28}$$

For conditions such as $\lambda_1 = 700$ nm, $\lambda_2 = 450$ nm, $\alpha = 1$ and $\Delta\alpha = 0.3$, calculations for the 'clear' model give an uncertainty $\Delta\rho_2$ of the order of 0.01, which is much greater than desired.

The accuracy is decidedly improved when the measurement is relative, i.e., it is the difference or ratio of reflectances at two neighboring wavelengths (λ_2 and λ_3). This yields

$$\Delta(\rho_2 - \rho_3) = \left(\frac{1}{T_2}\frac{\lambda_1}{\lambda_2} - \frac{1}{T_3}\frac{\lambda_1}{\lambda_3}\right) R_{a1}^A \alpha \Delta\alpha . \tag{29}$$

For the same conditions as above, the uncertainty is of the order of 0.001 for $\lambda_2 = 450$ nm and $\lambda_3 = 520$ nm. Significant evaluations of ocean color thus can be made with the aid of relative measurements between two neighboring wavelengths.

6. Example of Application

The efficiency of atmospheric corrections has to be evaluated relative to the accuracy necessary in the remote sensing of ocean color, and more specifically, relative to the retrieval of chlorophyll-like pigment content. The term 'chlorophyll-like pigment content' is used rather than 'chlorophyll content', because several different pigments absorb and modify the ocean spectral reflectance. Experimental results previously obtained are used to derive an interpretation model of ocean reflectances and to check the efficiency of the atmospheric corrections.

Interpretation Model

The results of previous low-altitude airborne experiments yield a relationship between chlorophyll-like pigment content and ocean spectral reflectances. This is illustrated in Figure 2, where the differences of the reflectances at 466 nm and

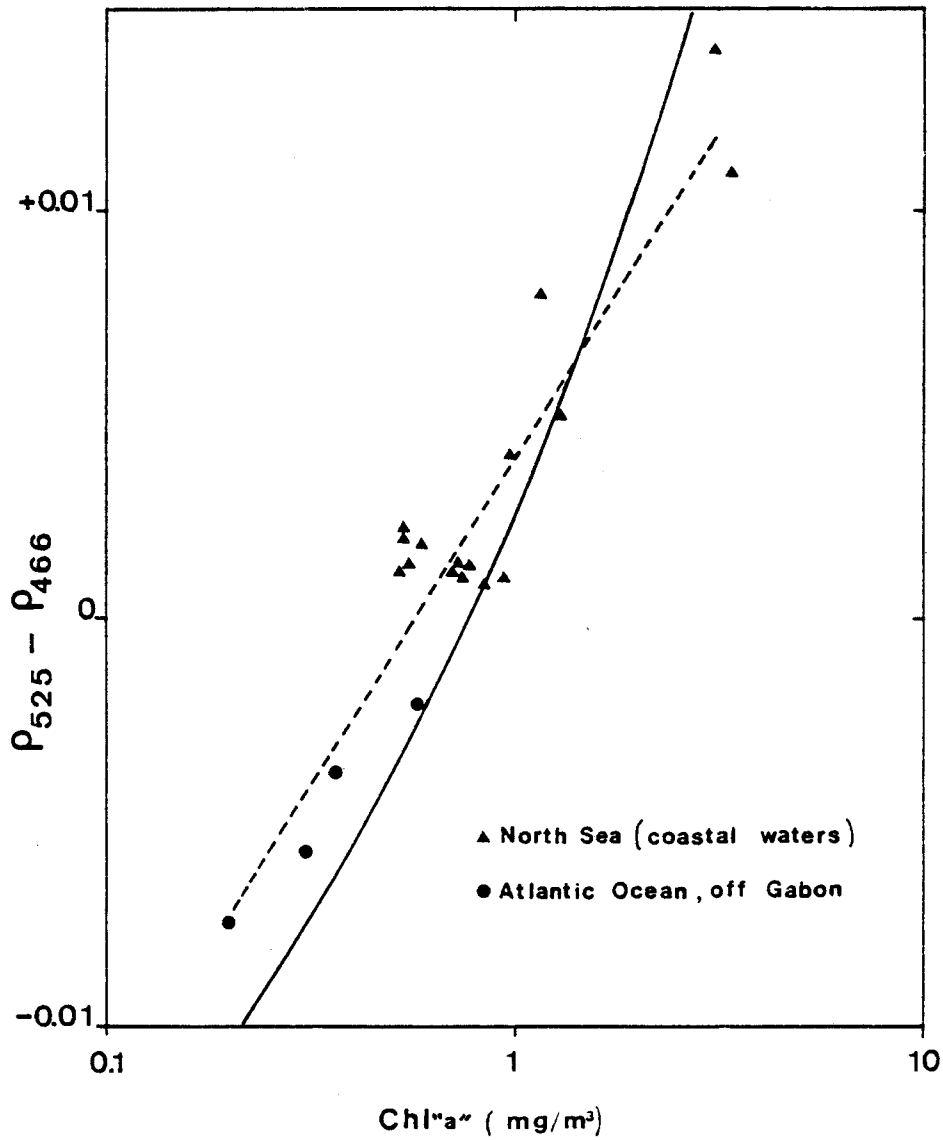

Fig. 2. Difference of reflectances at 525 and 466 nm versus chlorophyll-*a* concentration. *Dashed line*: experimental regression line from airborne measurements of reflectances at low altitude and from *in situ* measurements of chlorophyll-*a*. *Solid line*: theoretical relationship obtained by modelling.

525 nm are plotted versus the chlorophyll-*a* content measured *in situ* by spectrophotometric methods.

Two groups of points are noted. One group of 4 points corresponds to low concentrations of chlorophyll-*a* (from 0.2 to 0.8 mg m^{-3}) observed in the open ocean (see Deschamps *et al.*, 1977). The other group corresponds to higher concentrations (up to 3 mg m^{-3}) observed in a coastal region of the North Sea (see Viollier *et al.*,

1978b). Combining the two groups, one can find a best-fit regression line for all of the points. Uncertainty in chlorophyll-*a* concentration estimations made with this regression approach is less than one fourth of a log interval, which is acceptable for many biological applications.

The relationships between the difference of reflectances at two wavelengths and the chlorophyll-like pigment content can be approximated with the aid of a theoretical model. It is generally accepted that the diffuse reflectance of the ocean can be written

$$\rho_\lambda = m\frac{b_{0\lambda}}{a_\lambda} + n\frac{b_{p\lambda}}{a_\lambda} \tag{30}$$

where $b_{0\lambda}$ and $b_{p\lambda}$ are the coefficients for scattering due to molecules and particles contained in the water, and a_λ is the coefficient for absorption due to pure water and chlorophyll pigments. Viollier *et al.* (1978a) in this way calculated the theoretical variations of ρ_λ as a function of particle-scattering coefficient ($b_{p\lambda}$), and as a function of the chlorophyll pigment concentration (C), these being the main variables in Equation 30.

By assuming a linear relationship between the particle-scattering coefficient and the chlorophyll concentration, one obtains the theoretical relationship described in Figure 2. The differences between the theoretical and experimental curves are about one fourth of a log interval. We thus have a theoretical model furnishing an approximate relationship between ocean color and chlorophyll-like pigment concentration.

Atmospheric perturbations

By assuming that the above model is exact, it is proposed that the amplitude of the errors specific to atmospheric effects on chlorophyll retrieval be demonstrated. We have used daily measurements of atmospheric turbidity at an ocean site (Lajes, Azores, see Annex III). A case of low turbidity and a case of high turbidity are considered. The first is characterized by τ^A (1 μm) = 0.13 and the second by τ^A (1 μm) = 0.30, values corresponding to the minimum and maximum of the monthly average measurements of τ^A at this site in 1975. The annual average value α_m for the daily measurements of α was equal to 0.93, and the standard deviation $\Delta\alpha$ around this average was 0.3.

The efficiency of the atmospheric correction algorithm is tested by the following method:

(1) synthetic values of R at 466, 525 and 700 nm are computed for the cases of low and high atmospheric turbidity with $\alpha = 0.93$ and for various chlorophyll-*a* contents between 0.1 and 3 mg m^{-3}.

(2) the atmospheric correction algorithm (Equation 26) is applied to the reflectances at 466 and 525 nm, by introducing the values of ε, successively derived from the values of $\alpha = 0.93 \pm \Delta\alpha$. The differences of reflectances $\rho_{466}-\rho_{525}$ are then

TABLE VII

Comparison of initial and retrieval values of the chlorophyll concentration (mg m^{-3}) applying the atmospheric correction algorithm. The test is valid for a smooth sea and for turbidity conditions in the Azores Islands (see annex III). Upper part: low turbidity ($\tau^A(1\ \mu m) = 0.13$). Lower part: high turbidity ($\tau^A(1\ \mu m) = 0.3$). The computations were made for $\theta_0 = 41°$ and $\theta = 0°$

Initial	Retrieval from	to	Disparsity in log interval unit
0.1	0.07	0.15	0.18
0.31	0.23	0.41	0.14
1	0.84	1.22	0.09
3.13	2.75	3.66	0.06
0.1	0.03	0.25	0.50
0.31	0.17	0.61	0.29
1	0.65	1.61	0.21
3.13	2.24	4.49	0.15

calculated and the chlorophyll content C is deduced. The differences between the initial and retrieved value of C give the uncertainty in C which results from the uncertainty in α.

The results of this simulation are found in Table VII. It is noted that the error varies from 0.06 to 0.5 log interval depending upon the atmospheric turbidity and the diversity of the concentrations represented. Accuracy is best for high concentrations, which is explained by the fact that variations of the $\rho_{466} - \rho_{525}$ difference are then mainly due to variations of ρ_{525}, which is less subject to the atmospheric effect. It must be remembered that in this case the measurement is primarily of scattering coefficient b_p, which is assumed to be correlated with the pigment concentration. For lower concentrations, the correction accuracy is not as good. Just as with the atmospheric uncertainties, there is a 0.2 to 0.5 log interval error, indicating that chlorophyll-like pigment concentration can be estimated to within a factor of 1.5 to 3. Although this uncertainty is large, it nevertheless is consistent with the order of magnitude of other uncertainties encountered in the measurement of chlorophyll pigment concentration. For example, the uncertainty is found to be 0.20 log interval in the case of 'low turbidity', and thus is equal to the uncertainty which commonly is applied to the relationship between optical measurements made at the ocean level and corresponding chlorophyll pigment concentration.

7. Conclusion

Atmospheric effects between 400 and 700 nm are of two types: absorption by ozone and scattering by gases and aerosols. A correction for scattering, which is more complicated than a correction ozone absorption, was especially studied in this article.

The following points have been demonstrated:

(1) it is possible to calculate the Rayleigh scattering and the aerosol scattering separately for usual atmospheric turbidity conditions and nearly vertical sightings.

(2) the Rayleigh scattering effects (reflectance and diffuse transmittance) can very accurately be computed as a function of the geometric variables with the aid of simple formulas.

(3) aerosol scattering effects can be linearly extrapolated from one wavelength to another.

The correction algorithm constructed from these results allows the relative ocean reflectance values (ratio of difference of reflectances at two wavelengths) to be retrieved with good accuracy. By supposing that the relationship between the chlorophyll-like pigment concentration and the reflectances in the blue and green at sea level are known, it is shown that the chlorophyll-like pigment concentration can be retrieved to within a factor of 1.5 or 3, depending upon the atmospheric turbidity. These results demonstrate that significant results can be anticipated from visible images of the ocean observed from space.

ANNEX I

Absorption by Atmospheric Gases

Absorption between 400 and 700 nm is entirely due to ozone, which is situated high enough in the atmosphere for the absorption and scattering phenomena to be treated separately as follows:

$$R = T_{03}(R_a + \rho T)$$

where T_{03} represents the ozone transmittance and R_a, ρ and T are the scattering terms defined in Equation 3.

Transmittance T_{03}^{λ} can be given as

$$T_{03}^{\lambda} = \exp\left(-k_{\lambda} U\left(\frac{1}{\mu_0} + \frac{1}{\mu}\right)\right)$$

where k_{λ} is the ozone absorption coefficient, and U is the total quantity of ozone in the atmosphere. The only unknown is the quantity of ozone U, which is variable in time and space. The average values that are encountered increase from the equator ($U = 0.24$ cm atm) to the poles ($U = 0.38$ cm atm). A seasonal variation is also found, which increases with latitude (see London *et al.*, 1976). In Europe, average values change from 0.28 cm atm in autumn to 0.37 cm atm in spring. The accuracy necessary in the measurement of ozone content is of 0.05 atm cm if an accuracy of 0.002 is to be obtained in the absolute measurement of ocean reflectance. Thus it

seems that the estimation of T_{03} with the aid of the average seasonal ozone content suffices for atmospheric corrections.

ANNEX II

Evaluation of the Glitter Reflectance Equivalent

Capillary ripples and waves form a set of variably oriented facets which reflect direct solar radiation in many directions other than the direction of specular reflection. From space this is seen as a glitter pattern which is more or less extensive as a function of surface conditions. Under certain conditions (high sun, rough sea) it is difficult to avoid the reception of some glitter by an ocean color sensor, and this changes the useful signal and is incompatible with application of the atmospheric correction algorithm. It thus is essential that one be able to estimate glitter.

The distribution of surface-reflected solar radiation, and consequentially the wave slope distribution, was studied as a function of wind speed by Cox and Munk (1956). The distribution can be considered approximately isotropic and gaussian, with a variance equal to

$$\sigma^2 = 0.003 + 0.00512V \tag{A-1}$$

where V is the wind speed (m s^{-1}). The probability function for seeing glitter in direction (θ, ϕ) when the sun is in direction (θ_0, ϕ_0) is thus:

$$p(\theta, \phi; \theta_0, \phi_0, V) = \frac{1}{\pi\sigma^2} \exp\left(-\frac{z_x^2 + z_y^2}{\sigma^2}\right) \tag{A-2}$$

with

$$z_x^2 + z_y^2 = \tan^2 \theta_n \tag{A-3}$$

where z_x and z_y are the components of the slope vector (θ_n, ϕ_n) for which the specular reflection conditions are fulfilled (see Figure 3). With ω as the reflection angle, θ_n can be deduced from the following equations

$$\cos 2\omega = \cos\theta \cos\theta_0 + \sin\theta \sin\theta_0 \cos(\phi - \phi_0) \tag{A-4}$$

$$\theta_n = \arccos\left(\frac{\cos\theta + \cos\theta_0}{2\cos\omega}\right). \tag{A-5}$$

Cox and Munk established that the glitter radiance $L_g(\theta, \phi; \theta_0, \phi_0)$ is related to the probability function by the equation

$$L_g(\theta, \phi; \theta_0, \phi_0; V) = \frac{E_0 e^{-\tau/\mu_0}}{4} \frac{1}{\mu\mu_0^4} r(\omega) p(\theta, \phi; \theta_0, \phi_0; V) \tag{A-6}$$

where E_0 is the solar irradiance at the top of the atmosphere, τ is the atmospheric optical thickness (Rayleigh, aerosol and ozone), and $r(\omega)$ is the reflection factor given

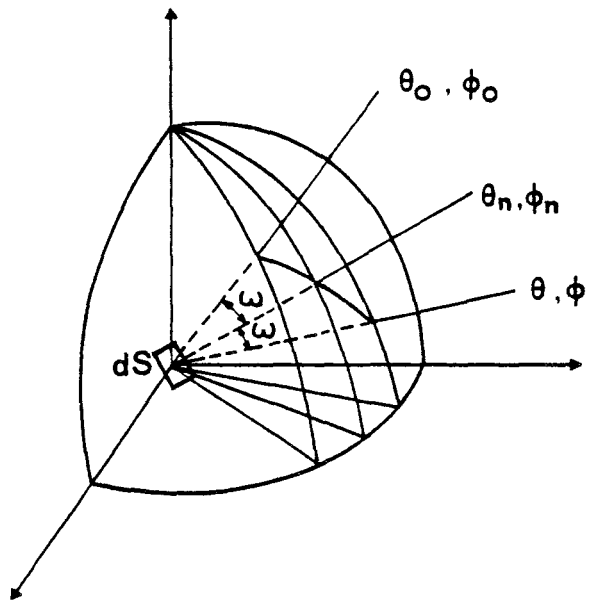

Fig. 3. Reflection geometry.

by Fresnel's law. The glitter reflectance at the top of the atmosphere

$$R_g(\theta, \phi; \theta_0, \phi_0; V) = \frac{\pi L_g(\theta, \phi; \theta_0, \phi_0; V) e^{-\tau/\mu}}{\mu_0 E_0} \qquad \text{(A-7)}$$

thus can be calculated as a function of (θ, ϕ), (θ_0, ϕ_0) and V by using Equations A–1 through A–6. It must be emphasized that the accuracy of this estimation is dependent upon the validity conditions of the Cox and Munk model. It seems that the model is valid only for homogeneous zones of open sea.

Table A–I shows the R_g values calculated for sighting angles ($\theta = 0, 15, 30, 45°$) in the plane perpendicular to the sun and solar angles ($\theta_0 = 30, 45, 60°$). For these calculations, the atmosphere was considered to be transparent ($\tau = 0$), which leads to a slight overestimation of the results (typically by 30%). It is noted that R_g is negligible ($<10^{-3}$) for solar angles of 45° and 60° when wind speed is low (5 m s^{-1} or 10 kt). Such is no longer the case for a wind speed of 14 m s^{-1} (28 kt). Thus either an exact measurement of glitter radiation, or lacking that, an estimation of wind speed at the sighted zone, seems to be necessary in the ocean color correction algorithms. When the wind speed is known to be low (typically less than 5 m s^{-1}), glitter reflectance can be ignored and the atmospheric correction algorithm described in this paper can be applied without modification.

TABLE A-I

Reflectance of glitter in a plane perpendicular to the plane of incidence. Windspeeds are 5 and 14 m s^{-1}.

$v = 5$ m/s θ_0 / θ	30	45	60
0	0.0189	0.0009	0.0000
15	0.0093	0.0003	0.0000
30	0.0009	0.0000	0.0000
45	0.0000	0.0000	0.0000

$v = 14$ m/s θ_0 / θ	30	45	60
0	0.0341	0.0133	0.0029
15	0.0273	0.0096	0.0017
30	0.0132	0.0033	0.0003
45	0.0033	0.0004	0.0000

ANNEX III

Statistical Study of Atmospheric Turbidity

Aerosol optical thickness depends on wavelength according to a power law characterized by coefficient α

$$\tau^A(\lambda_1) = \tau^A(\lambda_0)\left(\frac{\lambda_1}{\lambda_0}\right)^{-\alpha}.$$

The parameters characterizing atmospheric turbidity thus are α and $\tau^A(\lambda_0)$ where λ_0 is a reference wavelength, generally 1 μm.

The measurement of the optical thickness $\tau^A(\lambda)$ is deduced from the measurement of direct solar radiation $E_{s\lambda}$ by using the Lambert–Bouguer law

$$E_{s\lambda} = E_{0\lambda} \exp\left(-(\tau^M + \tau^G + \tau^A)m\right)$$

where $E_{0\lambda}$ is solar irradiance at the top of the atmosphere; τ^M = Rayleigh optical thickness; τ^G = absorption optical thickness (ozone); and m = air mass.

Coefficient α is deduced from measurements at two wavelengths

$$\alpha = \frac{\ln\left(\tau^A(\lambda_1)/\tau^A(\lambda_0)\right)}{\ln\left(\lambda_0/\lambda_1\right)}.$$

These measurements are made daily at some of the World Meteorological Organization network stations and are published (Anonymous 1977). From these data, those for the Lajes site (38°45 N, 27°05 W) were selected, as they are representative of oceanic conditions. Table A-II shows the monthly averages for τ^A

TABLE A-2

Monthly averages for atmospheric turbidity parameters $\tau^A(1\ \mu m)$ and α. Measurements made in Lajes, Azores (38° 45N, 27° 05W) obtained from Anonymous (1977)

Month	Number of measurements	$\tau^A(1\ \mu m)$	α
J	9	0.126	1.080
F	5	0.154	1.093
M	5	0.195	1.074
A	5	0.308	0.781
M	37	0.241	1.031
J	20	0.203	1.145
J	24	0.299	0.894
A	30	0.242	1.014
S	23	0.253	0.877
O	14	0.233	0.829
N	6	0.199	0.609
D	4	0.212	0.771

(1 μm) and α. The turbidity minimum is observed in January ($\tau^A(1\ \mu m) = 0.13$), whereas two maxima are observed, in April and July ($\tau^A(1\ \mu m) = 0.3$). The annual average and variance of α respectively are equal to 0.93 and 0.3. The range of α variation thus is relatively small for ocean sites.

Acknowledgments

This research was supported by the 'Centre National de la Recherche Scientifique' (C.N.R.S.) and by the 'Centre National d'Etudes Spatiales' (C.N.E.S.).

The authors wish to thank Dr. M. Herman and J. Lenoble for introducing them to the subject and for their helpful assistance, and L. F. Martin for his aid in the translation of this paper.

References

Anonymous: 1977, 'Global Monitoring of the Environment for Selected Atmospheric Constituents 1975', *Environmental Data Service – Asheville* NC 28801 U.S.A.

Arvesen, J. C., Millard, J. P., and Weaver, E. C.: 1973, 'Remote Sensing of Chlorophyll and Temperature in Marine and Fresh Waters', *Astronaut. Acta* **18**, 229–239.

Box, M. A., and Lo, S. Y.: 1976, 'Approximate Determination of Aerosol Size Distribution', *J. Appl. Meteorol.* **15**, 1068–1076.

Clarke, G. L., Ewing, G. C., and Lorensen, C. J.: 1970, 'Spectra of Backscattered Light from the Sea Obtained from Aircraft as a Measure of Chlorophyll Concentration', *Science* **167**, 1119–1121.

Cox, C., and Munk, W.: 1965, 'Slopes of the Sea Surface Deduced from Photographs of Sun Glitter', *Bull. Scripps Inst. Oceanogr. Univ. Calif.* **6**, 401–488.

Curran, R. L.: 1972, 'Ocean Color Determination through a Scattering Atmosphere', *Appl. Opt.* **11**, 1857–1866.

Deschamps, P. Y., Lecomte, P., and Viollier, M.: 1977, 'Remote Sensing of Ocean Color and Detection of Chlorophyll Content', *Proc. 11th Int. Symp. on Remote Sensing of Environment, Ann Arbor*, 1021–1033.

Gordon, H. R.: 1978, 'Removal of Atmospheric Effects from Satellite Imagery of the Oceans', *Appl. Opt.* **17**, 1631–1636.

Hovis, W. A., Forman, M. L., and Blaine, L. R.: 1973, 'Detection of Ocean Color Changes from High Altitude', *NASA* X-652-73-371.

Hovis, W. A.: 1978, 'The Coastal Zone Color Scanner (CZCS) Experiment', *The Nimbus 7 Users' Guide NASA*, G.S.F.C.

Hoyt, D. V.: 1977, 'A Redetermination of the Rayleigh Optical Depth and its Application to Selected Solar Radiation Problems', *J. Appl. Meteorol.*, **16**, 432–436.

Kattawar, G. W., and Humphreys, T. I.: 1976, 'Remote Sensing of Chlorophyll in an Atmosphere–Ocean Environment: A Theoretical Study', *Appl. Opt.* **15**, 273–282.

London, J., Bojkov, R. D., Oltsùans, S., and Kelly, J. I.: 1976, 'Atlas of the Global Distribution of Total Ozone', *NCAR/TN/133 + STR.*

McClatchey, R. A., Fenn, R. W., Selby, J. E. A., Voltz, F. E., and Garine, J. S.: 1971, 'Optical Properties of the Atmosphere', *AFCRL 71–0279 Envir. Res. Papers No. 354.*

Miller, J. R., Jain, S. C., O'Neill, N. T., McNeil, W. R., and Thompson, K. P. B.: 1977, 'Interpretation of Airborne Spectral Reflectance Measurements over Georgian Bay', *Remote Sensing Environ.* **6**, 183–200.

Plass, G. N., Kattawar, G. W., and Hitzfelder, S. J.: 1976, 'Multiple Scattered Radiation Emerging from Rayleigh and Continental Haze Layers. 1: Radiance, Polarization and Neutral Points', *Appl. Optics*, **15**, 632–647.

Sekera, Z., and Kahle, A. B.: 1966, 'Scattering Functions for Rayleigh Atmospheres of Arbitrary Thickness', *Rand Report R-452-PR.*

Tanré, D., and Herman, M.: 1978, 'Correction de l'effet de diffusion atmosphérique pour les données de télédétection', *Proceedings of an Int. Conf. on Earth Observation held at Toulouse ESA-SP 134*, 355–360.

Viollier, M., Deschamps, P. Y., and Lecomte, P.: 1978a, 'Airborne Remote Sensing of Chlorophyll Content under Cloudy Sky as Applied to the Tropical Waters in the Gulf of Guinea', *Remote Sensing of Environ.* **7**, 235–248.

Viollier, M., Lecomte, P., Bougard, M., and Richard, A.: 1978b, 'Expérience aéroportée de télédétection (température et couleur de la mer) dans le détroit du Pas de Calais, *Oceanologica Acta*, **1**, 265–269.

Wilson, W. M., Austin, R. W., and Smith, R. C.: 1978, 'Optical Remote Sensing of Chlorophyll in Ocean Waters', *Proc. of the 12th Int. Symp. on Remote Sensing of Environment* (Manila), 1103–1113.

ANNEXE 3

MODELING OF THE ATMOSPHERIC EFFECTS AND ITS APPLICATION TO THE REMOTE SENSING OF OCEAN COLOR

DESCHAMPS P.Y., HERMAN M., TANRE D.

Laboratoire d'Optique Atmosphérique

Université des Sciences et Techniques de Lille

59655 VILLENEUVE D'ASCQ CEDEX

ABSTRACT

The effect of atmospheric scattering on ocean color measurements from space is considered. It is shown that the modeling of the atmospheric effects can be improved by taking into account not only the direct but also the diffuse component of the atmospheric transmittance, and by a more precise formulation of the interaction between molecular and aerosol scatterings in the calculation of the atmospheric reflectance. This method, necessitating two near infrared channels, should be applied to future ocean color experiments in order to better correct for variable aerosol reflectance. The relative accuracy of the aerosol reflectance correction would then be to within 5 %, as opposed to the more than 10 % obtained with previous modelings.

I - INTRODUCTION

The feasability of spacecraft based observance of ocean color - i.e. the upwelled scattered radiance of seawater, and the use of this measurement in the monitoring of marine parameters such as derived pigment and suspended material concentrations, has been demonstrated by the present CZCS (Coastal Zone Color Scanner) experiment on NIMBUS-7[1,2]. Often more than 80 % of the radiance measured from space is due to atmospheric scattering, but it has been shown that some correction can be made for this atmospheric perturbation[3]. CZCS experiment results seem to indicate that pigment concentration (C) could be derived to better than a 0.5 log C accuracy[2], compared with in-situ measurements of marine optics, i.e. with no atmospheric interference, which report a 0.2 log C accuracy[3] (both figure numbers apply to the case of oceanic waters with no yellow substance absorption). The accuracy of CZCS results seems to be limited by the small number of channels available in this experiment (440, 520, 550 and 670 nm). This allows measurement inversion for only a limited number of sea water property unknowns, and the removal of the atmospheric effect has to be made on the mere basis of the information content of the 670 nm channel[3,5], which implies an overly simple and rather inaccurate atmospheric correction.

In accordance with recent recommandations[6], future experiments should include a larger number of channels. Additional near infrared channels would allow better evaluation of atmospheric effects and improvement in the accuracy with which pigment and suspended material concentrations are determined. This will be possible only if atmospheric scattering models are developped which account for some processes often neglected, namely the diffuse transmittance of the atmosphere, and the interaction between molecular and aerosol scattering in the atmosphere.

In what follows, an improved atmospheric correction scheme is proposed which uses two measurements at two wavelengths in the near infrared. Atmospheric modeling of scattering processes previously neglected has been developped. The accuracy of this method is compared to that of the cruder method[3,4] previously proposed on the basis of the single 670 nm CZCS channel.

II - RADIATIVE TRANSFER IN THE OCEAN-ATMOSPHERE SYSTEM

Optical properties of the ocean and of the atmosphere are simplified as follows (this study deals with monochromatic quantities, but the subscript λ will be omitted to simplify notation) :

(i) we consider a scattering and non absorbant atmosphere of optical thickness τ. Gazeous absorption, e.g., the ozone band around 600 nm, can be expressed as an attenuation of the measured radiance and independent of scattering processes. Aerosol absorption is neglected.

(ii) the radiance backscattered by the water column is supposed diffuse after the crossing of the sea-air interface. Consequently, the ocean-atmosphere system may be described as an atmosphere with a lower boundary of diffuse reflectance. The specular reflection of direct solar radiation by the sea surface, "glitter", and its interaction with atmospheric scattering are not hereby discussed. We also neglect the specular reflection of diffuse atmospheric components, but this term may be included in the atmospheric reflectance which will be defined later [5].

These are simplifications commonly encountered in the litterature. Experimental results and theoretical computations have shown that the above hypothesis allows the nearly exact description of the ocean-atmosphere system.

The apparent reflectance ρ', of a scattering atmosphere with a lower diffuse boundary, ρ_w, measured from space, is exactly given [8,9] by

$$\rho'(\theta_o, \theta, \varphi) = \rho_a(\theta_o, \theta, \varphi) + \rho_w \frac{T(\theta_o)\, T(\theta)}{1 - \rho_w s} \qquad (1)$$

θ_o is the zenith solar angle,

θ is the zenith observation angle

φ is the relative azimuth between the incident and observation vertical planes.

Eq. 1 allows the description of radiative transfer in a scattering atmosphere with the help of only three atmospheric functions : $\rho_a(\theta_o, \theta, \varphi)$ is the atmospheric reflectance, $T(\theta)$ is the total (i.e. direct plus diffuse) atmospheric transmittance and s is the spherical albedo of the atmosphere. Apparent reflectance ρ'($\rho' = \frac{\pi L'}{\cos \theta_o f}$, f is the solar constant) is used rather than the measured radiance L' in order to obtain dimensionless functions in Eq. (1). In the case of ocean color measurement through a clear atmosphere, ρ_w and s are small and Eq. (1) may be written,

$$\rho'(\theta_o, \theta, \varphi) \simeq \rho_a(\theta_o, \theta, \varphi) + \rho_w\, T(\theta_o)\, T(\theta) \qquad (2)$$

Based on Eq. (2), the scattering effect correction requires the knowledge of only two atmospheric functions. The main problem is the determination of atmospheric reflectance ρ_a (the atmospheric radiance L_a) with sufficient accuracy (typically 0.001). This point will be discussed in sections IV and V.

The assessment of the transmittance factor $T(\theta)\ T(\theta_o)$ is less critical but should be considered if we hope to markedly improve the accuracy of the pigment concentration determination. This is discussed in the following section.

III - ASSESSMENT OF TRANSMITTANCE FUNCTION

The radiance L' measured from space is frequently given[3] as

$$L'(\theta_o, \theta, \varphi) = L_a(\theta_o, \theta, \varphi) + L_w\, e^{-\tau/\cos\theta} \qquad (3)$$

where L_a is atmospheric radiance scattered by the atmosphere and L_w is the radiance backscattered by the water column at the bottom of the atmosphere. The definitions of $\rho_a(\theta_o, \theta, \varphi)$ in Eq. (1) and of $L_a(\theta_o, \theta, \varphi)$ in Eq. (3) are similar, and differ only by the normalisation factor $\frac{\pi f}{\cos\theta_o}$. But it must be noted that the formulation of the transmittance is incomplete or incorrect in Eq. (3) ;

(i) direct transmittance $e^{-\tau/\cos\theta}$ must be replaced in Eq. (3) by total transmittance $T(\theta)$,

(ii) L_w also depends on atmospheric scattering through the total irradiance available at the bottom of the atmosphere ; the corresponding term $\frac{T(\theta_o)}{1-\rho_w s} \simeq T(\theta_o)$ is included in L_w.

Ocean color measurements are frequently processed by using the ratio of reflectances backscattered by the sea water at two different wavelengths. In this way, it is easy to evaluate inaccuracy due to transmittance factor assessment. For example,[3] the pigment concentration C is derived from the ratio of two measurements at λ_1 and λ_2, by means of

$$\log_{10} C = a + b \log_{10}\left(\frac{L_w(\lambda_1)}{L_w(\lambda_2)}\right) \qquad (4)$$

with a = - 0.297, b = - 1,269 for λ_1 = 450 nm and λ_2 = 550 nm .

We first note that the ratio of radiances L_w used in Eq. (4) will depend slightly on the atmosphere and it should be more appropriate to use a ratio of reflectances :

$$\log_{10} C = a' + b' \log_{10}\left(\frac{\rho_w(\lambda_1)}{\rho_w(\lambda_2)}\right) \qquad (5)$$

The use of Eq. (3) and (4) instead of the more exact formula given in Eq. (2) and (5) will produce relative error $\frac{dC}{C}$ in the pigment concentration determination

$$\frac{dC}{C} = b \log_{10} \frac{T(\theta_o, \lambda_1)\, T(\theta, \lambda_1)\, e^{-\tau(\lambda_1)/\cos\theta}}{T(\theta_o, \lambda_2)\, T(\theta, \lambda_2)\, e^{-\tau(\lambda_2)/\cos\theta}} \qquad (6)$$

$\frac{dC}{C}$ is given in Table 1, as computed for three different scattering atmosphere models : (R) contains no aerosols and would correspond to the best measurement conditions, (V23) corresponds to ground visibility of 23 km and to standard measurement conditions, (V5) corresponds to ground visibility of 5 km and to extreme measurement conditions. The corresponding optical thicknesses have been calculated from the aerosol optical properties[10] and are given in Table 1. As shown in Table 2, the use of approximate Eq. (3) and (4) leads to errors which depend on geometrical conditions and are up to 6 % under standard conditions (V23) and up to 25 % under extreme atmospheric conditions (V5).

From this result, it can be concluded that the assessment of transmit-

tance factor is not a critical problem. The use of an approximate formulation would only explain a small part of the inaccuracies presently observed in the retrieval of pigment concentration. But use of the more exact Eq. (2) and (5) must be recommended to access ρ_w^λ to better remove the atmosphere influence in futur experiments. Once this point is clarified, there remains the main problem of the evaluation of the atmospheric reflectance $\rho_a(\theta_o, \theta, \phi)$.

IV - ATMOSPHERIC REFLECTANCE

IV.1 - Background

Under clear conditions, the atmospheric reflectance results from scattering by a rather constant number of molecules and a variable aerosol content.

When no aerosols are present, the molecular component of the atmospheric reflectance can easily be computed from the molecular optical properties known with sufficient accuracy. For practical use in an atmospheric correction algorithm the only problem is that the large value of the atmospheric reflectance to be corrected, about 0.1 at 450 nm, requires the precise calibration of the instrument against the solar constant, f, on the order of 1 %, if an accuracy of 0.001 in the reflectance is to be obtained[11,12].

The aerosol contribution to the atmospheric reflectance presents the same large variability in space and time as does the aerosol content. A few in situ ground measurements thus would not provide all of the aerosol parameters, and particularly the aerosol content, necessary for atmospheric correction at all locations on the satellite imagery. The estimation of the atmospheric reflectance must thus rely only on satellite measurements.

This problem may be solved by assuming the following approximate equations :

$$\rho_a(\theta_o, \theta, \varphi) = \rho_a^R(\theta_o, \theta, \varphi) + \rho_a^P(\theta_o, \theta, \varphi) \quad (7)$$

where R and P refer respectively to scattering by molecules or by aerosols.

$$\rho_a^P(\theta_o, \theta, \varphi) \sim \tau^P \quad (8)$$

$$\tau^P \sim \lambda^{-n} \quad (9)$$

where n, the Angström exponent, describes the wavelength variation of the aerosol optical thickness, τ^P.

Based on Eq. (7) to (9), the following atmospheric correction can be proposed

(i) the atmospheric reflectance $\rho_a(\theta_o, \theta, \varphi)$ is derived from measurements at wavelength $\lambda \geqslant 0.7\mu m$ where $\rho_w = 0$

(ii) the aerosol component $\rho_a^P(\theta_o, \theta, \varphi)$ is obtained by subtracting the computing molecular component $\rho_a^R(\theta_o, \theta, \varphi)$ from the total reflectance $\rho_a(\theta_o, \theta, \varphi)$

(iii) the aerosol component $\rho_a^P(\theta_o, \theta, \varphi)$ is then determined at the other wavelengths of interest for ocean color ($\lambda < 0,7$ m), by assuming $\rho_a^P(\theta_o, \theta, \varphi) \sim \lambda^{-n}$

(iiii) the atmospheric reflectance $\rho_a(\theta_o, \theta, \varphi)$ is finally obtained by adding the above aerosol component to a computed molecular component.

When only one channel is available at $\lambda \geqslant 0.7$ µm as in the CZCS experi-

ment, a mean value of the Angström exponent n has to be estimated which quickly limits the accuracy of the atmospheric correction. In the case of two or several channels at $\lambda \geqslant 0.7$ µm, n can be determined on the simple basis of the satellite experiment.

Eq. (7) and (8) are a valid approximation as far as the amount of multiple scattering is within reasonable limits, i.e. at small aerosol optical thickness τ^P. When τ^P increases, (i) multiple interactions between molecular and aerosol scatterings progressively invalidate Eq. (7), (ii) multiple scattering in the aerosol layer can slightly modify the wavelength dependence of aerosol reflectance given by Eqs. (8) and (9). Eq. (7) to (9) prove efficient at the small optical thicknesses which are currently observed[4], but it is interesting to investigate its validity at larger optical thicknesses. In what follows, exact computed results have been compared to the approximate results obtained by (7) to (9). A more complete and accurate formula for the determination of atmospheric reflectance is proposed to improve the atmospheric correction and to allow it to be extended to a lower solar elevation, higher aerosol content and shorter wavelength.

IV.2 - Validity of the adding of aerosol and molecular reflectances

The validity of the adding of aerosol and molecular components as given by Eq. (7), has been investigated. The exact atmospheric reflectance $\rho_a(\theta_o, \theta, \varphi)$ has been computed for different scattering atmosphere models with realistic optical properties and vertical profiles of aerosol concentration. The molecular component $\rho_a^R(\theta_o, \theta, \varphi)$ (i.e. with no aerosol) and the aerosol component $\rho_a^P(\theta_o, \theta, \varphi)$ (i.e. with no molecules present) have also been separately computed. The difference between the exact value and the approximation of Eq. (7) :

$$C^{R,P}(\theta_o, \theta, \varphi) = \rho_a(\theta_o, \theta, \varphi) - \rho_a^R(\theta_o, \theta, \varphi) - \rho_a^P(\theta_o, \theta, \varphi) \quad (10)$$

will be called the coupling term between the molecular and the aerosol scatterings. $C^{R,P}(\theta_o, \theta, \varphi)$ is obviously the error on $\rho_a(\theta_o, \theta, \varphi)$ introduced by using Eq. (7) if $\rho_a^P(\theta_o, \theta, \varphi)$ is perfectly known.

Fig. 1a to 1c show the dependance of the coupling term versus the solar zenith angle θ_o for a viewing at nadir ($\theta = 0$). Figures refer to different wavelengths, 450, 550 and 850 nm, and then to different molecular optical thicknesses, 0,216, 0,095 and 0,016, to which is added a variable aerosol optical thickness 0,264, 0,450 and 0,878. A cursory glance at the curves shows that they have similar shapes, $C^{R,P}(\theta_o, \theta, \varphi)$ is about nul at $\theta_o = 30°$. $C^{R,P}(\theta_o, \theta, \varphi)$ systematically increases with the molecular optical thickness i.e. at shorter wavelengths and with the aerosol content.

The coupling term $C^{R,P}$ is the error introduced into the estimation of the atmospheric reflectance by using Eq. (7). Reference must be made to the required accuracy of ρ_w, typically 0.001, to discuss the validity of Eq. (7). At low aerosol content ($\tau^P = 0.264$), this accuracy is obtained whatever may be solar zenith angle ($0 \leqslant \theta_o \leqslant 60°$) and the wavelength ($\lambda > 450$ nm). But the coupling term $C^{R,P}(\theta_o, \theta, \varphi)$ rapidly exceeds 0.001 with increased aerosol content or at shorter wavelengths, such as $\lambda = 400$ nm, ($\tau^R = 0.35$), which has been proposed to discriminate between the absorption by pigments and by yellow substances.

We thus conclude that Eq. (7) generally remains a rather good approximation, for a mean aerosol content, at least for the present utilisation of the CZCS. For this experiment, the fact that the Angström exponent n be unknown results in an error in the wavelength extrapolation of the aerosol component $\rho_a^P(\theta_o, \theta, \varphi)$ which is superior to the coupling term $C^{R,P}(\rho_o, \theta, \varphi)$. Nevertheless,

future experiments with an increased number of channels, for the estimation of n in the near infrared, and for the absorption type discrimination at λ = 400 nm, will require that the coupling term be accounted for in order to improve the accuracy in the atmospheric reflectance correction.

IV.3 - Modeling the coupling term between aerosols and molecules

An analytical formulation, giving a good approximation of the coupling term between scattering by aerosols and by molecules, has been searched for in order to be able to improve the accuracy of the atmospheric reflectance correction.

Most of the aerosol is located in the lower kilometers of the atmosphere and it seems reasonable to simplify the scattering atmosphere as a two layer model with molecules above the aerosols. Results of numerical tests show that, for $\theta < 30°$, the reflectances obtained with this simple model, are in agreement, within better than 0.001, with the reflectances obtained by using a more realistic vertical profile of the aerosol concentration such as given in (10).

For this two layer model, the formulation of Eq. (1) could be applied to the scattering molecular layer if the reflectance of the aerosol layer $\rho_a^P(\theta_o, \theta, \varphi)$ were Lambertien :

$$\rho_a(\theta_o, \theta, \varphi) = \rho_a^R(\theta_o, \theta, \varphi) + \rho_a^P(\theta_o, \theta, \varphi) \frac{T^R(\theta_o)\, T^R(\theta)}{1-\rho_a^P(\theta_o, \theta, \varphi) S^R} \qquad (11)$$

where $T^R(\theta)$ and S^R are the total transmittance and sperical albedo of the molecular layer

$$T^R(\theta) = e^{-\tau^R/\cos\theta} + E^R(\theta) \qquad (12)$$

where $E^R(\theta)$ is the diffuse transmittance of the molecular layer. Nevertheless the accuracy achieved by using Eq. (11) is not satisfactory and may be worse than that obtained with simpler Eq. (7).

To improve this modeling, one has to account for the anisotropy of the aerosol reflectances. Computations show that the angular dependance of the aerosol reflectance corresponds to an approximate law

$$\rho_a^P(\theta_o, \theta, \varphi) \sim \frac{1}{\mu} \qquad (13)$$

whatever the solar irradiance be, direct or diffuse (fig. 2a and 2b).

We thus define the following functions for a molecular layer illuminated by a unit irradiance but with an angular dependance $\frac{1}{\mu}$,

- diffuse transmittance $E'^R(\theta)$

- total transmittance $T'^R(\theta) = \frac{1}{2}\frac{e^{-\tau^R/\mu}}{\mu} + E'^R(\theta)$

- spherical albedo S'^R.

If ρ_a^P, A^P and S^P are the directionnal reflectance, the plane albedo, and the sperical albedo of the aerosol layer, we now can write the different interactions between the two layers as,

$$\rho_a(\theta_o, \theta, \varphi) = \rho_a^R(\theta_o, \theta, \varphi) + e^{-\tau^R/\cos\theta_o}\, \rho_a^P(\theta_o, \theta, \varphi)\, e^{-\tau^R/\cos\theta}$$
$$+ e^{-\tau^R/\cos\theta_o}\, A^P(\theta_o)\, E'^R(\theta)$$
$$+ E^R(\theta_o)\, S^P\, T'^R(\theta) \qquad (14)$$
$$+ T^R(\theta_o)\, \frac{S'^R (S^P)^2}{1 - S'^R S^P}\, T'^R(\theta)$$

Eq. (14) may be simply written

$$\rho_a(\theta_o, \theta, \varphi) = \rho_a^R(\theta_o, \theta, \varphi) + C_1^R\, \rho_a^P(\theta_o, \theta, \varphi) + C_2^R\, A^P(\theta_o) + C_2^R\, S^P \qquad (15)$$

where C_1^R, C_2^R, C_3^R and ρ_a^R can be computed at any wavelength for the molecular component.

Eq. (15) is obviously more complex than the simple Eq. (7) and requires the determination of three coefficients to account for the aerosol influence. Nevertheless, it will be seen that some correlation exists between $\rho_a^P(\theta_o, \theta, \varphi)$, $A_p(\theta_o)$, and S_p, and that Eq. (15) may in practice be used for the atmospheric correction.

From Table 3, where results obtained by Eq. 15 are compared to exact results, it may be seen that the accuracy of Eq. (15) is much better than the values of $\rho_a(\theta_o, \theta, \varphi)$ obtained by the Eq. (7). In table 3, values have been reported for the following conditions λ = 450 nm, two solar zenith angles θ_o = 15 and 60°, two optical thicknesses corresponding to ground visibilities of 23 and 5 km[10], and seven observation directions within 30° of nadir. But it must be

noted that the more approximate Eq. (7) appears to be sufficiently in most cases, because multiple interactions between Rayleigh and aerosols nearly perfectly balance the direct attenuation of the aerosol reflectance $\rho_a^P(\theta_o, \theta, \varphi)$ by the molecular layer, which is $\exp(-\tau_R/(\frac{1}{\mu} + \frac{1}{\mu_o}))$.

When $\tau_R.\tau_p$, the product of optical thicknesses is large, the coupling term $C^{R,P}(\theta_o, \theta, \varphi)$ cannot be neglected, and the use of Eq. (7) gives errors of a few 0.01 in $\rho_a(\theta_o, \theta, \varphi)$ while it may be seen that Eq. (15) still gives correct results and allows one to reduce the above error by a factor of 2 to 10.

V - Discussion

Based on the extrapolation of measurements acquired in the infrared, the atmospheric correction for ocean color will have two major sources of error : first, inaccuracy in the extrapolation of aerosol reflectance ρ_a^P from longer wavelengths ($\lambda > 0.7$ m), and second, the modeling of the coupling term between aerosol and molecular scatterings.

For the estimation of the first type of error, we will refer to the accuracy, with which the Angström exponent (n), may be determined (and this also includes the possible deviation of the wavelength dependance of the aerosol optical depth from the standard law, λ^{-n}, which has been assumed. The error $\varepsilon(\rho_a^P(\lambda))$ in the determination of $\rho_a^P(\lambda)$ is given by :

$$\frac{\varepsilon(\rho_a^P(\lambda))}{\rho_a^P(\lambda)} = (\frac{\lambda_o}{\lambda})^{\varepsilon(n)} - 1 \qquad (16)$$

where λ_o is the wavelength used in the infrared for the determination of ρ_a^P before the extrapolation, e.g. 0.7 m, and λ is the wavelength of interest for ocean color measurement, e.g. 0.45 m. It may be assumed that $\varepsilon(n) = 0.3$ in the case where only a mean value of n , $n \simeq 1$, can be used because only one channel is available in the near infrared for the atmospheric correction, like in the CZCS experiment[5]. An improved value of $\varepsilon(n)$, $\varepsilon(n) = 0.1$, could be anticipated with the use of the two near infrared channels proposed for some planned future experiments[7]. For $\lambda = 0.45\mu m$ and $\lambda_o = 0.70\mu m$, the relative error due to the extrapolation would then be equal to 4 % for $\varepsilon(n) = 0.1$, and 14 % for $\varepsilon(n) = 0.3$.

The estimation of the error introduced by the modeling of an atmosphere with aerosols and molecules has been derived from Table 3. At $\lambda = 0.45$ µm, for two solar zenith angles, $\theta_o = 15°$ and 60°, and for two aerosol contents, (V23) and (V5), the following values have been calculated for the set of angles θ within 30° from nadir : the mean value, $\overline{\rho_a^P}$ of the aerosol reflectance, and the standard deviation, $\varepsilon'(\rho_a^P)$, around the mean value introduced by using Eq. (7) or Eq. (15) on the retrieval of ρ_a^P. The corresponding relative error $\varepsilon'(\rho_a^P)/\overline{\rho_a^P}$ is given in Table 4 : the simple modeling of Eq. (7) gives errors of up to 12 %, while the more sophisticated Eq. (15) remains below 3 %.

Relative error given in Table 4 has to be compared with values of 4 % and 14 % for $\varepsilon(n) = 0.1$ and 0.3. It should be noted that the modeling given by Eq. (7) may be considered as satisfactory in the case of only one near infrared channel, as in the CZCS experiment, for the atmospheric correction. But an improved determination of the wavelength dependance of the aerosol reflectance from two near infrared channels, will in the future require, in order to be coherent, similar improvement of the scattering atmosphere model and the

use of more accurate formulas such as the one given by Eq. (15).

For practical application, the basic algorithm exposed in section IV-1 may be conserved with the following modifications :

(i) the Angström esponent is determined from the two near infrared derived values of ρ_a^P, at λ_o and λ'_o, after correcting for molecular scattering :

$$n = \frac{\text{Log } (\rho_a^P(\lambda_o)/\rho_a^P(\lambda'_o))}{\text{Log } (\lambda_o/\lambda'_o)} \qquad (17)$$

(ii) Eq. (7) is replaced by Eq. (15) when adding molecular and aerosol components at the shorter wavelengths. The use of Eq. (15) requires the estimation of the aerosol plane albedo, $A^P(\theta_o)$, and the spherical albedo, s^P, which may be obtained from an empirical relationship between the albedoes and the aerosol reflectance ρ_a^P, as demonstrated in Fig. 3a and 3b for several different aerosol models.

CONCLUSION

Present atmospheric correction for ocean color measurement from space can be improved in the two following ways.

1) - Not only the direct, but also the diffuse transmittances occuring during the two crossings of the scattering atmosphere must be taken into account for the calculation of the solar radiation backscattered by the ocean. Nethertheless, this only slightly improves on the accuracy of ocean color measurements.

2) - The comparison between the exact atmospheric reflectance ρ_a, and the value calculated by simply adding the molecular and aerosol components, $(\rho_a^R + \rho_a^P)$, shows errors which increase with the optical thickness, and are frequently above 10 % of the ρ_a^P value to be corrected. Nethertheless, this is presently adequate for the CZCS experiment considering the uncertainty in the spectral behaviour of the aerosol reflectance. A more accurate modeling of the interaction between molecular and aerosol scatterings is proposed, reducing the error to less than 3 % of the ρ_a^P value, which would allow improvement of ocean color measurements in future experiments, if the wavelength dependance of the aerosol reflectance is parallelly better determined by using two near infrared channels.

RÉFÉRENCES

1. *W.A. HOVIS, D.K. CLARK, F. ANDERSON, R.W. AUSTIN, W.H. WILSON, E.T. BAKER, D. BALL, H.R. GORDON, J.L. MUELLER, S.Z. EL-SAYED, B. STURM, R.C. WRIGLEY and C.S.YENTSCH,*
Science 210, 60 (1980).

2. *H.R. GORDON, D.K. CLARK, J.L. MUELLER and W.A. HOVIS,*
Science 210, 63 (1980).

3. *H.R. GORDON and D.K. CLARK,*
Boundary-Layer Meteorol. 18, 299 (1980).

4. *H.R. GORDON,*
Appl. Opt. 17, 1631 (1978).

5. *M. VIOLLIER, D. TANRE and P.Y. DESCHAMPS,*
Boundary-Layer Meteorol., 18, 247 (1980).

6. A Meeting of experts during the IURCM colloquium on "Passive Radiometry of the ocean", Sidney, B.C., june 1978 suggested additional channels at 745, 880, 1060 nm and 2.2 µm for an improved atmospheric and sun glitter corrections, see *A.Y. MOREL and H.R. GORDON,* Boundary-Layer Meteorol. 18, 343 (1980).

7. *P.Y. DESCHAMPS, D. TANRE and M. VIOLLIER,*
"Evaluation critique des exigences radiométrique pour un equipement mesurant à bord d'un satellite la couleur des océans", ESA-CR-1390, july 1980, (Agence Spatiale Européenne, 8-10 rue Mario Nikis, 75738 Paris Cédex 15, France).

8. *S. CHANDRASEKHAR,*
Radiative Transfer (Clarendon Press, London, 1950).

9. *D. TANRE, M. HERMAN, P.Y. DESCHAMPS and A. DE LEFFE,*
Appl. Opt. 18, 3587 (1979).

10. *M. CLATCHEY R.A., R.W. FENN, J.E.A. SELBY, F.E. VOLTZ and J.S. GARING,*
"Optical properties of the Atmosphere", AFCRL 71-0279, Environmental Research Paper 354 (1971).

11. *H.R. GORDON,*
Appl. Opt., 20, 207-210 (1981).

12. *M. VIOLLIER,*

Appl. Opt., (1982) (in press).

13. *D. DEIRMENDJIAN,*

Electromagnetic Scattering by Spherical polydispersions, American Elsevier, New York, N.Y., (1969).

14. *R.S. FRASER,*

Scattering properties of Atmospheric aerosols, Scientific Report n° 2, Contrat N°AF 19(604) - 2429, University of California, (1959).

	λ = 450 nm	λ = 550 nm	λ = 650 nm	λ = 850 nm
τ^R	0,2157	0,0948	0,0481	0,0163
τ^P (V23)	0,2801	0,2348	0,2011	0,1550
τ^P (V5)	0,9305	0,7801	0,6681	0,5151

TABLE 1

Optical thicknesses of the three scattering model atmosphere, (R), (V23) and (V5).

θ_o	θ	(R)	(V23)	(V 5)
0	0	+ 0,010	+ 0,061	+ 0,158
0	41,4	+ 0,052	+ 0,052	+ 0,251
60	0	- 0,054	- 0,001	+ 0,110
60	41,4	- 0,009	+ 0,061	+ 0,212

TABLE 2

Relative inaccuracy, $\frac{dC}{C}$, in the determination of pigment concentration, from the ratio of measurements at 440 and 450 nm, introduced by the incomplete formulation of atmospheric effects as given by Eq. (3).

	SOLAR ZENITH ANGLE = 15°						SOLAR ZENITH ANGLE = 60°					
θ_v, φ_v	(1)	(2)	(3)	(4)	(5)	(6)	(1)	(2)	(3)	(4)	(5)	(6)
2,84 0	0,1039	0,1054	0,0827	0,0237	-0,0010	-0,0008	0,1260	0,1271	0,0959	0,0290	0,0022	-0,0006
17,64 0	0,0950	0,0966	0,0779	0,0172	0,0015	-0,0011	0,1267	0,1260	0,0882	0,0389	-0,0011	0,0002
17,64 90	0,1041	0,1057	0,0839	0,0219	-0,0001	-0,0010	0,1339	0,1353	0,1023	0,0302	0,0028	-0,0001
17,64 180	0,1185	0,1194	0,0904	0,0331	-0,0041	-0,0009	0,1551	0,1588	0,1262	0,0292	0,0034	0,0000
32,48 0	0,0934	0,0946	0,0749	0,0169	0,0028	-0,0007	0,1429	0,1504	0,0960	0,0645	-0,0101	0,0021
32,48 90	0,1040	0,1058	0,0850	0,0186	0,0022	-0,0006	0,1500	0,1512	0,1120	0,0364	0,0028	0,0010
32,48 180	0,1220	0,1236	0,0967	0,0282	-0,0013	-0,0005	0,1999	0,2051	0,1623	0,0421	0,0007	0,0017

23

103

T A B L E 3-a

Computed atmospheric reflectances at λ = 450 nm, for a moderate aerosol content ((V23) model).

(1) Atmospheric reflectance, ρ_a, with the exact vertical profile of aerosol concentration,
(2) Atmospheric reflectance, ρ_a, with an aerosol layer below a molecular layer, refered to below as the exact atmospheric reflectance
(3) Molecular atmospheric reflectance, $\rho_a^R(\tau^P = 0)$.
(4) Aerosol atmospheric reflectance, $\rho_a^P(\tau^R = 0)$.
(5) Difference between the exact value and the result given by Eq. (7).
(6) difference between the exact value and the result given by Eq. (15).

	SOLAR ZENITH ANGLE = 15°						SOLAR ZENITH ANGLE = 60°					
θ_V, φ_V	(1)	(2)	(3)	(4)	(5)	(6)	(1)	(2)	(3)	(4)	(5)	(6)
2,84 0	0,1591	0,1599	0,0827	0,0830	-0,0058	-0,0034	0,2019	0,2022	0,0959	0,1167	-0,0104	-0,0006
17,64 0	0,1477	0,1487	0,0779	0,0716	-0,0008	-0,0034	0,2164	0,2144	0,0882	0,1486	-0,0224	0,0010
17,64 90	0,1597	0,1607	0,0839	0,0809	-0,0041	-0,0033	0,2133	0,2140	0,1023	0,1222	-0,0105	0,0002
17,64 180	0,1817	0,1817	0,0904	0,1036	-0,0123	-0,0033	0,2300	0,2338	0,1262	0,1143	-0,0067	0,0002
32,48 0	0,1318	0,1522	0,0749	0,0774	-0,0001	-0,0027	0,2721	0,2676	0,0960	0,2231	-0,0515	0,0047
32,48 90	0,1622	0,1633	0,0850	0,0791	-0,0008	-0,0028	0,2417	0,2423	0,1120	0,1454	-0,0151	0,0025
32,48 180	0,1858	0,1867	0,0967	0,0976	-0,0076	-0,0026	0,2871	0,2929	0,1623	0,1445	-0,0139	0,0032

T A B L E 3-b

Same as for Table 3-a, but for a high aerosol content ((V5) model).

	Eq. (7)	Eq. (15)
θ_o = 15° V = 23 km	10.5 %	1.0 %
θ_o = 60° V = 23 km	12.3 %	2.6 %
θ_o = 15° V = 5 km	5.3 %	0.4 %
θ_o = 60° V = 5 km	10.6 %	1.3 %

TABLE 4

Relative accuracy, $\varepsilon'(\overline{\rho_a^P})/\overline{\rho_a^P}$ of the modeling of the atmospheric reflectance by Eq. (7) and Eq. (15).

FIGURE CAPTIONS

Fig. 1-a : The coupling term $C^{R,P}(\theta_o, \theta, \varphi) = \rho_a - \rho_a^R - \rho_a^P$ at 450 nm, $\theta = 0$, as a function of the solar zenith angle θ_o, for 3 aerosol contents corresponding to a ground visibility, V of 23, 15 and 5 km.

Fig. 1-b : Same as Fig. 1-a, at 550 nm.

Fig. 1-c : Same as Fig. 1-a, at 850 nm.

Fig. 2-a : Aerosol atmospheric reflectance, ρ_a^P, at 450 nm, for $\theta_o = 15°$, and for (V23), as a function of the viewing zenith angle in the solar incidence plane ($\varphi = 0 - 180°$).

Fig. 2-b : Same as Fig. 2-a, for (V5).

Fig. 3-a : Empirical relationship between the albedo and the aerosol reflectance for several different aerosols models versus the diffusion angle at $\lambda = 650$ nm.

1 model C ; m = 1,33 (ref. 10)
1' model C ; m = 1,50 (ref. 10)
2 model D ; m = 1,33 (ref. 14)
3 haze M ; m = 1,33 (ref. 13).

Fig. 3-b : Same as Fig. 3-a, but at $\lambda = 850$ nm.

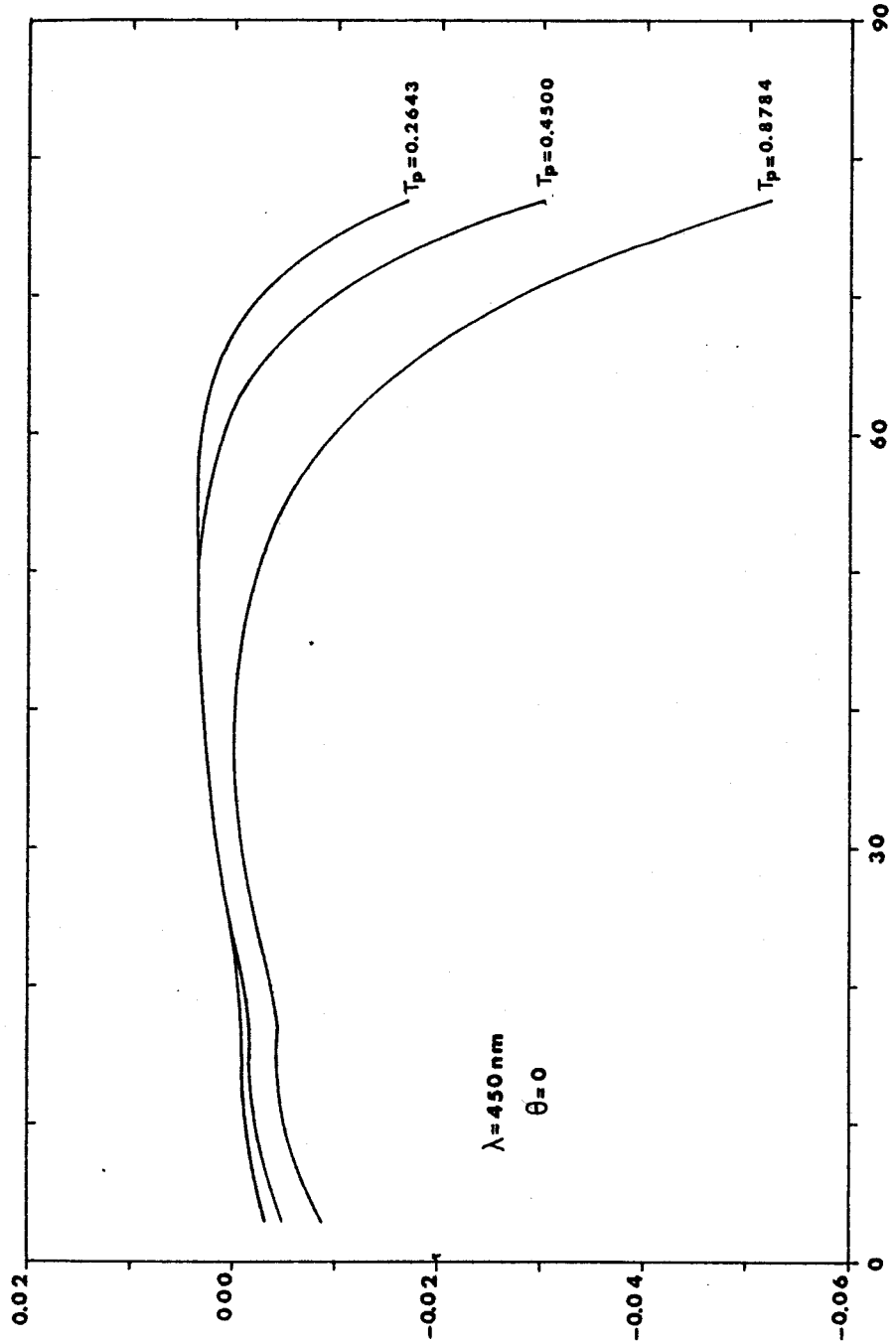

Fig. 1-a : The coupling term $C^{R,P}(\theta_o, \theta, \varphi) = \rho_a - \rho_a^R - \rho_a^P$ at 450 nm, $\theta = 0$, as a function of the solar zenith angle θ_o, for 3 aerosol contents corresponding to a ground visibility, V of 23, 15 and 5 km.

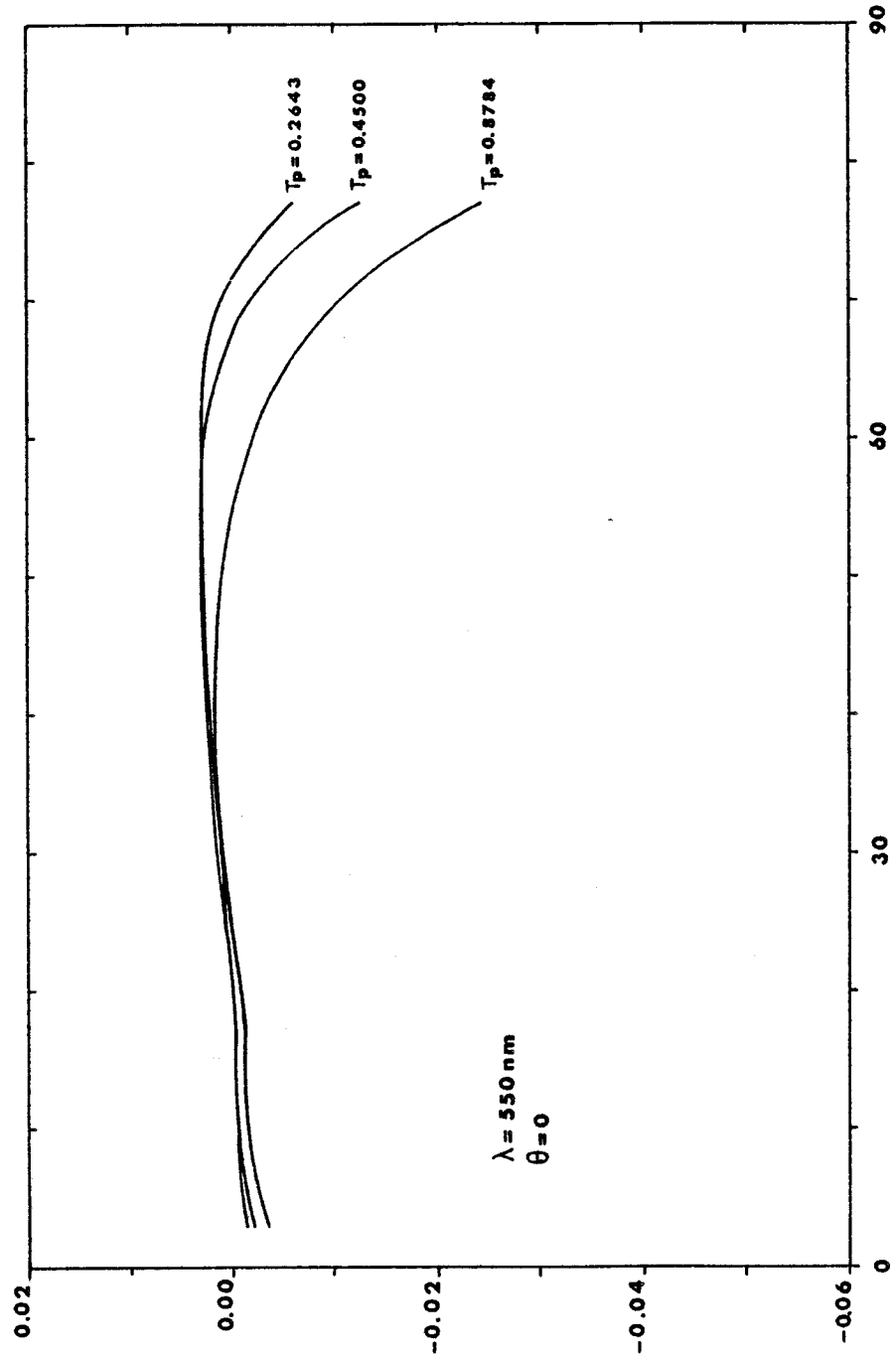

Fig. 1-b : Same as Fig. 1-a, at 550 nm.

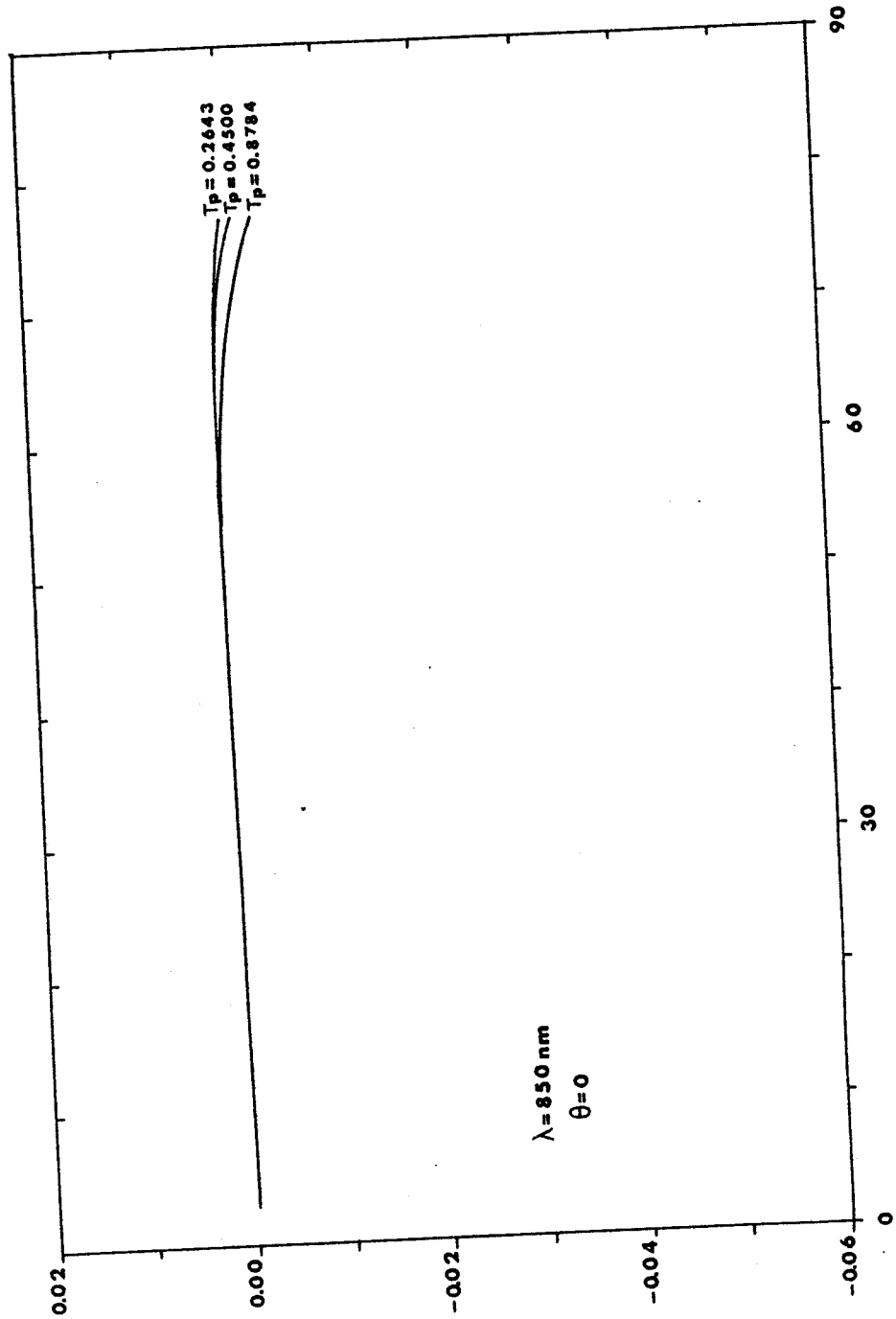
Tp=0.2643
Tp=0.4500
Tp=0.8784
λ=850nm
θ=0
0.02
0.00
-0.02
-0.04
-0.06
0
30
60
90

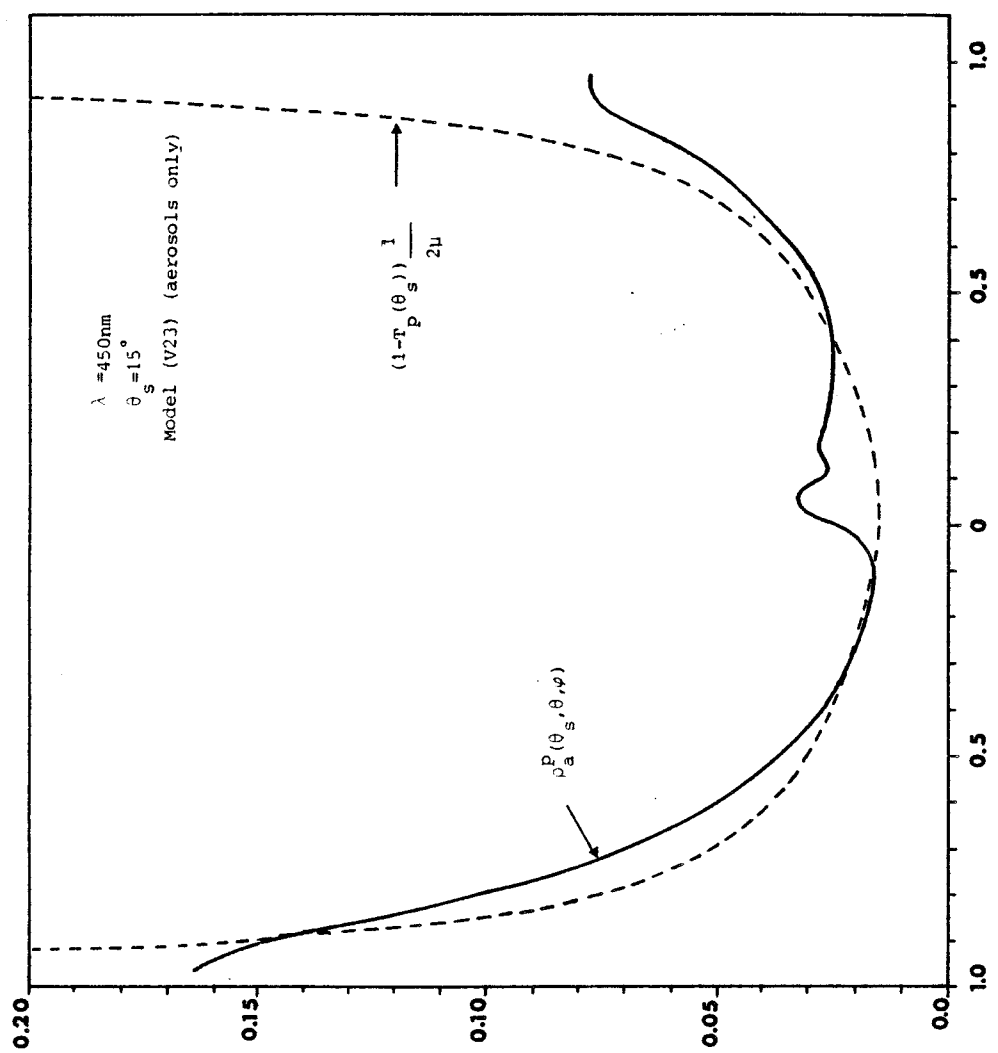

Fig. 2-a : Aerosol atmospheric reflectance, ρ_a^P, at 450 nm, for θ_o = 15°, and for (V23), as a function of the viewing zenith angle in the solar incidence plane (φ = 0 - 180°).

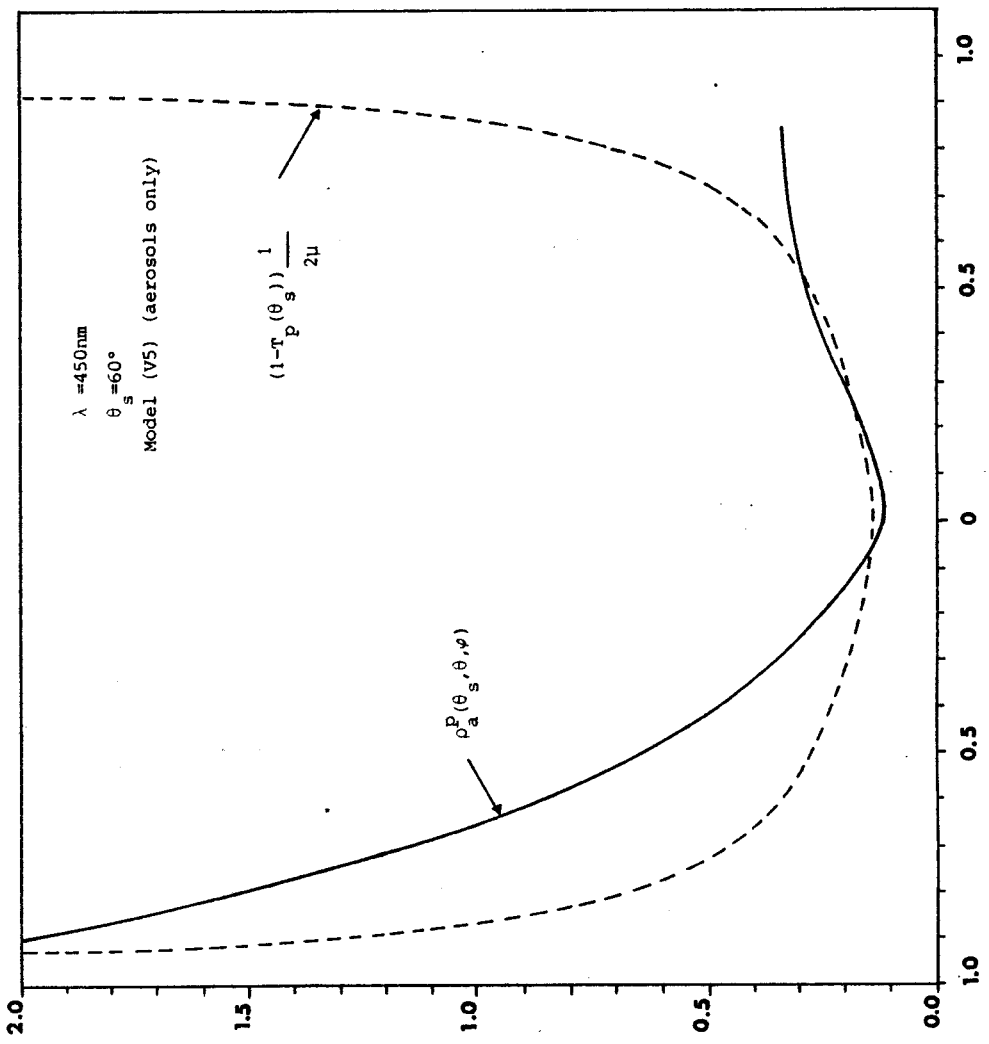

Fig. 2-b : Same as Fig. 2-a, for (V5).

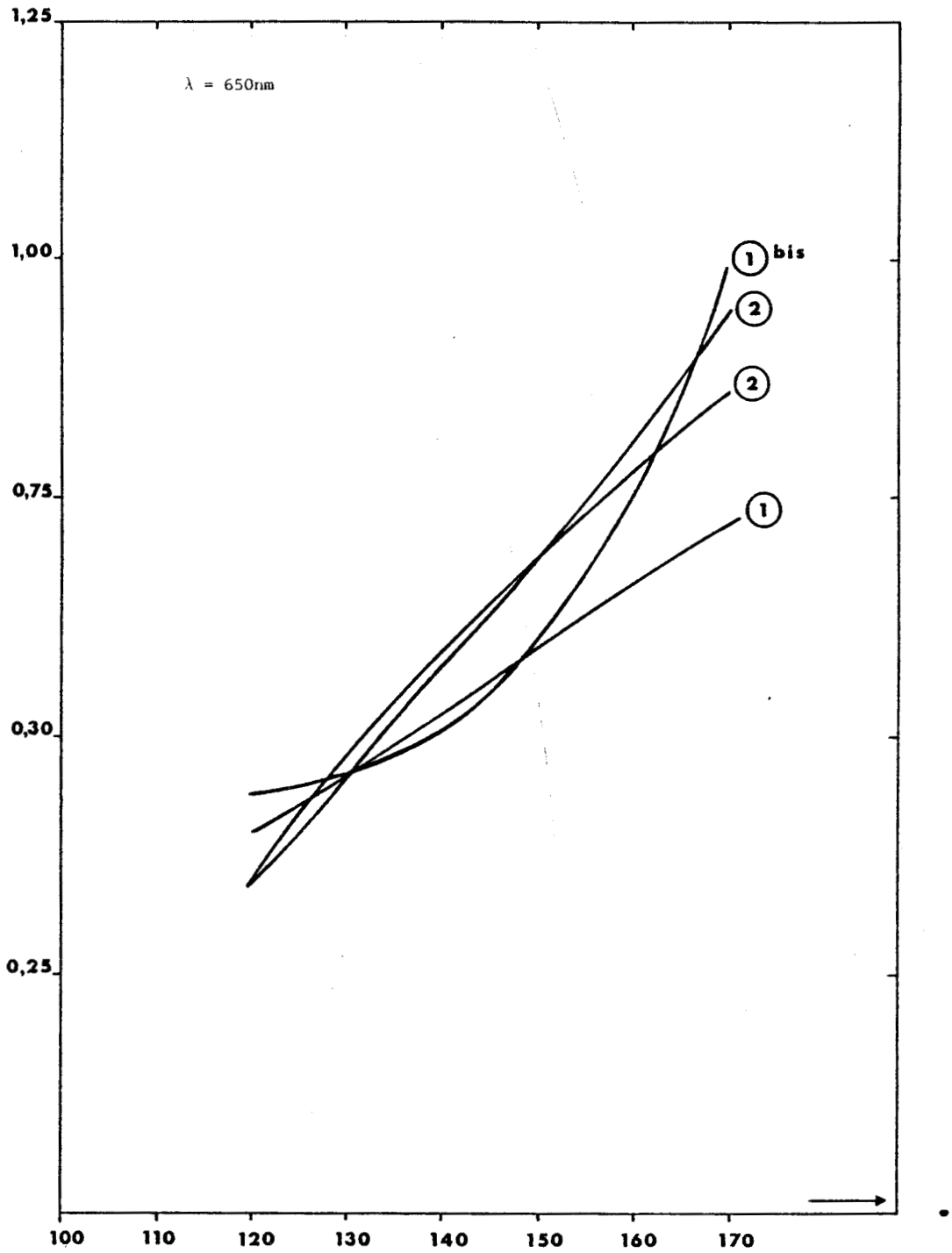

Fig. 3-a : Empirical relationship between the albedo and the aerosol reflectance for several different aerosols models versus the diffusion angle at λ = 650 nm.

1 model C ; m = 1,33 (ref. 10)
1' model C ; m = 1,50 (ref. 10)
2 model D ; m = 1,33 (ref. 14)
3 haze M ; m = 1,33 (ref. 13).

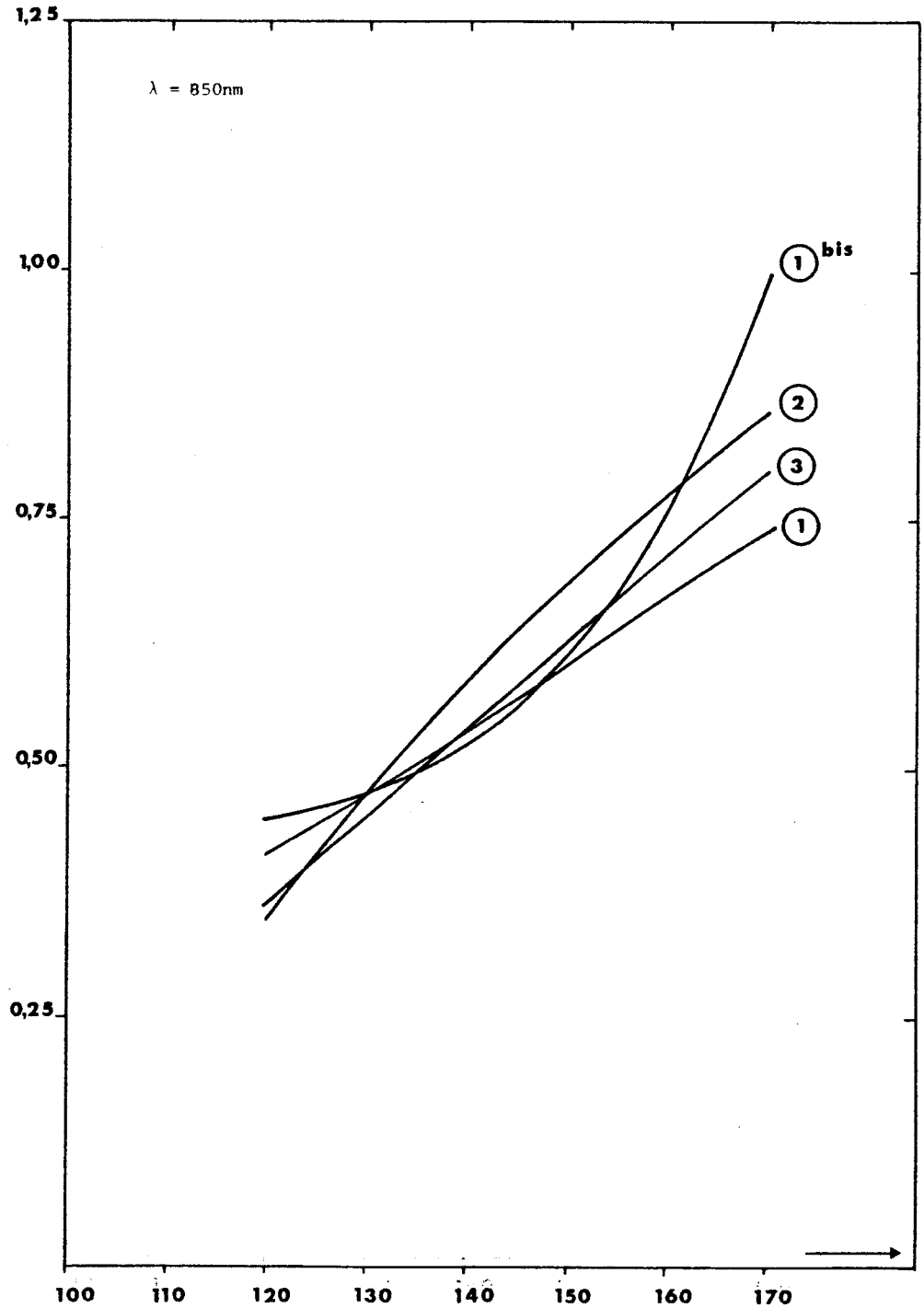

Fig. 3-b : Same as Fig. 3-a, but at λ = 850 nm.

III - APPLICATIONS EN RESSOURCES TERRESTRES (ANNEXES 4, 5, 6)

Pour l'étude de paysages terrestres dont les éléments (cas du parcellaire) peuvent atteindre de faibles dimensions (de l'ordre de la centaine de mètres), la diffusion atmosphérique provoque un mélange des signatures de cibles voisines. Dans une moindre mesure l'aspect directionnel des réflectances des cibles peut provoquer suivant la direction d'observation, des variations de réflectances équivalentes aux variations significatives permettant de séparer deux types de sol différents.

Avant d'étudier ces deux problèmes, regardons simplement l'ordre de grandeur du signal que nous voulons atteindre pour quelques exemples de sol.

Le cas des surfaces végétales est particulièrement important. Leur spectre est très typique, nettement marqué par les fortes bandes d'absorption de la chlorophylle dans le visible. La réflectance des végétaux, forte dans le proche infra-rouge, s'effondre ainsi assez brutalement à partir de 700 nm, la chlorophylle ne laissant subsister que le pic de réflectance secondaire, vers 500 nm, caractéristique de sa couleur verte.

Les spectres des terres nues et arides sont beaucoup plus monotones, et, sauf dans le cas du sable (plages, déserts), la réflectance reste généralement assez faible.

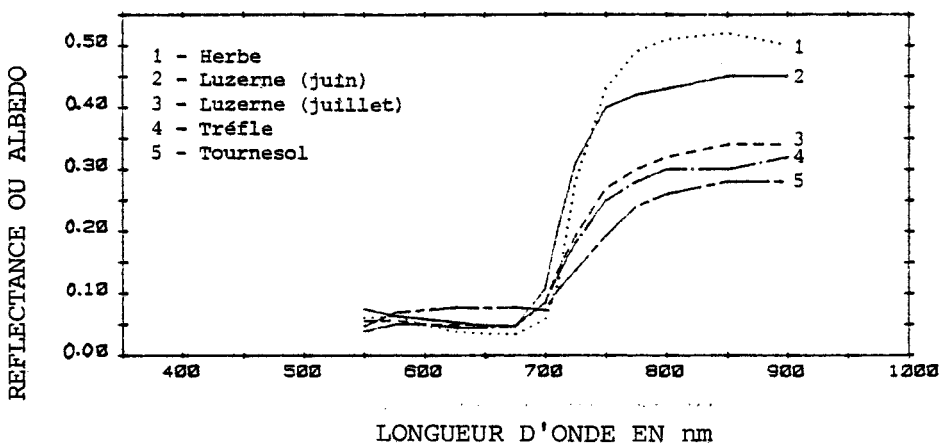

Dépendance spectrale de l'albédo pour différents types de végétation. (Réf. : KONDRATIEV et al., Pure Appl. Geophys. 59, 207, (1964)).

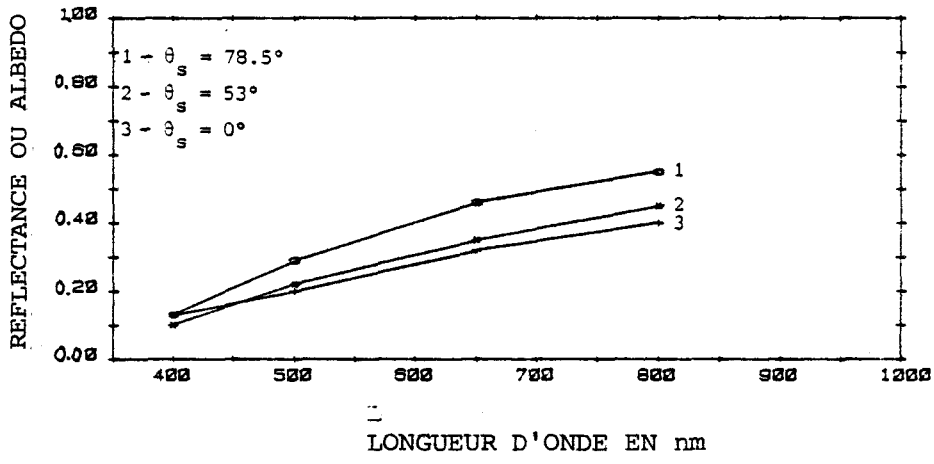

Dépendance spectrale de l'albédo du sable.
Albédo plan, pour différents angles d'incidence, θ_s,
du faisceau solaire. (Ref. : Manual of remote sensing, American society of Photogrammetry, Falls Chruch, Virginia, 1975, p. 100).

Une visualisation commode des effets directionnels est donnée par les indicatrices de réflectance, qui sont des représentations polaires dans un plan vertical donné de la réflectance bidirectionnelle $\rho(\theta_s, \theta, \phi)$, en fonction de θ, pour une incidence θ_s fixe. L'indicatrice d'un réflecteur de Lambert se réduira à un demi cercle de rayon ρ.

Les figures suivantes montrent des exemples d'indicatrices de réflectance pour la savanne et une forêt. Les résultats correspondent au plan vertical qui contient le soleil et où l'effet directionnel est maximum. Deux directions d'incidence, visualisées sur les figures, sont considérées dans chaque cas.

Ces résultats ne sont qu'indicatifs. Ici par exemple le minimum de réflectance observé à 90° de la direction d'incidence environ correspond à un poids maximum des ombres portées dans le signal.

Ces figures sont cependant représentatives des gammes de variation angulaire de la réflectance auxquelles on peut s'attendre au dessus des sites terrestres.

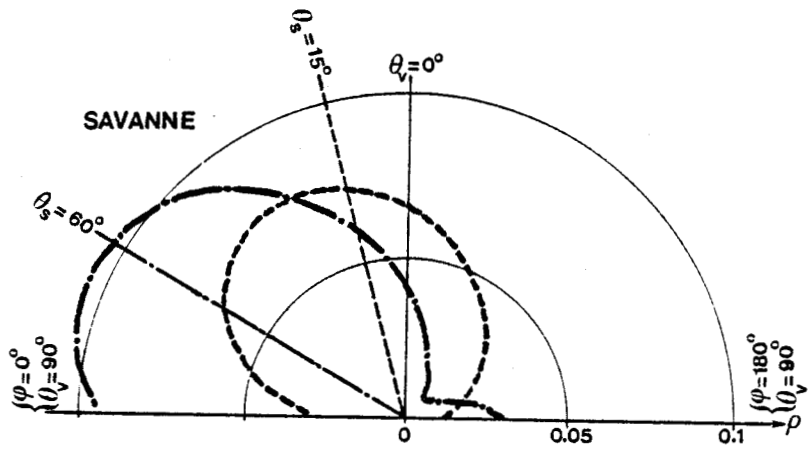

Indicatrices de réflectance observées dans le plan d'incidence du soleil, au dessus de la savanne. Les résultats sont donnés pour deux valeurs de l'angle d'incidence θ_s.

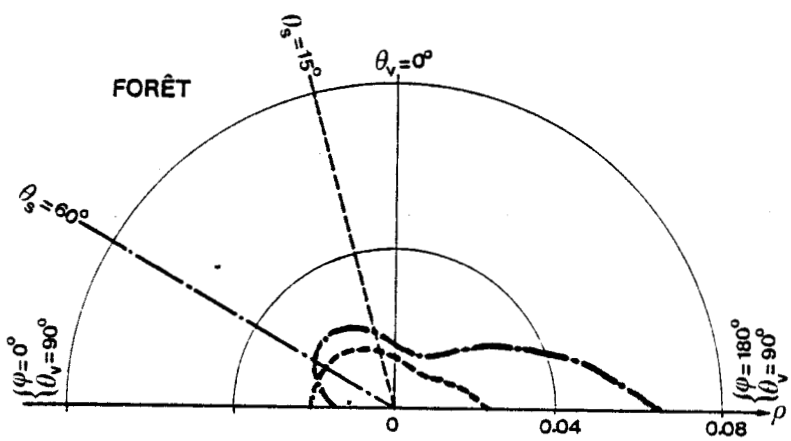

Indicatrices de réflectance observées dans le plan d'incidence du soleil, au dessus de la forêt. Les résultats sont donnés pour deux valeurs de l'angle d'incidence θ_s.

A partir de ces ordres de grandeur, il apparait que la partie intéressante des spectres de la végétation, à partir de 700 nm, sera surtout perturbée par les phénomènes d'environnement. En effet, les réflectances à mesurer sont de l'ordre de 30 à 50 %, alors que la réflectance atmosphérique atteint 10 % pour des conditions limites d'observation et vaut généralement quelques pourcents.

III-1 - PHENOMENES D'ENVIRONNEMENT (Annexe 4)

Ce travail a fait l'objet d'une publication et pour plus de détails, on se reportera à l'annexe 4, nous nous contenterons de rappeler les résultats.

Le problème est celui de la détermination de la fonction d'environnement $F(r)$, et de l'étude de sa sensibilité aux différents paramètres atmosphériques.

Les épaisseurs optiques des molécules (τ^R) et des aérosols (τ^P) jouent sur les phénomènes d'environnement par l'intermédiaire des fonctions de transmission $T(\theta_s)$ et $T(\theta_v)$, l'allure de la fonction d'environnement $F(r)$ ne dépendant que du rapport de ces épaisseurs optiques τ^R/τ^P.

Pour la répartition en altitude des aérosols, on montre que suivant la distance r entre le point considéré et le point visé, la contribution au signal provient principalement d'une couche bien localisée en altitude, ce que nous écrirons sous la forme :

$$F(r) \sim \int_0^{Z(r)} N^* (z)\, dz \qquad \text{(III-1)}$$

où N^* représente la densité relative des aérosols.

Quant à la fonction de phase, son influence apparaitra sur le niveau effectif $Z(r)$.

Un calcul rigoureux de la fonction d'environnement nécessite donc la connaissance précise de la concentration et de la nature des aérosols en fonction de l'altitude. On pourra cependant obtenir une bonne estimation de $F(r)$ en faisant les approximations suivantes.

En effet, les processus de diffusion moléculaire et aérosols peuvent se linéariser et s'écrire sous la forme,

$$F(r) \simeq \frac{t_{dR}(\theta_v)\ F_R(r) + t_{dp}(\theta_v)\ F_p(r)}{t_{dR}(\theta_v) + t_{dp}(\theta_v)} \qquad \text{(III-2)}$$

où t_{dR} et t_{dp} sont les facteurs de transmission diffus et correspondent respectivement à l'atmosphère moléculaire pure et à une atmosphère ne contenant plus que les seuls aérosols.

Les phénomènes d'environnement peuvent donc être pris en compte à l'aide de l'équation III-2, $F_R(r)$ étant calculée exactement et $F_p(r)$ estimée à partir d'un modèle moyen d'aérosols. La restitution de la fonction F(2) à l'aide de l'équation III-2 est correcte, le seul paramètre à connaitre de manière précise est alors l'épaisseur optique τ_p.

Enfin, on montre que dans le cas pratique d'une cible quelconque de réflectance ρ_1 dans un environnement de réflectance ρ_o, l'approximation qui consiste à poser

$$\rho_e = \rho_1\ F(\bar{r}) + \rho_o(1 - F(\bar{r})) \qquad \text{(III-3)}$$

où l'on a défini une dimension caractéristique $\bar{r}$ de la cible, prend en compte la majeure partie des phénomènes d'environnement.

Le formalisme développé dans le cas de sols inhomogènes nous a permis de dégager l'influence des différents paramètres :

- épaisseurs optiques moléculaire et aérosols ;
- fonction de phase des aérosols ;
- répartition en altitude des aérosols,

des formules de correction simples restituant la plupart des effets sont aussi proposées.

Nous allons maintenant envisager le cas de cibles présentant un caractère directionnel ; comment formuler de manière simple le signal et comment interpréter des mesures effectuées sous des conditions géométriques différentes.

III-2 - EFFETS DIRECTIONNELS (annexe 5)

Supposons que l'on veuille mesurer les effets bidirectionnels que peut présenter la cible et considérons un site sensiblement uniforme (pour négliger les effets d'environnement), de réflectance non lambertienne $\rho(\theta_s, \theta_v, \varphi)$.

Si l'on reprend la formulation (I-24) nous surestimons la dégradation atmosphérique des contrastes directionnels.

En effet, une étude plus poussée des effets directionnels (annexe 5) nous a amené aux conclusions suivantes.

La formulation (I-24) peut être remplacée par une expression plus précise qui tient compte de l'allure du rayonnement éclairant le cible. Il suffit pour cela de définir trois réflectances moyennes $\bar{\rho}$, $\bar{\rho}'$ et $\bar{\bar{\rho}}$ telles que :

$$\bar{\rho} = \frac{\int_0^{2\pi} \int_0^1 \mu' \, L\bar{a}_o(\mu_s, \mu', \phi') \, \rho(\mu', \mu_v, \phi', \phi) \, d\mu' d\phi'}{\int_0^{2\pi} \int_0^{'} \mu' \, L\bar{a}_o(\mu_s, \mu', \phi') \, d\mu' d\phi'}$$

$$\bar{\rho}' = \frac{\int_0^{2\pi} \int_0^1 \mu' \, \rho(\mu_s, \mu', \phi', \phi) \, L\bar{a}_o(\mu', \mu_v, \phi') \, d\mu' d\phi'}{\int_0^{2\pi} \int_0^{'} \mu' \, L\bar{a}_o(\mu_s, \mu', \phi') \, d\mu' d\phi'} \qquad \text{(III-4)}$$

$$\bar{\bar{\rho}} = \frac{\int_0^{2\pi} d\phi' \int_0^1 \mu' d\mu' \int_0^{2\pi} d\phi'' \int_0^1 \mu'' d\mu'' \; L\bar{a}_o(\mu_s, \mu', \phi') \, \rho(\mu', \mu'', \phi', \phi'') \, L\bar{a}_o(\mu'', \mu_v, \phi)}{E_d(\mu_s) \; E_d(\mu_v)}$$

En négligeant les interactions multiples, la réflectance apparente s'écrit alors sous la forme,

$$\rho^* = \rho_a + \rho_e^{-\tau m} + \bar{\rho} \, t_d(\mu_s) \, e^{-\tau/\mu_v} + \bar{\rho}' \, e^{-\tau/\mu_s} t_d(\mu_v) + \bar{\bar{\rho}} t_d(\mu_s) \, t_d(\mu_v) \qquad \text{(III-5)}$$

En fait, on montre théoriquement que les deux réflectances moyennes $\bar{\rho}$ et $\bar{\rho}'$ sont identiques, le problème se limite donc au calcul de $\bar{\rho}$ et $\bar{\bar{\rho}}$.

Des simulations numériques effectuées sur différents types de sol et pour plusieurs modèles d'atmosphère indiquent que la forte pointe de diffusion avant des aérosols permet de retrouver dans les réflectances moyennes $\bar{\rho}$ et $\bar{\bar{\rho}}$ une partie de l'information. En première approximation, on peut ainsi poser

$$\bar{\rho} = a\,\rho + b$$
$$\text{et} \quad \bar{\bar{\rho}} = a^2\rho + b \qquad \text{(III-6)}$$

où a représente le pourcentage de directionnalité qui subsiste dans l'éclairement diffus et où b est directement relié à l'albedo sphérique du sol.

A partir de cette modélisation, nous pouvons effectuer une simulation d'une mesure des propriétés directionnelles et estimer la faisabilité d'une telle expérience.

Il apparait que mises à part des mesures effectuées dans l'infrarouge avec de bonnes conditions de visibilités, il est pratiquement impossible de remonter à l'aspect directionnel de la réflectance si on ne veut pas corriger les mesures autrement qu'en prenant une réflectance atmosphérique standard lambertienne ; les deux principales sources de perturbation sont,

(i) l'aspect directionnel de la réflectance atmosphérique, des variations de quelques pourcents étant observées dans le plan d'incidence pour des directions symétriques par rapport à la verticale.

(ii) la dégradation des contrastes par les fonctions de transmission sur les trajets soleil-sol, sol-satellite.

Pour éviter d'avoir à évaluer le diagramme directionnel de la réflectance atmosphérique, on peut envisager d'utiliser des mesures multispectrales. Il est alors possible par différence entre canaux de s'affranchir de la plus grosse part de l'erreur et de remonter à la réflectance vraie même pour des conditions de visibilité assez médiocres.

III-3 - MESURE SATELLITAIRE DE L'EPAISSEUR OPTIQUE, APPLICATION A LANDSAT : (Annexe 6)

Les études précédentes précisent les grandeurs dont la connaissance est nécessaire pour corriger l'influence de l'atmosphère sur les mesures satellitaires. Ce sont principalement,

- l'épaisseur optique d'aérosols τ_p,
- leur coefficient de rétrodiffusion b_p.

On propose une méthode permettant de remonter à l'un de ces paramètres τ_p, méthode basée sur un traitement mathématique de l'image d'une zone donnée. En effet l'écart en réflectance entre cibles voisines est atténué d'un facteur $\exp(-f(\tau))$ par l'atmosphère. En faisant un histogramme de référence sur un site connu, supposé invariant dans le temps, la déformation de cet histogramme donnera l'épaisseur optique.

Dans un premier temps, nous rappellerons le principe de la méthode et présenterons ensuite une étude de faisabilité dans le cas du satellite LANDSAT, étude qui a fait l'objet d'une publication (annexe 6).

III-3-a) Principe de la méthode

Le formalisme développé précédemment nous permet d'écrire la réflectance apparente ρ^* dans le cas d'un sol lambertien non homogène

$$\rho^*(\tau,\mu,\mu_s,\phi) = \rho^a(\tau,\mu_s,\mu,\phi) + \rho\, T(\mu_s)\, e^{-\tau/\mu} + \rho_e\, T(\mu_s)\, t_d(\mu) \quad \text{(III-7)}$$

où $T(\mu_s)$ est la fonction de transmission total au niveau du sol,

$t_d(\mu)$ la transmission diffuse de l'atmosphère dans le direction μ,

ρ la réflectance de la cible

et ρ_e la réflectance moyenne de son environnement.

Soit ρ^*_{ij} la réflectance mesurée au point M(i,j), i et j représentent

les coordonnées du point (i, la ligne, j la colonne) et $\rho^*_{i,j+i}$, la réflectance mesurée au point i, j+1.

Si on soustrait les réflectances de deux points adjacents, on obtient,

$$\Delta\rho^*_{i,j}(\tau,\mu,\mu_s) = \rho^*_{i,j}(\tau,\mu,\mu_s) - \rho^*_{i,j+1}(\tau,\mu,\mu_s)$$

$$= \Delta\rho^a_{i,j}(\tau,\mu,\mu_s) + \Delta\rho_{ij}\, T(\mu_s)\, e^{-\tau/\mu} \qquad \text{(III-8)}$$

$$+ \Delta\rho_{e_{i,j}}\, T(\mu_s)\, E(\mu)$$

Pour des points voisins, on peut raisonnablement poser

$$\rho^a_{i,j} = \rho^a_{i,j+1} \qquad \text{(III-9)}$$

et $\rho_{e_{i,j}} = \rho_{e_{i,j+1}}$,

les échelles spatiales de ces phénomènes étant de l'ordre du kilomètre et la résolution d'un satellite d'observation de la terre de quelques dizaines de mètres.

L'équation III-8 s'écrit alors,

$$\Delta\rho^*_{i,j}(\tau,\ \mu,\ \mu_s) = \Delta\rho_{ij}\, T(\mu_s)\, e^{-\tau/\mu} \qquad \text{(III-10)}$$

Nous avons à notre disposition plusieurs expressions analytiques de la fonction $T(\mu_s)$ basées sur des méthodes approchées (méthode d'Eddington, méthode à deux flux...).

Reprenons l'expression analytique de la fonction de transmission diffuse donnée dans l'annexe 1 (p 3590, Eq 12b) à laquelle nous ajoutons la fonction de transmission directe. Celà nous donne l'Eq. III-11 pour la fonction de transmission totale.

$$T(\mu_s) = \exp\left(-\frac{b\tau}{\mu_s}\right) \qquad \text{(III-11)}$$

où b est relié au facteur d'assymétrie g par

$$b = \frac{1}{2}\,(1 - g) \qquad \text{(III-12)}$$

Les écarts en réflectance se mettent donc sous la forme

$$\Delta\rho^{*}_{i,j}(\tau,\ \mu,\ \mu_s) = \Delta\rho_{i,j}\ \exp\left(-\ \tau_P\left(\frac{1}{\mu}+\frac{1}{\mu_s}-\frac{b_P}{\mu_s}\right)\right) \exp\left(-\ \tau_R\left(\frac{1}{\mu}+\frac{1}{\mu_s}-\frac{b_R}{\mu_s}\right)\right) \qquad \text{(III-3)}$$

où l'indice R se rapporte à la diffusion moléculaire et l'indice P aux aérosols.

Si l'on considère les moments d'ordre n de l'histogramme, définis par

$$M^n = \int_o^\infty (\Delta\rho)^M\ P(\Delta\rho)\ d(\Delta\rho) \qquad \text{(III-4)}$$

où $P(\Delta\rho)$ est la probabilité de rencontrer un écart en réflectance de $\Delta\rho$, alors on peut écrire

$$M^{*n} = M^n\ \exp\left(-\ n\tau_P\left(\frac{1}{\mu}+\frac{1}{\mu_s}-\frac{b_P}{\mu_s}\right)\right)\ \exp\left(-\ n\tau_R\left(\frac{1}{\mu}+\frac{1}{\mu_s}-\frac{b_R}{\mu_s}\right)\right) \qquad \text{(III-5)}$$

où M^{*n} est le moment d'ordre n des écarts en réflectance apparente et M^n celui des écarts en réflectance vraie de la scène.

La déformation de l'histogramme peut donc dans le principe fournir l'épaisseur optique au dessus d'un site invariant dans le temps.

III-3-b) Application au satellite LANDSAT

Pour tester la validité de cette méthode, n'ayant pas à notre disposition d'histogramme de référence sur un site invariant dans le temps, nous avons travaillé sur des images LANDSAT.

En effet ce satellite survole la même scène à une journée d'intervalle. En supposant que les réflectances de sol n'ont pas varié sur une période de temps aussi courte, les variations sur les écarts en réflectance peuvent être attribuées aux seules variations des caractéristiques de l'atmosphère.

Les conditions géométriques étant identiques sur les deux jours, on peut écrire

$$\frac{M^{*n}(t_1)}{M^{*n}(t_2)} = \exp(-n(\tau(t_1) - \tau(t_2))\ (\frac{1}{\mu} + \frac{1}{\mu_s} - \frac{b_P}{\mu_s})) \qquad \text{(III-6)}$$

et espèrer ainsi atteindre les variations d'épaisseur optique $\Delta\tau_P$ à l'aide de

$$\Delta\tau_P = -\left[n(\frac{1}{\mu} + \frac{1}{\mu_s} - \frac{b_P}{\mu_s})\right]^{-1} \text{Log}\ \frac{M^{*n}(t_1)}{M^{*n}(t_2)} \qquad \text{(III-7)}$$

Si on se fixe une valeur standard de b_P, obtenue par un modèle réaliste d'aérosols, les conditions géométriques étant connues, on remontera à $\Delta\tau_P$.

Nous avons choisi de travailler sur une zone légèrement au Sud de Carpentras. On constate (annexe 6) que les valeurs de $\Delta\tau_P$ obtenues indépendamment, c'est à dire soit sur des zones différentes d'une même scène, soit en utilisant des moments différents, sont tout à fait cohérents compte tenu de la dispersion moyenne des résultats.

Les principales origines de cette dispersion sont de deux types,

- les erreurs intrinséques à la méthode, c'est à dire les erreurs dues soit au recalage des deux scènes soit à l'incertitude sur la position du pixel par rapport à un gradient de réflectance.
- les erreurs dues à l'application de la méthode au cas de LANDSAT, variations des réflectances vraies, changement du type de particules (Δb_P), variations locales de l'épaisseur optique ($\delta(\Delta\tau_P)$), variations des conditions géométriques ($\Delta(\frac{1}{\mu} + \frac{1}{\mu_s})$).

Le premier type d'erreur pourrait être éventuellement modélisé dans une étude plus poussée mais il semble difficile de chiffrer l'ensemble des incertitudes. L'incertitude totale de l'ordre de 0,03 semble être une caractéristique de la méthode. Cette précision n'est pas ridicule, des mesures in-situ donnent une précision de l'ordre de 0,01 à 0,02.

ANNEXE 4

Reprinted from Applied Optics, Vol. 20, page 3676, October 15, 1981

Influence of the background contribution upon space measurements of ground reflectance

D. Tanre, M. Herman, and P. Y. Deschamps

The influence of background contamination on the apparent reflectance of a target as viewed from space has been studied as a function of the characteristics of atmospheric aerosols and the simple geometry of the target. For relatively common aerosol characteristics, the main features of the environment effect may be accounted for by simple correction terms, which depend only upon the optical thicknesses of aerosols and the molecular scattering of the atmosphere.

I. Introduction

With the advent of earth observation satellites, much effort has been devoted to the problem of accounting for atmospheric effects, which disturb the remote measurement of surface reflectances.

In many analyses of these effects, the surface reflectance is assumed to be uniform.[1-4] Such calculations accurately evaluate the intrinsic atmospheric radiance, which is in fact the major term of the atmospheric perturbation when observing areas with low reflectivities, as in oceanographic investigations.[5,6] Moreover, this 1-D treatment is suitable for targets of very large dimensions (like oceans or forests), or to the contrary, of very small dimensions, such that only the radiance reflected by the target modifies the signal which otherwise comes from a uniform background.[7,8]

It can be shown that the relative contributions of the object pixel and of its environment become nearly equivalent at wavelengths shorter than ~0.8 μm.[9] We first shall try to define the minimum or maximum scales for which the reflectance of the observed area has to be uniform so that one or the other of these approximations is correct.

In any event, this environment effect will induce a contrast degradation near the boundary between contrasted areas. For scenes exhibiting a patchy structure, this blurring effect may lead to reflectance errors as important as the atmospheric reflectance itself,[9] and it has to be taken into account.

Careful computations of multiple scattering and multiple reflection effects may be made by the Monte Carlo method (e.g., Ref. 10). A general solution to the problem may also be obtained by Fourier analysis.[11] Here the atmospheric function $rp(r)$ will be used, which gives the probability that the points on the surface separated by a distance r from the object pixel can contribute to the signal. Approximate evaluations of $rp(r)$ have been made by way of calculations of primary scattering.[12,13] The accuracy of such estimations will be examined, and we will investigate how this probability function depends upon the main parameters of the problem, i.e., the observation wavelength, the number density profile of the aerosols, and their optical properties.

Although this environmental effect is quite variable, it will be shown that simple correcting formulas may eliminate the major part of the environment perturbation found in the worst case of patchy structures, provided that the aerosol optical thickness is known.

II. Signal Analysis

A. Atmospheric Models

The atmosphere is horizontally homogeneous, and bidirectional effects of the ground reflectivity are negligible. Lambert's reflectance law is assumed to pertain to any point on the surface.

In all the models, a mean molecular component is assumed (Table I). This pure molecular atmosphere will be denoted model R.

For the aerosol component, the Junge-type model of McClatchey *et al.*[14] is taken as a reference. The particle phase function, computed from the Mie theory with the

The authors are with Université des Sciences et Techniques de Lille, Laboratoire d'Optique Atmosphérique, 59655 Villeneuve d'Ascq Cedex, France.

Received 6 February 1981.
0003-6935/81/203676-09$00.50/0.

Table I. Optical Thickness for Molecules τ_R and Aerosols τ_P for the *MC*23 and *MC*5 Models

$\lambda_{\mu m}$	τ_R	τ_P (*MC*23)	τ_P (*MC*5)
0.4500	0.2157	0.2801	0.9305
0.8500	0.0163	0.1550	0.5151

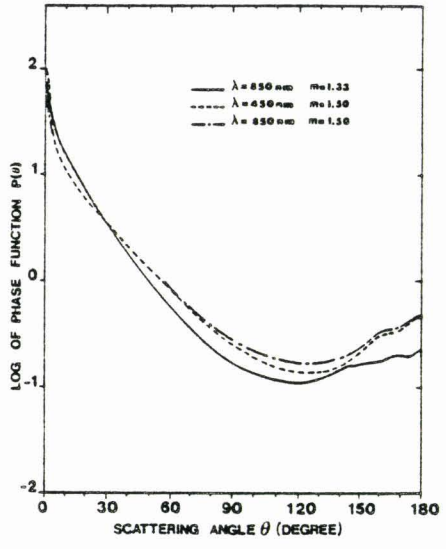

Fig. 1. Scattering phase function $P(\theta)$ of aerosol. For the size distribution and the refractive index (m = 1.50) of the model of McClatchey *et al.*,[14] the results are shown for λ = 850 and 450 nm. For λ = 850 nm, $P(\theta)$ is also shown for the same size distribution but for an assumed refractive index m = 1.33.

refractive index m = 1.50, for λ = 450 nm and λ = 850 nm (Fig. 1), is weakly dependent upon wavelength λ. The particle number density profiles $N(z)$, from Eq. (14), are drawn in Fig. 2. Figure 3 gives the corresponding reduced quantities

$$\int_0^z N(z')dz' / \int_0^\infty N(z')dz'. \tag{1}$$

The optical thicknesses for molecules τ_R and for aerosols τ_P, for these *MC*23 and *MC*5 models, are given in Table I as a function of wavelength.

To estimate the influence of aerosol properties upon the atmospheric effect, these basic models have been modified in two respects.

In models *MC.I.*23 and *MC.I.*5, the relative particle number density profiles and the optical thicknesses τ_P are the same as those in the *MC*23 and *MC*5 models, but the aerosol phase function is computed with the refractive index m = 1.33 (Fig. 1).

In models *MC.P.*23 and *MC.P.*5, the optical thicknesses τ_P and the phase function are those of the *MC*23 and *MC*5 models, but the particle number density is assumed to be constant from the ground to altitude z = 2 km and then decreases exponentially from z = 2 to $z \simeq 4$ or 5 km, respectively, where the standard profile is rejoined (Figs. 2 and 3).

B. Formulation of the Signal

Rather than being expressed as radiance I, the various quantities will be expressed in terms of equivalent reflectance defined as

$$\rho^* = \pi I/(\mu_0 f), \tag{2}$$

where f is the solar flux at the top of the atmosphere, and $\theta_0 = \arccos\mu_0$ is the solar zenith angle.

It is convenient to express signal ρ^* received by the satellite as a series of the successive orders of radiation interactions in the coupled ground–atmosphere system (e.g., Refs. 9, 15, and 16). Let ρ be the ground reflectance; then, for a uniform surface respecting Lambert's law,

$$\rho^*(\mu_0,\mu,\phi) = \rho_a(\mu_0,\mu,\phi) + \frac{1}{1-\rho s}[\rho \cdot A(\tau,\mu_0,\mu) + \rho \cdot B(\tau,\mu_0,\mu)], \tag{3}$$

with

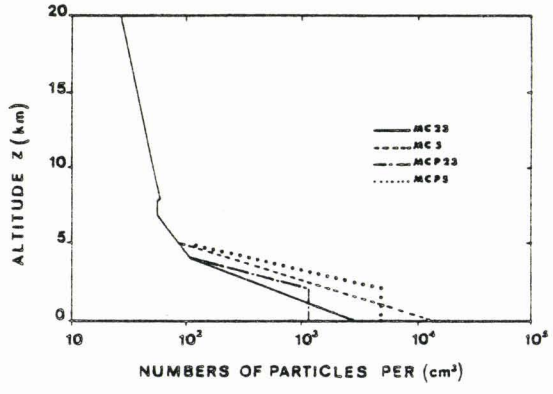

Fig. 2. Aerosol number density profiles for the two basic models *MC*23 and *MC*5 and for the modified models *MC.P.*23 and *MC.P.*5.

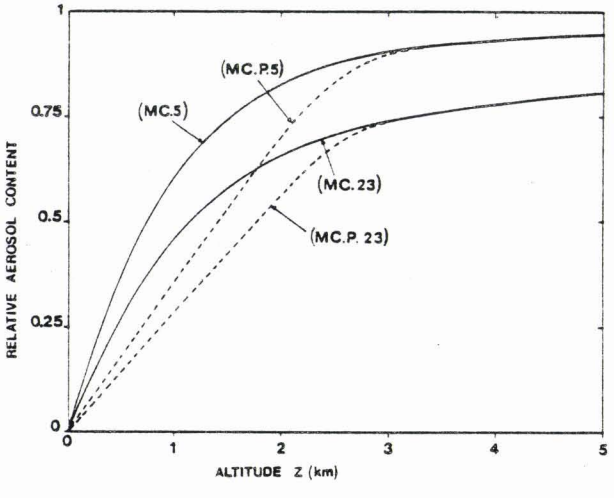

Fig. 3. Relative integrated aerosol content

$$\int_0^z N(z')dz' \Big/ \int_0^\infty N(z')dz'$$

as a function of altitude z for the four aerosol number-density profiles given in Fig. 2.

Table II. Values of ρ_a, A, and B for the $MC23$ and $MC5$ Models [a]

Solar zenith angle	Model	λ = 450 nm ρ_a	λ = 450 nm A	λ = 450 nm B	λ = 850 nm ρ_a	λ = 850 nm A	λ = 850 nm B
15	$MC23$	0.105	0.525	0.224	0.021	0.814	0.121
60	$MC23$	0.128	0.452	0.192	0.025	0.769	0.114
15	$MC5$	0.160	0.250	0.378	0.056	0.535	0.298
60	$MC5$	0.203	0.198	0.298	0.075	0.463	0.258

[a] Results are given for two wavelengths (450 and 850 nm), for two solar zenith angles ($\theta_0 = 15°$ and $\theta_0 = 60°$), and for a vertical observation ($\mu = 1$).

$$A(\tau,\mu_0,\mu) = T(\tau,\mu_0)\exp(-\tau/\mu),$$
$$B(\tau,\mu_0,\mu) = T(\tau,\mu_0)E(\tau,\mu),$$
$$T(\tau,\mu_0) = E(\tau,\mu_0) + \exp(-\tau/\mu_0), \quad (4)$$

where τ is the total optical thickness of the atmosphere, $\theta = \arccos\mu$ is the zenith viewing angle, and ϕ is the azimuthal angle.

$\rho_a(\mu_0,\mu,\phi)$ is the intrinsic atmospheric signal component in terms of reflectance.

$\rho \cdot A(\tau,\mu_0,\mu)$ is the first-order signal component due to the object pixel, which is reflected by the object, is directly transmitted through the atmosphere to the sensor, and results from the direct $[\exp(-\tau/\mu_0)]$ plus the diffuse $[E(\tau,\mu_0)]$ solar flux.

$\rho \cdot B(\tau,\mu_0,\mu)$, the first-order signal component due to the background, results from the direct plus the diffuse solar flux reflected by the background but is transmitted to the sensor by atmospheric scattering $[E(\tau,\mu)]$.

The second and higher orders of radiance–ground interactions are taken into account by the factor $(1 - \rho s)^{-1}$, where s is the spherical albedo of the atmosphere as viewed from the surface.

The reciprocity principle allows that the diffuse illumination term and the diffuse transmission term in A and B, respectively, may be expressed by the same atmospheric function $E(\tau,\mu)$. Simple approximative analytical expressions for atmospheric terms $E(\tau,\mu)$ and $s(\tau)$ may be obtained as a function of optical thicknesses τ_R and τ_P and of asymmetry parameters $\langle\cos\theta\rangle_R$ and $\langle\cos\theta\rangle_P$ for the molecular and aerosol scattering,[9] and

$$E(\tau,\mu) \simeq \exp\left(-\frac{\tau_R + \tau_P}{\mu}\right)\left[\exp\left(+\frac{\alpha_R\tau_R + \alpha_P\tau_P}{\mu}\right) - 1\right] \quad (5)$$

with

$$\alpha_R = \frac{1 + \langle\cos\theta\rangle_R}{2}; \qquad \alpha_P = \frac{1 + \langle\cos\theta\rangle_P}{2}, \quad (6)$$

that is, $\alpha_R = 1/2$ and $\alpha_P \simeq 5/6$.

Table II gives some values of coefficients A and B in Eq. (3) for the $MC23$ and $MC5$ models at a vertical observation. The corresponding atmospheric reflectances ρ_a are also given. Calculations were made by the successive orders of the scattering method. Except for long wavelengths and very good visibility conditions, the relative weight of the background of the object pixel (term B) is one fourth to one half of that of the entire surface (term $A + B$).

To give the magnitude of this effect, suppose a reflectance difference $\Delta\rho \simeq 0.10$ between the very small object pixel and its environment. The background contribution corresponding to this value $\Delta\rho = 0.10$ introduces an error $\Delta\rho^* \simeq 0.02$–0.05, which is comparable with ρ_a itself.

For the case of an inhomogeneous surface, Eq. (3) will be generalized into the form

$$\rho^*(M,\mu_0,\mu,\phi) = \rho_a(\mu_0,\mu,\phi) + \frac{1}{1 - \langle\rho(M)\rangle s} \times [\rho(M) \cdot A(\tau,\mu_0,\mu) + \langle\rho(M)\rangle \cdot B(\tau,\mu_0,\mu)], \quad (7)$$

where $\rho(M)$ is the reflectance of the object pixel M, located at the origin of the x,y coordinate system, and $\langle\rho(M)\rangle$ is the average reflectance of its environment. For the first order of the environment contribution, $\langle\rho(M)\rangle$ will be given by

$$\langle\rho(M)\rangle = \frac{1}{E(\mu)}\iint \rho(x,y)e(x,y,\mu)dxdy, \quad (3)$$

where $e(x,y,\mu)$ is the contribution to the diffuse transmission $E(\mu)$ per unit area of an isotropic unit source placed at a point on the surface with coordinates (x,y).

The use of the same average reflectance $\langle\rho(M)\rangle$ for the higher orders of interaction [that is, the $(1 - \langle\rho(M)\rangle s)^{-1}$ term] is incorrect but reasonable, as it may be shown that, in practical cases, the contribution from these terms does not exceed 10–15% of the contribution from the first-order term $(\rho_a + \rho A + \langle\rho\rangle B)$.[9,13]

III. Environment Functions $rp(r)$ and $F(r)$

A. Calculation

We will restrict the study to the case of vertical observations, and Eq. (8) will be written

$$\langle\rho(M)\rangle = \int_0^{2\pi}\int_0^{\infty} \rho(r,\psi)rp(r)drd\psi \quad (9)$$

with

$$rp(r) = \frac{re(r,\psi,+1)}{E(+1)}, \quad (10)$$

where (r,ψ) are the polar coordinates of a given surface point with object pixel M at the origin.

For the exact evaluation of $rp(r)$, Monte Carlo calculations have been used in conjunction with the reciprocity principle. Photons are injected from space at the nadir toward M. Let $N(r)\Delta r$ be the number of

Table III. Relative Contributions of Primary and Secondary Scattering Orders, to the Function $E(\mu)$, for Two Viewing Zenith Angles and Two Observation Wavelengths [a]

Viewing zenith angle (deg)	Model	Wavelength (nm)	$\rho_a^{(1)}/\rho_a$	$\rho_a^{(1)} + \rho_a^{(2)}/\rho_a$
2.84	*MC*23	450	0.71	0.90
28.77	*MC*23	450	0.67	0.86
2.84	*MC*5	450	0.51	0.75
28.77	*MC*5	450	0.47	0.72
2.84	*MC*23	850	0.89	0.98
28.77	*MC*23	850	0.87	0.98
2.84	*MC*5	850	0.72	0.91
28.77	*MC*5	850	0.70	0.90

[a] Results are for *MC*23 and *MC*5 models.

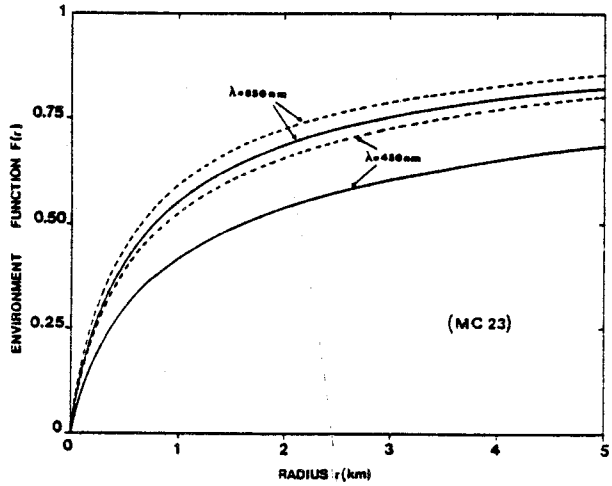

Fig. 4. Comparison of the exact results for $F(r)$ (solid lines) with the single-scattering approximation (dashed lines). The results are for the *MC*23 model for $\lambda = 850$ nm (upper curves) and $\lambda = 450$ nm (lower curves).

photons arriving at the surface in the annular area $2\pi r\Delta r$ and N_0 be the total number of these transmitted photons. Then

$$2\pi \overline{rp(r)}\,\Delta r = \frac{N(r)\Delta r}{N_0} \tag{11}$$

will define the probability function.

Given the large contribution to $E(\tau,\mu)$ that the single-scattered photons make in most cases (Table III), it may be hoped that a single-scattering approximation is valid. Then $rp(r)$ will be directly obtained by

$$rp(r) = \frac{1}{2\pi} \frac{\int_0^\infty k(z)P(\theta,z)t(z,r)rz(r^2+z^2)^{-3/2}dz}{\int_0^\infty dr \int_0^\infty k(z)P(\theta,z)t(z,r)rz(r^2+z^2)^{-3/2}dz}, \tag{12}$$

with

$$t(z,r) = \exp[-\tau(z)] \exp(-|[\tau(z) - \tau] \cdot (r^2+z^2)^{1/2} \cdot z^{-1}|).$$

It should be noted that the scattering coefficient $k(z)$ and the phase function $P(\theta,z)$ depend on the altitude z in the inhomogeneous models we are dealing with.

As Monte Carlo calculations give poorly resolved $rp(r)$ functions, the comparison between the exact results and the approximate results will rather be done through the integral function

$$F(r) = \int_0^r 2\pi r' p(r')dr', \tag{13}$$

which gives the relative contribution to $\langle \rho(M) \rangle$ of surface points not farther than a distance r apart from the origin. Figure 4 shows the $F(r)$ functions obtained from Eqs. (11) and (12) for the *MC*23 model at wavelengths of 850 and 450 nm, respectively.

For large wavelengths, the single-scattering approximation is good and of value in quantitative estimations. The systematic errors are not larger than those caused by uncertainties about the aerosol parameters as will be discussed later.

At shorter wavelengths, the optical thickness becomes greater, and the use of the single-scattering approximation gives a systematic underestimation of the environment signal because of the transmission term $t(z,r)$ used in Eq. (12).

B. Variability of the Environment Functions

Due to the forward character of the aerosol scattering law, the paths of multiply scattered photons have a good chance of being very close to the path of primary scattered photons; and the major defect of single scattering calculations is the underestimation introduced by the transmission terms in Eq. (12). As a matter of fact the results of Monte Carlo calculations performed for the *MC*23 model do not vary within a few percent when increasing threefold the particle number density at each atmospheric level. So the total aerosol content is of direct importance to the respective weights A and B of the object pixel and of its background [Eq. (7)], but the behavior of $rp(r)$ and $F(r)$ will depend only upon the ratio of the optical thicknesses τ_R/τ_P and upon the relative number density profile for the aerosols:

$$N^*(z) = N(z) \Big/ \int_0^\infty N(z')dz'. \tag{14}$$

This last result implies that the aerosol contributions to the environment weighting functions corresponding to the *MC*23, *MC.P.*23, MC5, and *MC.P.*5 models may be considered as representatives of four different relative particle number density profiles, whatever the associated optical thickness for the aerosols may be.

The exact functions $F(r)$, corresponding to the *MC*23, *MC.P.*23, *MC*5, and *MC.P.*5 models, are shown in Fig. 5 for $\lambda = 850$ nm and in Fig. 6 for $\lambda = 450$ nm. When changing the observation wavelength, the variations of the aerosol scattering cross section do not by themselves modify $F(r)$, as has been shown, or are the very small variations of their phase function important (Fig. 1). The transition from Fig. 5 to 6 corresponds to the increasing influence of the molecular scattering, and this spectral variation can easily be accounted for. When writing Eq. (5) into the approximate form

$$E(\tau,\mu) \simeq \exp\left(-\frac{\tau_R + \tau_P}{\mu}\right)(\alpha_R\tau_R + \alpha_P\tau_P), \tag{15}$$

it looks as though the aerosols and the molecules, apart from a common transmission term, transmit the back-

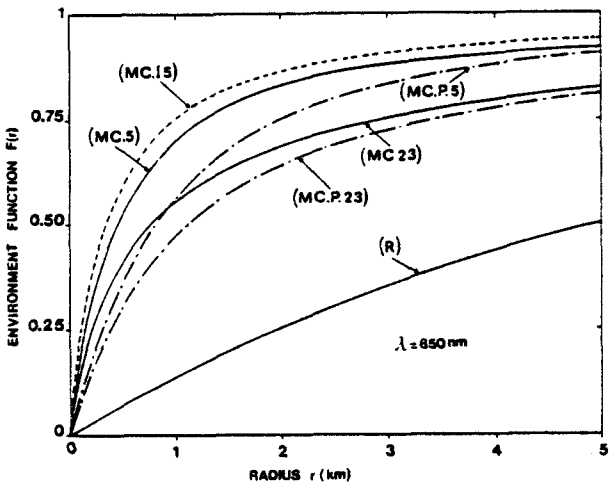

Fig. 5. Function $F(r)$ for pure molecular scattering (model R) for four different aerosol number density profiles (models $MC5$, $MC.P.5$, $MC23$, and $MC.P.23$) and for the $MC.I.5$ model. Comparison of the $MC5$ with the $MC.I.5$ results shows the influence of the aerosol phase function. Results are for λ = 850 nm.

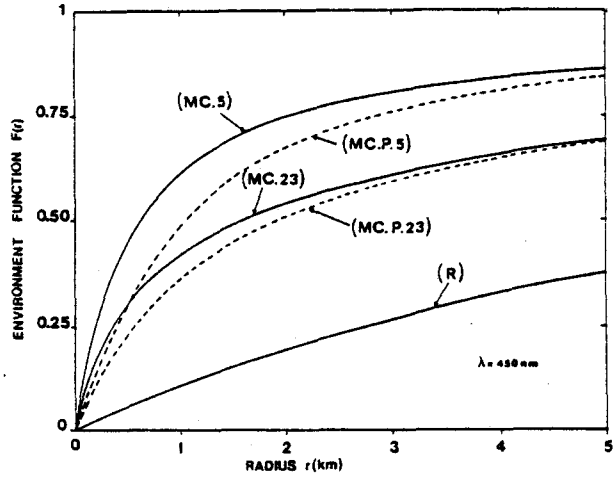

Fig. 6. Same as Fig. 5 for λ = 450 nm. $MC.I.5$ results have been omitted.

ground contribution with respective efficiencies $\alpha_R\tau_R$ and $\alpha_P\tau_P$. A valuable interpolation formula for $rp(r)$ or $F(r)$ as a function of the wavelength is then

$$F(r) = \frac{\alpha_P\tau_P \cdot F_P(r) + \alpha_R\tau_R F_R(r)}{\alpha_P\tau_P + \alpha_R\tau_R}, \tag{16}$$

where τ_R and τ_P depend upon the wavelength; $F_R(r)$ is the result for the molecular model R; and $F_P(r)$ corresponds only to the aerosol influence with profile $N^*(z)$. Practically, when using for $F_P(r)$ the results obtained for λ = 850 nm (Fig. 5) and for $F_R(r)$, the results obtained for λ = 450 nm, Eq. (16) gives the results for λ = 450 nm within a few percent (maximum 3%).

Apart from this molecular influence, the environment effect depends mainly upon the aerosol relative number density profile, as shown when comparing the behavior of Fig. 5, which is nearly representative of the aerosol effect, with Fig. 3. The very good correlation between the general features of these curves is clear when one considers the relative contribution of each atmospheric level to the value of $rp(r)$, corresponding to a given point of the environment, as shown in Fig. 7. The contribution of single-scattered photons from points at a given distance r from the origin tends to be the consequence of scattering at a rather well-localized atmospheric level $z(r)$. It must therefore be expected that

$$F(r) \sim \int_0^{z(r)} N^*(z')dz'. \tag{17}$$

Such a simple result is only true for constant aerosol optical properties, as the results corresponding to the $MC.I.5$ model show in Fig. 5. Given the aerosol relative number density profile, large modifications of their forward scattering law (see Fig. 1 for the phase function for the $MC.I.5$ model) will somewhat modify the effective level $z(r)$ in Eq. (17) and thus the environment weighting function.

In summary, the variability of the environment weighting function $F(r)$ proves to be rather tractable. (1) The molecular scattering is a major factor governing the enlarged contribution of the background when decreasing the observation wavelength. This effect may be linearized and accounted for by Eq. (16). (2) The aerosol term $F_P(r)$ in Eq. (16) depends principally upon the relative number density profile $N^*(z)$ and, to a lesser extent, upon the particle phase function. But it may be seen that the mean features of the environment effect may be restored by using any of the functions given in Fig. 5 in conjunction with the actual aerosol optical thickness τ_P.

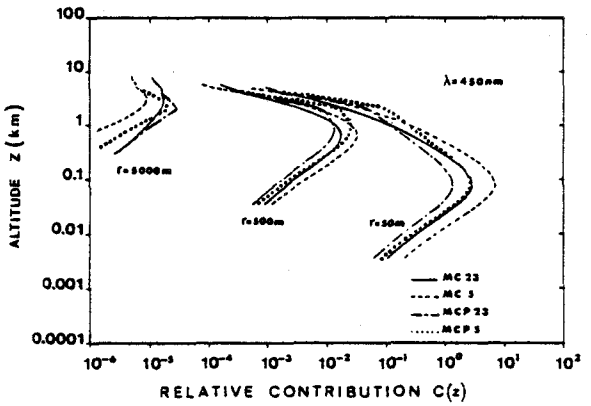

Fig. 7. Relative contribution $C(z)$ from the various atmospheric layers to the environment weighting function $rp(r)$ with

$$rp(r) = \int_0^\infty C(z)rdz$$

for three fixed values of distance r. Four aerosol number density profiles given in Fig. 2 are investigated. Results are for λ = 450 nm and correspond to single-scattering calculations.

IV. Examples of Contrast Degradation

Some simulations of the environment effect have been made with Eqs. (7), (5), and (9) for the case of two adjacent half planes with respective uniform reflectances ρ_0 and ρ_1 and for the case of a square target with reflectance ρ_1 within a uniform background with reflectance ρ_0.

For these bireflectance structures, let us put

$$\langle \rho(P) \rangle^* = \iint_{S_1} rp(r) dr d\psi, \tag{18}$$

where the integral is restricted to the surface S_1 whose reflectance $\rho_1 \cdot \langle \rho(P) \rangle^*$ will depend only on the geometry of the problem.

Then the mean background reflectance, from Eq. (9), will be

$$\langle \rho(P) \rangle = \rho_0 + (\rho_1 - \rho_0) \langle \rho(P) \rangle^*. \tag{19}$$

Neglecting the small contribution from higher-order interactions, $\langle \rho(P) \rangle s$ in Eq. (7), ρ^* will be given by

$$\rho^*(P) = \rho_a + A\rho(P) + B\rho_0 + B(\rho_1 - \rho_0) \langle \rho(P) \rangle^*. \tag{20}$$

Instead of ρ^* which depends on ρ_a and on the actual contrast $(\rho_1 - \rho_0)$, it is interesting to study the contrast degradation expressed as

$$\frac{\rho^*(P_1) - \rho^*(P_2)}{\rho_1 - \rho_0} = C(P_1) - C(P_2), \tag{21}$$

where the $C(P)$ function is independent of $(\rho_1 - \rho_0)$ and may be written

$$C(P) = \epsilon(P)A + B\langle \rho(P) \rangle^*, \tag{22}$$

where $\epsilon(P)$ equals 0 when ground reflectance at P is ρ_0 and 1 otherwise.

Using the computation of the intrinsic function $C(P)$ in Eq. (22), it is possible to evaluate the cross effect for any value of ρ_0 and ρ_1.

The contrast functions $C(P)$, for the case of two adjacent half-planes, are given in Fig. 8 as a function of the distance from P to the boundary. The results are for two observation wavelengths (850 and 450 nm) and for the two aerosol contents corresponding to the $MC23$ and $MC5$ models. The values of atmospheric functions A and B (in Table II) correspond to a solar zenith angle of 60°. So as to distinguish the various curves in Fig. 8, each curve was translated by a constant factor $-(A + B)/2$, which makes them symmetrical with respect to the boundary.

For the four pairs of data (τ_R, τ_P), two extreme values of $C(P)$ have been calculated, using for $rp(r)$ in Eq. (18) the two extreme results obtained for the $MC.I.5$ and $MC.P.23$ models (Figs. 5 and 6).

The general features of the results are already known.[9,10,13] The space scale of the environment effect is of the order of 1–2 km; this corresponds, for example, to the distance in which the land influence characteristically perturbs water color gradients in oceanic coastal investigations.

It may be seen that the mean features of the effect depend mainly upon the aerosol optical thickness τ_P, which is the principal factor governing the strength of the contrast degradation, and to a lesser extent upon the contribution to $rp(r)$ of the molecular scattering, which slightly increases the scale of the effect in blue light. But the results are not very sensitive to large variations of the aerosol characteristics. A mean standard function $rp_P(r)$ could be used for the contribution of the aerosols to $rp(r)$. Figure 8 shows that errors in $C(P)$ would be less than $\Delta C_P \simeq 0.02$ for contrasting scenes with $\Delta\rho \simeq 0.20$, and Eq. (21) suggests that systematic errors $\delta(\Delta\rho^*)$ so introduced would not exceed 1% of apparent reflectance for the high aerosol content and half of a percent for the low aerosol content.

The same calculations have been performed for the case of a square target. Three different target sizes were considered. The contrast functions corresponding to the four pairs (τ_R, τ_P) are given in Figs. 9–12 as a function of the distance from P to the center of the square.

The contrast degradation depends mainly upon the leading term A in Eq. (7). But, for these targets of intermediate size, the environment effect is not negligible, and the variations of the contribution from the B term, as a function of the size of the target, may be quite noticeable.

Here again it appears that, whatever the exact characteristics of the particle may be, the environment effect may be accounted for rather well with a mean aerosol model, provided that the optical thickness is known.

V. Approximate Evaluation of the Environment Effect. Range of Validity of the 1-D Approximations

Within the range of the target sizes, in Figs. 9–12, the contrast gradients are not very large except near the boundaries. With a mean ground resolution of the order of 50 m and a digitization level of 0.005 in reflectance, the observations would be nearly constant all over

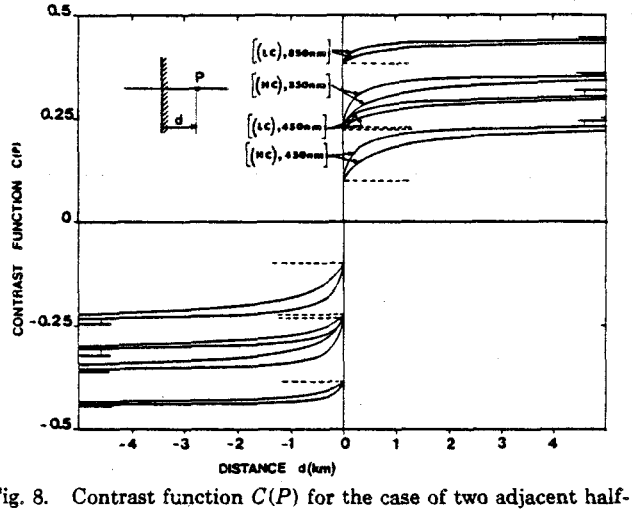

Fig. 8. Contrast function $C(P)$ for the case of two adjacent half-planes as a function of the distance d from P to the boundary. Solar zenith angle is 60°. Two aerosol contents of the $MC5$ and $MC23$ models and two observation wavelengths, 850 and 450 nm, have been considered. For each case, $C(P)$ was calculated with the environment functions corresponding to the $MC.I.5$ model (upper contrast) and to the $MC.P.23$ model (lower contrast). Results labeled HC correspond to the high aerosol content of the $MC5$ model. LC corresponds to the low aerosol content of the $MC23$ model.

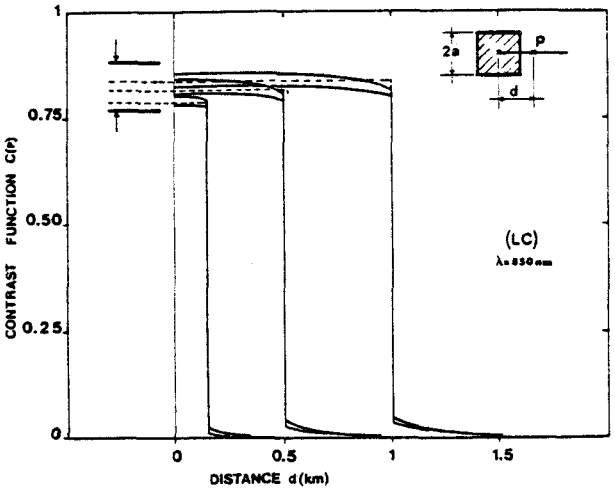

Fig. 9. Contrast function $C(P)$, for the case of a square target, as a function of distance d from P to the center of the target. Solar zenith angle is 60°. Results are shown only for positive values of d. Three different target sizes are considered: $2a = 0.3$, 1, and 2 km. Aerosol contents, observation wavelengths, and extreme environment weighting functions are the same as for Fig. 8. Results in Fig. 9 are for the low aerosol content LC and for $\lambda = 850$ nm. Horizontal dashed lines correspond to approximate values for $C(P)$ (see text). Horizontal solid lines with arrows show extreme values of $C(d)$ with the center of a very small (lower) or very large (upper) target.

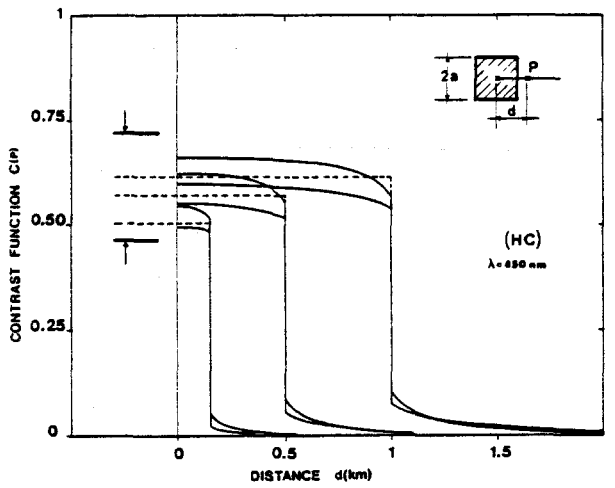

Fig. 10. Same as Fig. 9 for high aerosol content HC and $\lambda = 850$ nm.

the target, apart from one or two pixels across the boundaries. It seems valuable to search for a simple constant correction term which accounts for the environmental effect.

Let $\bar{r}$ be the characteristic size of a target whose geometry is not too nearly linear and whose reflectance ρ_1 is uniform. Let ρ_0 be the mean reflectance of the background. When the target is considered to be a circular targer of radius $\bar{r}$, an approximate value for $\langle \rho(P) \rangle$ all over the target will be given by

$$\langle \rho(P) \rangle = \rho_1 F(\bar{r}) + \rho_0 [1 - F(\bar{r})] \tag{23}$$

or

$$\langle \rho(P) \rangle^* = F(\bar{r}). \tag{24}$$

In Figs. 9–12, the contrast functions $C_a(P)$, resulting from the approximate Eq. (24) and which are constant all over the target, have been drawn. The $F(\bar{r})$ values were obtained from Eq. (16), where a mean value of the results in Fig. 5 was used for the aerosol contribution $F_P(\bar{r})$, and the results for the model R at 450 nm were used from the molecular contribution $F_R(\bar{r})$:

$$\begin{aligned} F_P(r) &\simeq 1 - [0.375 \exp(-0.2r) + 0.625 \exp(-1.83r)] \\ F_R(r) &\simeq 1 - [0.930 \exp(-0.08r) + 0.070 \exp(-1.10r)] \end{aligned} \quad (r \text{ in km}). \tag{25}$$

It may be seen that the major part of the environment effect is rather well accounted for by these approximations.

More generally, this approximation may be used to test the range of validity of the 1-D approximations of the environment effect where the target is considered as very large or very small. The question is: for which minimum or maximum size $\bar{r}$ can one neglect the background contribution or, respectively, the contribution from the target itself to the diffuse signal component?

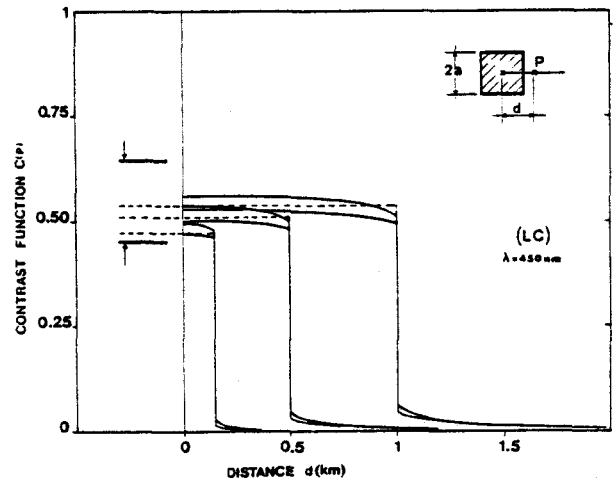

Fig. 11. Same as Fig. 9 for low aerosol content LC and $\lambda = 450$ nm.

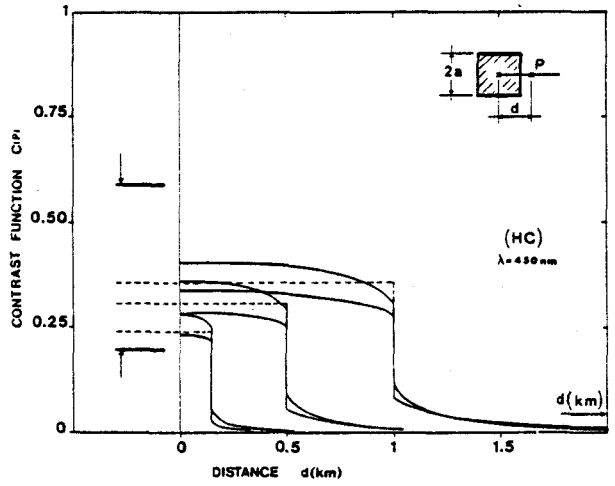

Fig. 12. Same as Fig. 9 for high aerosol content HC and $\lambda = 450$ nm.

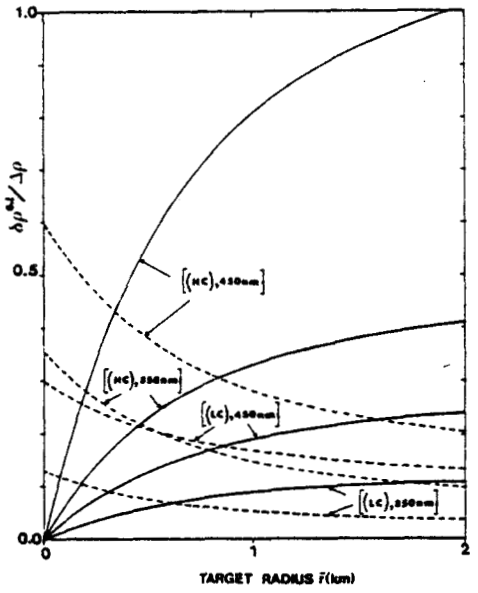

Fig. 13. Accuracy of small and large target approximations. $\Delta\rho$ is the actual environment correction. $\delta\rho$ is the error on the retrieved $\Delta\rho$ due to the approximations. Ratios $\delta\rho/\Delta\rho$ are given for, respectively, the small target approximation (full line) and large target approximation (dashed line).

It has been shown that nearly all over the target the measurements will give

$$\rho^* = \rho_a + \rho_1[A + BF(\bar{r})] + \rho_0 B[1 - F(\bar{r})]. \quad (26)$$

A target assumed to be either very small or very large may be respectively attributed approximate reflectances ρ_1^s and ρ_1^l so that

$$\rho^* = \rho_a + \rho_1^s A + \rho_0 B \quad (27)$$

$$\rho^* = \rho_a + \rho_1^l (A + B). \quad (28)$$

The systematic errors in absolute reflectance so introduced will be given by

$$\frac{\delta\rho_1^s}{\Delta\rho} = \frac{\rho_1^s - \rho_1}{\rho_1 - \rho_0} = \frac{BF(\bar{r})}{A} \quad (29)$$

$$\frac{\delta\rho_1^l}{\Delta\rho} = \frac{\rho_1^l - \rho_1}{\rho_1 - \rho_0} = \frac{B[1 - F(\bar{r})]}{A + B}. \quad (30)$$

These errors are shown in Fig. 13 as a function of the characteristic size $\bar{r}$ of the target for the two observation wavelengths of 850 and 450 nm and for the two aerosol contents corresponding to the $MC5$ and $MC23$ models. The solar zenith angle is 60°, and the mean approximate value of $F(\bar{r})$ [Eqs. (16) and (25)] was used.

Even for rather good visibility conditions, the environment effect will induce systematic errors larger than ~1% in absolute reflectance, as soon as the reflectance differences between the target and its background exceed 0.10. For patchy structures whose cell sizes are in the range of hundreds of meters, neither of the two 1-D approximations is good; the approximate Eqs. (29) and (30) then can account for the major part of these errors.

On the other hand, for this range of *a priori* rather small cell sizes, and for classification purposes, Fig. 13 shows that it is illusory to hope for data correction from Eq. (27) when using the small target approximation. The variability of the residual errors as a function of $\bar{r}$ would be larger [with a factor of $(A + B)/A$; Eqs. (29) and (30)] than when using the large target approximation. The classification errors will be smaller when the targets which have the same apparent reflectance ρ^* are affected to the same reflectance class.

The atmospheric effects need to be taken into account only for determination of the absolute value of a reflectance class; in such a determination, the environment effect could be partially accounted for by applying Eq. (30) to some reference targets of the considered class.

VI. Conclusions

The influence of the background contribution upon the apparent reflectance has been studied as a function of some atmospheric parameters and for simple target geometries.

The main defect of the single-scattering approximation of this environment effect corresponds to the overestimation of the transmission terms so introduced. More accurate values for $rp(r)$ would be obtained by just omitting the transmission terms $t(z,r)$ in Eq. (12).

The environment effect depends mainly upon the aerosol optical thickness τ_P. This parameter, along with the molecular optical thickness τ_R, defines the respective weights A and B of the object pixel and its background in the signal. Environment weighting functions, $rp(r)$ or $F(r)$, may be defined to describe the scale of the environment effect. These functions may be linearized as follows: $F(r) \simeq [\alpha_P\tau_P F_P(r) + \alpha_R\tau_R F_R(r)]/(\alpha_P\tau_P + \alpha_R\tau_R)$, where the respective contributions of aerosols and molecules are again given by optical parameters $\alpha_R\tau_R$ and $\alpha_P\tau_P$. Except for very unusual aerosol models, the aerosol environment weighting function $F_P(r)$ is reasonably accounted for with a mean standard function. Horizontal scales of the environment effect are typically 1 km for aerosol scattering and 10 km for molecular scattering.

For uniform targets whose sizes are in the intermediate range of hundreds of meters, where neither the small nor the large target approximation is accurate, the reflectance gradients are seen to be small enough to allow simple formulas to account for the major part of the atmospheric effect. For multispectral classification purposes, approximate Eqs. (29) and (30) could be helpful in the estimation of systematic errors induced by the environment effect.

The authors are indebted to A. De Leffe, Centre National d'Etudes Spatiales de Toulouse, for his helpful suggestions about this work and to J. Lenoble, Université des Sciences et Techniques de Lille, for her useful comments about this paper. Thanks go to L. F. Martin for his aid in the translation of this paper and to M. Doribreux who typed the manuscript. This work has been supported by the Centre National d'Etudes Spatiales under contract CNES/77/0737.

References

1. R. S. Fraser, in *Interaction Mechanisms within the Atmosphere, Manual of Remote Sensing*, R. G. Reaves, Ed. (American Association of Photogrammetry, Falls Church, Va.), p. 181.
2. T. Takashima, C. I. Taggart, and E. G. Morrissey, Astrophys. Space Sci. **40**, 157 (1976).
3. G. W. Kattawar and G. N. Plass, Appl. Opt. **7**, 1519 (1968).
4. R. E. Turner and M. M. Spencer, "Atmospheric Model for Correction of Spacecraft Data," in *Proceedings, Eighth International Symposium on Remote Sensing of Environment* (ERIM, Ann Arbor, Mich., 1972), p. 895.
5. H. R. Gordon, Appl. Opt. **17**, 1631 (1978).
6. M. Viollier, D. Tanre, and P. Y. Deschamps, Boundary-Layer Meteorol. **18**, 247 (1980).
7. A. P. Odell and J. A. Weinman, J. Geophys. Res. **80**, 5035 (1975).
8. S. Q. Duntley, A. R. Boileau, and R. W. Preisendorfer, J. Opt. Soc. Am. **47**, 499 (1957).
9. D. Tanre, M. Herman, P. Y. Deschamps, and A. De Leffe, Appl. Opt. **18**, 3587 (1979).
10. W. A. Pearce, "A Study of the Effects of the Atmosphere on Thematic Mapper Observations," NASA contract NAS 5-23639, Report 004-77, prepared for NASA Goddard Space Flight Center, Greenbelt, Md. (1977).
11. Y. Kawata, Y. Haba, T. Kusaka, Y. Terashita, and S. Ueno, "Atmospheric Effects and their Correction in Airborne Sensor and Landsat MSS Data," in *Proceedings, Twelfth International Symposium on Remote Sensing of Environment* (ERIM, Ann Arbor, Mich., 1978), p. 1241.
12. S. Ueno, Y. Haba, Y. Kawata, T. Kusaka, and Y. Terashita, *The Atmospheric Blurring Effect on Remotely Sensed Earth Imagery, in Remote Sensing of the Atmosphere: Inversion Methods and Applications*, A. L. Fymat and V. E. Zuev, Eds. (Elsevier, New York, 1978), p. 305.
13. J. Otterman and R. S. Fraser, Appl. Opt. **18**, 2852 (1979).
14. McClatchey, R. A. Fenn, J. E. A. Selby, F. E. Volz, and J. S. Garing, "Optical Properties of the Atmosphere," AFCRL 71-0279, Environmental Research Papers 354 (1971).
15. S. Chandrasekhar, *Radiative Transfer* (Clarendon, Oxford, 1950).
16. K. L. Coulson, E. L. Gray, and G. M. Bouricius, "A Study of the Reflection and Polarization Characteristics of Selected Natural and Artificial Surfaces," Technical Information Series, Report R 655 D4, Space Sciences Laboratory, General Electric Co. (1965).

ANNEXE 5

INFLUENCE OF THE ATMOSPHERE UPON SPACE MEASUREMENTS OF DIRECTIONAL PROPERTIES

TANRE D., HERMAN M., DESCHAMPS P.Y.

Laboratoire d'Optique Atmosphérique

Université des Sciences et Techniques de Lille

59655 Villeneuve d'Ascq Cédex

ABSTRACT

To compare measurements performed under different geometrical conditions, it is necessary to take into account the angular anisotropy of the reflection properties of natural surfaces. As the use, in the radiative transfer codes, of the exact boundary conditions seems prohibitive, a simple but accurate formulation of the problem has been searched for.

In this paper, two average angular reflectances are defined from which the reflected radiance may be deduced for any distribution of the downward radiance. Calculations made for different atmospheric models, show that the solar directionality is partly preserved in the downward radiation field, so that the average reflectances can be written as a linear combination of the actual reflectance and of the spherical albedo of the surface.

Finally, the feasability to detect directional properties from space measurements is discussed.

I - INTRODUCTION

To compute the solar radiation which is backscattered by the earth ground-atmosphere system, the ground reflectance is generally assumed to be given by a simple Lambert's law.

For most purpose, this is a good approximation ; but actually, ground reflectances exhibit generally some bidirectionnal properties. These bidirectionnal effects may be considered as an interesting information, to be looked for in the atmospheric signal ; or, on the contrary, as a perturbation term to be corrected (for the case of stereoscopic measurements, for example). In any case, evaluations of the atmospheric signal, taking into account the bidirectionnal properties of the ground reflectance, are valuable, at least as reference computations.

Exact computations will not be tried here, because these rigourous results depend, in an intrincated way, upon the ground reflectance law and upon the atmospheric optical properties. We will rather search for an approximate formulation of the signal, where the ground and the atmosphere parameters will be separated. This is possible, with a good accuracy, for not too highly anisotropic bidirectionnal reflectance laws.

From this approximate formulation, it is easy to determine to what extent the anisotropy effects of the ground reflectance are preserved in the atmospheric signal, and to compare them with anisotropy effects due to the atmospheric scattering. These two effects generally will be quite comparable. The ground bidirectionnal reflectance retrieval, from space measurements, is so somewhat delicate, and its feasability for vegetated surfaces, from multi-

spectral measurements is discussed.

II - BIDIRECTIONNAL REFLECTANCES

The atmospheric signal must be evaluated for reflectance laws representative of the bidirectionnal effects actually encountered over natural surfaces.

Many measurements of bidirectionnal reflectances have been made in the litterature[1-3] ; but, to be quite useful in radiative transfer computations, $\rho(\theta_s,\theta_v,\varphi_v)$ must be known as a function of the incident direction θ_s as well as, as a function of the scattered or observation direction θ_v,φ_v (φ_v is the relative azimuth between the incidence and observation planes). Very few examples of such complete measurements of $\rho(\theta_s,\theta_v,\varphi_v)$ exist ; we wil refer here to the results presented by Kriebel[4].

Three cases have been retained, from these observations, corresponding to vegetated surfaces : pasture, forest and Savannah. Fig. 1a to 1c show typical results, as reported by Kriebel, for $\rho(\theta_s,\theta_v,\varphi_v)$ in the principal solar incidence plane, for λ = 520 nm. Fig 1d shows that, except for the albedo scaling factor, the bidirectionnal effect does not depend very much upon the wavelength.

These experimental data are compared, Fig. 1a to 1d, with polar diagrams, corresponding for the reflectance, to analytical law in the form

$$\rho(\theta_s,\theta_v,\varphi_v) = \sum_s (2-\delta_{os}) \cos s\varphi \sum_\ell \sum_m \rho^s_{\ell m} P^s_\ell(\theta_s) P^s_m(\theta_v) \qquad (1)$$

$\rho^s_{\ell m}$ were adjusted to fit coarsely the experimental results. We put $\rho^s_{\ell m}=\rho^s_{m\ell}$, so as to assure the reciprocity principle.

From eq. (1) $\rho(\theta_s,\theta_v,\varphi_v)$ may be computed very easily for any geometric condition. Fig. 1a to 1c show that this equation, in conjunction with adequate values for $\rho^s_{\ell m}$, compares quite well with representative experimental results. From now the 3 bidirectionnal reflectance laws corresponding to the results of eq. (1) in these Figures will be considered as our reference test cases : it is for these theoretical and somewhat artificial, but reasonably realistic, reflectances that the atmospheric signal will be simulated.

III - EXPRESSION OF THE ATMOSPHERIC SIGNAL

One will not solve exactly the radiative transfer problem, but will search for an approximate formulation of the backscattered solar radiation, in which the atmospere and the ground reflectance parameters could be separated.

Classically the signal received by the satellite will be expressed as a function of the successive orders of radiation interactions, in the coupled ground-atmosphere system. We will distinct here :

(i) the purely atmospheric signal, (Fig. 2a);

(ii) the direct signal, corresponding to photons which go directly from the sun to the target and from the target to the satellite, through the atmosphere (Fig. 2b). This is the useful signal, which contains the whole information about the bidirectionnel properties of the target ;

(iii) the signal corresponding to the diffuse solar radiation, reflected by the target and then going directly through the atmosphere (Fig. 2c) ;

(iv) the signal corresponding to the direct solar radiation reflected by the ground (the surface is assumed to be homogeneous to neglect the environment effect) and then going diffusely through the atmosphere, (fig. 2d) to the satellite, we will see that these (iii) and (iv) signals are partly useful signals ;

(v) the signal corresponding to photons which go diffusely from the sun to the surface and then from the surface to the satellite (fig. 2e) ;

(vi) and finally the signal corresponding to photons which has suffered 2, 3... reflexions on the ground (fig. 2f).

Typically for mean atmospheric conditions, the respective weights of the signals (ii) to (v) are 70,10, 10 and 1 per cent for λ = 750 nm (respectively 40, 20, 20, and a few percent for λ = 400 nm). Clearly to obtain a good accuracy in the atmospheric signal formulation, it is sufficient to search for a correct estimation of these terms (i) to (iv), that is of the terms (ii) (iii) and (iv), for the bidirectionnal properties influence.

Let τ be the optical thickness of the atmosphere, θ_s = Arcos μ_s, the solar zenith angle, θ_v = Arcos μ_v, the zenith wiewing angle and $\downarrow L a_o$ the diffuse downward solar radiation.

To each component of the radiation field, one well associate a particular reflectance

- the acutal reflectance ρ will correspond to the photons directly transmitted on the two paths : $(e^{-\tau/\mu_s}\ \rho\ e^{-\tau/\mu_v})$ (Fig. 2b).

- the reflectance $\bar{\rho}$ will correspond to the photons diffusely transmitted to the surface ($E(\mu_s)$), reflected by the ground ($\bar{\rho}$) and then directly transmitted through the atmosphere ($e^{-\tau/\mu_v}$) (Fig. 2c) that is

$$\bar{\rho}(\theta_s,\theta_v,\varphi_v) = \frac{\int_0^{2\pi}\int_0^1 \downarrow L a_o(\theta_s,\theta',\varphi')\ \rho(\theta_v,\theta',\varphi')\ d\Omega'}{E(\theta_s)} \qquad (2)$$

with $E(\theta_s)$ defined by

$$E(\theta_s) = \int_0^{2\pi}\int_0^1 L_a^{\downarrow}(\theta_s,\theta,\varphi)d\Omega$$

where $L_a^{\downarrow}$ is the downward diffuse radiance and $d\Omega$ the solid angle about the direction Ω.

- The reflectance $\bar{\rho}'$ will correspond to the photons directly transmitted through the atmosphere $(e^{-\tau/\mu_s})$, reflected by the ground $(\bar{\rho}')$ then diffusely transmitted through the atmosphere in the observation direction $(E(\mu_v))$ (fig. 2d), that is

$$\bar{\rho}'(\theta_s,\theta_v,\varphi_v) = \frac{\int_0^{2\pi}\int_0^1 \rho(\theta_s,\theta',\varphi')\, L_a^{\downarrow}(\theta',\theta_v,\varphi')d\Omega'}{E(\theta_v)} \qquad (3)$$

In fact, then two average reflectances $\bar{\rho}(\theta_s,\theta_v,\varphi_v)$ et $\bar{\rho}'(\theta_s,\theta_v,\varphi_v)$ are identical according to the reciprocity principle. For more details, the reader is referred to ANNEX I.

Finally, the reflectance $\bar{\bar{\rho}}(\theta_s,\theta_v,\varphi_v)$ will correspond to the radiance diffused through the atmosphere which gives a diffuse flux $E(\mu_s)$, reflected by the ground $\bar{\bar{\rho}}$ and then diffused by the atmosphere in the observation direction with the function $E(\mu_v)$. The exact definition of $\bar{\bar{\rho}}$ is detailed in ANNEX II (cf. eq. (A-II-5)).

If we neglect the multiple interactions between the atmosphere and the ground, and express the various quantities in terms of equivalent reflectance, the apparent reflectance can be written as[6]

$$\begin{aligned}\rho^*(\tau,\mu_s,\mu_v,\varphi_v) = {} & \rho_a(\tau,\mu_s,\mu_v,\varphi_v) + \rho(\mu_s,\mu_v,\varphi_v)\, e^{-\tau/\mu_s}\, e^{-\tau/\mu_v} \\ & + \bar{\rho}(\tau,\mu_s,\mu_v,\varphi_v)\left[\bar{t}_d(\mu_s)e^{-\tau/\mu_v} + e^{-\tau/\mu_s}t_d(\mu_v)\right] \qquad (4) \\ & + \bar{\bar{\rho}}(\tau,\mu_s,\mu_v,\varphi_v)\, t_d(\mu_s)\, t_d(\mu_v)\end{aligned}$$

where $t_d(\mu)$ is the diffuse transmittance.

We will apply this formulation to our 3 kinds of ground reflectance law and to different atmosphere models. From these cpmputations, we will search which parameters are important for the average reflectances $\bar{\rho}$ and $\bar{\bar{\rho}}$.

IV - MEAN REFLECTANCE $\bar{\rho}$

Besides the 3 bidirectionneal reflectance laws (Eq.1) we have considered three different scattering atmospheric models : (R) contains no aerosols and would correspond to the best measurement conditions, (V23) corresponds to ground visibility of 23 km according to the Mc Clatchey et al's model ; it corresponds to standart measurements conditions. (V5) corresponds to a ground visibility of 5 km and to extreme measurements conditions.

For these 3 atmospheric models the intrinsic atmospheric radiances L_{ao} were first computed by the successive orders of scattering method, assuming the ground reflectances to be null. The upward radiances give the atmospheric reflectances ρ_a in Eq (4).

The downward radiances which are to be used in eq. (2), (3) and (A-II-5 to give the mean reflectances $\bar{\rho}$, and $\bar{\bar{\rho}}$, are drawn on Fig. 3a and 3-b, (in polar coordinates), we see on these figures that the strong forward scattering of the aerosols is retrieved in the downward diffuse radiance. This suggest that we should write the downward radiance as a linear combination of an isotropic component and of a dirac function.

We have computed, for several geometrical conditions - i.e. several solar zenith angles and several observation angles, the two average reflectance $\bar{\rho}$ and $\bar{\bar{\rho}}$ from eq.(2) and eq.(A-II-5) for the 9 different combinaisons of ground

reflectance law and atmosphere model precedently defined. For each case,we have drawn $\bar{\rho}$ versus ρ, for any geometric condition, in Fig. 4a to 4c, for λ = 450 nm. For the Savannah, Fig. 4d (λ= 850 nm) shows the wavelength influence.

From Fig. 4a to 4c, it may be seen that in $\bar{\rho}$ (and in $\bar{\bar{\rho}}$ to a lesser extent, Fig. 4e) the bidirectional effect is partly preserved, and $\bar{\rho}$ can be approximately written as

$$\bar{\rho} = a\rho + b \qquad (5)$$

In the same way (Fig. 4e)

$$\bar{\bar{\rho}} = a'\rho + b'$$

From a linear regression, these coefficients a, a', b and b' where estimated (table 2) and the corresponding results Eq.5 are compared (Fig. 4a to 4e) to the exact values $\bar{\rho}$ and $\bar{\bar{\rho}}$.

It is seen, Table 2, that the coefficients a and b don't depend very much upon the assumed ground reflectance law. These coefficients depend essentially upon the atmospheric diffuse radiation field (that is, upon the atmospheric parameters), so that, from eq. (5), we obtain the desired separation between the atmospheric parameters and the ground reflectance parameters, with a reasonable accuracy.

The conservation of the bidirectional effects in $\bar{\rho}$ is quite understandable, from Fig. 3a and 3b, where it is seen that solar beam directionnality is preserved, to a large degree, into the downward diffused radiation field $L_{ao}^{\downarrow}$, due to the forward scattering of the aerosols.

More precisely, from eq. (3), it is clear that eq. (5) is evident for a diffused radiation field $L_{ao}^{\downarrow}$ in the form

$$\frac{L_{a_o}^{\downarrow}(\tau,\mu_s,\mu_v,\varphi_v)}{\mu_s \; f \; E(\mu_s)} = A \; \delta(\mu_v,\mu_s) + B \qquad (6)$$

with $A + B = 1$

where $\delta(\mu_v,\mu_s)$ is the dirac function. From the exact computations of $L_{ao}^{\downarrow}$, for different solar zenith angles, we have estimed the coefficients A and B with a least square method ; the corresponding values for the three atmosphere models are reported in table 1 for λ = 450 nm and λ = 850 nm.

The values of A (Table 1) and a (Table 2) compare well, and we will consider that

$$a \simeq A, \qquad (7)$$

that is,a, in eq. (5), corresponds to the remaining directionnality in the downward diffuse radiation field. For the second order term, we will put

$$a' \simeq A^2 \qquad (8)$$

In the same way, the ground spherical albedo γ is defined by

$$\gamma = \frac{\int_o^{2\pi} d\varphi_v \int_o^{2\pi} d\varphi_s \int_o^1 \mu_v d\mu_v \int_o^1 \mu_s d\mu_s \; \rho(\mu_s,\mu_v,\varphi_v,\varphi_s)}{\int_o^{2\pi} d\varphi_v \int_o^{2\pi} d\varphi_s \int_o^1 \mu_v d\mu_v \int_o^1 \mu_s d\mu_s} \qquad (9)$$

From eq. (5) and (6), b is to be compared to the predict of the ground spherical albedo by the pourcentage of isotropic radiance (that is B) in the diffuse radiation field. The results indicate a good correlation between b and γB (Table 3).

In firt approach, the average reflectance $\bar{\rho}$ and $\bar{\bar{\rho}}$ can be written a good accuracy as

$$\bar{\rho} = a\rho + b \qquad ; \qquad \bar{\bar{\rho}} = a^2\rho + b \tag{10}$$

where the coefficient a, which depends essentially upon the atmospheric model corresponds to the remaining directionality, in the downward diffuse radiation field; and where the coefficient b is the product of the ground spherical γ albedo by the intensity B of the isotropic component in the downward radiation field.

V - APPLICATIONS

The above formalism Eqs. 4 and 10 allows to write, with a good accuracy, the apparent reflectance ρ^* as,

$$\rho^*(\tau,\mu_s,\mu_v,\varphi_v) = \rho_a(\tau,\mu_s,\mu_v,\varphi_v) + \rho(\mu_s,\mu_v,\varphi_v)(e^{-\tau/\mu_s}+a\ t_d(\mu_s))(e^{-\tau/\mu_v}+a\ t_d(\mu_v)) + b(T(\mu_s)\ T(\mu_v) - e^{-\tau/\mu_s}\ e^{-\tau/\mu_v}) \tag{11}$$

where $T(\mu)$ (direct + diffuse atmospheric transmittance) and a being atmospheric parameters the separation between the atmospheric and ground reflectance properties is effectively obtained.

From this formulation (Eq. 11) it is now very easy to determine how the ground anisotropy effects influence the atmospheric signal. We will use here this formulation to examine the feasability to detect the ground bidirectionnal effects from satellite measurements, assuming that a same target can be observed from different directions. Then the perturbing term is the atmospheric reflectance ρ_a, which exhibits also large directionnal effects.

A first solution is to study in what conditions these directionnal effects of ρ_a are merely negligible in front of the ground effects. Let $\Delta\rho^*$ be the difference between two satellite measurements, we suppose the observations are made in the solar incident plane in directions θ_v, φ_v=0 and θ_v, φ_v=180, then

$$\Delta\rho^*_{\Delta\varphi} = \Delta\rho^a_{\Delta\varphi} + \Delta\rho_{\Delta\varphi} \left[e^{-\tau/\mu_s} + a\, t_d(\mu_s)\right]\left[e^{-\tau/\mu_v} + a\, t_d(\mu_v)\right]$$

where $\Delta\rho^*_{\Delta\varphi} = \rho^*(\tau,\theta_s,\theta_v,\varphi_v = 0) - \rho^*(\tau,\theta_s,\theta_v,\varphi_v = 180)$

$$\Delta\rho^a_{\Delta\varphi} = \rho_a(\tau,\theta_s,\theta_v,\varphi_v = 0) - \rho_a(\tau,\theta_s,\theta_v,\varphi_v = 180) \qquad (12)$$

$$\Delta\rho_{\Delta\varphi} = \rho(\theta_s,\theta_v,\varphi_v = 0) - \rho(\theta_s,\theta_v,\varphi_v = 180)$$

with $\Delta\varphi$ the azimuth difference between the two measurements.

To derive from the measurement, $\Delta\rho^*_{\Delta\varphi}$, the information about the ground signal $\Delta\rho_{\Delta\varphi}$, without taking into account the atmospheric perturbation, it is necessary that the standard deviation of the atmospheric reflectance ρ_a, from an isotropic law, be small, that is

$$\Delta\rho^a_{\Delta\varphi} \ll \Delta\rho_{\Delta\varphi} \left(e^{-\tau/\mu_s} + a\, t_d(\mu_s)\right)\left(e^{-\tau/\mu_v} + a\, t_d(\mu_v)\right) \qquad (13)$$

These different terms regard monochromatic quantities, but subscript λ will be omitted to simplify notation. We study the spectral variations of Eq 13 to determine the spectral range where the information can be derived.

We will suppose that the angular dependance of the reflectance is nearly independant of the wavelength (cf. Fig. 1c and 1d) that is

$$\Delta\rho_{\Delta\varphi} = \gamma \, \Delta\rho^{r}_{\Delta\varphi} \tag{14}$$

where $\Delta\rho^{r}_{\Delta\varphi}$ does not depend upon the wavelength for fixed geometrical conditions, and where γ is the spherical albedo of the surface.

The relative angular variations $\Delta\rho^{r}_{\Delta\varphi}$ of the reflectance must be so that

$$\Delta\rho^{r}_{\Delta\varphi} \geqslant \frac{\overline{\Delta\rho^{a}_{\Delta\varphi}}}{\gamma} \quad \frac{1}{(e^{-\tau/\mu_s} + a\, t_d(\mu_s))(e^{-\tau/\mu_v} + a\, t_d(\mu_v))} \tag{15}$$

From the exact atmospheric reflectance computations, for our three atmospheric models, we have estimated $\frac{\overline{\Delta\rho^{a}_{\Delta\varphi}}}{\gamma}$ as a function of λ, for observations within a cone of 40° in the incident plane. For the spectral variations of the albedo γ, we have considered the case of the vegetation and we have taken the values given by Kondratiev et al.[5].

The spectral variations of $\frac{\overline{\Delta\rho^{a}_{\Delta\varphi}}}{\gamma} \frac{1}{T_s(\mu_s)\, T_s(\mu_v)}$ where we have noted $T_s(\mu)$ the transmittance defined as

$$T_s(\mu) = e^{-\tau/\mu} + a\, E(\mu) \tag{16}$$

are reported on figure 5-a. The calculation are made for the three atmosphere models at two solar zenith angles (θ_s = 15 and 60°). If the atmospheric reflectance is unknown and is supposed isotropic, one will have very large errors on the ground estimated bidirectionnal effect, all over the visible range ($\lambda \lesssim 0{,}8$ m). In the near infrared, the ground effect will be attanable only for very good conditions of visibility. In fact, the knowledge of the angular dependance of $\rho_a(\theta_s, \theta_v, \varphi_v)$ could increase largely the possibilities to detect the ground directionnal contrast. In effect, from the computations made for the different atmosphere models, it is clear that the atmospheric reflectance ρ_a directionnal features are partly somewhat independant of the aerosols content or of the aerosols properties ; so that a mean standard atmospheric reflectance $\bar{\rho}_a$ could be defined, as a function of the geometric conditions, and be substracted from the measurements.

Nevertheless in order to avoid this somewhat difficult problem, we propose to use multi-spectral measurements which permit to escape the ρ_a evaluation. Indeed, the albedo of vegetation surfaces has a minimum at 650 nm and becomes maximum near 750 nm ; on the other hand, the atmospheric reflectance $\rho_a(\theta_s, \theta_v, \varphi_v)$ and the "specular transmittance" $T_s(\mu)$ have a smoth wavelength dependance (as λ^{-1}). So we can hope to eliminate most of the errors in substracting the apparent reflectances measured at 650 nm and 850 nm.

From Eq. 11, we write

$$(\rho^{*}_{\lambda_1}(\theta_1) - \rho^{*}_{\lambda_2}(\theta_1)) - (\rho^{*}_{\lambda_1}(\theta_2) - \rho^{*}_{\lambda_2}(\theta_2)) = \Delta\rho^{a}_{\Delta\varphi,\lambda_1} - \Delta\rho^{a}_{\Delta\varphi,\lambda_2} + \Delta\rho_{\Delta\varphi,\lambda_1} T_{s,\lambda_1} - \Delta\rho_{\Delta\varphi,\lambda_2} T_{s,\lambda_2} \quad (17)$$

To obtain some information, the relative angular variations have now to be such as

$$\Delta\rho^{r}_{\Delta\varphi} \gg \frac{\Delta\rho^{a}_{\Delta\varphi,\lambda_1} - \Delta\rho^{a}_{\Delta\varphi,\lambda_2}}{\gamma_{\lambda_1} T_{s,\lambda_1} - \gamma_{\lambda_2} T_{s,\lambda_2}} \quad (18)$$

This condition is much less restrictive than Eq. 15. The fig. 5b shows that this method allows to remote small angular variations of the reflectance, even for extreme condition of visibility.

CONCLUSION

An accurate analytical expression of the measured reflectance was established for the case of a non Lambertien ground. The formulation of the signal as described can be quite practical. It allows a fast and simple evaluation of the two average angular reflectance as a function of atmospheric and ground properties.

Using multispectral measurements, it seems possible to obtain informations about the angular variations of the ground reflectances even with high aerosol contents in the atmosphere, from space measurements.

REFERENCES

1 - CHANCE I.E., and E.W. LEMASTER, Appl. Opt. 16, 407, (1977).

2 - SUITS G.H., Remote Sensing Environ. 2, 117, (1972).

3 - COULSON K.L., G.M. BOURICIUS and E.L. GRAY, J. Geophys. Res. 70, 4601, (1965).

4 - KRIEBEL K.T., Appl. Opt. 17, 253, (1978).

5 - KONDRATIEV K.Y., Z.F. MIRONOVA and A.N. OTTO, Pure Appli. Geophys. 59, 207, (1964).

6 - TANRE D., M. HERMAN, P.Y. DESCHAMPS and A. DE LEFFE, Appl. Opt. 18, 3587, (1979).

ANNEXE I

IDENTITY BETWEEN THE TWO AVERAGE ANGULAR REFLECTANCES $\bar{\rho}$ AND $\overline{\rho'}$

Let $\mu_o L(\Omega_o) d\Omega_o$ be the radiance **incident** in the solid angle $d\Omega_o$ about the direction Ω_o where θ_o = Arcos μ_o is the angle between the incident radiation and the normal to the atmosphere.

Let $P(\Omega_o, \Omega) d\Omega$ be the probability that the incident radiation at Ω_o will be scattered into an element of solid angle $d\Omega$ about the direction Ω.

We define $\bar{\rho}$ which corresponds to the radiation diffused over the entire hemispherical space, and reflected in direction Ω by

$$\bar{\rho}(\Omega_o, \Omega) = \frac{\int_o^{2\pi} \int_o^1 \rho(\Omega', \Omega) L(\Omega') \mu' d\Omega'}{\int_o^{2\pi} \int_o^1 I(\Omega') \mu' d\Omega'} \qquad (I-1)$$

where $L(\Omega') \mu' d\Omega'$ is the radiance diffused by the atmosphere in any direction Ω', that will be written

$$L(\Omega') d\Omega' = P(\Omega_o, \Omega') d\Omega' [L(\Omega_o)\mu_o d\Omega_o] \qquad (I-2)$$

So, the average angular reflectance $\bar{\rho}$ is written

$$\bar{\rho}(\Omega_o, \Omega) = \frac{\int_o^{2\pi} \int_o^1 \rho(\Omega', \Omega) P(\Omega_o, \Omega')\mu' d\Omega'}{\int_o^{2\pi} \int_o^1 P(\Omega_o, \Omega')\mu' d\Omega'} \qquad (I-3)$$

In the same way, we define $\bar{\rho}'$ which corresponds to the radiation directly transmitted to the ground, reflected in any direction and diffusely transmitted in Ω direction,

$$\bar{\rho}'(\Omega_o, \Omega) = \frac{dL(\Omega)}{L(\Omega_o)\ \mu_o\ d\Omega_o} \qquad (I\text{-}4)$$

$dL(\Omega)$ is the radiance diffused by the atmosphere in Ω direction, that will be written as :

$$dL(\Omega) = \frac{\int_o^{2\pi} \int_o^1 P(\Omega', \Omega)\ L(\Omega')\ \mu'\ d\Omega'}{\int_o^{2\pi} \int_o^1 P(\Omega', \Omega)\ \mu'\ d\Omega'} \qquad (I\text{-}5)$$

where $L(\Omega')$ represents the radiance reflected by the ground, that is

$$L(\Omega') = \rho(\Omega_o, \Omega')\ L(\Omega_o)\ \mu_o\ d\ \Omega_o \qquad (I\text{-}6)$$

The average reflectance $\bar{\rho}'$ can be written again as

$$\bar{\rho}'(\Omega_o, \Omega) = \frac{\int_o^{2\pi} \int_o^1 P(\Omega', \Omega)\ \rho(\Omega_o, \Omega')\ \mu'\ d\Omega'}{\int_o^{2\pi} \int_o^1 P(\Omega', \Omega)\ \mu'\ d\Omega'} \qquad (I\text{-}7)$$

In accordance with the reciprocity principle, we have

$$\begin{aligned} P(\Omega, \Omega_o) &= P(\Omega_o, \Omega) \\ \rho(\Omega, \Omega_o) &= \rho(\Omega_o, \Omega) \end{aligned} \qquad (I\text{-}8)$$

With the relations I-8 into Eqs I-3 and I-7, we note the strict identity between the two average angular reflectances $\bar{\rho}$ and $\bar{\rho}'$.

ANNEXE II

DEFINITION OF THE AVERAGE REFLECTANCE $\bar{\bar{\rho}}$

We consider the reflectance which corresponds to the radiation incident on the surface from all directions in the hemispherical space after scattering in the atmosphere and the radiation reflected over the entire hemispherical space then diffused again in Ω direction. We can so write

$$\bar{\bar{\rho}} = \frac{dL(\Omega)}{I(\Omega_o)\ \mu_o\ d\Omega_o} \qquad \text{(II-1)}$$

From Eq I-5, $dL(\Omega)$ is written

$$dL(\Omega) = \frac{\int_o^{2\pi} \int_o^1 P(\Omega', \Omega)\ L(\Omega')\ \mu'\ d\Omega'}{\int_o^{2\pi} \int_o^1 P(\Omega', \Omega)\ \mu'\ d\Omega'} \qquad \text{(II-2)}$$

$L(\Omega')$ corresponds to the radiation reflected in direction Ω' when the radiation is incident on the surface from all directions in the hemispherical space, that is

$$L(\Omega') = \int_o^{2\pi} \int_o^1 \rho(\Omega'', \Omega')\ L(\Omega'')\ \mu''\ d\Omega'' \qquad \text{(II-3)}$$

As $L(\Omega'')$ is the diffused radiation through the atmosphere with an incident radiation $\mu_o L(\Omega_o)\ d\Omega_o$, it can be written

$$L(\Omega'') = P(\Omega_o, \Omega'')\ \mu''\ d\Omega''\ [L(\Omega_o)\ \mu_o\ d\Omega_o] \qquad \text{(II-4)}$$

From Eqs II-2 to II-4, the average reflectance $\bar{\bar{\rho}}$ is given by

$$\bar{\bar{\rho}}(\Omega_o, \Omega) = \int_o^{2\pi}\int_o^1 \mu'' d\Omega'' \int_o^{2\pi}\int_o^1 \mu' d\Omega' \; P(\Omega', \Omega)\, \rho(\Omega'', \Omega')\, P(\Omega_o, \Omega'') \quad \text{(II-5)}$$

	λ = 450 nm		λ = 850 nm	
	A	B	A	B
{ R}	0.10	0.90	0.12	0.88
{23}	0.28	0.72	0.40	0.60
{ 5}	0.24	0.76	0.35	0.63

TABLE 1

Coefficients A and B of development of the diffused radiation field.

	coefficient a				coefficient a'
	λ = 450 nm			λ = 850 nm	λ = 450 nm
	savannah	pasture	forest	savannah	savannah
{R}	0.097	0.120	0.158	0.100	0.014
{23}	0.331	0.338	0.329	0.328	0.128
{5}	0.302	0.323	0.300	0.469	0.114

TABLE 2

Coefficients a and a' of the linear regression of $\bar{\rho}$ and $\bar{\bar{\rho}}$.

	λ = 450 nm			λ = 850 nm	λ = 450 nm
	Savannah	Pasture	forest	Savannah	Savannah
γ	0,045	0,057	0,021	0,186	0,045
{R} b	0,041	0,042	0,015	0,153	b' 0,042
{R} γB	0,041	0,051	0,019	0,164	0,041
{23} b	0,032	0,031	0,011	0,085	b' 0,038
{23} γB	0,032	0,041	0,015	0,112	0,032
{5} b	0,035	0,032	0,011	0,102	b' 0,040
{5} γB	0,034	0,043	0,016	0,121	0,034

TABLE 3

Comparaison between coefficient b of the linear regression of $\bar{\rho}$ and $\bar{\bar{\rho}}$ and coefficient γB of the diffused radiation field and of the ground.

FIGURE CAPTIONS

Fig. 1-a Reflectance of the pasture (in polar coordinates) in the principal solar incidence plane, for three zenith solar angles, at λ = 520 nm.

Fig. 1-b Same as Fig. 1-a but for the forest

Fig. 1-c Same as Fig. 1-a but for the savannah

Fig. 1-d Same as Fig. 1-a but for the savannah at λ = 860 nm.

Fig. 2 Successive orders of radiation interactions in the coupled ground-atmosphere system.

Fig. 3-a Downward radiances (polar coordinates) for two zenith solar angles and the three atmosphere models, at λ = 450 nm.

Fig. 3-b Same as Fig. 3-a, but at λ = 850 nm.

Fig. 4-a Average angular reflectance $\bar{\rho}$ versus the actual reflectance ρ for the pasture (The different points are obtained for different geometrical conditions) at λ = 450 nm

Fig. 4-b Same as Fig. 4-a, but for the forest.

Fig. 4-c Same as Fig. 4-a, but for the savannah.

Fig. 4-d Same as Fig. 4-a, but for the savannah at λ = 850 nm.

Fig. 4-e Average angular reflectance $\bar{\rho}$ versus the actual reflectance ρ for the savannah (The different points are obtained for different geometrical conditions) at λ = 450 nm.

Fig. 5-a Spectral variations of $\frac{\Delta\rho^a_{\Delta\varphi}}{\gamma} \frac{1}{T_s(\mu_s)T_s(\mu_v)}$ (see the text) for the three atmosphere models and two zenith solar angles.

Fig. 5-b Spectral variations of

$$\frac{\Delta\rho^a_{\Delta\varphi,\lambda_1} - \Delta\rho^a_{\Delta\varphi,\lambda_2}}{\gamma_{\lambda_1} T_{s,\lambda_1} - \gamma_{\lambda_2} T_{s,\lambda_2}}$$

(see the text) where λ_1 = 650 nm for the extreme atmosphere model (V5) and two zenith solar angles.

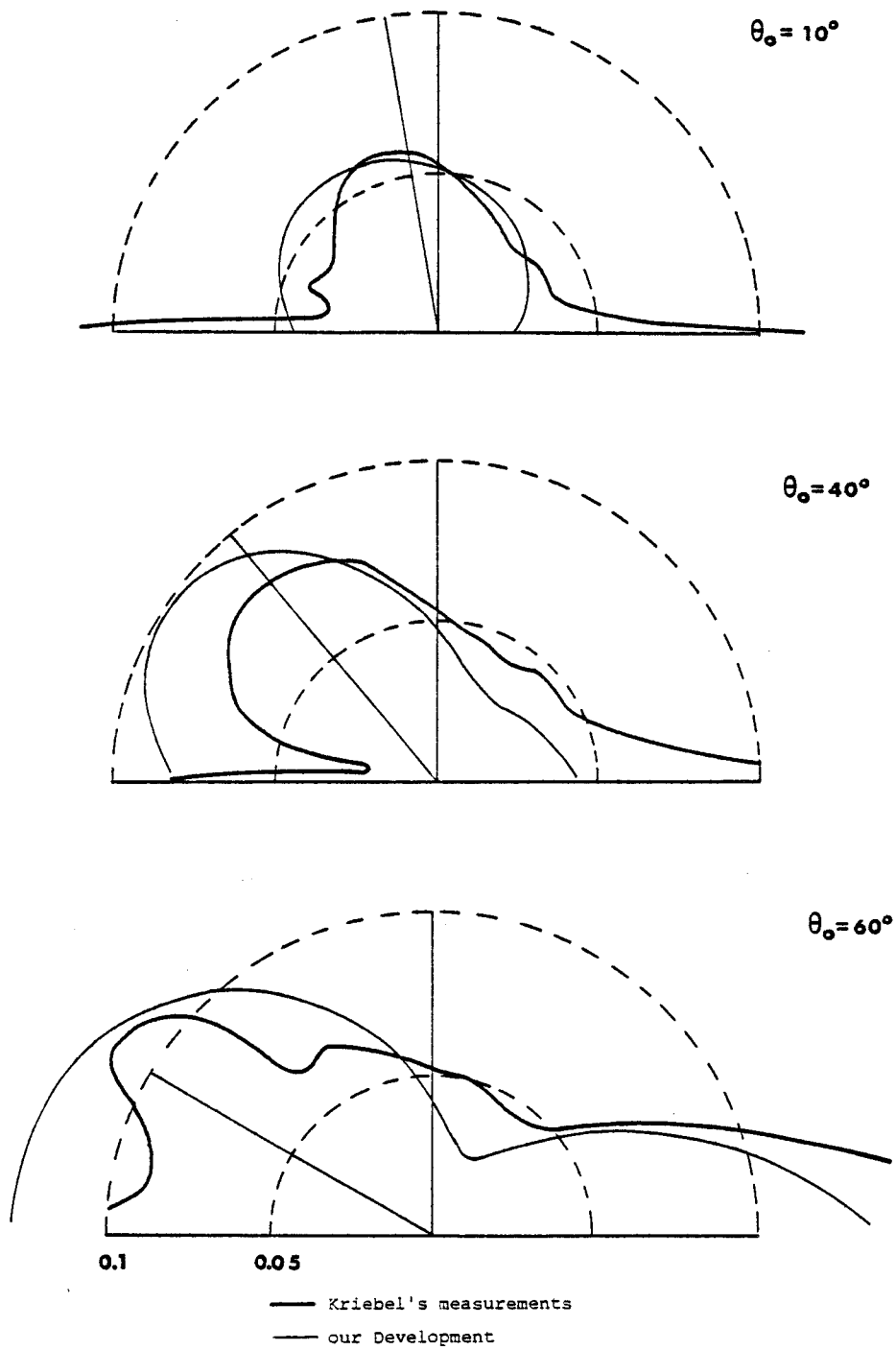

Fig. 1-a Reflectance of the pasture (in polar coordinates) in the principal solar incidance plane, for three zenith solar angles, at λ = 520 nm.

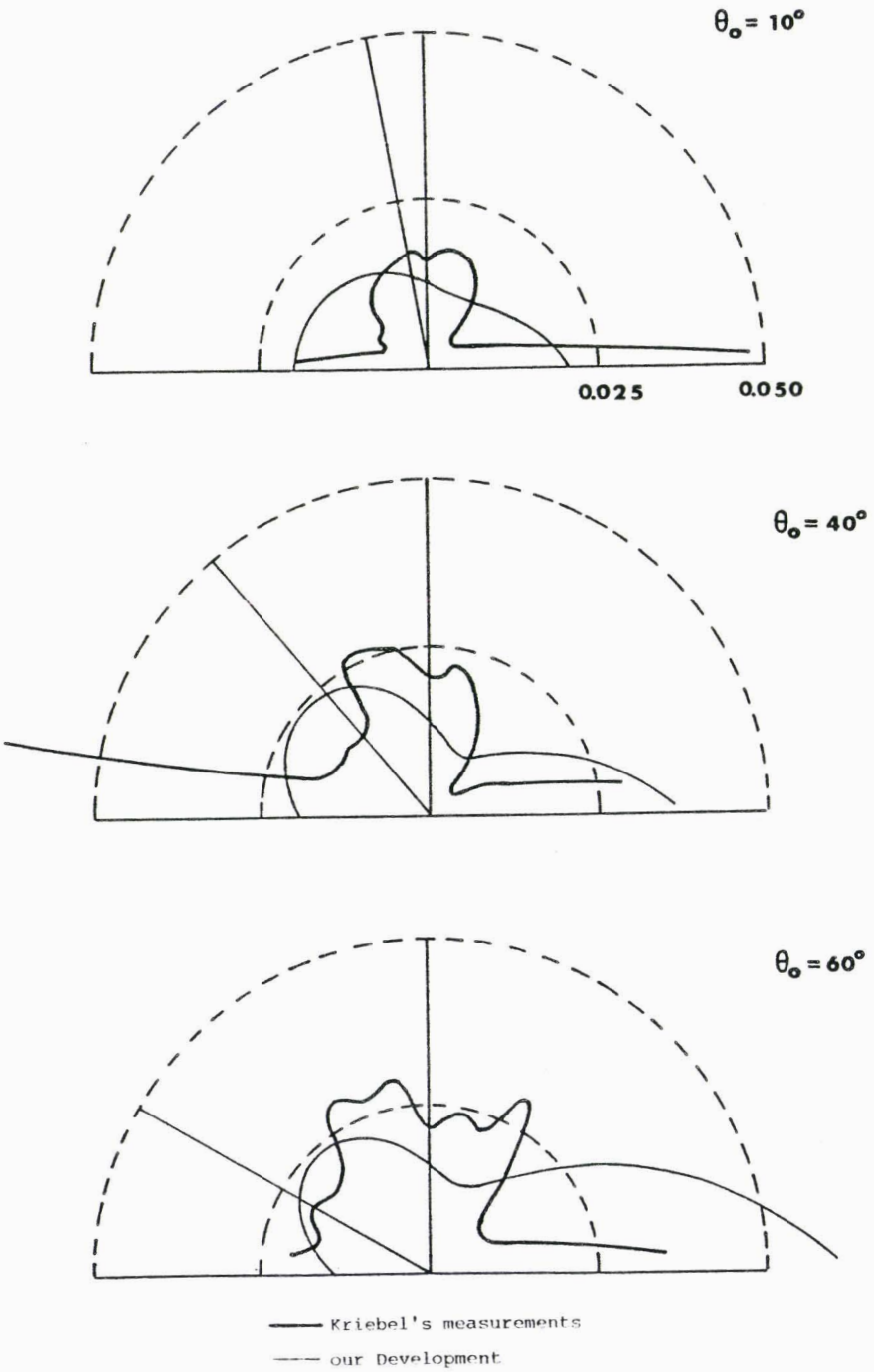

Fig. 1-b Same as Fig. 1-a but for the forest

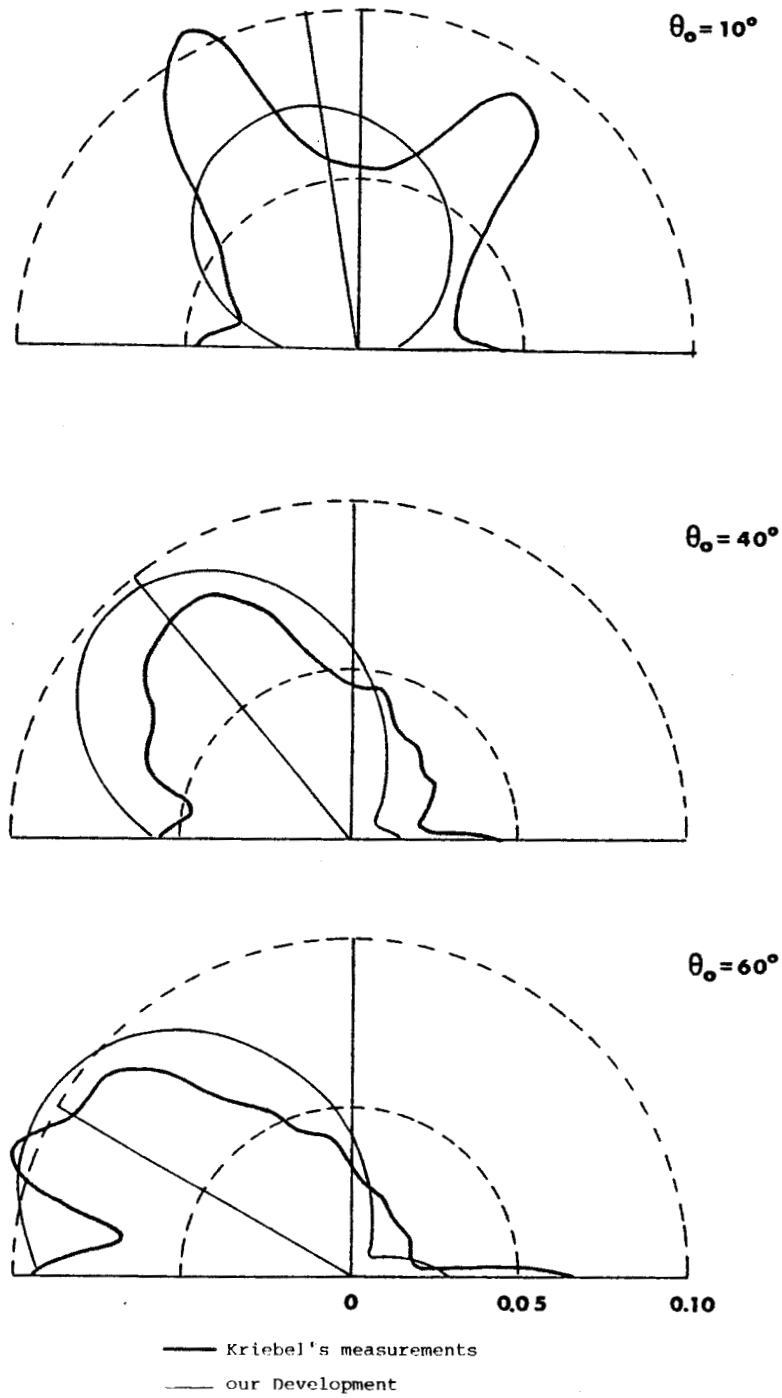

Fig. 1-c Same as Fig. 1-a but for the savannah

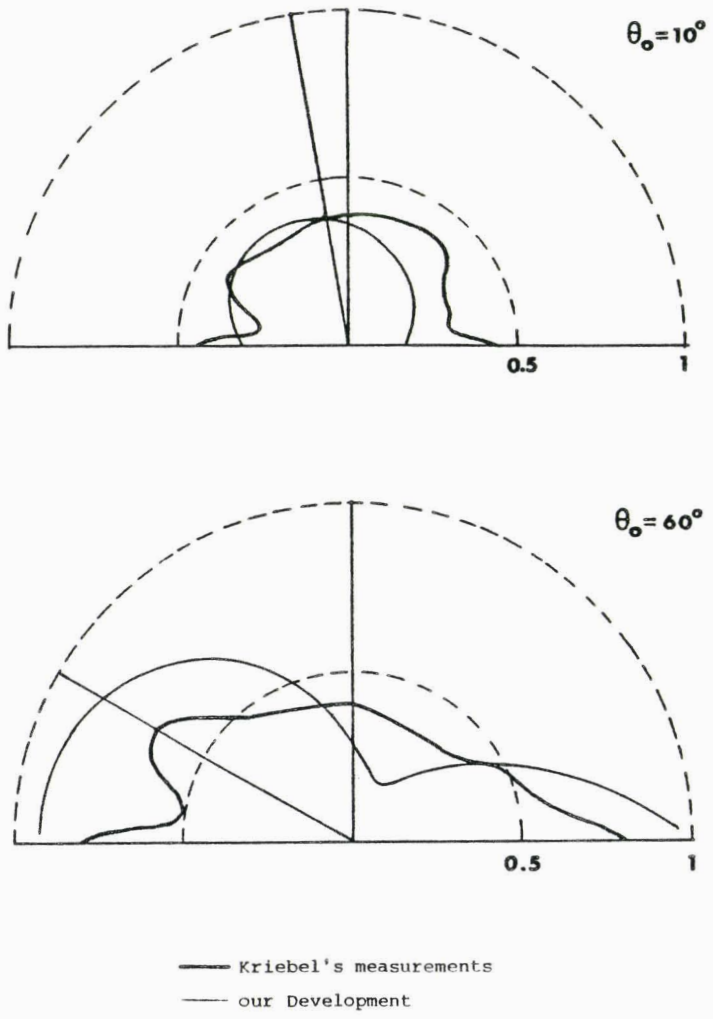

Fig. 1-d Same as Fig. 1-a but for the savannah at λ = 860 nm.

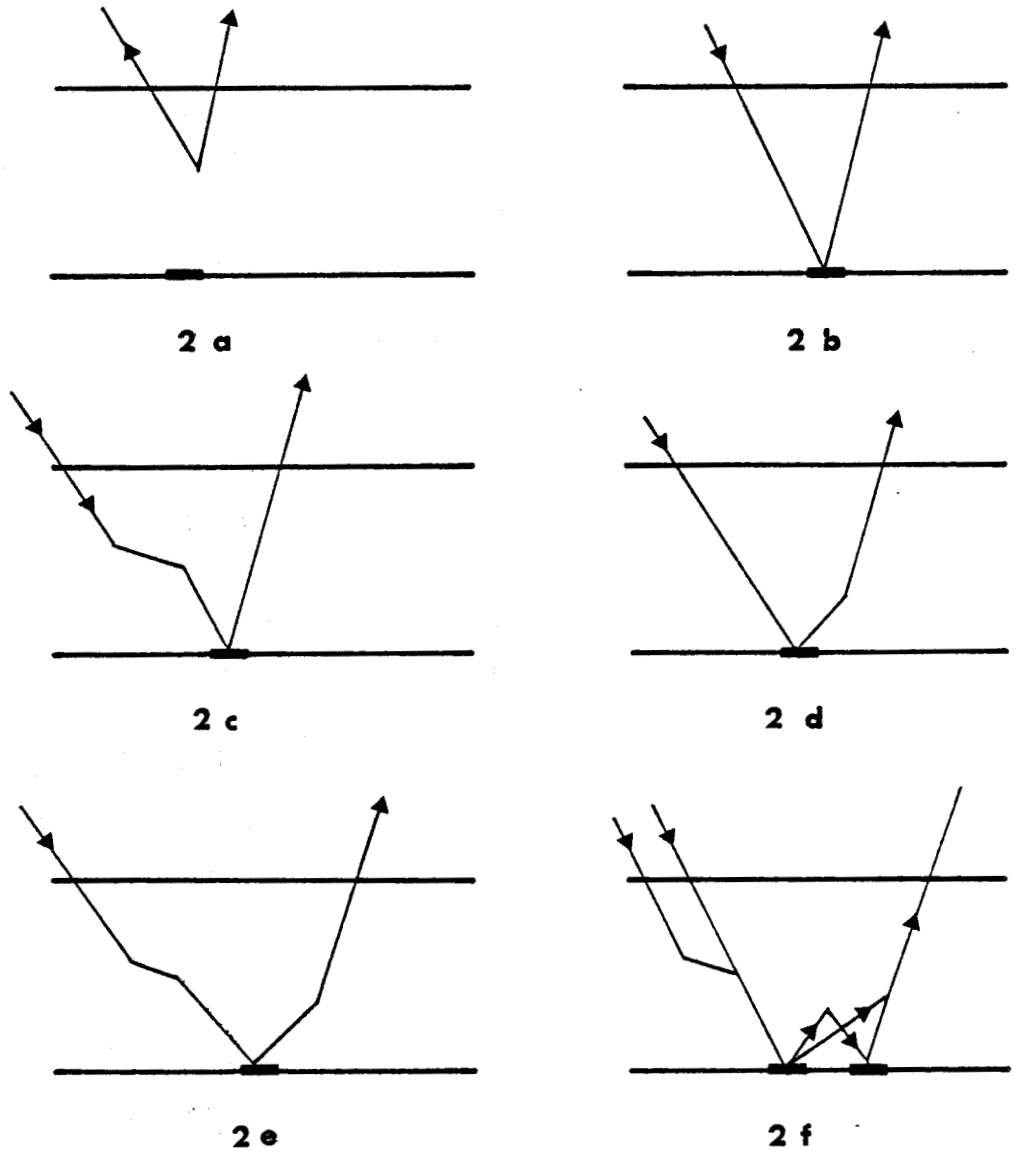

Fig. 2 Successive orders of radiation interactions in the coupled ground-atmosphere system.

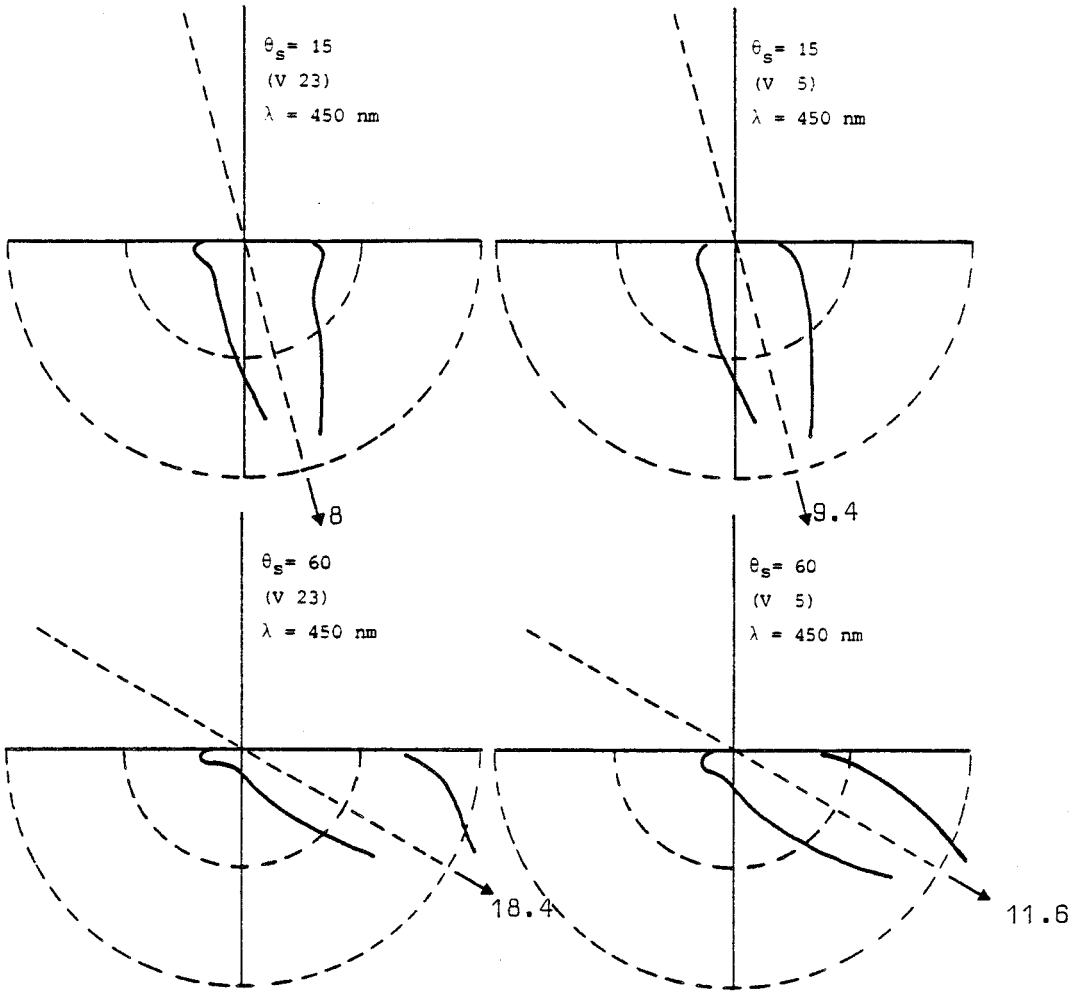

Fig. 3-a Downward radiances (polar coordinates) for two zenith solar angles and the three atmosphere models, at λ = 450 nm.

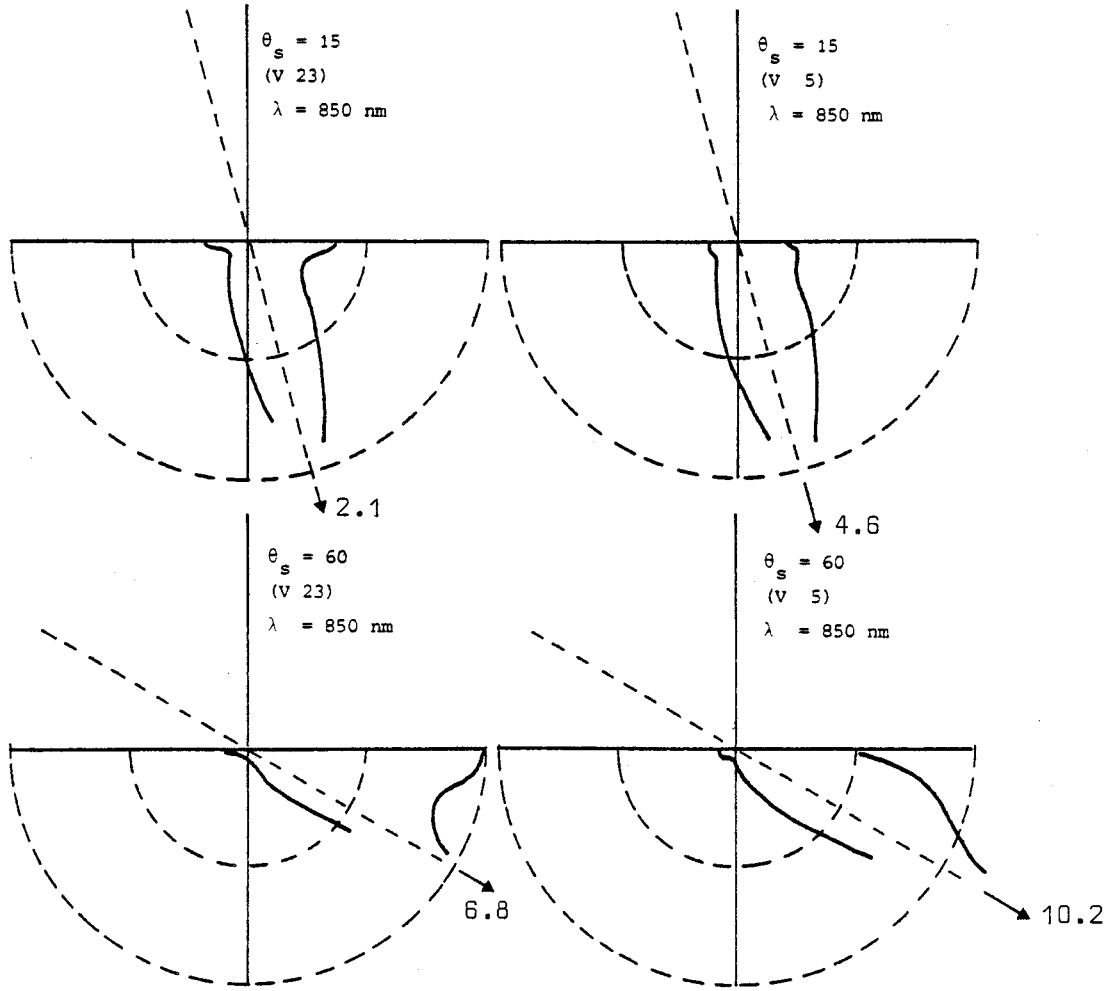

Fig. 3-b Same as Fig. 3-a, but at λ = 850 nm.

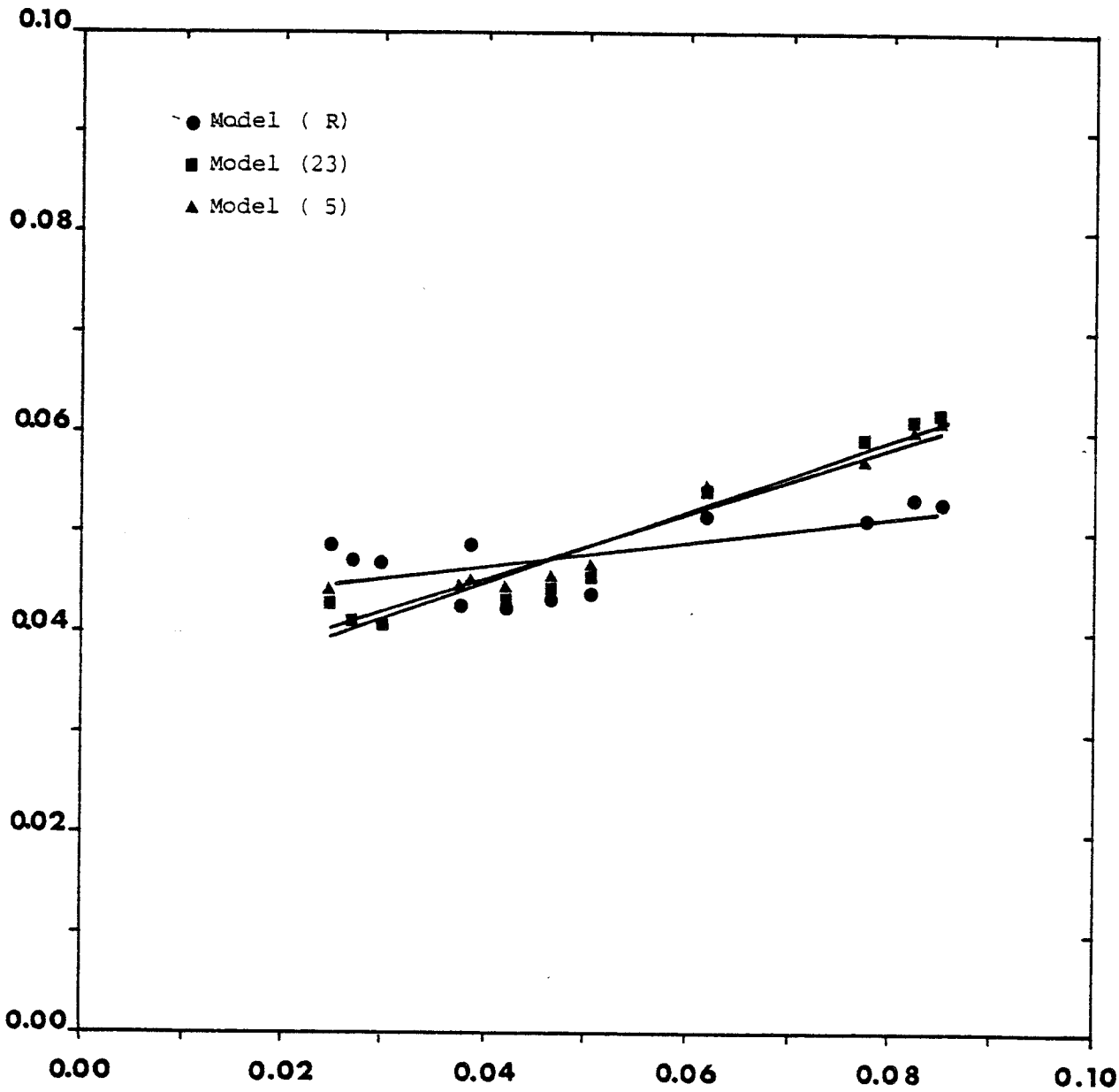

Fig. 4-a Average angular reflectance $\bar{\rho}$ versus the actual reflectance ρ for the pasture (The different points are obtained for different geometrical conditions) at λ = 450 nm

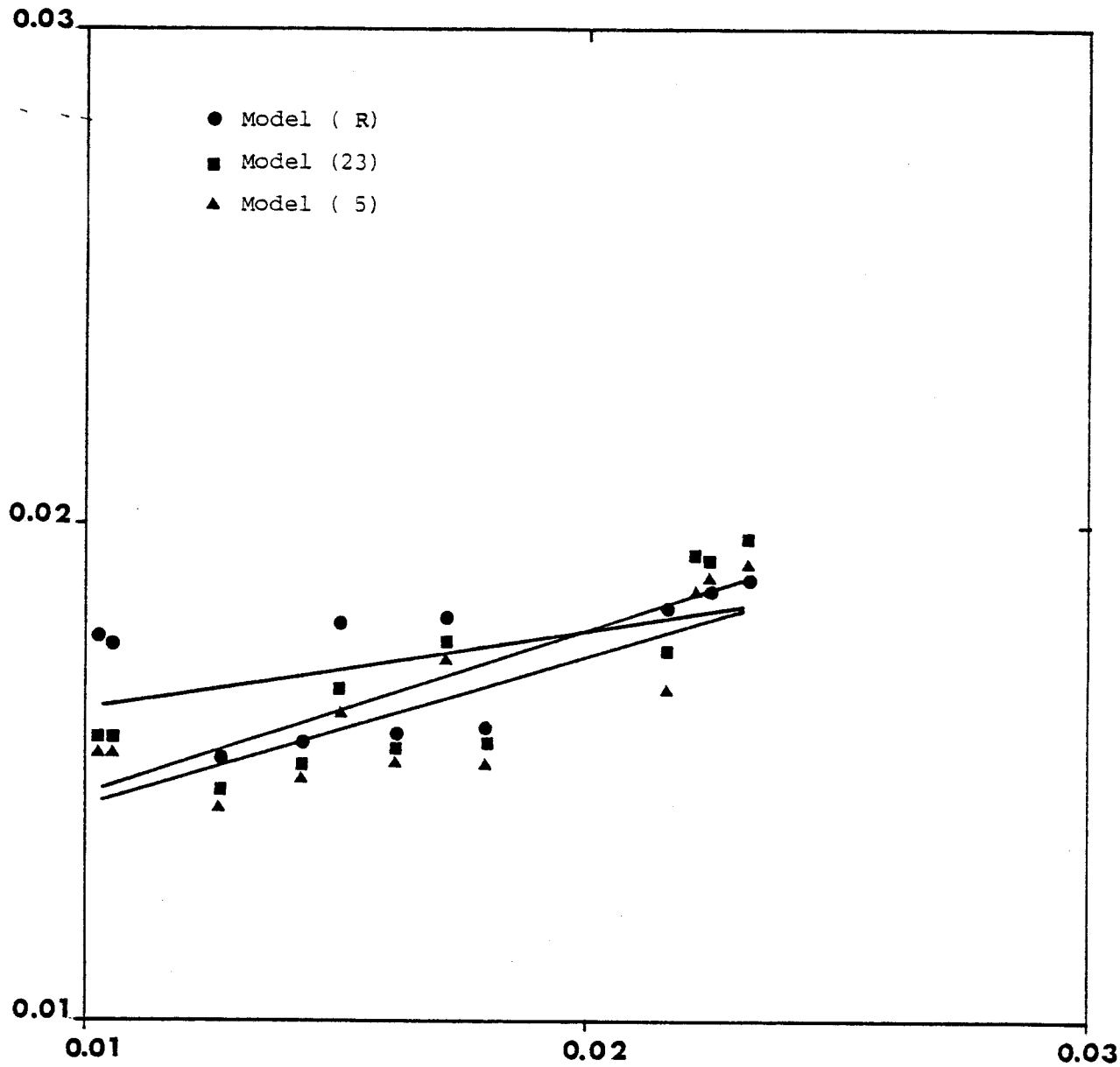

Fig. 4-b Same as Fig. 4-a, but for the forest.

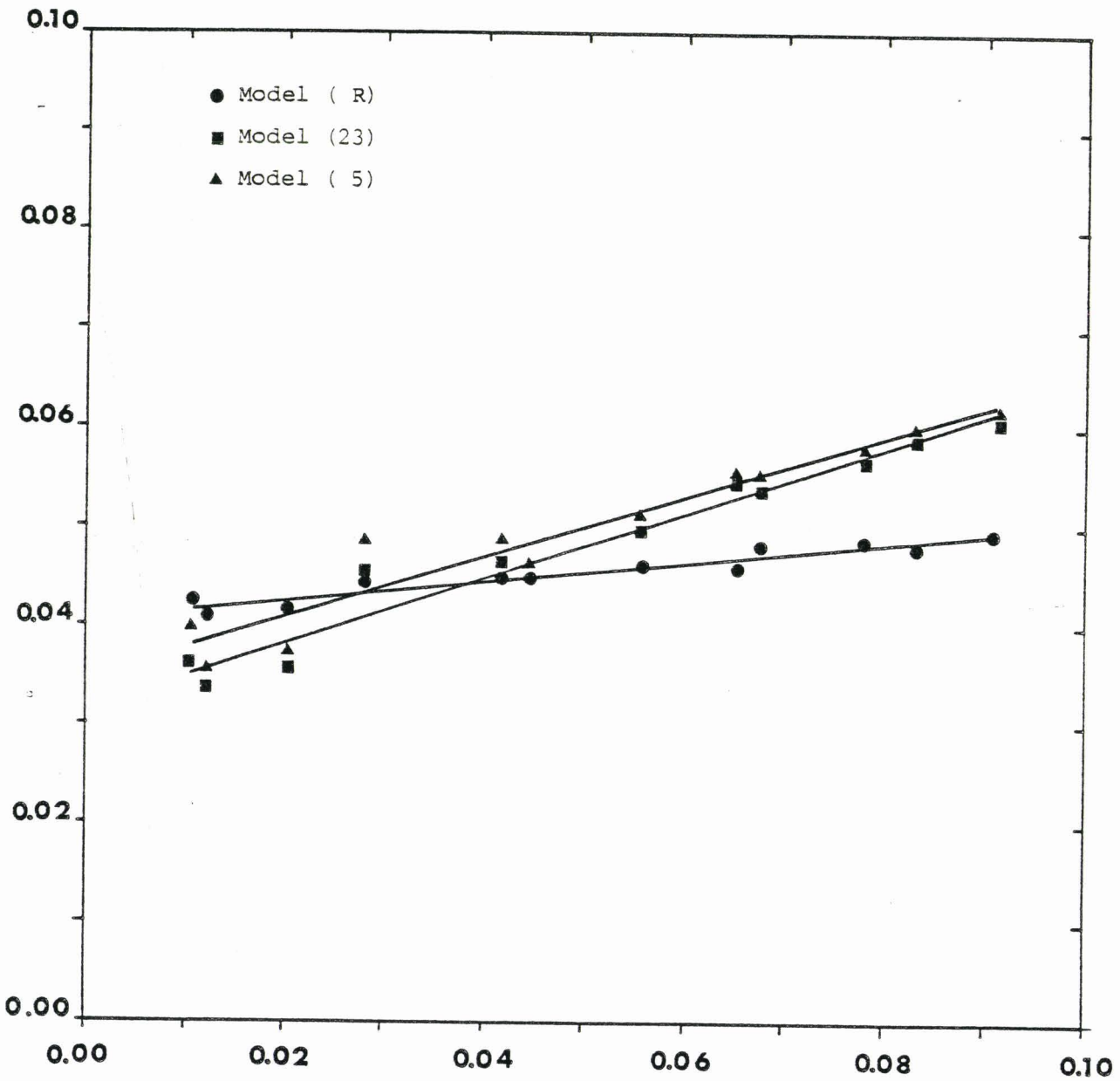

Fig. 4-c Same as Fig. 4-a, but for the savannah.

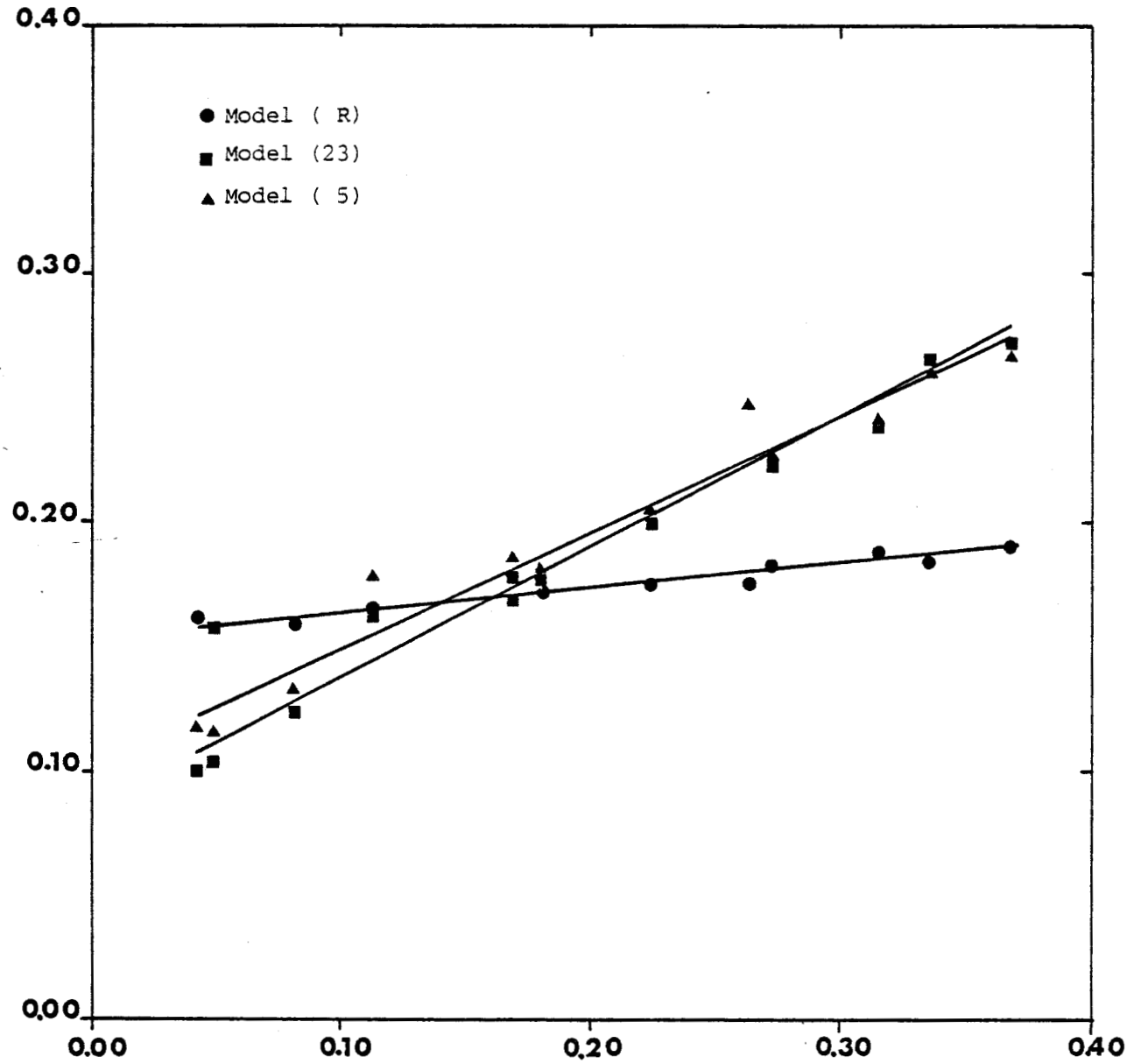

Fig. 4-d Same as Fig. 4-a, but for the savannah at λ = 850 nm.

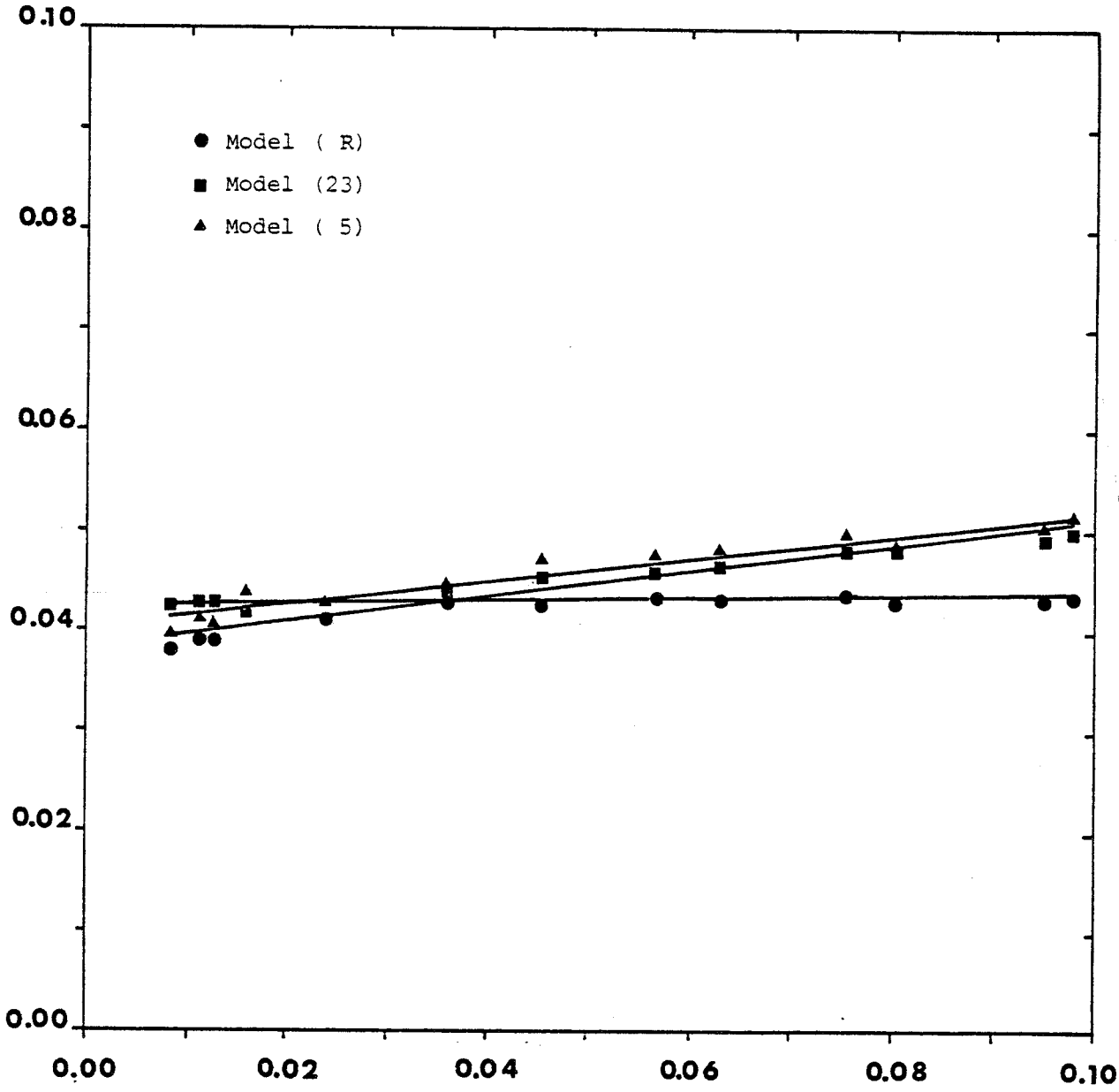

Fig. 4-e Average angular reflectance $\bar{\bar{\rho}}$ versus the actual reflectance ρ for the savannah (The different points are obtained for different geometrical conditions) at λ = 450 nm.

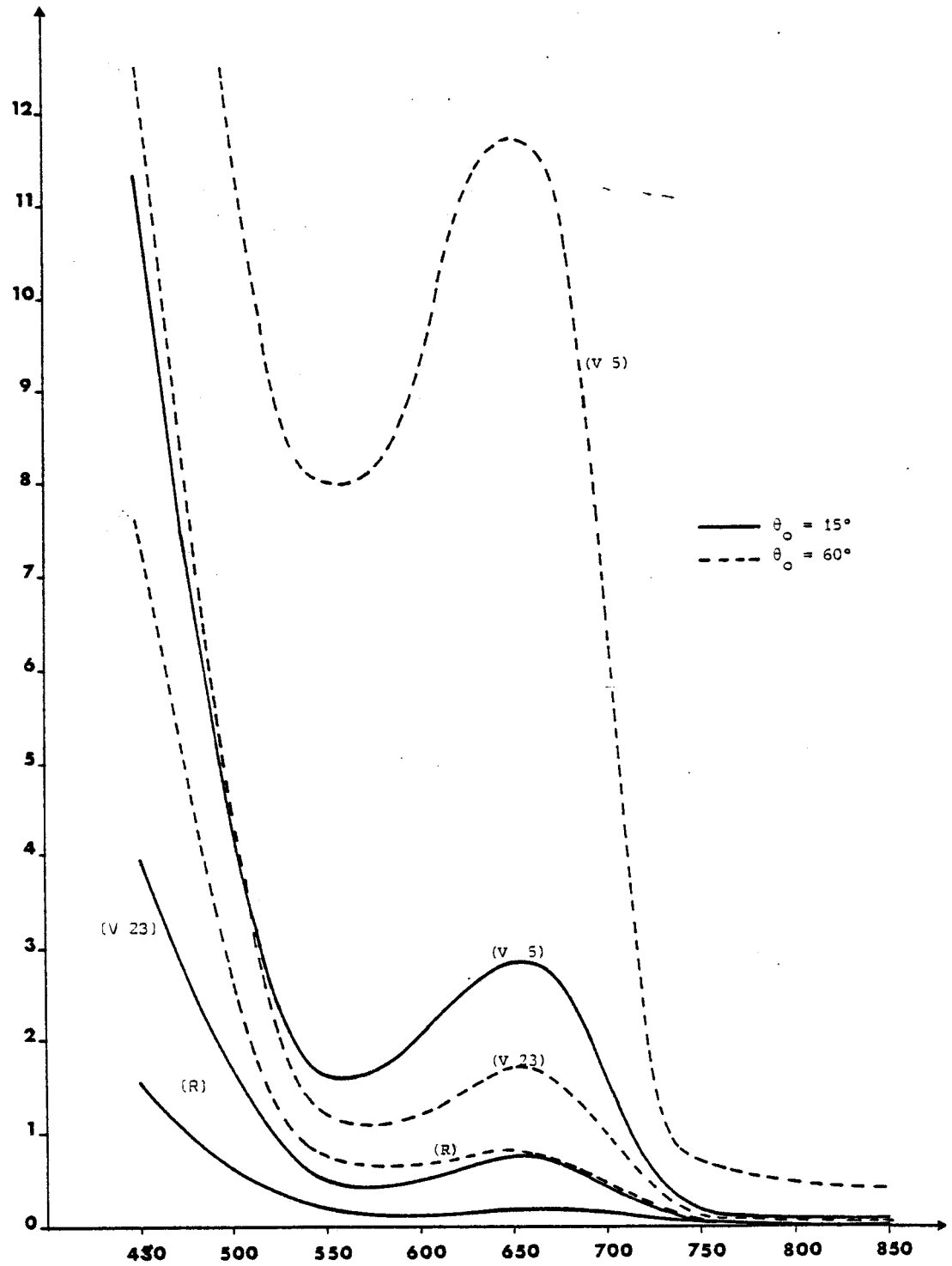

Fig. 5-a Spectral variations of $\frac{\Delta\rho^a_{\lambda\omega}}{\gamma} \frac{1}{T_s(\mu_s)T_s(\mu_v)}$ (see the text) for the three atmosphere models and two zenith solar angles.

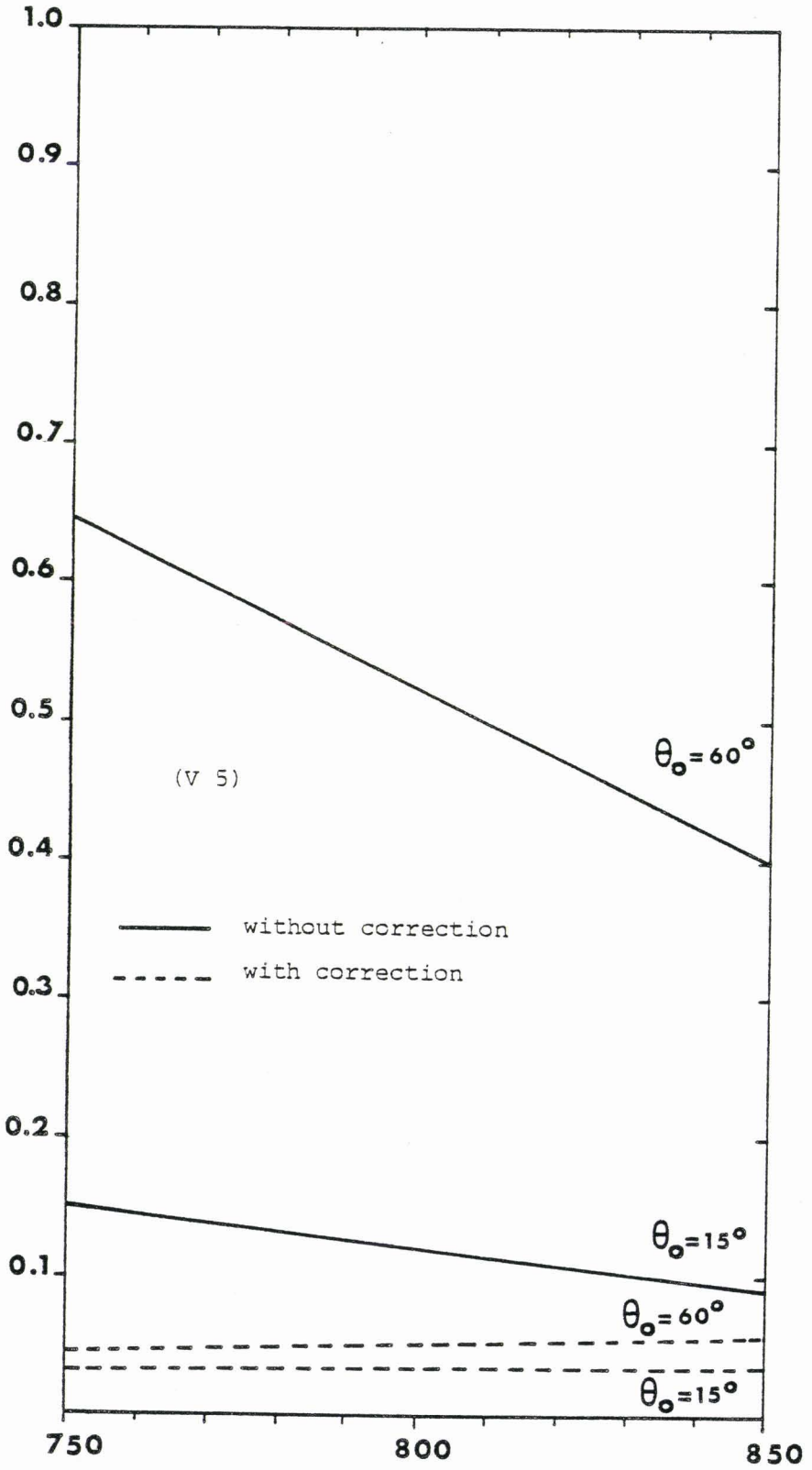

Fig. 5-b Spectral variations of

$$\frac{\Delta\rho^{a}_{\Delta\varphi,\lambda_1} - \Delta\rho^{a}_{\Delta\varphi,\lambda_2}}{\gamma_{\lambda_1} T_{s,\lambda_1} - \gamma_{\lambda_2} T_{s,\lambda_2}}$$

(see the text) where λ_1 = 650 nm for the extreme atmosphere model (V5) and two zenith solar angles.

ANNEXE 6

450

CORRECTION OF THE ATMOSPHERIC SCATTERING EFFECTS ON REMOTE SENSING OF THE GROUND ALBEDO

P.Y. Deschamps, M. Herman, J. Lenoble, D. Tanré

Laboratoire d'Optique Atmosphérique - ERA 466
Université des Sciences et Techniques de Lille I
59655 Villeneuve d'Ascq Cedex - FRANCE

1. INTRODUCTION

The atmosphere modifies the ground reflectance observed from space by three main mechanisms : - backscattering by aerosols and molecules changes the reflectance levels ; - the target reflectance is blurred by the environnement contribution, in case of non uniform sites; - the bidirectional reflectance of the target is smoothed by the diffuse part of the irradiance.

We will first analyse the signal in term of its components, introducing two average reflectances. Then we will show that the variation of contrast between two neighbouring points can be related to the variation of the aerosol optical thickness and we will suggest a method to obtain this important parameter. Finally an example of retrieval is given using Landsat data.

2. MODELISATION OF THE SIGNAL (Tanré et al, 1979)

The apparent reflectance ρ^+ measured at a point M in a direction (μ,ϕ), for an incident solar illumination in the direction (μ_o,o), and with an atmosphere of total optical thickness $\tau = \tau_R+\tau_p$, can be written as

$$\rho^+(M,\mu_o,\mu,\phi,\tau) = \rho_a(\mu_o,\mu,\phi,\tau) + \rho(M,\mu_o,\mu,\phi)\, e^{-\tau(\frac{1}{\mu}+\frac{1}{\mu_o})}$$

$$+ \bar{\rho}(M,\mu_o,\mu,\phi)\, e^{-\tau/\mu} E(\mu_o) + \langle\rho(M,\mu_o,\mu,\phi)\rangle\,(E(\mu_o) + e^{-\tau/\mu_o})E(\mu) \quad (1)$$

where $-\rho_a(\mu_o,\mu,\phi,\tau)$ is the atmosphere reflectance

$-\rho(M,\mu_o,\mu,\phi)$ is the target reflectance,

$-\bar{\rho}(M,\mu_o,\mu,\phi)\, e^{-\tau/\mu} E(\mu_o)$ defines the angular average reflectance $\bar{\rho}$ of the target with the diffuse sky irradiance $E(\mu_o)$,

$-\langle\rho(M,\mu_o,\mu,\phi)\rangle\,(E(\mu_o) + e^{-\tau/\mu_o})E(\mu)$ represents the first order of the environment contribution and defines a spatial average reflectance $\langle\rho\rangle$ of the ground.

A last term corresponding to multiple interactions between the ground and the atmosphere has been omitted in equation (1) ; it contributes generally for less than 10 % to the signal.

3. DETERMINATION OF AEROSOL OPTICAL THICKNESS

Numerical tests have proved that the main parameters in equation (1) are the aerosol optical thickness τ_p and the aerosol backscattering coefficient β_p (Herman and Tanré, 1978). These parameters have to be determined in order to correct remote sensed ground reflectances.

On the other hand, inversion of equation (1) can be used to retrieve the aerosol optical thickness or at least its temporal variations from the satellite images.

Assuming the observed target has a lambertian reflectance, equation (1) can be written

$$\rho^{+}_{ij}(\mu,\mu_o,\phi,\tau) = \rho^{a}_{ij}(\mu,\mu_o,\phi,\tau) + \rho_{ij}\{E(\mu_o) + e^{-\tau/\mu_o}\} e^{-\tau/\mu} + {}^{<\rho>}_{ij}\{E(\mu_o) + e^{-\tau/\mu_o}\} E(\mu) \quad (2)$$

where (i,j) refer to the coordinates of point M.

If we consider two neighbouring points M(i,j) and M(i,j+1), we can reasonnably assume that

$$\rho^{a}_{i,j} = \rho^{a}_{i,j+1} \quad \text{et} \quad <\rho_{i,j}> = <\rho_{i,j+1}> \quad , \quad (3)$$

and the difference of apparent reflectance between the two points is

$$\Delta\rho^{+}_{i,j}(\mu,\mu_o,\phi,\tau) = \rho^{+}_{i,j} - \rho^{+}_{i,j+1} = \Delta\rho_{i,j}(E(\mu_o) + e^{-\tau/\mu_o}) e^{-\tau/\mu} \quad (4)$$

where $\Delta\rho_{i,j} = \rho_{i,j} - \rho_{i,j+1}$, is the difference of the actual reflectances.

From equation (4) we can write the moments of order n of the histogram obtained for the $\Delta\rho^{+}_{i,j}$ on the satellite image, as

$$M^{+n} = M^{n}(E(\mu_o) + e^{-\tau/\mu_o}) e^{-\tau/\mu} \quad (5)$$

where M^n is the same moment for the $\Delta\rho_{i,j}$.

Introducing a simple approximate form for $E(\mu_o)$ (Tanré et al, 1979), equation (5) leads to

$$M^{+n} = M^{n} \exp(-n\tau_p(\frac{1}{\mu} + \frac{1}{\mu_o} - \frac{\beta_p}{\mu_o}))\exp(-n\tau_R(\frac{1}{\mu} + \frac{1}{\mu_o} - \frac{\beta_r}{\mu_o})) \quad (6)$$

If M^n is known from ground based observations, and if β_p can be fixed to a reasonable value for a known type of aerosols, then the value of M^{+n} with equation (6) gives the aerosol optical thickness τ_p.

4. APPLICATION TO LANDSAT DATA

To check the method, we have used data from the satellite

LANDSAT, which observes a third of the same scene during two successive days ; it seems therefore reasonable to assume that the ground reflectance remains the same, as well as the type of particles, for the successive passages at time t_1 and t_2. From equation (6) we can get

$$M^{+n}(t_1) = M^{+n}(t_2) \exp(-n \Delta\tau_p (\frac{1}{\mu} + \frac{1}{\mu_o} - \frac{\beta_p}{\mu_o})) \qquad (7)$$

where $\Delta\tau_p$ is the variation of optical thickness from t_1 to t_2.

The first results obtained in the south-east of France are plotted on figure 1. The different moments give values in good agreement.

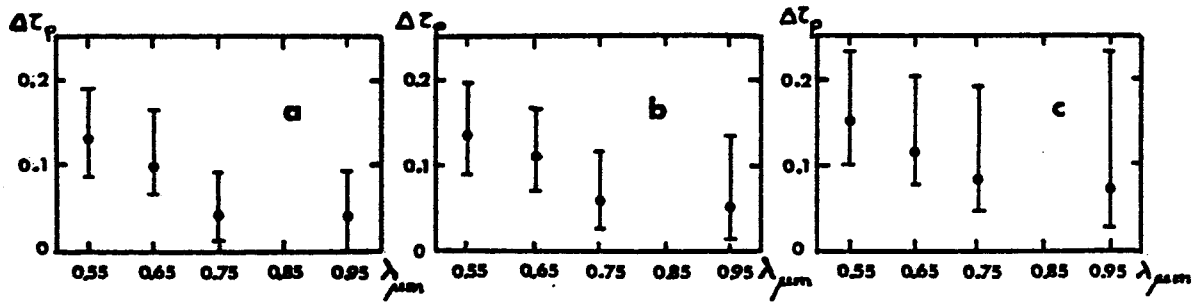

Fig. 1 : Values of $\Delta\tau_p$ obtained with the first three moments (curve (a) $-{}^pM^1$ - (b)M^2 - (c)M^3) vs the wavelenght ; the error bars correspond to different zones (60x60 pixels) of the scene (256x256 pixels).

5. CONCLUSION

The modelisation of the apparent reflectance of a target observed from space suggests a method for remote sensing of the aerosol optical thickness, using the variation of contrast during successive observations of the same scene. A first check of the method seems encouraging. Further investigations, including ground-truth experiments, remain to be done.

6. REFERENCES

Herman M., and D.Tanré, (september 1978) : Etude des effets d'atmosphère sur les mesures de réflectance faites dans le visible à partir de satellite. Rapport C.N.E.S. - Convention 77-0737 - Université de Lille I.

Tanré D., M. Herman, P.Y. Deschamps, and De Leffe A., (1979) : Atmospheric modeling for space measurements of ground reflectances, including bidirectionnal properties. Applied Optics, 18, 3587-3594.

This research was supported by the "Centre National d'Etudes Spatiales"(C.N.E.S.) and by the "Centre National de la Recherche Scientifique" (C.N.R.S.).

CONCLUSION

Nous avons montré que la réflectance apparente mesurée à partir de l'espace est fonction de la réflectance atmosphérique intrinséque, de la réflectance vraie de la cible, et de deux réflectances moyennes angulaire et spatiale. Une étude de ces différents termes nous a amené aux conclusions suivantes.

- il est possible de séparer dans la réflectance atmosphérique propre, les contributions des molécules et des aérosols, soit d'une manière très simple si on désire une précision de quelques millièmes, soit à l'aide d'une formule plus élaborée pour une précision de l'ordre du millième.
- Les effets d'environnement qui à priori nécessitent une connaissance complète de l'atmosphère sont généralement bien restitués à l'aide d'expressions analytiques simples obtenues pour une atmosphère moyenne.
- Quant à l'aspect directionnel des réflectances, seules des mesures multispectrales permettent d'obtenir des informations sur l'anisotropie de la surface.

Enfin, le paramètre primordial, très variable en fonction du lieu et des conditions d'observations, l'épaisseur optique en aérosols, pourrait être estimé à l'aide de mesures uniquement satellitaires ; le problème étant de trouver des sites tests (s'ils existent) tels que leur histogramme $\Delta\rho_{i,j}^{vrai}$ reste invariant.

PARTIE II

EFFET CLIMATIQUE DES AEROSOLS

Avec l'évolution des modèles climatiques qui deviennent de plus en plus performants, on envisage d'y inclure l'effet des aérosols mais leur impact climatique est difficile à cerner. On peut se demander de quelle façon ils contribuent au climat et quelle est leur influence sur le bilan énergétique de la planète.

Leur contribution peut se décomposer globalement en deux types d'effets. A côté d'effets directs, par leur influence sur le rayonnement (modification de l'albédo de la planète et du profil d'absorption solaire, modification des phénomènes d'émission absorption dans l'infra rouge) on peut penser à des phénomènes de couplage ou de feedback plus complexes. Les aérosols peuvent agir indirectement sur la stabilité du profil de température (par absorption visible et par absorption/émission du rayonnement infrarouge), sur le niveau de condensation, et sur les propriétés radiatives des nuages (par modification de leurs propriétés optiques). Les différents effets influencent le bilan climatique de manière très différente. L'absorption par les aérosols, que ce soit en visible ou en infra-rouge aura toujours pour effet de provoquer un réchauffement de la planète. Or ce phénomène d'absorption apparaît généralement en même temps que le phénomène de diffusion, qui peut provoquer soit un refroidissement soit un réchauffement ; la rétrodiffusion vers l'espace du rayonnement solaire incident aura tendance à refroidir l'atmosphère, par contre la rétrodiffusion vers le bas des rayonnements solaires réfléchi et émis par le sol aura tendance à réchauffer l'atmosphère ; ce deuxième effet dépendant d'ailleurs de l'albédo du sol. L'impact climatique des aérosols est donc difficile à cerner compte tenu des phénomènes de feedback entre les différents paramètres climatiques.

Dans ce qui constitue une première approche, nous nous sommes limités aux problème des aérosols stratosphériques. Il forment une couche diffusante bien séparée du reste de l'atmosphère (aérosols troposphériques, nuages), les interactions avec les autres paramètres sont moins importantes et peuvent être raisonnablement négligées. De plus, les données sur ce type d'aérosols sont de plus en plus nombreuses (expériences SAM et SAGE) et les modèles de plus en plus réalistes.

En séparant les interactions successives entre les deux couches (stratosphère, troposphère et sol), le formalisme de la partie I a été adapté au calcul des flux radiatifs pour la partie visible du spectre (cf annexe 7) et on a inclu de manière très simple, la partie infrarouge. On obtient ainsi une expression analytique approchée de l'effet radiatif où n'interviennent que les valeurs moyennées sur tout le spectre,de l'albédo du système troposphère-sol, de l'absorption propre des aérosols, du coefficient d'anisotropie, de leur fonction de phase et du rapport des coefficients d'absorption visible et infrarouge. Les comparaisons effectuées avec des calculs plus précis montrent que la précision obtenue est tout à fait satisfaisante.

Cette formulation a ensuite été intégrée à un modèle climatique très simple, celui de Budyko (cf Annexe 8). Les résultats obtenus dépendent très fortement des propriétés radiatives des aérosols et il s'avère primordial d'améliorer nos connaissances sur leurs caractéristiques optiques. Nous avons utilisé les deux modèles de la Commission Internationale du Rayonnement (IAMAP), un modèle moyen constitué de particules de H_2SO_4 et un modèle volcanique. Pour une couche d'épaisseur optique de 0,1, on observe une décroissance de la température de surface de 3,5° et de 1,5° pour les deux modèles respectivement ; ces deux modèles ont des albédos de 0,998 et de 0,944, ce qui montrent l'importance de l'absorption propre des particules (leurs coefficients d'anisotropie étant pratiquement identiques) sur le bilan climatique. Un tel refroidissement, s'il était maintenu sur une longue période de temps, entraine une évolution de la limite des glaces vers l'équateur qui amplifie le phénomène de refroidissement d'un facteur 2 ou 3.

Ces résultats ne sont qu'indicatifs et montrent simplement la cohérence de notre méthode lorsqu'on les compare aux résultats obtenus par d'autres auteurs, l'effet dépend fortement du modèle climatique choisi (comment les phénomènes de feedback sont pris en compte, quels phénomènes sont négligés) et du type d'aérosols retenu, particulièrement de leur albédo qui peut entrainer un refroidissement s'ils sont peu absorbants ou un réchauffement s'ils sont très absorbants.

Le travail présenté ici est avant tout une première approche, nous envisageons d'inclure notre formalisme dans un modèle à trois dimensions et d'utiliser les données fournies par l'expérience SAGE qui permet une couverture de l'épaisseur optique à l'échelle du globe. Par contre, ces données ne permettent pas d'accéder à l'albédo qui reste le paramètre le plus mal connu et le plus difficile à atteindre.

ANNEXE 7

A SIMPLE METHOD TO COMPUTE THE CHANGE IN EARTH-ATMOSPHERE RADIATIVE BALANCE DUE TO A STRATOSPHERIC AEROSOL LAYER.

I - THEORETICAL FORMULATION

J. LENOBLE, D. TANRE, P.Y. DESCHAMPS, M. HERMAN

Laboratoire d'Optique Atmosphérique - (ERA 466)
Université des Sciences et Techniques de Lille
59655 VILLENEUVE D'ASCQ CEDEX (FRANCE)

Abstract - A simple modelisation of the earth atmosphere system including tropospheric and stratospheric aerosols has been derived. Analytical expressions are obtained for the albedo variation due to a thin stratospheric aerosol layer. They outlined the physical procedures and the respective influence of the main parameters : aerosol optical thickness, single scattering albedo and asymetry factor, and sublayer albedo. The accuracy has been tested in comparison with HERMAN's et al (1976) exact computations.

1 - Introduction

The role of stratospheric aerosols in modifying the earth radiation balance, and therefore the global climate, is expected to be important due to their long term of residence and to their extended transport in the stratosphere.

This influence is twofold, including a modification of the solar reflection and an increase of the infrared opacity. This last effect leads to a warming, depending on the aerosol infrared absorption ; but it has been shown (LUTHER, 1976 ; HARSHVARDHAN and CESS, 1976) to be in any case smaller than the effect on solar reflection. The first model calculations, including a crude treatment of the radiative problem, have shown that the aerosol loading generally results in an enhancement of the planet reflection and therefore in a cooling of the earth surface and of the troposphere ; however they have pointed to a possible inverse effect, warming instead of cooling, in the case of absorbing aerosol above clouds, or high reflecting ground (CHARLSON and PILAT, 1969, ATWATER, 1970 ; RASOOL and SCHNEIDER, 1971 ; SCHNEIDER, 1971). Further more detailed studies have confirmed this result (YAMAMOTO and TANAKA, 1972 ; CHYLEK and COAKLEY, 1974 ; WANG and DOMOTO, 1974 ; RECK, 1974 ; HERMAN and BROWNING, 1975 ; POLLACK et al. 1976 ; COAKLEY and GRAMS, 1976). HERMAN et al. (1976) have demonstrated the sensitivity to solar elevation angle. Their paper contains a complete modelisation of the earth-atmosphere, including tropospheric aerosols ; the radiative transfer computations use the Gauss-Seidel iteration technique (HERMAN and BROWNING, 1965) which is assumed to give results accurate within better than 1 %, or so-called "exact data".

More recently HARSHARDHAN (1979) has examined the albedo sensitivity of the planet to a stratospheric aerosol layer, both on the global and on the zonal scale. He uses a simple analytical formulation, based on primary scattering with a first order expansion in τ for the thin stratospheric scattering layer and assumes the albedo of the sublayer (ground and troposphere) as known ; satellite-derived planetary albedos are used in the numerical computations ; the aerosols are assumed to be 75 % $H_2 SO_4$ non absorbing particles.

In this paper (Part I) a simple analytical formulation based on the two-stream approximation is worked out for both the troposphere and the stratosphere. The results accuracy is checked in comparison with the exact computations of HERMAN et al.(1976) and appears quite reasonable ; for the stratospheric layer it prooves generally a little better than the primary scattering approximation.

In a companion paper (Part II) the formulation is applied to study the zonal influence of a stratospheric aerosol layer, including the weak infrared effect, and using a BUDYKO-type climate model . Two different aerosol models are considered, and the feedback effect, mainly due to the polar ice sheet variation is introduced.

2 - General formulation

Let us first consider a scattering atmosphere illuminated by the solar beam above a lambertian ground (or sublayer). The bidirectional reflectance is defined by

$$\rho(\tau;\ \mu_o,\mu,\phi) = \frac{\pi\ I^+(o;\mu,\phi)}{\mu_o\ f} \qquad (1)$$

and the albedo by

$$A(\mu_o) = \frac{1}{\pi} \int_0^{2\pi} \int_{-0}^{+1} \mu \, \rho(\tau;\mu_o,\mu,\phi) \, d\mu \, d\phi \quad , \qquad (2)$$

where τ is the atmosphere optical thickness,

Arc cos μ_o the solar zenith angle,

Arc cos μ the observation zenith angle,

ϕ the azimuth angle between the observation and the sun vertical planes,

$I^+(o;\mu,\phi)$ the reflected radiance in the direction (μ,ϕ),

f the solar irradiance.

Considering the successive interactions between the atmosphere and the ground (or sublayer) (TANRE et al, 1979 , DESCHAMPS et al, 1980) , the bidirectional reflectance can be written as

$$\rho(\tau;\mu_o,\mu,\phi) = \pi \, S(\tau;\mu_o,\mu,\phi) + \frac{A_G \, T(\mu) \, T(\mu_o)}{1 - A_G \, \bar{S}} \quad , \qquad (3)$$

where $\pi \, S(\tau;\mu_o,\mu,\phi)$ is the atmospheric contribution (with no ground reflection),

$\bar{S}$ is the atmosphere spherical albedo (with no ground reflection),

$T(\mu) = e^{-\tau/\mu} + t(\mu)$ is the total (direct + diffuse) atmospheric flux transmittance,

A_G is the ground (or sublayer) albedo.

The system exact albedo comes from Eq. (2) and Eq. (3) as

$$A(\mu_o) = S(\mu_o) + \frac{A_G\, T(\mu_o)\, \bar{T}}{1 - A_G\, \bar{S}} \quad , \tag{4}$$

where $S(\mu_o)$ is the intrinsic atmosphere contribution to the flux reflectance ,

$$\bar{T} = 2\, E_3(\tau) + \bar{t} \quad ,$$

$$\bar{t} = 2 \int_o^1 \mu\, t(\mu)\, d\mu \quad ,$$

$E_3(\tau)$ is the exponential integral function of order 3.

The spherical or planetary albedo is

$$A = 2 \int_o^1 \mu_o\, A(\mu_o)\, d\,\mu_o \quad , \tag{5}$$

$$A = \bar{S} + \frac{A_G\, \bar{T}^2}{1 - A_G\, \bar{S}} \quad . \tag{6}$$

We can also definie a mean daily value of the local albedo

$$A(\bar{\mu}_o(t_o)) = \frac{1}{\bar{\mu}_o(t_o)} \int_o^{t_o} \mu_o(t)\, A(\mu_o)\, dt \quad , \tag{7}$$

with

$$\bar{\mu}_o(t_o) = \frac{1}{t_o} \int_o^{t_o} \mu_o(t)\, dt \quad ,$$

where t_o is the half-day length depending on season and latitude.

The perturbations of albedo introduced by the atmosphere write respectively as

$$\Delta A(\mu_o) = A(\mu_o) - A_G \quad ,$$

$$\Delta A = A - A_G \quad . \tag{8}$$

If the underlying layer is not lambertian Eq. (3) does not apply. A similar treatment leads to a much more complex equation involving the ground bidirectional reflectance $\rho_G(\mu_o,\mu,\phi)$ instead of A_G. Average values $\langle\rho_G(\mu_o)\rangle$ can be introduced, but they are defined with different weighting functions for each process of ground-atmosphere interactions (DESCHAMPS et al, 1980) and a simple combination of the terms as in Eq. (3) cannot be achieved. A rough approximation consists in replacing all the $\langle\rho_G(\mu_o)\rangle$ by the ground albedo $A_G(\mu_o)$ which leads to an equation similar to Eq. (3). Then $A(\mu_o)$ reads as in Eq. (4) with $A_G(\mu_o)$ instead of A_G (HARSHVARDHAN, 1979). We will also use this approximation in the case of the stratospheric layer above the troposphere which is not a lambertian reflector. A similar approximation on the average values of $A_G(\mu_o)$ leads to Eq. (6).

3 - Approximate expressions of the scattering and transmission functions

The scattering (S) and transmission (T) functions can be obtained with all the required accuracy by various methods (Radiation Commission, 1977) ; they are complex functions of the atmosphere optical thickness τ, single scattering albedo $\bar{\omega}$ and phase function $p(\mu,\phi;\mu'\phi')$. However as they appear in Eq. (4) by their mean values as flux trans-

mittance or reflectance, approximate analytical methods can probably be used. Moreover the optical thickness for stratospheric aerosols is small, allowing further approximations.

The modified two stream approximation (IRVINE, 1968) has proved to give generally reasonably accurate results. The usual formulae for conservative scattering ($\bar{\omega} = 1$) are

$$T(\mu_o) = \{1 + \frac{b\tau}{\mu_o}\}^{-1} \quad , \qquad (9)$$

$$S(\mu_o) = 1 - T(\mu_o) \quad ,$$

where b is choosen as

$$b = \frac{1}{2}(1-g) \quad , \qquad (10)$$

where g is the phase function asymetry factor.

In non conservative case the two-stream formulation is much more difficult to handle than Eq. (9) and we have tried the more approximate expressions

$$S(\mu_o) = \bar{\omega}\, S_{\bar{\omega}=1}(\mu_o) \quad , \qquad (11)$$

$$t(\mu_o) = \bar{\omega}\, t_{\bar{\omega}=1}(\mu_o) \quad .$$

Eq. (11) should hold when $\bar{\omega}$ is near to 1 or when primary scattering is predominant, i.e. when τ is small. Table 1 shows the comparison of the

diffuse transmission computed by the two stream method with exact values, including a separate test of Eq. (11) for four optical thicknesses and two zenith angles.

The accuracy of the two stream method (Eq. 9) coupled with the approximation (Eq. 11) remains better than 10 % for $\bar{\omega} \geqslant 0.6$, $\tau \lesssim 0.5$ and normal incidence. When μ_o decreases the conditions on $\bar{\omega}$ or τ become a lettle more restrictive. Anyhow, as the aerosol albedo is generally larger than 0.9 in the solar spectrum, the method should apply with a good accuracy for most atmospheric problems.

For small optical thickness, as met in stratosphere, the functions can be expanded to the first order in τ, and with Eq. (9), Eq. (10) and Eq. (11), we get

$$S(\mu_o) = \bar{\omega}\, \frac{b\tau}{\mu_o} \quad ,$$

$$T(\mu_o) = 1 - \frac{\bar{\omega} b\tau}{\mu_o} - (1-\bar{\omega})\, \frac{\tau}{\mu_o} \quad , \qquad (12)$$

$$\bar{S} = 2\, \bar{\omega} b\, \tau \quad ,$$

$$\bar{T} = 1 - 2\, \bar{\omega}\, b\tau - 2(1-\bar{\omega})\tau \quad .$$

In such cases of small optical thickness, it may seem more sensible to use the primary scattering expressions for S and T functions. On table 2 the values obtained by the primary scattering formulation are compared with exact and two-stream values. For μ_o near to 1 the two stream gives better results except for very small optical thickness ($\tau = 0.01$) but even in this case, it accuracy remains very good. For μ_o near to 0.5,

the two stream becomes less accurate but the magnitude of the differences with the exact values are comparable with those obtained by the primary scattering formulation.

If there is not a definitive advantage for any method, from a practical point of view, it would seem convenient to keep the same formalism for the stratosphere and for the troposphere. However further comparisons of both methods will be presented in the test computations.

4 - Modelisation

The stratospheric aerosols are considered as a thin scattering layer above the troposphere which is assumed to comprise all the scattering molecules and tropospheric aerosols. Both the stratosphere and the troposphere are characterized only by their optical thickness τ_s or τ_t, their single scattering albedo $\bar{\omega}_s$ or $\bar{\omega}_t$ and the asymetry factor of their phase functions g_s or g_t ; subscript s will refer to all quantities in the stratosphere and subscript t to the troposphere. Parameters τ_t, $\bar{\omega}_t$ and g_t are evaluated taking into account both the molecules and the tropospheric aerosols, with

$$\tau_t = \tau^{Rayl} + \tau^{aer} \quad ,$$

$$\bar{\omega}_t = (1-\delta)\,\bar{\omega}^{aer} + \delta\,\bar{\omega}^{Rayl} \quad , \text{ where } \delta \text{ is the Rayleigh scattering ratio}$$

$$b_t\,\tau_t = b^{Rayl}\,\tau^{Rayl} + b^{aer}\,\tau^{aer} \quad . \qquad (13)$$

This formulation assumes a negligeable influence of the altitude variation of the aerosols mixing ratio

The ground is assumed to be homogeneous and to reflect according to the LAMBERT's law.

The tropospheric albedo $A_t(\mu_o)$ is computed from Eq. (4) where the tropospheric scattering S_t and transmission T_t functions are obtained by the modified two stream approximation (Eqs. (9), (10), (11)).

Then the stratospheric albedo $A_S(\mu_o)$ derives from Eq. (4) where A_G is replaced by $A_t(\mu_o)$ and the stratospheric scattering S_S and transmission T_S functions are given by the approximate relations Eq. (12) for small optical thickness.

The perturbation introduced by the stratospheric aerosol layer on the local, or on the global albedo appears to be proportional to its optical thickness τ_S and can be expressed as

$$\Delta A(\mu_o)/\tau_S = \bar{\omega}_S\, b_S\, \{1-A_t(\mu_o)\}\, \{\frac{1}{\mu_o} - 2\, A_t(\mu_o)\} - (1-\bar{\omega}_S)\, (\frac{1}{\mu_o} + 2) A_t(\mu_o)\,, \tag{14a}$$

$$\Delta A/\tau_S = 2\, \bar{\omega}_S\, b_S (1-A_t)^2 - 4\, (1-\bar{\omega}_S)\, A_t \quad . \tag{14b}$$

This analytic formulation is in fact very similar to the formulation obtained by the primary scattering approximation. The planetary albedo (Eq. (14b)) derives clearly from the local albedo (Eq. (14a)) by taking the average incidence $\bar{\mu}_o$ for a planet which is equal to 0.5.

The physical meaning of the various terms in Eqs. (14) is quite ob-

vious :

$-(1-\bar{\omega}_S)\ (\frac{1}{\mu_o} + 2)\ A_t(\mu_o)$ corresponds to the radiation absorbed by the aerosols before and after the reflection,

$\bar{\omega}_S\ b_S(1-A_t(\mu_o))\ (\frac{1}{\mu_o} - 2A_t(\mu_o))$ corresponds to the radiation scattered by the aerosols with three different contributions :

$\frac{\bar{\omega}_S\ b_S}{\mu_o}$ is the atmospheric contribution ;

$-\ \bar{\omega}_S\ b_S(\frac{1}{\mu_o} + 2)\ A_t(\mu_o)$ corresponds to the radiation los by scattering before and after the reflection,

$2\bar{\omega}_S\ b_s\ A_t^2(\mu_o)$ corresponds to the radiation scattered downwards by the atmosphere and reflected twice by the sublayer .

It is easy to study the influence of the various parameters $\bar{\omega}_S$, b_S, A_t and μ_o in Eqs. (14). In particular as ΔA appears as a balance between positive and negative terms, the resulting effect can be either an enhancement or a reduction of the albedo ; an equilibrium value of the single scattering albedo $\bar{\omega}_S^{eq}$ corresponds to an exact compensation and no effect.

5 - Test of the method

In order to test the above described method we have choosen to apply it to the model used by HERMAN et al (1976), who give results at λ = 0.5 µm obtained by a complete and accurate resolution of the transfer problem ; their model will be quoted as H.B.R. in what follows.

5-1 - Atmospheric model

Troposphere : - molecular optical thickness $\tau^{Rayl} = 0.1$

- aerosols characteristics :
  - . optical thickness $\tau^{aer} = 0.145$
  - . size distribution $n(r) = C\ r^{-3.5}$
  - . Elterman's profile
  - . refractive index $m = 1.54 - 0.00i$

Stratosphere : - aerosol uniform layer between 15 and 25 km

- size distribution (log. normal)

$$n(r) = \frac{C}{(2\pi)^{1/2}\ \sigma r} \exp\{-(\ell n(r/\bar{r}))^2/2\sigma^2\} ,$$

$\sigma = 1.3$; $\bar{r} = 0.3$ µm

- real part of refractive index $m_r = 1.54$.

The stratospheric aerosol mass loading is varied between 0 and 3.2 $\mu g.m^{-3}$, which corresponds to an optical thickness τ_S between 0 and 0.1216. The aerosol absorption is also kept variable with a single scattering albedo $\bar{\omega}_S$ between 1 and 0.6. Three ground albedo A_G= 0.1, 0.3, 0.9 and three solar zenith angle Arc cos μ_o = 15°, 45°, 65° are considered.

5-2 - Results for the tropospheric albedo

Table 3 shows the comparison of our results with H.B.R. results for the three ground albedos and the three solar zenith angles.

The agreement is always better than 1 %, which validates the assumption of homogeneity and the use of the two stream method.

5-3 - Results for the stratospheric aerosol influence

Both the two-stream and the primary scattering approximations, expanded to the first order in τ have been used.

Table 4 compares the equilibrium single scattering albedo $\bar{\omega}_S^{eq}$ obtained by both methods with H.B.R. exact values.

Table 5 gives a similar comparison for the slopes $\Delta A(\mu_o)/\tau_S$ for 5 values of $\bar{\omega}_S$ between 0.6 and 1.

All the comparisons are done for the three ground albedos and the three solar zenith angles.
For 15° and 45° solar zenith distance, the two-stream results are better than the primary scattering results, the equilibrium single scattering albedo are nearly exact, and the slopes agree within better than 10 % with the exact values. For 65° solar zenith distance the inverse becomes true, with a little better agreement of the primary scattering values with the exact ones. Anyhow the difference between both methods are very small. The advantage remains to the two-stream method, considering the larger influence of small solar incidences on the radiation balance.

However the method may fail for near grazing incidences, where moreover the earth curvature should have to be taken account. On the other hand the accuracy of the method seems to increase with the ground albedo ; this may have some compensating effect at high latitude, where the sun is low, but the ice or snow covered ground highly reflective. (ELLIS and VONDER HAAR, 1976). Finally Fig. 1 reproduces H.B.R. figs. 2,3,4, in comparison with our results plotted in the same form.

6 - Conclusion

A simple formalism based on the two stream approximation allows to describe the whole atmosphere including both tropospheric and stratospheric aerosols. Therefore the radiative characteristics of either the troposphere or the stratosphere can be separately adjusted to describe any atmospheric state. The accuracy has been checked on a realistic model by comparison with exact computations results. The local and planetary albedo are retrieved nearly exactly and the variations of albedo due to a stratospheric aerosols layer are reproduced with an accuracy of ten percent in the worst cases and generally much better. The discribed method will be used now to study the climatic impact of stratospheric aerosol, with a degree of confidence which was not achieved in the previous similar studies.

References

ATWATER, M.A., 1970, Planetary albedo changes due to aerosols, Science 170, 64-66.

CHARLSON, R.J. and PILAT, M.J., 1969, Climate;the influence of aerosols, J. Appl. Meteor. 8, 1001-1002.

CHYLEK, P. and COAKLEY JR, J.A., 1974, Aerosols and climate, Science 183, 75-77.

COAKLEY, J.A. and GRAMS, G.W., 1976, Relative influence of visible and infrared optical properties of a stratospheric aerosol layer on the global climate, J. Appl. Meteor. 15, 679-691.

DESCHAMPS P.Y., HERMAN, M., LENOBLE, J., TANRE, D., VIOLLIER, M., 1980, Atmospheric effects in remote sensing of ground and ocean reflectances, in "Remote Sensing of Atmospheres and Oceans" edit. by A. DEEPAK, Academic Press, New York.

ELLIS, J. and VONDER HAAR, T.H., 1976, Zonal average earth radiation budget measurements from satellites for climate studies, Atmos. Sci. Paper n° 240, Colorado State University, 50 pp. (NTIS N 77 - 13588/7GA).

HARSHVARDHAN and CESS, R.D., 1976, Stratospheric aerosols : Effect upon atmospheric temperature and global climate, Tellus 1,1-10.

HARSHVARDHAN, 1979, Perturbation of the zonal radiation balance by a stratosphere aerosol layer, J. Atmos. Sci. 36, 1274-1285.

HERMAN, B.M. and BROWNING, S.R., 1965, A numerical solution to the equations of radiative transfer, J. Atmos. Sci. 22, 559-566.

HERMAN, B.M. and BROWNING, S.R., 1975, The effect of aerosols on the earth-atmosphere albedo, J. Atmos. Sci. 32, 1430-1445.

HERMAN, B.M., BROWNING, S.R. and RABINOFF, R., 1976, The change in earth-atmosphere albedo and radiational equilibrium temperatures due to stratospheric pollution, J. Appl. Meteor. 13, 1057-1067.

IRVINE, W.M., 1968, Multiple scattering by large particles. II - Optically thick layers, Astroph. J. 152, 823.

LUTHER, F.M., 1976, Relative influence of stratospheric aerosols on solar and longwave radiative fluxes for a tropical atmosphere, J. Appl. Meteor. 15, 951-955.

POLLACK, J.B., TOON, O.B., SAGAN, C., SUMMERS, A., BALDWIN, B. and VAN CAMP, W., 1976, Volcanic explosions and climatic change : a theoretical assessement, J. Geophys. Res. 81, 1071-1083.

RADIATION COMMISSION OF IAMAP, 1977, Standard Procedures to Compute Atmospheric Radiative Transfer in a Scattering Atmosphere, Edit by J. LENOBLE, Université des Sciences et Techniques de Lille - France. (Available from Dr. S. RUTTENBERG, NCAR, Boulder Colorado 80307, USA).

RASOOL, S.I. and SCHNEIDER, S.H., 1971, Atmospheric carbon dioxide and aerosols effects of large increases on global climate, Science 173, 138-141.

RECK, R.A., 1974, Influence of surface albedo on the change in the atmospheric radiation balance due to aerosols, Atmos. Environ. 8, 823-833.

SCHNEIDER, S.H., 1971, A comment on "Climate : the influence of aerosols", J. Appl. Meteor. 10, 840-841.

TANRE, D., HERMAN, M., DESCHAMPS, P.Y. and DE LEFFE, A., 1979, Atmospheric modeling for space measurements of ground reflectances, including bidirectional properties, Appl. Opt. 18, 3587-3594.

WANG, W. and DOMOTO, G.A., 1974, The radiative effect of aerosols in the earth's atmosphere, J. Appl. Meteor. 13, 521-534.

YAMAMOTO, G. and TANAKA, M., 1972, Increase of global albedo due to air pollution, J. Atmos. Sci. 29, 1405-1412.

	ω_o = 1.0	ω_o = 0.9	ω_o = 0.8	ω_o = 0.7	ω_o = 0.6
(1)	0.0089	0.0080	0.0071	0.0062	0.0053
τ = 0.010 (2)	0.0089	0.0080	0.0071	0.0062	0.0053
μ_o = 0.999 (3)	0.0082	0.0074	0.0065	0.0057	0.0049
(1)	0.0452	0.0405	0.0358	0.0312	0.0266
τ = 0.052 (2)	0.0452	0.0407	0.0362	0.0316	0.0271
μ_o = 0.999 (3)	0.0415	0.0373	0.0332	0.0290	0.0249
(1)	0.1078	0.0960	0.0845	0.0732	0.0622
τ = 0.130 (2)	0.1078	0.0970	0.0862	0.0755	0.0647
μ_o = 0.999 (3)	0.0993	0.0893	0.0794	0.0965	0.0596
(1)	0.3452	0.2980	0.2548	0.2150	0.1780
τ = 0.520 (2)	0.3452	0.3107	0.2762	0.2416	0.2071
μ_o = 0.999 (3)	0.3206	0.2885	0.2565	0.2244	0.1923
(1)	0.0150	0.0135	0.0120	0.0105	0.0090
τ = 0.010 (2)	0.0150	0.0135	0.0120	0.0105	0.0090
μ_o = 0.523 (3)	0.0155	0.0140	0.0124	0.0109	0.0093
(1)	0.0744	0.0665	0.0586	0.0509	0.0433
τ = 0.052 (2)	0.0744	0.0670	0.0595	0.0521	0.0446
μ_o = 0.523 (3)	0.0771	0.0694	0.0617	0.0540	0.0463
(1)	0.1704	0.1506	0.1315	0.1131	0.0953
τ = 0.130 (2)	0.1704	0.1534	0.1363	0.1193	0.1023
μ_o = 0.523 (3)	0.1774	0.1597	0.1419	0.1242	0.1064
(1)	0.4537	0.3810	0.3176	0.2617	0.2120
τ = 0.520 (2)	0.4537	0.4083	0.3630	0.3176	0.2722
μ_o = 0.523 (3)	0.4788	0.4309	0.3830	0.3351	0.2873

Table 1 - Comparison of the diffuse transmission $t(\mu_o)$ computed exactly (1), by using the approximation $t(\mu_o) = \bar{\omega}\, t_{\bar{\omega}=1}(\mu_o)$ where $t_{\omega=1}(\mu_o)$ is the exact computation (2), and by the two-stream method including the previous approximation (3).

	$\omega_o = 1.0$	$\omega_o = 0.9$	$\omega_o = 0.8$	$\omega_o = 0.7$	$\omega_o = 0.6$
(1)	0.0089	0.0080	0.0071	0.0062	0.0053
$\tau=0.010$ (2)	0.0082	0.0074	0.0066	0.0058	0.0049
$\mu_o=0.999$ (3)	0.0090	0.0081	0.0072	0.0063	0.0054
(1)	0.0452	0.0405	0.0358	0.0312	0.0266
$\tau=0.052$ (2)	0.0427	0.0385	0.0342	0.0299	0.0256
$\mu_o=0.999$ (3)	0.0466	0.0420	0.0373	0.0326	0.0280
(1)	0.1078	0.0960	0.0845	0.0732	0.0622
$\tau=0.130$ (2)	0.1063	0.0962	0.0855	0.0748	0.0641
$\mu_o=0.999$ (3)	0.1166	0.1049	0.0933	0.0816	0.0700
(1)	0.0150	0.0135	0.0120	0.0105	0.0090
$\tau=0.010$ (2)	0.0157	0.0141	0.0126	0.0110	0.0094
$\mu_o=0.523$ (3)	0.0152	0.0137	0.0122	0.0106	0.0091
(1)	0.0744	0.0665	0.0586	0.0509	0.0433
$\tau=0.052$ (2)	0.0816	0.0734	0.0653	0.0571	0.0490
$\mu_o=0.523$ (3)	0.0791	0.0712	0.0633	0.0554	0.0475
(1)	0.1704	0.1506	0.1315	0.1131	0.0953
$\tau=0.130$ (2)	0.2040	0.1836	0.1632	0.1428	0.1224
$\mu_o=0.523$ (3)	0.1978	0.1780	0.1382	0.1384	0.1187

Table 2 - Comparison of the diffuse transmion $t(\mu_o)$ computed exactly (1), by two-stream method and primary scattering expression expanded to the first order in τ (respectively (2) and (3)).

A_G \ θ_o	(1) 15°	(2)	(1) 43°	(2)	(1) 65°	(2)
0.1	0.155	0.156	0.132	0.132	0.105	0.103
0.3	0.315	0.312	0.245	0.243	0.167	0.165
0.9	0.860	0.861	0.635	0.632	0.380	0.381

Table 3 - Comparison of the reflected fluxes at the top of the troposphere between H.B.R. results (1) and our results (2). The computations are given for the three ground albedos and the three solar zenith angles.

A_G \ θ_o	(1) 15°	(2)	(3)	(1) 45°	(2)	(3)	(1) 65°	(2)	(3)
0.1	0.88	0.88	0.96	0.85	0.87	0.90	0.82	0.87	0.82
0.3	0.98	0.97	/	0.95	0.95	0.98	0.90	0.94	0.92
0.9	/	/	/	/	/	/	/	/	/

Table 4 - Comparison of the equilibrium single scattering albedo $\bar{\omega}_S^{eq}$ obtained by both methods (two-stream (2) and primary scattering (3) approximations) with H.B.R. exact values (1). The results are given for the three ground albedos and three solar zenith angles. No value means cases where equilibrium das not exist (always warming).

	$\bar{\omega}_s$ \ A_G	0,1 (1)	0,1 (2)	0,1 (3)	0,3 (1)	0,3 (2)	0,3 (3)	0,9 (1)	0,9 (2)	0,9 (3)
θ_o=15°	0.6	-0.140	-0.155	-0.185	-0.334	-0.374	-0.405	-0.987	-1.088	-1.096
	0.7	-0.093	-0.099	-0.135	-0.268	-0.273	-0.309	-0.770	-0.818	-0.828
	0.8	-0.045	-0.043	-0.084	-0.185	-0.172	-0.213	-0.553	-0.549	-0.560
	0.9	X	+0.013	-0.033	-0.083	-0.071	-0.117	-0.316	-0.279	-0.292
	1.0	+0.064	+0.069	+0.018	X	+0.031	-0.021	-0.051	-0.009	-0.024
θ_o=45°	0.6	-0.172	-0.196	-0.212	-0.381	-0.436	-0.455	-1.128	-1.223	-1.230
	0.7	-0.106	-0.122	-0.142	-0.296	-0.313	-0.336	-0.902	-0.919	-0.926
	0.8	-0.035	-0.049	-0.071	-0.184	-0.190	-0.216	-0.621	-0.614	-0.623
	0.9	+0.042	+0.025	0.000	-0.057	-0.068	-0.096	-0.338	-0.309	-0.319
	1.0	+0.080	+0.098	+0.071	+0.066	+0.055	+0.023	X	-0.005	-0.015
θ_o=65°	0.6	-0.259	-0.327	-0.287	-0.519	-0.615	-0.588	-1.354	-1.571	-1.569
	0.7	-0.142	-0.204	-0.157	-0.360	-0.433	-0.401	-1.039	-1.176	-1.175
	0.8	X	-0.081	-0.028	-0.189	-0.251	-0.215	-0.767	-0.782	-0.780
	0.9	+0.125	+0.042	+0.102	0.000	-0.070	-0.029	-0.471	-0.388	-0.386
	1.0	+0.271	+0.165	+0.231	+0.189	+0.112	+0.157	X	+0.006	+0.009

X : Difficult to estimate from the Figures in Herman and al (1976).

Table 5 - Same as table 3 but for the slopes $\Delta A(\mu_o)/\tau$. The results are given for the three ground albedos and for five values of $\bar{\omega}_s$.

LIST OF CAPTION

Fig. 1-a : Comparison of reflected flux as a function of the stratospheric aerosol albedo for five values of the stratospheric aerosol loading for unit incident solar flux (left : HBR results, right : our results). Incident solar angle $\Theta_o = 15°$.

Fig. 1-b : Same as fig. 1-a but for $\Theta_o = 45°$.

Fig. 1-c : Same as fig. 1-a but for $\Theta_o = 65°$.

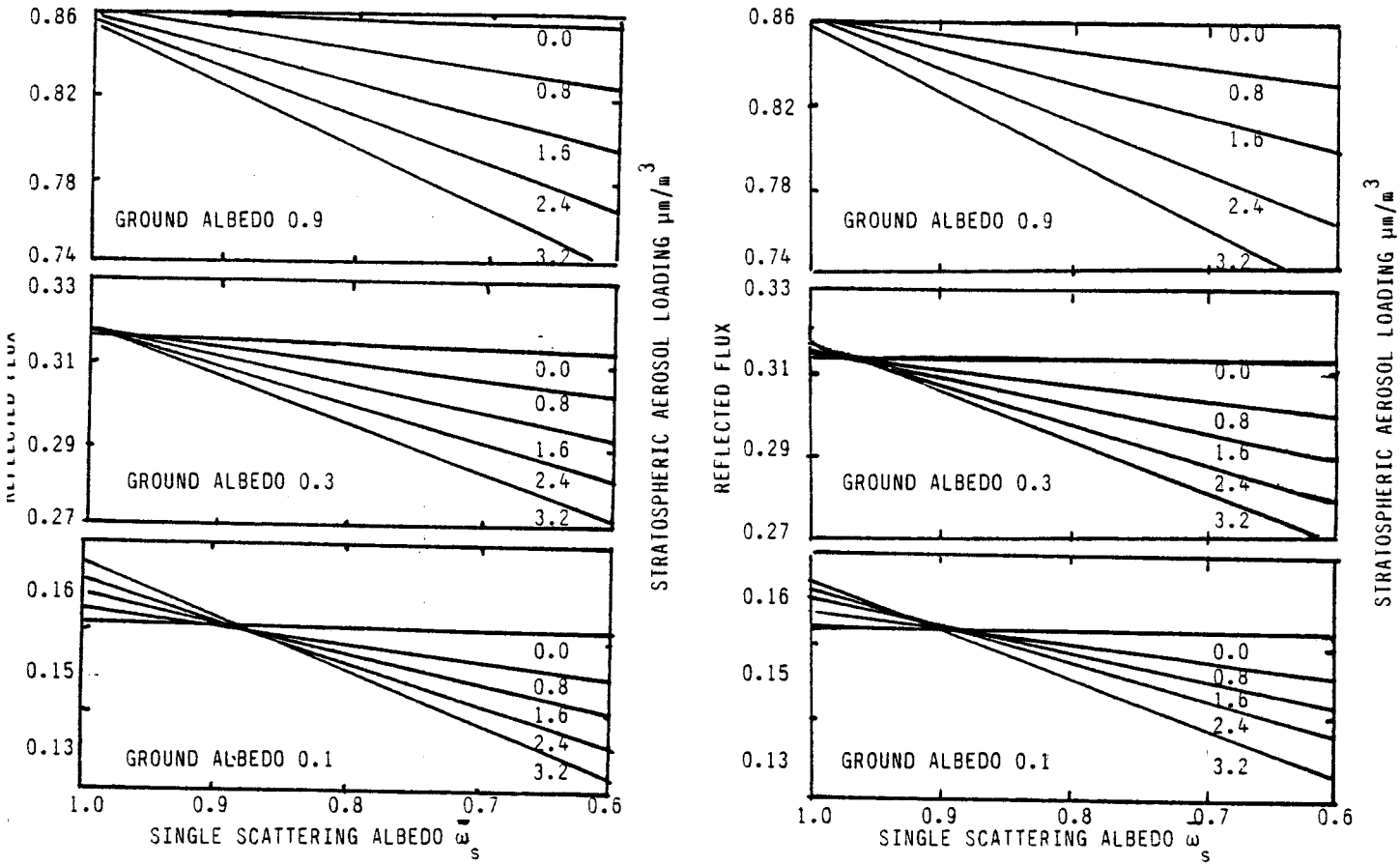
0.86
0.82
0.78
0.74
GROUND ALBEDO 0.9
0.0
0.8
1.6
2.4
3.2
0.33
0.31
0.29
0.27
GROUND ALBEDO 0.3
0.16
0.15
0.13
GROUND ALBEDO 0.1
1.0
0.9
0.8
0.7
0.6
SINGLE SCATTERING ALBEDO $\bar{\omega}_s$
REFLECTED FLUX
STRATOSPHERIC AEROSOL LOADING μm/m^3

Fig. 1-a

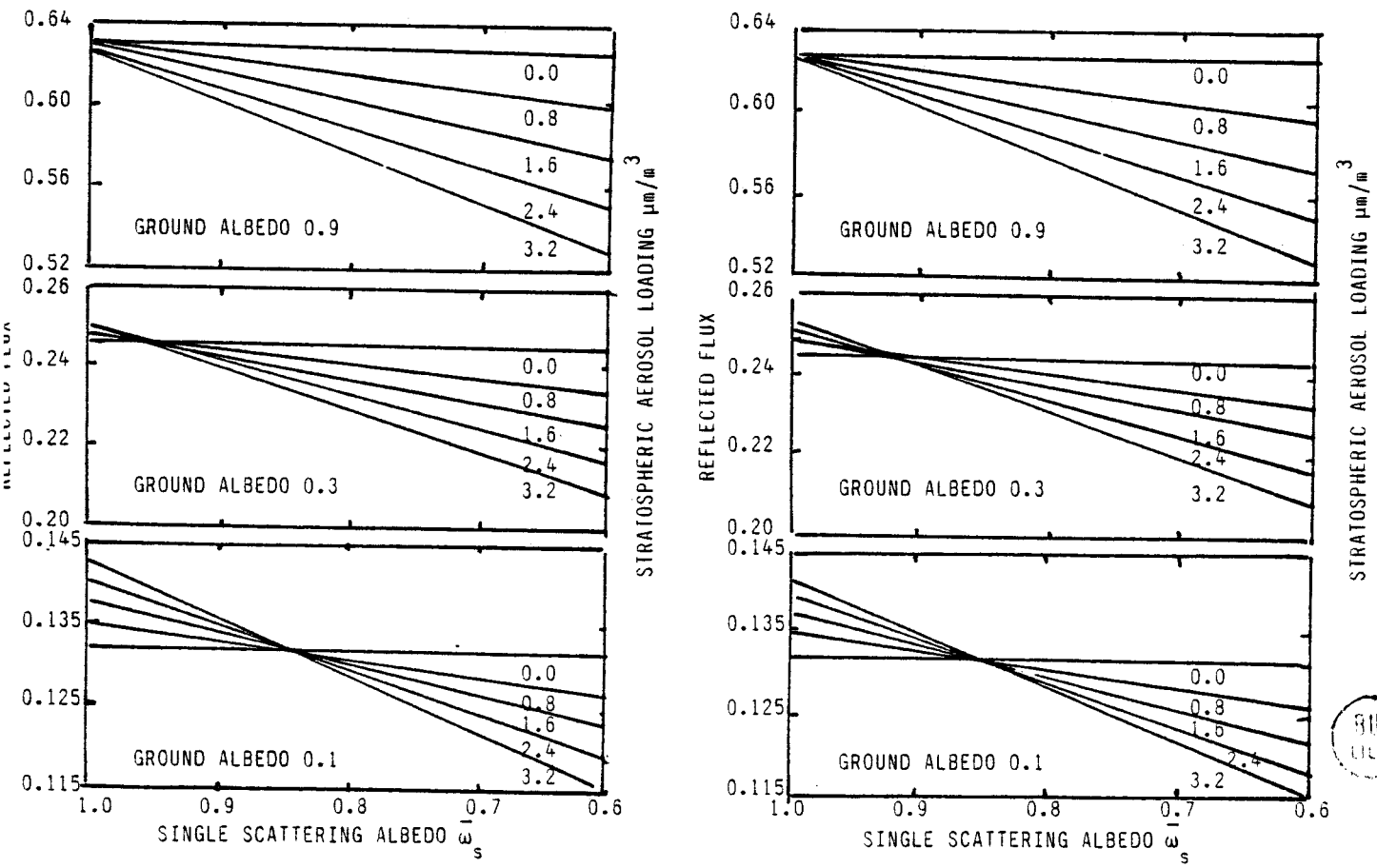
0.64
0.60
0.56
0.52
GROUND ALBEDO 0.9
0.0
0.8
1.6
2.4
3.2
0.26
0.24
0.22
0.20
GROUND ALBEDO 0.3
0.145
0.135
0.125
0.115
GROUND ALBEDO 0.1
1.0
0.9
0.8
0.7
0.6
SINGLE SCATTERING ALBEDO $\bar{\omega}_s$
REFLECTED FLUX
STRATOSPHERIC AEROSOL LOADING μm/m^3

Fig. 1-b

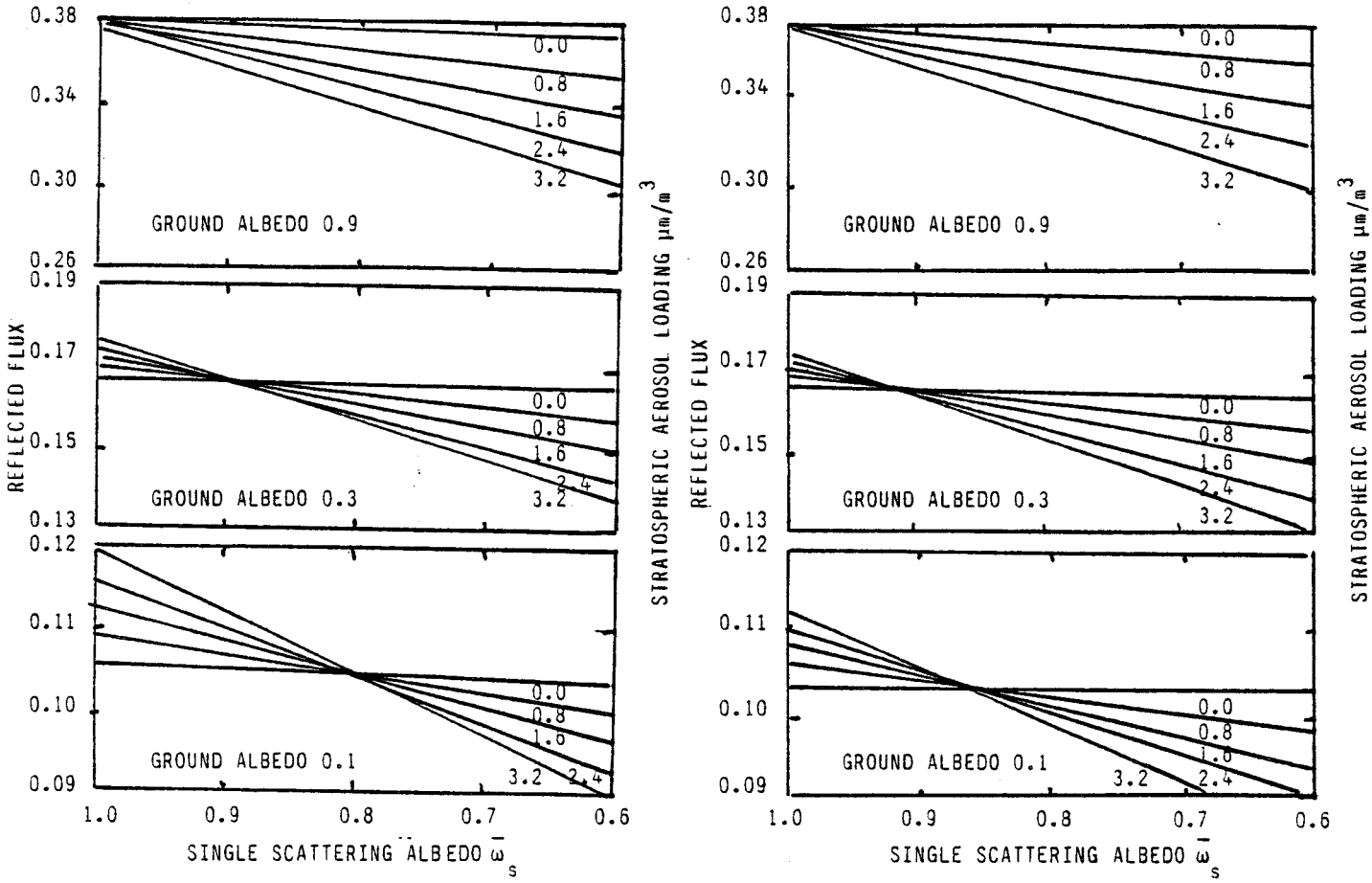

Fig. 1-c

ANNEXE 8

A SIMPLE METHOD TO COMPUTE THE CHANGE IN EARTH-ATMOSPHERE RADIATIVE BALANCE DUE TO A STRATOSPHERIC AEROSOL LAYER

II : APPLICATIONS

D. TANRE, J. LENOBLE, P.Y. DESCHAMPS, M. HERMAN

Laboratoire d'Optique Atmosphérique - (ERA 466)

Université des Sciences et Techniques de Lille

59655 VILLENEUVE D'ASCQ Cédex (FRANCE)

Abstract

The method described in (Lenoble et al, 1981) is applied to compute the variation of the zonal albedo and of the planetary radiation balance due to a stratospheric aerosol layer of background SO_4H_2 particles and of volcanic ashes (Mc Clatchey et al, 1980). The resulting ground temperature perturbation is evaluated, using a Budyko type climate model ; the feedback of a shift of the polar ice cap is considered.

1 - Introduction

In a companion paper (Lenoble et al., 1981 henceforth called Part I) we have worked out a simple analytical formulation of the albedo perturbation due to an enhancement of the stratospheric aerosol layer.

The purpose of the present study is to analyse the climatic impact of stratospheric aerosols of two types, background SO_4H_2 particles and volcanic ashes, as they are described in the models proposed by the IAMAP radiation commission (Mc Clatchey et al., 1980).

In the first section, the formalism of part I is applied to the variation of the zonal albedo ; then the influence of the aerosol layer on the planetary radiation balance is considered, including the infrared opacity increase. Finaly the aerosol perturbation, both of the albedo and of the emissivity, is introduced into a Budyko type climate model ; the resulting surface temperature variation is computed. On a long time scale, this can lead to a shift of the polar ice cap edge ; this shift is evaluated and its feedback influence on the temperature variation is outlined.

2 - Stratospheric aerosol Models

The IAMAP Radiation Commission (Mc Clatchey et al., 1980) has recently proposed standard atmospheric models for use in radiation calculations. They are based on our best present knowledge and represent a fairly realistic description, even if they cannot be expected to describe all the possible conditions of the real atmosphere. Their main purpose is to furnish a small number of well defined atmospheres useful for

intercomparisons.

In this paper we are using the two stratospheric aerosol models of the Standard Radiation Atmosphere (refered as SRA). The background stratospheric aerosol (BSA), made of 75% SO_4H_2 solution,and the volcanic aerosol (VA) are characterized by their complex refractive index (Mc Clatchey et al., 1980, table 7) and their size distribution given by a modified gamma function

$$n(r) = Ar^{\alpha} \exp(-br^{\gamma}) \quad ; \tag{1}$$

the coefficients α, b, γ are listed in table 1 ; A is just a normalisation constant related to the total number of particles, or to the optical thickness. The main parameters of the stratospheric aerosol layer (see part I of this paper) are the optical thickness τ_s, the single scattering albedo $\bar{\omega}_s$ and the backscattering coefficient $b_s = (1-g_s)/2$, related to the asymetry factor g_s. They are computed for a series of wavelengths from the Mie theory. As we are interested in the aerosol influence over the whole solar spectrum, we will define the following effective values

$$\tau_s^{eff} = \frac{\int_o^{\infty} \tau_{s\lambda} \, f_\lambda \, d\lambda}{\int_o^{\infty} f_\lambda \, d\lambda} \quad , \tag{2}$$

$$\bar{\omega}_s^{eff} = \frac{1}{\tau_s^{eff}} \frac{\int_o^{\infty} \bar{\omega}_{s\lambda} \, \tau_\lambda \, f_\lambda \, d\lambda}{\int_o^{\infty} f_\lambda \, d\lambda} \quad , \tag{3}$$

$$b_s^{eff} = \frac{1}{\bar{\omega}_s^{eff} \, \tau_s^{eff}} \frac{\int_o^{\infty} b_{s\lambda} \, \omega_{s\lambda} \, \tau_{s\lambda} \, f_\lambda \, d\lambda}{\int_o^{\infty} f_\lambda \, d\lambda} \quad , \tag{4}$$

where the weighting function f_λ is the incoming solar monochromatic

irradiance. Table 1 gives the values of $\bar{\omega}_s^{eff}$ and b_s^{eff} for both SRA models. Similarly we will define an effective infrared optical thickness

$$\tau_{s\ IR}^{eff} = \frac{1}{\sigma T_s^4} \int_o^\infty \tau_{s\lambda}\ B_\lambda(T_s) d\lambda = C_s \tau_s^{eff}, \qquad (5)$$

weighted by the blackbody radiance B_λ at the stratospheric temperature taken as T_s = 215 K. The ratio $C_s = \tau_{s\ IR}^{eff} / \tau_s^{eff}$ is also given in table 1.

3 - Aerosol influence on the zonal albedo

In part I of this paper, we have worked out a simple expression which gives the albedo variation due to a stratospheric aerosol layer as

$$\Delta A = \bar{\omega}_s\ b_s\ \tau_s (1-A)(\frac{1}{\mu_0} - 2A) - (1-\bar{\omega}_s)\ A\tau_s(\frac{1}{\mu_0} + 2) \qquad (6)$$

where A is the albedo of the unperturbed atmosphere and Arccos μ_0 the sun zenith angle.

Equation (6) has been applied to the monthly albedo sensitivity for 10° latitude belts. The mean solar zenith angle is taken for the 21 of each month and the mean latitude of the zone. The unperturbed atmosphere albedo is taken to be the mean monthly values quoted in Ellis and Von der Haar (1976). As this albedo is only known by its average value over the solar spectrum, it seems more sensitive to use for τ_s, $\bar{\omega}_s$ and b_s the average effective values of the stratospheric parameters as defined by Eqs. (2), (3) and (4) rather than to repeat the computations for a series of wavelengths.

Figure 1 compares our results with those obtained by Harshvardhan (1979) and by Herman et al. (1976) ; it shows the isopleths in percent

of change of albedo for the Northern Hemisphere. The aerosol parameters are taken as

$$\bar{\omega}_s = 1 \quad ; \quad b_s = 0.135 \quad ; \quad \tau_s = 0.03,$$

which are the same conditions as used by Harshvardhan, except than he includes a very slight absorption in the near infrared. The solar averaged values are obtained by Harshvardhan in averaging over the albedo itself, instead of averaging over the aerosols parameters. Herman's results corresponds to a slightly different phase function and to a different unperturbed atmosphere model. The three sets of curves agree quite perfectly except for two points :

- at high latitude our data confirm the higher values obtained by Harshvardhan than by Herman, due probably to the ground albedo difference as outlined by Harshvardhan ;
- the large area of small albedo changes extending from high latitude winter to nearly the whole year at low latitudes is due to a compensating influence of A and μ_0 leading to a factor $(1-A)\ (1/\mu_0-2A)$ which is nearly constant ; in this area the gradients of ΔA are so small, that the deformations of the isopleth 0.3 % cannot be considered as significant.

Figure 2 shows the results obtained for the two SRA aerosol models for both hemispheres ; the optical thickness has been kept to $\tau_s = 0.03$ and the unpertunbed albedo is always taken from Ellis and Von der Haar (1976). Comparisons of the two diagrams of figure 2 together and with figure 1-a outline the influence of the aerosol model. Of course the three diagrams display the same general pattern, with a large seasonal variation at high latitudes due to the solar incidence variation, a slight seasonal variation at mean latitudes where the winter increase of albedo is partly compensated by the decrease of μ_0, and a nearly constant value

of ΔA at low latitudes where both A and μ_0 do not vary much. The influence of the rather strong absorption assumed in the SRA volcanic model shows up in strongly reducing the increase of albedo ; with volcanic aerosols, one can even trace in the Northern Hemisphere an isopleth 0 % corresponding to a complete compensation and a slight decrease of albedo at high latitudes in summer. The backscattering coefficient has a small influence, ΔA increasing slightly with b_s.

4 - Aerosol influence on the planetary balance

The global planetary balance expresses the equilibrium between the absorbed solar flux and the infrared emitted flux ; it can be written as

$$f(1-A_P) = 4\sigma T_P^4, \qquad (7)$$

where A_P is the planetary (or spherical) albedo,

T_P an effective planetary temperature,

f the solar irradiance,

σ the Stefan Boltzman constant.

The addition of a stratospheric aerosol layer modifies the planetary albedo (see part I) by

$$\Delta A_P = 2\bar{\omega}_s \tau_s b_s (1-A_P)^2 - 4(1-\bar{\omega}_s)\tau_s A_P \quad , \qquad (8)$$

and the emitted infrared flux by

$$\Delta F_{IR} = [\varepsilon_s \sigma T_s^4 + (1-\varepsilon_s)\sigma T_P^4] - \sigma T_P^4, \qquad (9)$$

where ε_s is the emissivity of the aerosol layer assumed to be at a uniform temperature T_s different from T_P.

In the longwave spectrum the aerosol scattering can be neglected and the monochromatic flux emissivity is given by

$$\varepsilon_\lambda = 1 - 2\, E_3(\tau_\lambda) \simeq 2\tau_\lambda, \qquad (10)$$

where the exponential integral function E_3 has been expanded to the first order for a thin layer. A mean effective emissivity is given from the infrared effective optical thickness defined by Eq. (5) as

$$\varepsilon_s = 2\, C_s\, \tau_s \qquad (11)$$

Equation (7) with equation (9) yields to a planetary budget

$$\Delta B = -f\, \Delta A_P + 4\varepsilon\sigma(T_P^4 - T_S^4) \quad , \qquad (12)$$

which is a variation from the B = 0 equilibrium value ; ΔB is a flux by unit surface and is counted as positive if gained by the planet.

Assuming $T_s^4 = T_P^4/2$, which is approximately verified ($T_s \simeq 215$ K, $T_P \simeq 255$ K), and using Eq (11) and Eq (7) yields to

$$\Delta B = -f\, \Delta A_P + f(1-A_P) C_s\, \tau_s \quad , \qquad (13)$$

$$\Delta B = -f(\Delta A_P + \Delta A_P'), \qquad (14)$$

where ΔA_P is given by Eq (8) ; the infrared greenhouse effect of the aerosols can be taken into account by a further "equivalent variation of albedo"

$$\Delta A_P' = -(1-A_P) C_s\, \bar{\tau}_s \quad . \qquad (15)$$

Table 2 gives the modification of the planetary budget due to a stratospheric aerosol layer of optical thickness (averaged over the solar spectrum) $\tau_s = 0.03$ for both the SRA aerosol models ; the planetary albedo $A_P = 0.309$ is taken from Ellis and Von der Haar (1976). The contributions due to aerosol scattering, aerosol solar absorption and aerosol

infrared emission are shown separately. It clearly appears that the back-scattering term is commanding ; but the two other terms cannot be neglected, especially for absorbing aerosols, as in the volcanic case.

For a given aerosol size distribution, b_s is nearly independant of the imaginary refractive index ; C_s varies slightly with the visible and infrared absorption, but as the emissivity term is only a small contribution, we have kept C_s as constant and sought for the solar absorption (fixed by $\bar{\omega}_s$) which will lead to a complete compensation ($\Delta B = 0$). The results as expected are quite similar for both model and we have found $\bar{\omega}_s^{eq} = 0.891$ and $\bar{\omega}_s^{eq} = 0.895$ respectively for the background and the volcanic aerosols. This means absorption much stronger than it seems reasonnable to assume in our present state of knowledge. It seems therefore likely that a stratospheric aerosol increase will lead to a cooling of the planet.

5 - Climatic impact of the stratospheric aerosols.

Using a global climate model, the modification of the planetary radiation balance due to the stratospheric aerosols can be translated into a mean ground temperature variation. A simple Budyko-type model (Budyko, 1969;Chylekand Coakley, 1975) will be applied with the two SRA aerosol models and the results compared with those obtained by Harshvardhan and Cess (1976). In a last step the possible feedback due to the variation of the polar ice cap limit will be emphasized.

5.1 - Budyko-type climate model

In the climate model of Budyko (1969), the energy balance at any latitude ϕ is expressed by

$$\frac{f}{4} S(\phi) (1 - A(\phi)) - F_{IR}(\phi) = D(\phi), \qquad (16)$$

where

$\frac{f}{4} S(\phi)$ is the annual average incoming solar flux at the top of the atmosphere at the latitude ϕ,

$A(\phi)$ the annual average albedo,

$F_{IR}(\phi)$ the annual average outgoing infrared radiation flux

$D(\phi)$ the heat divergence resulting from the horizontal redistribution by the oceanic and atmospheric circulations ;

$S(\phi)$ is normalized by

$$\int_0^1 S(x)\, dx = 1, \text{ with} \qquad (17)$$

$$x = \sin \phi. \qquad (18)$$

Budyko assumes a constant cloudiness distribution of 50 % and gives an empirical expression of the infrared flux

$$F_{IR}(\phi) = a + BT(\phi), \qquad (19)$$

where $T(\phi)$ is the average surface temperature, and a, B, two empirical coefficients ($a = 202$ W m^{-2}, $B = 1{,}46$ W m^{-2}K^{-1}).

Similarly the transport of heat is parametrized by

$$D(\phi) = \beta(F_{IR}(\phi) - \bar{F}_{IR}), \qquad (20)$$

$$\bar{F}_{IR} = a + B\bar{T}, \qquad (21)$$

where $\bar{T}$ is the hemispherical (or planetary) mean surface temperature ;

β = 2.61 is an empirical coefficient.

5.2 - Planetary mean surface temperature

On the planetary scale, the radiative equilibrium is achieved and the integration of Eq (16) over an hemisphere with Eqs (17) and (21) leads to

$$\frac{f}{4}(1 - A_P) = \bar{F}_{IR} = a + B\bar{T}, \qquad (22)$$

where A_P is the planetary albedo defined previously.

From Eq (22), the planetary average surface temperature derives as

$$\bar{T} = \frac{f(1 - A_P) - 4a}{4B} \quad . \qquad (23)$$

When a stratospheric aerosol layer is added to the unperturbed atmosphere, the planetary albedo is changed from A_P to $A_P + \Delta A_P + \Delta A'_P$, with ΔA_P given by Eq (8) and $\Delta A'_P$ by Eq (15).
It finally results into a temperature variation

$$\Delta\bar{T} = -\frac{f}{4B}(\Delta A_P + \Delta A'_P) \qquad (24)$$

Figure 3 shows the variation $\Delta\bar{T}$ versus τ_s for the aerosol model used by Harshvardhan and Cess (1976) and characterized by ($\bar{\omega}_s$ = 1 ; b_s = 0.185 ; C_s = 0.0408). Fig. 3a includes the aerosol infrared effect and Fig. 3b is without infrared effect. As expected the infrared greenhouse effect results into a small decrease of the cooling ΔT (from -1,3°C to -1°C for τ_s = 0.03). The comparison of our values with those of Cess and Harshvardhan exhibits a very good agreement, with our values slightly

smaller without infrared and slightly higher with infrared included. On figure 4, the same data are plotted for the two SRA models. All results are for A_p = 0,309 taken from Ellis and Von der Haar. For the same optical thickness the cooling is smaller for the volcanic aerosol (ΔT = -1.5°C for τ_s = 0.1) than for the background aerosol (ΔT = -3,5°C for τ_s = 0.1) which gives the sames results than the Harshvardhan and Cess model (ΔT = -3.5°C for τ_s = 0.1). This is mainly due to the compensating influence of the solar radiation absorption when $\bar{\omega}_o$ decreases. The infrared emissivity influence increases slightly with the ratio C_s of the infrared and shortwave optical thicknesses.

5.3 - Ice cap limit and feedback

In the Budyko climate model it is possible to infer the stratospheric aerosol influence on the polar ice cap limit. This variation by modifying the ground albedo, has a feedback effect on the surface temperature which can be taken into account.

In what follows we will assume, based on Budyko's paper, that the unperturbed atmosphere local albedo has the form of a step function with a discontinuity at the edge of the ice cap and we will write

$$\begin{aligned} A(x,x_s) = A_1 &= 0,32 \text{ for } x < x_s \ , \\ A_s &= 0,50 \text{ for } x = x_s \ , \\ A_2 &= 0,62 \text{ for } x > x_s \ ; \end{aligned} \qquad (25)$$

the latitude of the ice edge is ϕ_s = Arc sin x_s and its temperature is fixed at $T(\phi_s) = T_s$ = - 9°C. For the present climate ϕ_s is found to be 72°. The planetary albedo $A_p(x_s)$ corresponding to the local albedo given in Eq. (25)

is 0.328 for $x_s = 72°$ slightly different from the Ellis and Von der Haar value $A_p = 0{,}309$. The influence of this modification has been checked to be small (for $\tau_s = 0{,}08$, the cooling ΔT changes from 2,8°C to 2,6°C for the background aerosols and from 1,2°C to 1,0°C for the volcanic aerosols).

The local balance at latitude ϕ_s can be written from Eq. (16) and Eq. (20) with the variable x

$$\frac{f}{4} S(x_s)(1 - A(x_s,x_s)) - F_{IR}(x_s) = D(x_s) = \beta(F_{IR}(x_s) - \bar{F}_{IR}), \quad (26)$$

and the global balance from Eq. (22)

$$\frac{f}{4} (1 - A_p(x_s)) = \bar{F}_{IR} \; ; \quad (27)$$

$A(x,x_s)$ means the albedo at latitude x, when the ice edge is at x_s and $A(x_s,x_s) = A_s$.

From Eqs (26) and (27) we can get

$$1 - A_p(x_s) = \frac{4 F_{IR}(x_s)}{f} \frac{1 + \beta}{\beta} - \frac{S(x_s)(1-A(x_s,x_s))}{\beta}, \quad (28)$$

where the unknown variable is x_s.

In order to solve explicitly Eq (28) we will assume a polynomial expansion of order N

$$S(x) = \sum_{i=0}^{N} a_i x^i \quad , \quad (29)$$

for the solar flux ; the a_i's are obtained by a least squares fit to the values of S(x) listed in table 1 of Chylek and Coakley (1975).

With Eq (29) we can rewrite the planetary albedo as

$$A_p(x_s) = (A_1 - A_2) \sum_{i=0}^{N} a_i \frac{x_s^{i+1}}{i+1} + A_2 \sum_{i=0}^{N} \frac{a_i}{i+1} \quad ; \quad (30)$$

substituting Eqs (29) and (30) into Eq (28) we get an equation of degree N + 1 for x_s

$$1-(A_1-A_2)\sum_{i=0}^{N} a_i\frac{x_s^{i+1}}{i+1} + \frac{(1-A_s)}{\beta}\sum_{i=0}^{N} a_i x_s^i - A_2\sum_{i=0}^{N}\frac{a_i}{i+1} - \frac{4F_{IR}(x_s)}{f}\frac{(1+\beta)}{\beta} = 0 \qquad (31)$$

Among the (N+1) roots of Eq (31), only two are real ; one of them (x_s = 72°) is the solution for the present climate ; the other real root has no physical meaning, as an increase of the solar constant will then cause a shift of the ice cap toward the equator (Chylek and Coakley, 1976 ; Frederiksen, 1976 ; North, 1975).

The stratospheric aerosol layer modify the planetary albedo $A_P(x_s)$ in Eq (30) by a quantity $\Delta A_P + \Delta A'_P$ given by Eqs (8) and (15) in terms of $A_P(x_s)$. Introduction of this term in Eq (31) results into a modification of the solution x_s. On figure 5 the latitude ϕ_s of the ice cap edge is plotted versus the aerosol optical thickness for the two SRA models, with and without the infrared effect included. The ice edge shift is much faster for the non absorbing background aerosols than for the volcanic aerosols ; inclusion of the infrared greenhouse effect slows down a little the shift. An optical thickness of 0.095 of SO_4H_2 aerosol leads to an ice limit at a latitude of 50° ; this effect is similar to a decrease of 1,6 % of the solar constant.

As the single scattering albedo is the commanding parameter, we have varied it for both models keeping b_s and C_s as constant. The results, similar as expected for both models, are plotted on figure 6, which shows the variation of the ice limit latitude ϕ_s versus $\bar{\omega}_s$ for different optical

thickness τ_s.

The shift is towards the equator for large $\bar{\omega}_s$ and towards the pole for small $\bar{\omega}_s$ (strongly absorbing aerosols). The equilibrium value $\bar{\omega}_s^{eq}$ which appears, corresponds to an exact compensation of the aerosols effects and no modification of the radiation balance ; the values are respectively $\bar{\omega}_s^{eq} \simeq 0{,}909$ and $\bar{\omega}_s^{eq} \simeq 0{,}906$ for the background and the volcanic models ; these values are slightly different from those found in section 4 (0.891 and 0.895) due to the different value of the unperturbed atmosphere albedo (respectively 0.328 and 0.309).

Finaly we have considered the feedback of this ice cap limit shift due to the aerosol cooling (or warming), which modify the planetary albedo A_p, on the mean surface temperature variations computed from Eqs (24), (8) and (15).

Results are presented on figure 7 versus the optical thickness τ_s for both SRA models. Figure 8 outlines the influence of the single scattering albedo for various τ_s, keeping the other characteristics of the model as constant. For comparison the curves of ΔT variations without feedback have been redrawn on figures 7 and 8, using the Budyko planetary albedo. The feedback amplifies the temperature decrease from 2.6°C to 7.2°C for a background aerosol layer of optical thickness 0.08 ; an effect of the same order is reached only with a layer of volcanic aerosols of optical thickness 0.24 (ΔT = 3°C and 6.5°C respectively without and with feedback).

On figure 8, we find again the equilibrium value $\bar{\omega}_s^{eq} \simeq 0.905$ between the cooling due to the most frequent aerosols and the possible warming by very strongly absorbing aerosols.

It seems worth to have a look at the time constants involved in the earth-ocean-atmosphere system in order to get a better understanding of the real possible influence of the stratospheric aerosols.

The time constant of the thermal energy reservoir is of about 100 days (Gierash et al. 1979), therefore it doesnot limit the climatic answer to an enhancement of the stratospheric aerosol loading, as due to a volcanic eruption, which has a typical life time up to 2 or 3 years.

The ocean-atmosphere system has a time constant of about 4 years, due to the high thermal capacity of the ocean (Schneider and Dickinson, 1974 ; Bryson, 1974). A volcanic enhancement during 2 or 3 years cannot completely perturb the system and our evaluation is probably a little in excess.

For the ice cap evolution, the time constant is quite large ; the last glacial period had a duration of about 10^3 years. Therefore the feedback effect has to be neglected when considering periods shorter than 100 years ; for longer periods it has to be taken into account, but probably not on its full scale and the values given above are probably surestimated.

6 - Conclusion

The climatic impact of a stratospheric aerosol layer has been investigated, considering the two aerosol models of the Standard Radiation Atmosphere proposed by the IAMAP Radiation Commission (Mc Clatchey et al., 1980). The background stratospheric aerosol model (SO_4H_2 particles) leads

to results quite similar to those found previously by Harshvardhan (1979) and Harshvardhan and Cess (1976), whereas the volcanic aerosol model has a much smaller influence due to the opposite and partially compensating influence of the aerosol scattering and aerosol absorption of solar radiation. In this last case, one can even observe a slight decrease of the zonal albedo at high latitudes in summer, which means an heating effect of the aerosol. However on the planetary scale both models lead to a loss of energy of respectively 27 $W.m^{-2}$ and 23 $W.m^{-2}$, for an optical thickness of 0.03 including the small infrared greenhouse effect i.e. to a cooling effect. The possibility of heating will appear only for much more absorbing aerosols with a single scattering albedo smaller than 0.9.Using a simple Budyko-type model this can be related to a surface temperature decrease of 3.5°C and 1.5°C respectively for a layer of background and volcanic aerosols with an optical thickness 0.1. Such a cooling if maintained over a long period of time could lead to a shift of the ice cap edge towards the equator, which in turn amplifies the temperature decrease by a factor between 2 and 3.

References

BRYSON, R.A., 1974 A perspective on climatic change, Science 184, 733.

BUDYKO, M.I., 1969, The effect of solar radiation variations on the climate of the earth, Tellus 21, 611-619.

CHYLEK, P., and J.A. COAKLEY, Jr, 1975, Analytical Analysis of a Budyko-type climate model, J. Atmos. Sci 32, 675-679.

ELLIS, J. and T.H. VON DER HAAR, 1976, Zonal average earth radiation budget measurements from satellites for climate studies, Atmos. Sci. Paper n° 240, Colorado State University, 50 pp, (NTIS N77-13588/7 GA).

FREDERIKSEN, J.S., 1976, Nonlinear albedo-temperature coupling in climate models, J. Atmos. Sci. 33, 2267-2272.

GIERASCH, P.R.,R.M.GOODY and P. STONE, 1970, The energy balance of planetary atmospheres, Geophys. Fluid Dyn. 1, 1.

HARSHVARDHAN and R.D. CESS, 1976, Stratospheric aerosols : Effect upon atmospheric temperature and global climate, Tellus 1, 1-10.

HARSHVARDHAN, 1979, Perturbation of the zonal radiation balance by a stratosphere aerosol layer, J. Atmos. Sci. 36, 1274-1285.

HERMAN, B.M., S.R. BROWNING, and R. RABINOFF, 1976, The change in earth-atmosphere albedo and radiational equilibrium temperatures due to stratospheric pollution, J. Appl. Meteor. 13, 1057-1067.

LENOBLE, J., D., TANRE, P.Y., DESCHAMPS, and M., HERMAN, 1982, A simple Method to compute the change in earth-atmosphere radiative balance due to a stratospheric aerosol layer, Part. I, Theoritical formulation, submitted to J. Atmos. Sci.

NORTH, G.R., 1975, Theory of Energy-Balance Climate Models, J. Atmos. Sci. 32, 2033-2043.

Mc CLATCHEY, R.A., H.J., BOLLE, K., YA KONDRATYEV , 1980, Report of the IAMAP Radiation Commission working group on a Standard Radiation Atmosphere, WMO/IAMAP (available from R.A. Mc Clatchey, AFGL, Hanscom AFB, Mass. 01731, USA).

SCHNEIDER, S.H., and R.E., DICKINSON, 1974, Climate Modeling, Rev. Geophys. Space Phys. 12, 447-493.

Aerosol Model	$\bar{\omega}_s^{eff}$	b_s^{eff}	$C_s = \tau_{IR}^{eff}/\tau_s^{eff}$	α	b	γ
B.S.A.	0.998	0.189	$3.83.10^{-2}$	1.0	18	1.0
V.A.	0.944	0.169	$2.17.10^{-2}$	1.0	16	0.5

TABLE I : Characteristics of the aerosol models (see text)

Aerosol Model	$-2\bar{\omega}_s\ b_s\ \tau_s(1-A_P)^2 f$	$4(1-\bar{\omega}_s)\tau_s\ A_P f$	$(1-A_P)\tau^{IR}\ f$	ΔB
B.S.A.	$-2.85.10^{1}$	$9.23.10^{-2}$	$1.56.10^{0}$	$-2.68.10^{1}$
V.A.	$-2.64.10^{1}$	$2.28.10^{0}$	$8.87.10^{-1}$	$-2.32.10^{1}$

TABLE II : Modification of the planetary budget $\Delta B(W.m^{-2})$ for the two SRA aerosol models with $\tau_s = 0.03$.

Relative contribution of :

1. Scattering $-2\bar{\omega}_s\ b_s\ \tau_s(1-A_P)^2 f$
2. Solar absorption $4(1-\bar{\omega}_s)\tau_s\ A_P\ f$
3. Emission $(1-A_P)\tau^{IR}\ f$

Captions

Fig. 1 : Change in zonal albedo in percent with addition of a stratospheric aerosol layer (τ_s = 0.03, $\bar{\omega}_s$ = 1, b_s = 0,135) comparison of our results (a), with Harshvardhan (1979) (b) and Herman et al (1976) (c).

Fig. 2 : Change in zonal albedo in percent with addition of a stratospheric aerosol layer (τ_s = 0.03) for the two SRA models. (a) Background aerosols ; (b) volcanic aerosols.

Fig. 3 : Variation of the average planetary surface temperature $\overline{\Delta T}$ versus the stratospheric aerosol optical thickness τ_s, $\bar{\omega}_s$ = 1, b_s = 0,185, C_s = 0,0408, A_p = 0,309.

a - infrared included

b - Infrared neglected

——— Harshvardhan and Cess (1976)

------ our results.

Fig. 4 : Variation of the average planetary surface temperature $\overline{\Delta T}$ versus the stratosphere aerosol optical thickness for the SRA aerosol models (infrared included)

——— Background aerosols

------ Volcanic aerosols

Fig. 5 : Latitude ϕ_s of the ice cap edge versus stratospheric aerosols optical thickness τ_s. Background stratospheric aerosols (BSA), Volcanic aerosols (VA).

——— Infrared neglected

------ Infrared included

Fig. 6 : Variation of the ice cap edge latitude ϕ_s with the single scattering albedo $\bar{\omega}_s$ for various τ_s

a. b_s, C_s values of BSA

b. b_s, C_s values of VA

Fig. 7 : Variation of the average planetary surface temperature $\overline{\Delta T}$ versus the stratospheric aerosol optical thickness τ_s with (———) and without (----) ice edge shift feeback (infrared included, A_p = 0.328)

a. background aerosols

b. volcanic aerosols

Fig. 8 : Variation of the average planetary surface temperature $\overline{\Delta T}$ with the single scattering albedo.

——— τ_s = 0.10
------ τ_s = 0.05 } with ice feedback
— - — τ_s = 0.01

+++ τ_s = 0.05 without ice feedback

a. background aerosols

b. volcanic aerosols

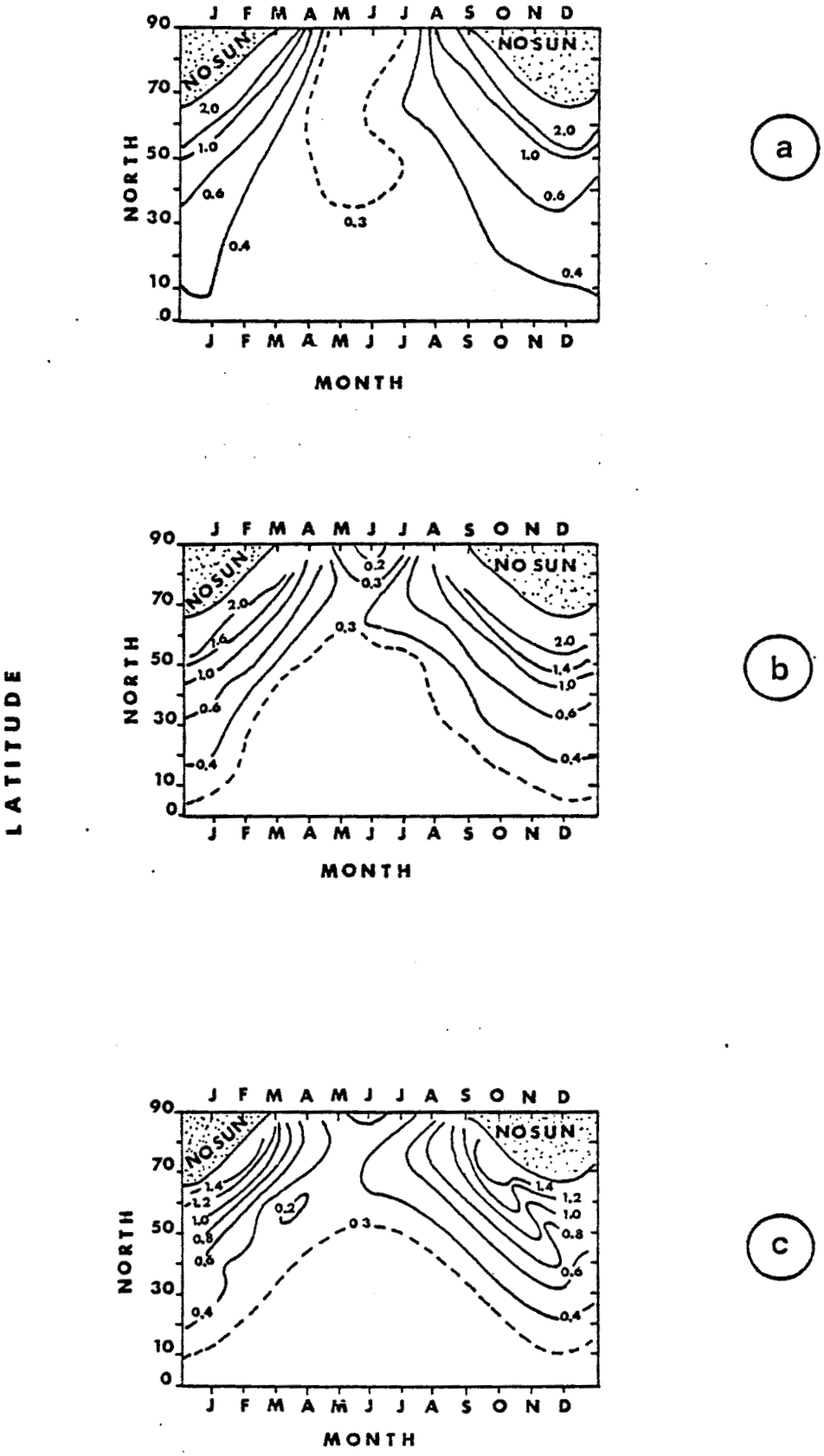

Fig. 1 : Change in zonal albedo in percent with addition of a stratospheric aerosol layer (τ_s = 0.03, $\bar{\omega}_s$ = 1, b_s = 0,135) comparison of our results (a), with Harshvardhan (1979) (b) and Herman et al (1976) (c).

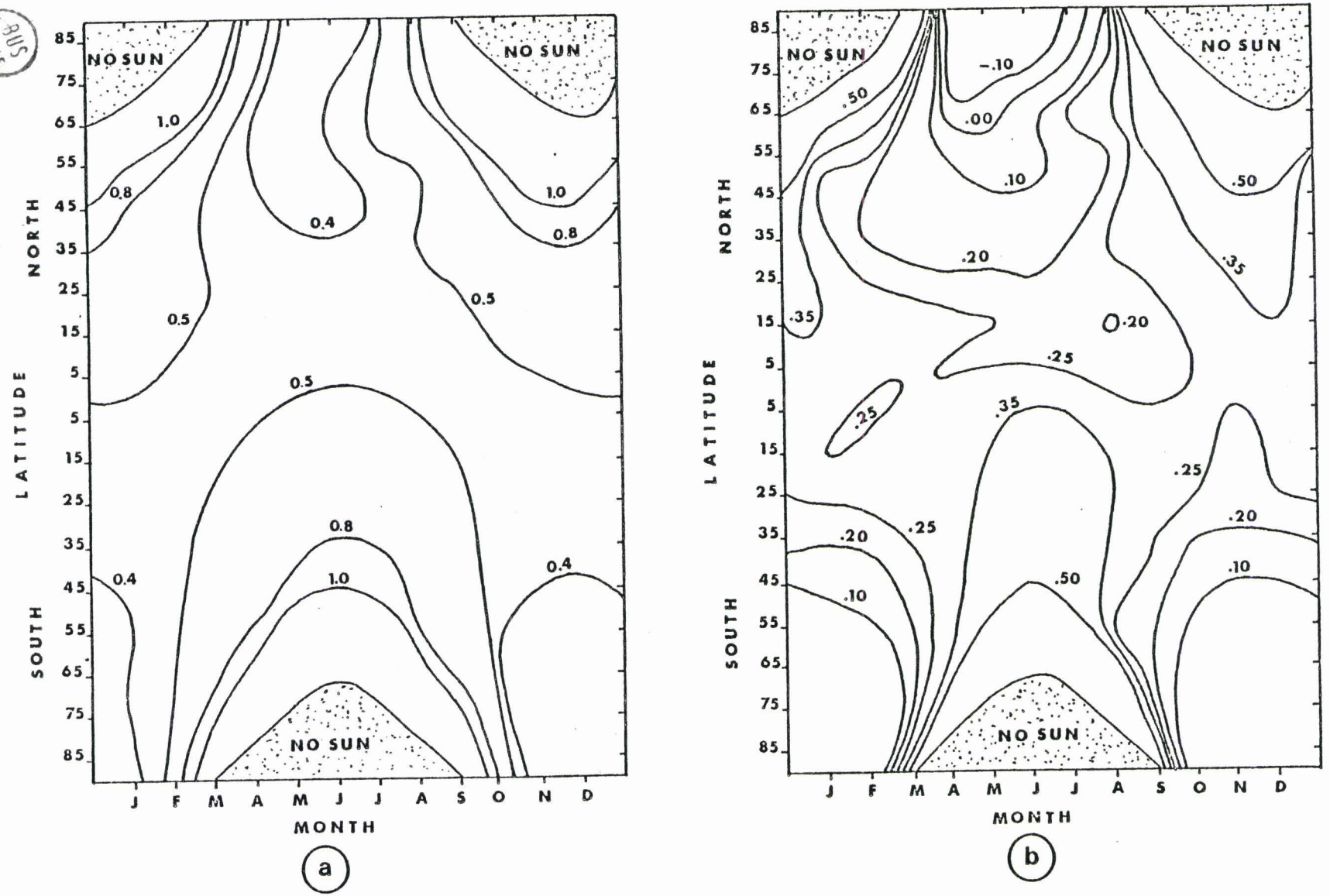

Fig. 2 : Change in zonal albedo in percent with addition of a stratospheric aerosol layer (τ_s = 0.03) for the two SRA models. (a) Background aerosols ; (b) volcanic aerosols.

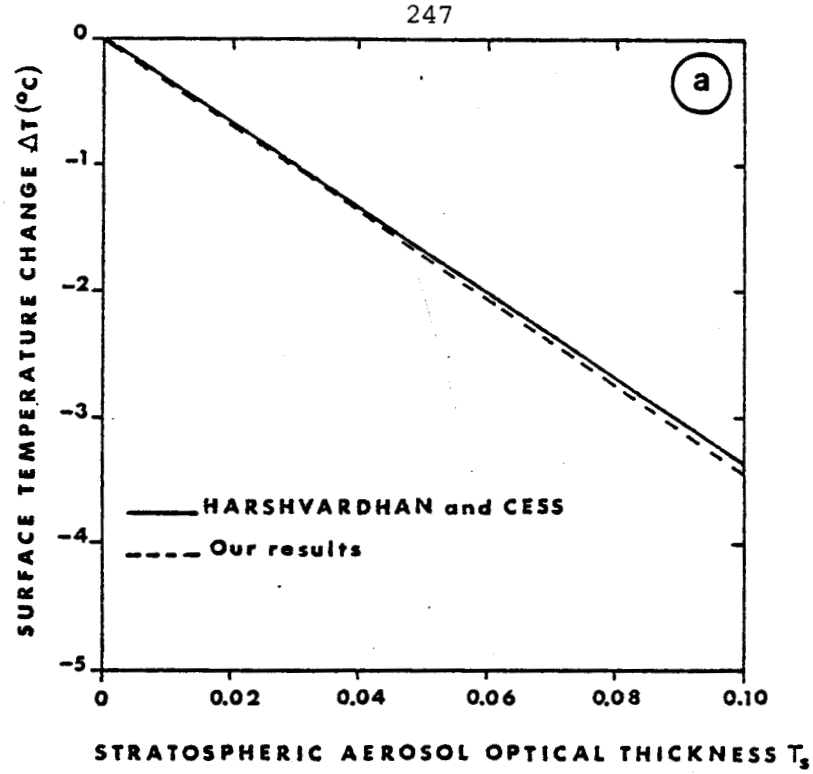

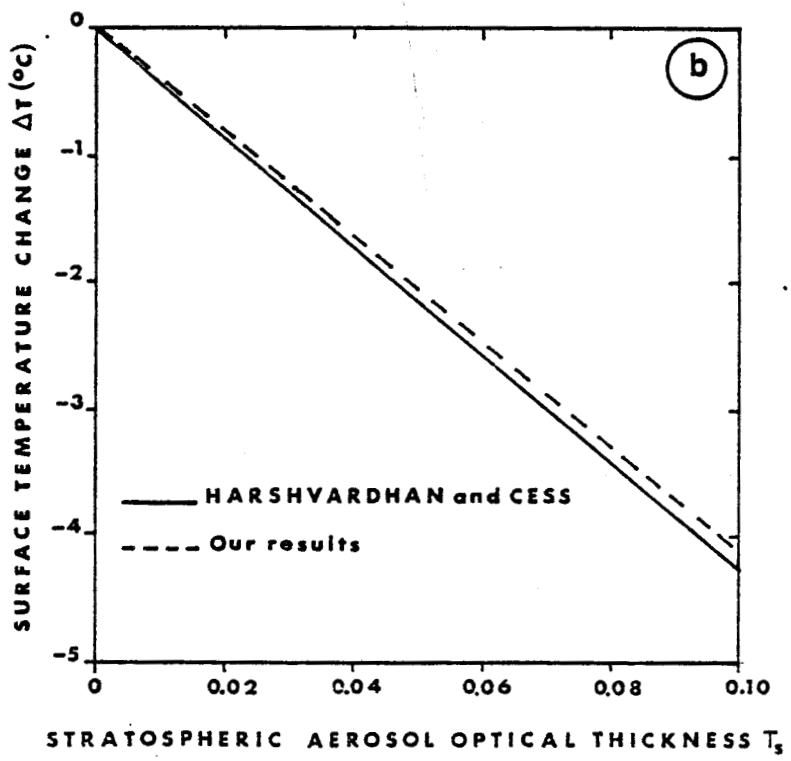

Fig. 3 : Variation of the average planetary surface temperature $\overline{\Delta T}$ versus the stratospheric aerosol optical thickness τ_s, $\bar{\omega}_s = 1$, $b_s = 0,185$, $C_s = 0,0408$, $A_p = 0,309$.

a - infrared included

b - Infrared neglected

——— Harshvardhan and Cess (1976)

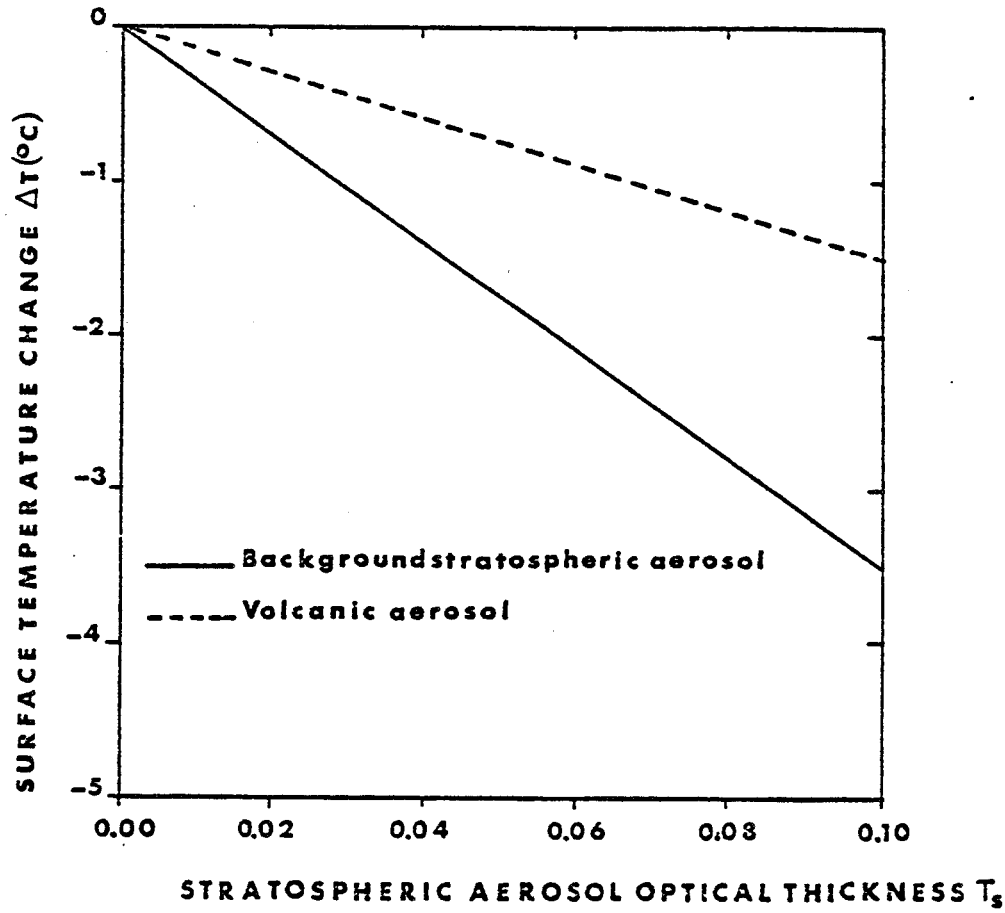

Fig. 4 : Variation of the average planetary surface temperature $\overline{\Delta T}$ versus the stratosphere aerosol optical thickness for the SRA aerosol models (infrared included)

——— Background aerosols

------ Volcanic aerosols

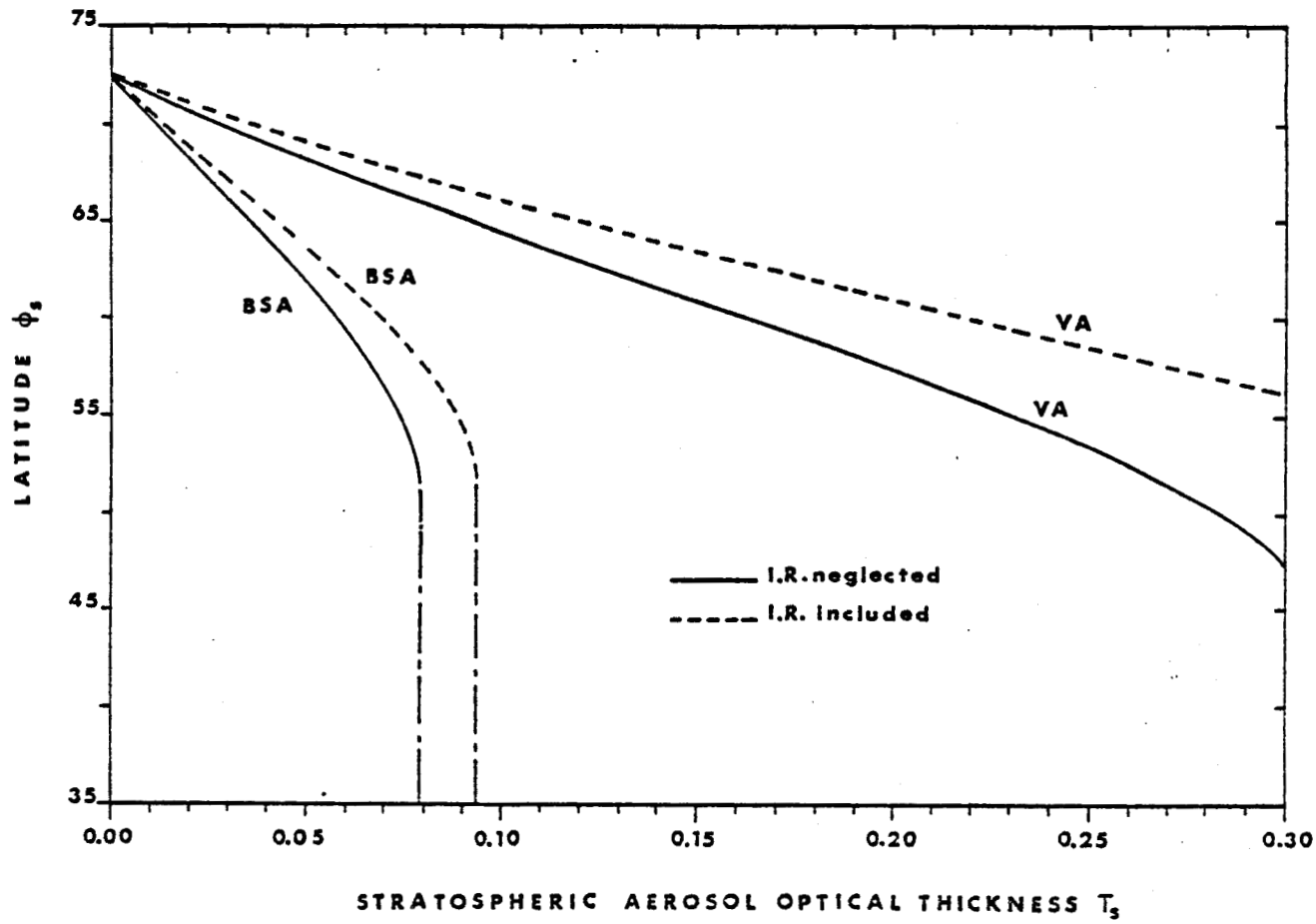

Fig. 5 : Latitude ϕ_s of the ice cap edge versus stratospheric aerosols optical thickness τ_s. Background stratospheric aerosols (BSA), Volcanic aerosols (VA).

——— Infrared neglected

------ Infrared included

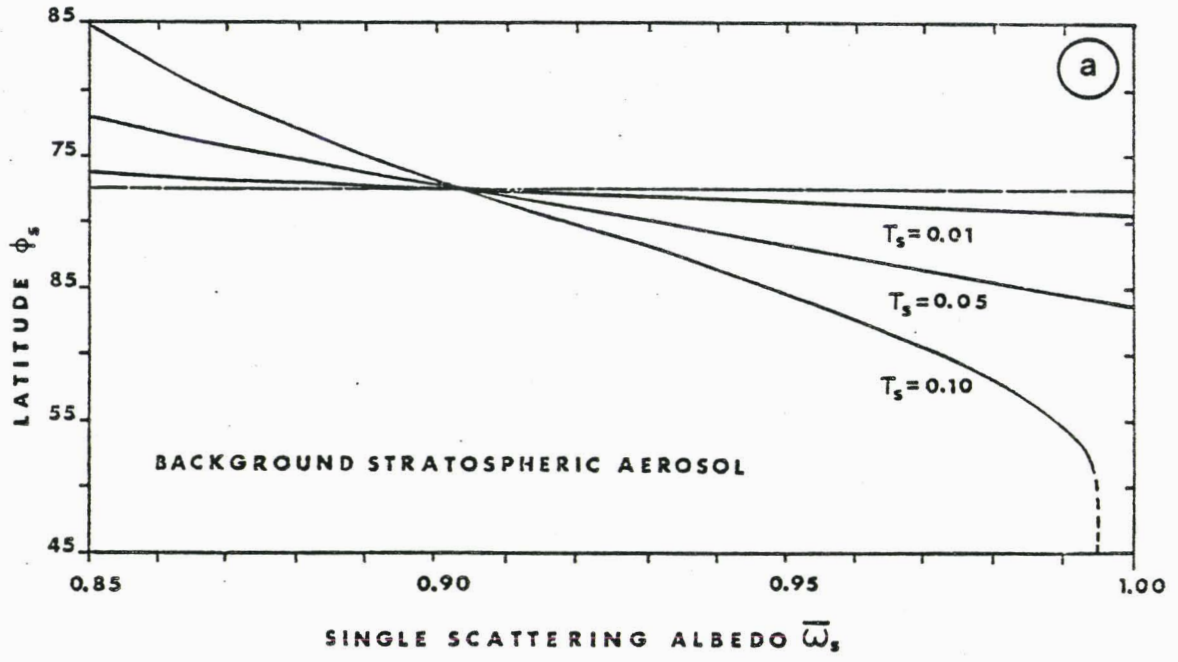

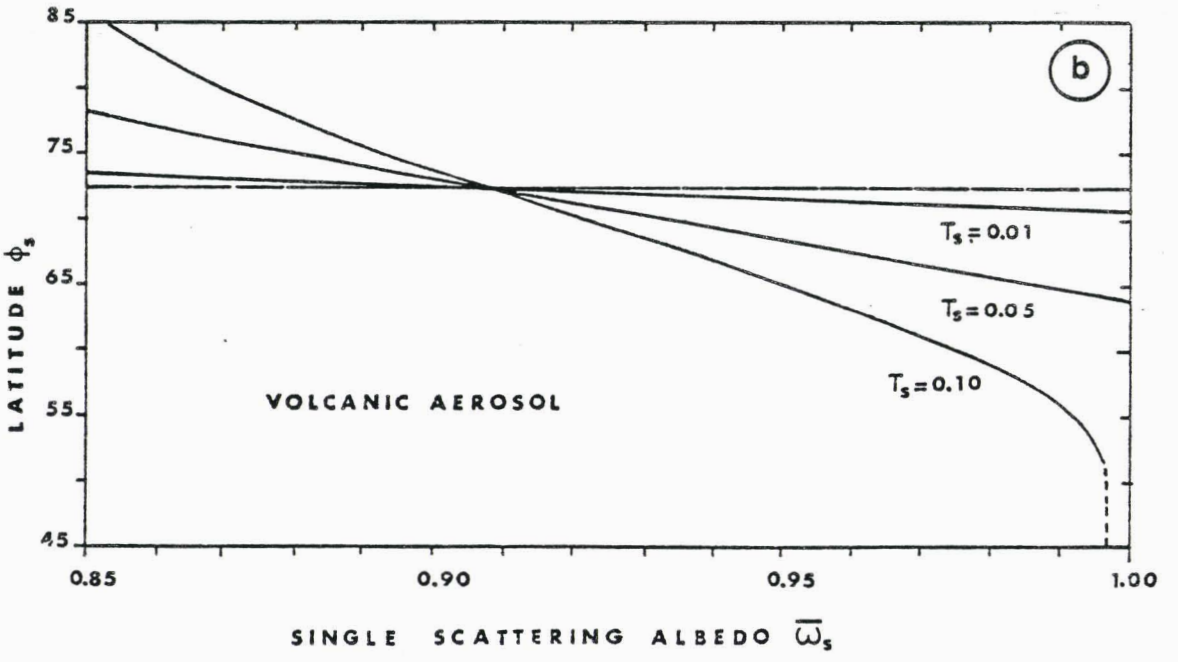

Fig. 6 : Variation of the ice cap edge latitude ϕ_s with the single scattering albedo $\bar{\omega}_s$ for various τ_s

a. b_s, C_s values of BSA

b. b_s, C_s values of VA

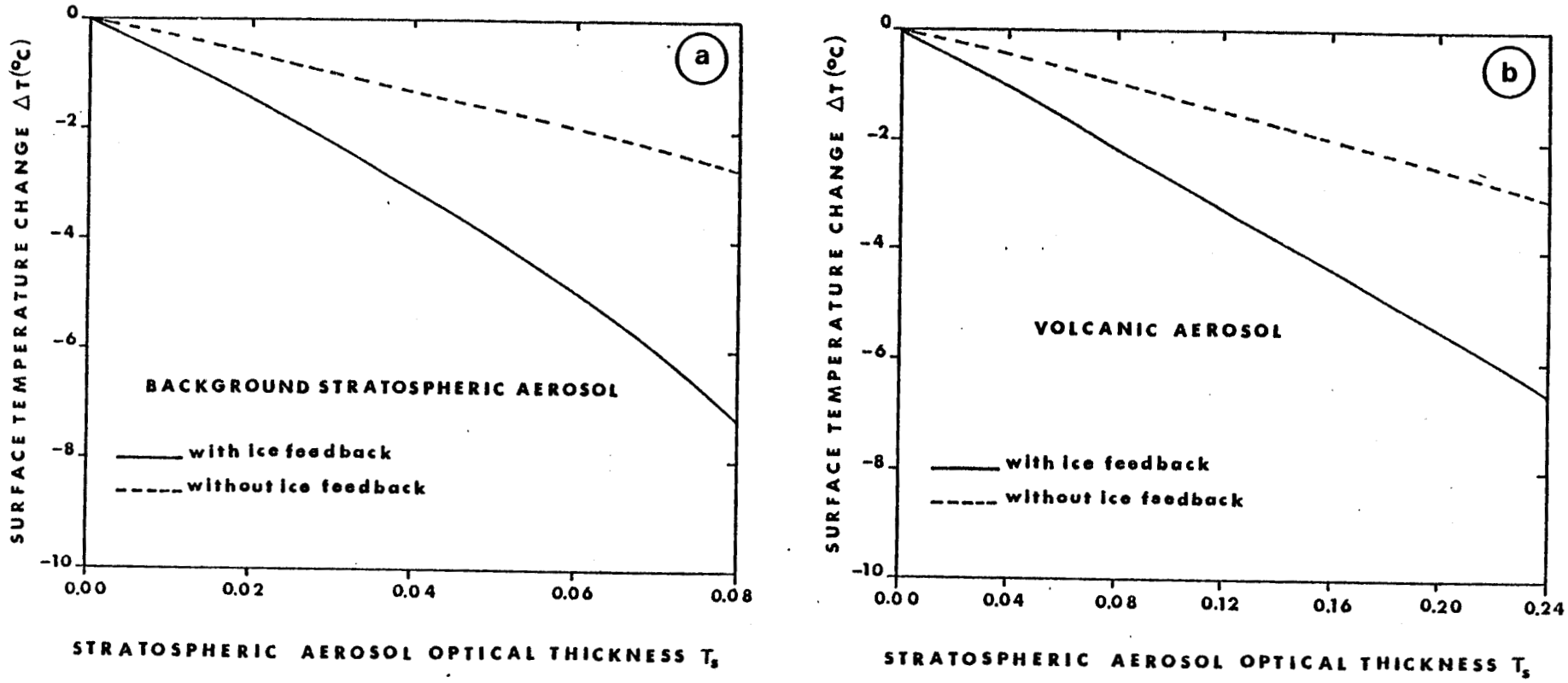

Fig. 7 : Variation of the average planetary surface temperature $\overline{\Delta T}$ versus the stratospheric aerosol optical thickness τ_s with (——) and without (----) ice edge shift feeback (infrared included, A_P = 0.328)

a. background aerosols

b. volcanic aerosols

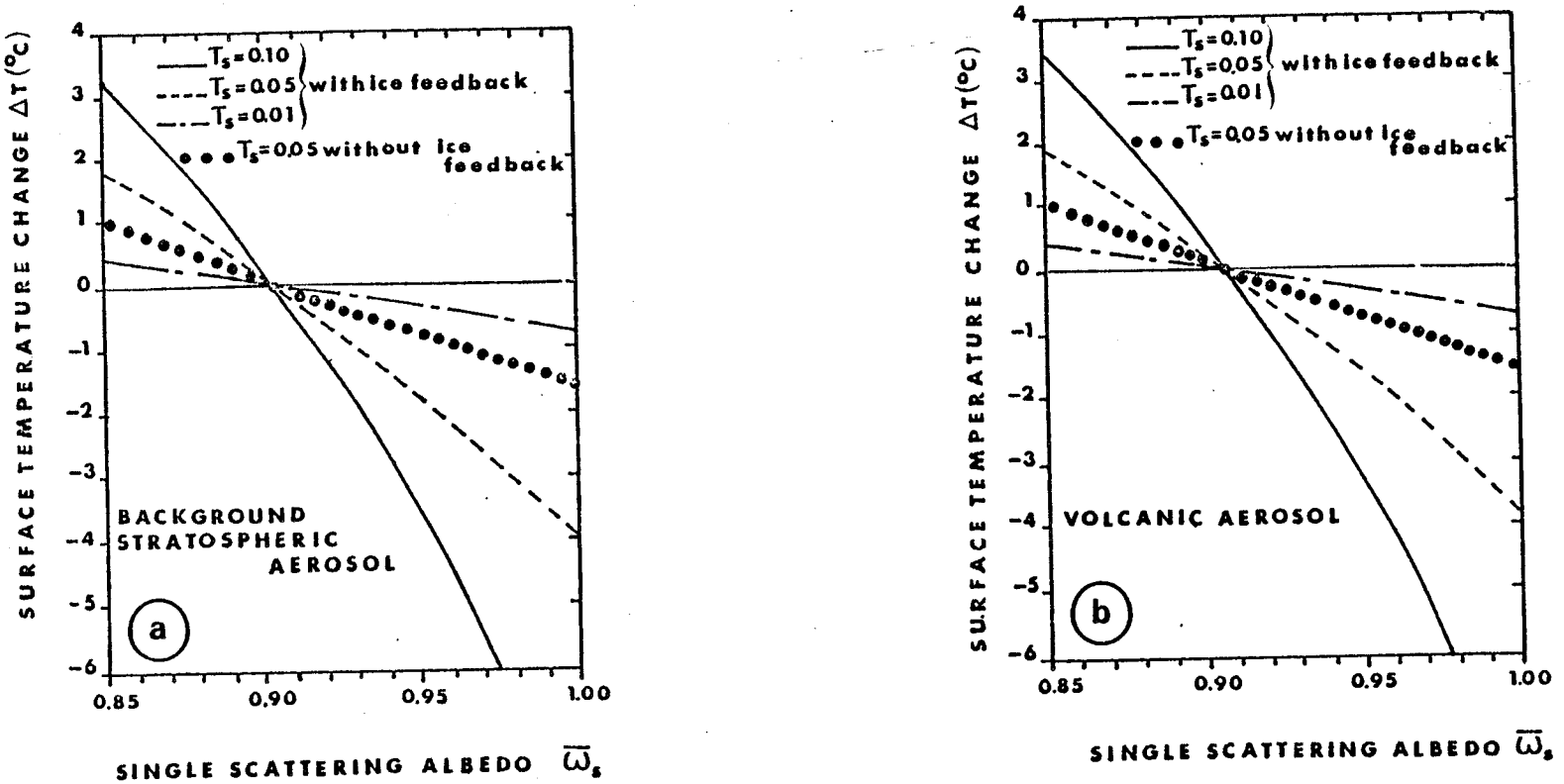

Fig. 8 : Variation of the average planetary surface temperature $\overline{\Delta T}$ with the single scattering albedo.

——— τ_s = 0.10
------ τ_s = 0.05 } with ice feedback
— - — τ_s = 0.01

+++ τ_s = 0.05 without ice feedback

a. background aerosols

b. volcanic aerosols

CONCLUSION

L'étude que nous avons faite a porté sur quelques uns des problèmes qu'implique pour le rayonnement terrestre, la présence d'aérosols.

Des calculs exacts ont d'abord été effectués pour des modèles tenant compte aussi finement que possible des conditions effectivement rencontrées lors de la mesure (inhomogénéités verticales, réflectance de sol non homogène et non lambertienne).

La complexité du problème nous a amené à développer un formalisme simple mais assez rigoureux pour restituer la plupart des caractéristiques du rayonnement rétrodiffusé. Cette modélisation nous a permis de linériser le signal satellitaire en fonction de quatre grandeurs :

- La réflectance atmosphérique proprement dite qui correspond au rayonnement uniquement diffusé dans l'atmosphère et qui n'a pas interagi avec le sol.
- La réflectance réelle de la cible visée.
- Une réflectance moyenne directionnelle qui tient compte de l'allure du champ de rayonnement diffus éclairant la cible.
- Une réflectance moyenne spatiale qui tient compte de la contribution des points environnant la cible.

Comme nous l'avons vu, dans le cas de sites marins de faibles réflectances, c'est essentiellement la réflectance atmosphérique propre qui perturbe le signal, et doit être éliminée. Pour la modéliser, nous nous sommes attaché à séparer la contribution moléculaire, stable et connue, de la contribution des aérosols. La réflectance de la composante en aérosol est fonction principalement de deux paramètres, l'épaisseur optique τ_p des aérosols et leur fonction de diffusion.

Au lieu d'une simple addition des deux réflectances (réflectance de la couche moléculaire et réflectance de la couche d'aérosols) on a amélioré cette première approche en tenant compte du couplage entre molécules et aérosols. Ceci permet d'augmenter la précision sur la réflectance atmosphérique d'un facteur 2 à 10 (suivant les conditions géométriques et les conditions de turbidité). La précision de l'ordre de 0,005 obtenue sur la réflectance, devient d'ailleurs nécessaire pour utiliser pleinement les données qui seront obtenues avec les futurs programmes spatiaux où le nombre de canaux disponibles permet d'envisager de nouveaux algorithmes de correction.

En ressources terrestres, le problème est différent, les réflectances à mesurer sont élevées et la principale perturbation provient des phénomènes d'environnement.

Pour étudier, dans le cas de paysages morcellés, cette influence de l'environnement de la cible, nous avons introduit la réflectance moyenne ρ_e. On peut exprimer ρ_e en fonction de l'épaisseur optique d'aérosols τ_p, et d'une fonction atmosphérique standard, établie pour un modèle moyen d'atmosphère. Une étude des effets de dégradation de contrastes pour différents types de parcellaires nous a permis de mettre au point une formulation analytique approchée tenant compte de l'effet principal de la perturbation, et permettant de corriger la mesure satellitaire.

Enfin, dans le cas de cibles directionnelles, la structure du rayonnement permet, compte tenu de la forte diffusion avant des aérosols de retrouver une partie du signal utile, cette information reste malgré tout difficile à atteindre et seules des mesures multispectrales permettent de remonter aux écarts à la loi de Lambert de la plupart des réflectances de surface. Bien que cet effet soit relativement minime et du 2° ordre par rapport aux effets d'environnement, il reste intéressant à étudier pour chiffrer son impact dans le cas de satellites effectuant un dépointage c'est à dire observant la même scène sous des conditions géométriques différentes.

Ces différentes études ont montré l'importance capitale de la quantité en aérosols τ_p. La méthode proposée pour remonter à ce paramètre est basée sur l'analyse fine des histogrammes de réflectances d'une scène donnée.

Les premiers résultants obtenus à l'aide d'images LANDSAT sont encourageants et prometteurs. Une restitution de τ_p avec une erreur de l'ordre de 0,03 semble possible.

La deuxième partie de cette étude a été consacrée à une approche de l'impact énergétique des aérosols. La modélisation du signal atmosphérique développée plus particulièrement pour les problèmes de télédétection, a été facilement appliquée au calcul du bilan radiatif. Dans cette première approche, on n'a abordé que le cas simple des aérosols stratosphériques.

En séparant les interactions successives entre les aérosols stratosphériques et la troposphère, on aboutit à une expression analytique de l'albédo zonal ou global très simple où interviennent l'albédo de la sous couche, l'absorption propre des aérosols, leur coefficient d'anisotropie et leur épaisseur optique ; la comparaison effectuée avec des calculs exacts montre que sa précision est tout à fait satisfaisante.

Une application réalisée à l'aide d'un modèle climatique simple, celui de Budyko, nous a permis de chiffrer l'impact climatique sur la température de surface et sur l'évolution de la limite des glaces. Cet impact dépend en grande partie du type d'aérosols retenu. Nous avons choisi les deux types d'aérosols stratosphériques de la commission internationale du rayonnement. Ils entrainent une diminution de la température de surface de l'ordre de 1 à 2° pour une épaisseur optique de 0.05. Un tel refroidissement maintenu sur une longue période peut entrainer une évolution de la limite des glaces vers l'équateur, ce qui peut amplifier les phénomènes d'un facteur 2 ou 3. Mais rappelons que tout dépend des propriétés radiatives des aérosols particulièrement de leur albédo qui peut entrainer un refroidissement ou un réchauffement suivant qu'ils sont peu ou très absorbants ; les données sur la stratosphère sont de plus en plus nombreuses et les modèles de plus en plus réalistes mais l'albédo propre des particules est difficile à atteindre et reste encore mal connu. Signalons de même que les ordres de grandeur donnés dans ce travail dépendent du modèle climatique choisi, le modèle de Budyko a été retenu à cause de sa cimplicité mais le formalisme développé peut s'inclure dans des modèles plus élaborés.

En résumé, la modélisation du signal atmosphérique proposée dans ce travail correspondait à un certain besoin que ce soit en télédétection ou en climatologie mais quelques problèmes restent encore à résoudre.

Pour l'aspect télédétection, nous avons dégagé les paramètres optiques qui régissent le champ de rayonnement ; le problème est maintenant de parvenir à les mesurer. Les premiers résultats obtenus à partir des données LANDSAT montrent que la méthode proposée pour atteindre à l'épaisseur optique semble prometteuse. Une corrélation des résultats satellitaires avec des mesures sol est à étudier pour s'assurer de la faisabilité ; ce travail est actuellement en cours, conjointement avec le C.N.E.S.. Il restera ensuite à trouver un nombre suffisant de sites tests invariants dans le temps (villes, surfaces d'eau par exemple) ; nous nous proposons de préciser ce point par une étude statistique. Pour les autres paramètres(principalement la fonction de phase), une étude en polarisation pourrait s'avérer intéressante ; un gros travail sur les algorithmes d'inversion reste à faire.

Pour l'aspect climatique, la formulation très simple obtenue pour les calculs de flux pourrait entrer dans les modèles de circulation générale sans alourdir exagérément les temps de calcul. Nous nous proposons de faire entrer les différents modèles d'aérosols, qu'ils soient stratosphériques ou troposphériques, dans le modèle du Centre Européen pour les prévisions météorologiques à moyen terme (Grande Bretagne).

Pour les aérosols troposphériques, nous envisageons d'effectuer plusieurs passages pour tester les différents effets, les effets directs sur l'albédo de la planète et sur le spectre infra-rouge, les effets indirects provenant des phénomènes de couplage ou de "feedback" entre les aérosols et la nébulosité. Ce travail doit se faire en collaboration principalement avec l'institut de Météorologie et de Géophysique d'Innsbruck (Autriche). Parallèlement, nous envisageons d'utiliser les données SAM et SAGE afin d'améliorer la caractérisation des aérosols stratosphériques.